2006

Synthesis and characterization of novel silica polyamine composites and their application to the reclamation of hazardous mining wastewater and tailings

Daniel J. Nielsen
The University of Montana

NOTE TO USERS

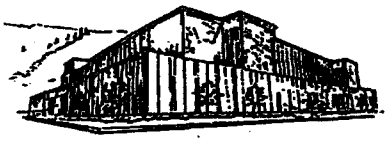

SYNTHESIS AND CHARACTERIZATION OF NOVEL SILICA POLYAMINE COMPOSITES AND THEIR APPLICATION TO THE RECLAMATION OF HAZARDOUS MINING WASTEWATER AND TAILINGS

by

Daniel J. Nielsen

B.A. Chemistry and Physics, SUNY College at Potsdam, 1999

presented in partial fulfillment of the requirements

for the degree of

Doctor of Philosophy

The University of Montana

May, 2006

Approved by:

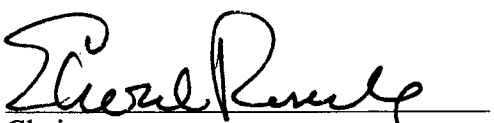

Chairperson

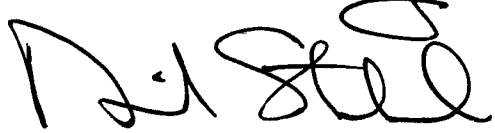

Dean, Graduate School

4-25-06

Date

Nielsen, Daniel J. Ph.D., May, 2006 Chemistry

Synthesis and Characterization of Novel Silica Polyamine Composites and Their Application to the Reclamation of Hazardous Mining Wastewater and Tailings

Chairperson: Edward Rosenberg

Toxic and hazardous metals contaminate waters on a global scale. Presently, metal laden liquid waste streams are frequently discharged into riverian systems without treatment. A plethora of mine waste and acid leach bodies are contained worldwide, some in perpetuity. Solid metal containing wastes and mine tailings are dispersed around the globe some of which have been relocated to designated repositories. In an effort to address these problems the further development of solid phase adsorbents composed of supramolecular composite materials is proposed. The focus of this thesis is to:

1. Develop novel silica composite materials for the recovery of manganese, ferric iron, gallium, lanthanide and actinide cations.
2. Construct a series of composites utilizing phosphorous based functional groups.
3. Characterize selected gels and composites at various stages of synthesis by the use of solid state nuclear magnetic resonance (NMR) spectroscopy.
4. Investigate the surface structure, kinetics, and capacity of composite materials incorporating mixtures of silanes in the lateral polymerization synthetic step of composite synthesis.
5. Generate and test separation strategies for the extraction of salable metals from contaminated waters and sediment.
6. Engineer a single column system that allows for accurate assessment of pilot scale flow treatment.

Selected composites will be employed for the capture and recovery of selected metals from synthetic solutions as well as from genuine solutions such as The Berkeley Pit Lake (Butte, Montana), Mt. Weld Leachate (Laverton, Australia), and contaminated sediments/tailings from the Philipsburg District, Montana. Bench-scale testing of these materials will provide the necessary physiochemical information for the implementation of future pilot-scale operations at these and other similar sites.

Acknowledgments

This work was completed under the advisement of Professor Ed Rosenberg, University of Montana. I am and will always be grateful for the support, opportunities, and sincerity that Ed has provided me with since September of 2000. I would also like to thank Bob Fischer and Carolyn Hart for their guidance and training. Countless hours of testing and analysis contributing to this work was shared by undergraduate researchers Joel Clancey and Jeff McKenzie, may you both find the future success you deserve. Thanks to my friends for sharing much frustration and success. Thank you Autumn for your patience, love and inspiration. Most importantly thanks to Mom and Dad for your continual guidance, loving support and encouragement. This research was funded by the Montana Board of Research & Commercialization Technology, and I gratefully acknowledge their support.

Table of Contents

ACKNOWLEDGMENTS III
TABLE OF CONTENTS IV
INDEX OF TABLES VI
INDEX OF FIGURES VII
INDEX OF EQUATIONS XII

1 INTRODUCTION 1

2 BACKGROUND 5

2.1 SILICA GEL 5
2.2 CHLOROPROPYL GEL 8
2.3 POLYAMINE COMPOSITES (WP-1, BP-1, VP-1) 8
2.4 ACETATE POLYAMINE COMPOSITES (WP-2, BP-2) 10
2.5 PICOLYLAMINE COMPOSITE (CUWRAM) 10
2.6 METAL SELECTIVITY 11
2.7 MULTI-COLUMN CONTINUOUS TREATMENT SYSTEMS 13
2.8 COMPARISON WITH OTHER METAL RECOVERY TECHNOLOGIES 14
2.8.1 ELECTROWINNING 14
2.8.2 POLYSTYRENE ION-EXCHANGE RESINS 16
2.8.3 COMPETITIVE SILICA BASED ION-EXCHANGE MATERIALS 18
2.8.4 LIME TREATMENT FOR ACID MINE DRAINAGE (THE BERKELEY PIT LAKE) 20
2.8.5 SULFATE REDUCING BACTERIA TREATMENT 22

3 RESULTS AND DISCUSSION – COMPOSITE MATERIALS 23

3.1 COMPOSITE CHARACTERIZATION 23
3.2 PERFORMANCE TESTING OF COMPOSITES 24
3.3 IMPACT OF SILICA GEL ON COMPOSITE PERFORMANCE 30
3.4 CHLOROPROPYL GEL 31
3.5 LATERAL POLYMERIZATION OF MIXED TRIFUNCTIONAL SILANES 37
3.6 POLYAMINE COMPOSITES (WP-1, BP-1) 42
3.7 OXINE POLYETHYLENEIMINE COMPOSITE (WP-4) 45
3.8 SUCCINAMIC ACID POLYALLYLAMINE COMPOSITE (BPSU) 46
3.9 TETRA-ACETATE POLYALLYAMINE COMPOSITE (BPDT) 50
3.10 AMINO-δ-KETO PHOSPHONIC ACID POLYALLYLAMINE COMPOSITE (BPMA) 51
3.11 PHOSPHONIC ACID POLYALLYLAMINE COMPOSITE VIA CMPD (BPCD) 52
3.12 PHOSPHONIC ACID POLYALLYLAMINE COMPOSITE BY MANNICH (BPAP) 54
3.13 PHOSPHINIC ACID POLYALLYLAMINE COMPOSITE (BP-5) 84
3.14 METHYL/DIMETHYL PHOSPHONATE POLYALLYLAMINE COMPOSITE (BP-6) 85
3.15 METHYL/DIMETHYL PHOSPHONATE POLYALLYLAMINE COMPOSITE (BP-7) 89

4 RESULTS AND DISCUSSION – ADDITIONAL APPLICATIONS 91

4.1 PILOT SCALE COLUMN TESTING 91
4.2 RARE EARTH ELEMENT SEPARATION 94

4.3 ACTINIDE ELEMENT SEPARATION 102
4.4 ACID MINE DRAINAGE TREATMENT 105
4.5 METAL RECOVERY FROM MINING TAILINGS 127

5 CONCLUSIONS AND FUTURE WORK 129

5.1 LATERAL POLYMERIZATION OF MIXED TRIFUNCTIONAL SILANES 129
5.2 PHOSPHOROUS BASED SILICA POLYAMINE COMPOSITES 130
5.3 MINING WASTE TREATMENT 131

6 EXPERIMENTAL 133

6.1 REAGENTS AND SYNTHETIC PROCEDURES 133
6.2 SYNTHESIS OF CLEANED HYDRATED GEL 136
6.3 SYNTHESIS OF CHLOROPROPYL GEL (CP GEL) 137
6.4 SYNTHESIS OF MIXED SILANE GEL 138
6.5 SYNTHESIS OF POLYAMINE COMPOSITES (WP-1, BP-1) 139
6.6 SYNTHESIS OF TETHERED POLYALLYLAMINE COMPOSITE (BP-1-T) 141
6.7 SYNTHESIS OF ACETATE POLYAMINE COMPOSITES (WP-2, BP-2) 141
6.8 SYNTHESIS OF PICOLYLAMINE COMPOSITE (CUWRAM) 142
6.9 SYNTHESIS OF OXINE POLYALLYLAMINE COMPOSITE (WP-4) 142
6.10 SYNTHESIS OF SUCCINAMIC ACID POLYALLYLAMINE COMPOSITE (BPSU) 143
6.11 SYNTHESIS OF TETRA-ACETATE POLYALLYAMINE COMPOSITE (BPDT) 144
6.12 SYNTHESIS OF KETO PHOSPHONIC ACID POLYAMINE COMPOSITE (BPMA) 145
6.13 SYNTHESIS OF PHOSPHONIC ACID COMPOSITE VIA CMPD (BPCD) 145
6.14 SYNTHESIS OF PHOSPHONIC ACID COMPOSITE BY MANNICH REACTION (BPAP) 146
6.15 SYNTHESIS OF METHYLATED BPAP (PHOSPHONATE) 147
6.16 SYNTHESIS OF PHOSPHINIC ACID POLYALLYLAMINE COMPOSITE (BP-5) 148
6.17 SYNTHESIS OF METHYL/DIMETHYL PHOSPHONATE COMPOSITE (BP-6) 148
6.18 SYNTHESIS OF METHYL/DIMETHYL PHOSPHONATE COMPOSITE (BP-7) 150

APPENDIX A – ELEMENTAL ANALYSIS RESULTS 151

REFERENCES 152

Index of Tables

Table 1. Physical characteristics of various silica gels. 6
Table 2. Elemental analyses of CP Gels. 35
Table 3. CP Gel-CF and QH surface coverage of chloropropyl anchor. 35
Table 4. Mixed silane gel coverage density results. 40
Table 5. Elemental analyses of polyamine composites WP-1 and BP-1. 43
Table 6. Elemental analysis of WP-4. 46
Table 7. Elemental analysis of BPSU. 48
Table 8. Eu(III) batch testing on BPSU. 49
Table 9. Elemental analysis of BPMA. 52
Table 10. Elemental analysis of BPCD. 53
Table 11. Elemental analysis of WPAP, BPAP, and BPAP-t. 55
Table 12. Elemental analysis of BP-5. 84
Table 13. Elemental analysis of BP-6. 86
Table 14. Elemental analysis of BP-7. 90
Table 15. Metal concentrations (mg/L) of Berkeley Pit Lake water (at various depths), and Montana water quality standards. 106
Table 16. Berkeley Pit Lake metal ion recovery data. 112
Table 17. Elemental Analysis of various gels and composites. 151

Index of Figures

Figure 1. Micrograph of Qingdao Haiyang silica gel. 6
Figure 2. Mercury porosimetry analyses for Crosfield (top) and Qingdao Haiyang silica gels (bottom). 7
Figure 3. (a) WP-1 silica poly(ethyleneimine) composite, (b) BP-1 silica poly(allylamine) composite, (c) VP-1 silica poly(vinylamine) composite. 9
Figure 4. Schematic structure of WP-2 (left), and BP-2 (right). 10
Figure 5. Schematic structure of CuWRAM chelating a copper ion. 11
Figure 6. The Irving-Williams effect. 13
Figure 7. Multi-column continuous treatment systems; ISEP (left), SepTor (right). 14
Figure 8. Conventional electrowinning (left), and EMEW® electrowinning cell (right). 15
Figure 9. Diphonix resin polymer matrix. 16
Figure 10. Breakthrough curves comparing Diphonix resin (left) to BPAP-CF composite (right). 17
Figure 11. Longevity testing comparing Diphonix resin (left) to BPAP-CF composite (right). 17
Figure 12. Breakthrough curves for Nd(III) using phosphonic acid ICAB. 19
Figure 13. Molecular diagram of SAMMS technology and example functionalities. 20
Figure 14. The Berkeley Pit, 1981 (left) & Lake, 1999 (right), Butte, Montana. 21
Figure 15. Breakthrough testing cartoon. 26
Figure 16. BPAP-CF 041504-DN, Eu(III) average breakthrough curve with standard deviation of three trials, 0.50 CV/min., pH 1.0, 50 mg/g Eu(III) capacity. 27
Figure 17. Standard addition for Cu(II) in Berkeley Pit Lake matrix. 29
Figure 18. BPAP-CF 041504-DN and BPAP-QH 082503-DN, Fe(III) breakthrough curves, 0.50 CV/min., pH 1.5, 2.9 g/L Fe(III). 31
Figure 19. Hydration apparatus for silica gel and typical hydration curve. 32
Figure 20. Lateral (left) and vertical (right) polymerization on hydrated silica gel. 33
Figure 21. Two hydration experiments on Crosfield silica gel (% H_2O and H_2O:Si-OH). 34
Figure 22. ^{13}C NMR CP/MAS of the non-hydrated CP Gel (left), and hydrated CP Gel (right). 34
Figure 23. Schematic structure (left) and ^{13}C NMR spectra of CP Gel (right). 36
Figure 24. Schematic structure CP Gel (left), ^{29}Si CP/MAS NMR spectrum of CP Gel (middle), ^{29}Si BD/MS spectrum of CP Gel (right). 37
Figure 25. BD/MAS ^{29}Si NMR spectra; CP Gel (A) (top, left), 1.3:1 CP/M Gel (B) (top, right), M Gel (D) (bottom, left), deconvolution CP Gel (A) (bottom, right). 40
Figure 26. BPAP-QH mixed silane study: Fe(III) breakthrough curves, 0.50 CV/min., pH 1.5, 3.1 g/L Fe(III) (top); strip curves, 0.50 CV/min., 9.0 N H_2SO_4 (bottom). 42
Figure 27. Schematic structure (left) and ^{13}C NMR spectra of BP-1 (right). 44
Figure 28. Schematic structure (left) and ^{13}C NMR spectra of WP-1 (right). 45
Figure 29. Schematic structure (left) and ^{13}C NMR spectra of WP-4 (right). 46
Figure 30. Molecular structure of BPSU. 47
Figure 31. 500 MHz CP/MAS ^{13}C NMR spectrum of BPSU. 48
Figure 32. BPSU-CF 032202-DN; breakthrough curve, 0.50 CV/min., pH 3.0 (left); strip profile, 0.50 CV/min., 8.0 N H_2SO_4, 92 % stripped (right). 49
Figure 33. BPSU-CF 080404-DN; breakthrough curve, 0.50 CV/min., pH 1.5 (left); strip profile, 0.50 CV/min., 9.0 N H_2SO_4, 84 % stripped (right). 49

Figure 34. Schematic structure of BPDT. 50
Figure 35. BPSU-CF 082202-DN, BPDT-CF 033002-DN; Mn(II) breakthrough curves, 0.50 CV/min., pH 3.0, 200 mg/L Mn(II). 51
Figure 36. Schematic structure (left), ^{13}C (center) and ^{31}P (right) NMR spectra of BPAP. 58
Figure 37. $^{1}H - ^{31}P$ HETCOR NMR spectrum of BPAP. 59
Figure 38. BPAP-CF 082003-DN, BPAP-QH 082503-DN; Fe(III) breakthrough curves, 0.50 CV/min., pH 1.5, 2.9 g/L Fe(III) (top); strip curves, 0.50 CV/min., 7.5 N H_2SO_4 (bottom). 61
Figure 39. Batch profile silica gel study using BPAP, pH 1.5. 62
Figure 40. Silica gel study using BPAP breakthrough curves, 0.50 CV/min. (1.0 CV/min. BPAP-CF), pH 1.5, 459 mg/L Fe(III). 63
Figure 41. WPAP-CF 090803-DN, BPAP-CF 100203-DN; Fe(III) breakthrough curves, 0.50 CV/min., pH 1.5, 1.5 g/L Fe(III)/0.50 g/L Cu(II) (top); strip curves, 0.50 CV/min., 7.5 N H_2SO_4 (bottom). 64
Figure 42. Fe(III) and Eu(III) batch capacity pH profile for BPAP. 65
Figure 43. BPAP-CF 041504-DN, Fe(III) concentration dependent adsorption isotherm, pH 1.7. 67
Figure 44. BPAP-CF 041504-DN, Fe(III) Langmuir plot. 68
Figure 45. Rare earth element (RE) coordination by phosphonic acid ester ligand. 68
Figure 46. BPAP-QH 053003B-DN, breakthrough curves, 0.50 CV/min., pH 1.5, 456 mg.L Fe(III), 339 mg/L Eu(III). 69
Figure 47. BPAP-QH 053003B-DN, Fe(III) strip curves, 0.25 and 0.50 CV/min., 7.5 N H_2SO_4. 70
Figure 48. WPAP-CF 090803-DN, BPAP-CF 100203-DN, BPAP-CF 091103-DN (0.3 g H_3PO_3/g); breakthrough curves, 0.50 CV/min., pH 1.5, 1.5 g/L Fe(III), 0.50 g/L Cu(II) (top); strip curves, 0.50 CV/min., 7.5 N H_2SO_4 (bottom). 71
Figure 49. BPAP-CF 041504-DN, BPAP-t-CF 071504-DN; breakthrough curves, 0.50 CV/min., pH 1.5, 3.1 g/L Fe(III) (left); strip curves, 0.50 CV/min., 9.0 N H_2SO_4 (right). 72
Figure 50. BPAP-QH 081303-MT, initial stripping study. 73
Figure 51. BPAP-CF methylation study; breakthrough curves, 0.50 CV/min, pH 1.5, 3.0 g/L Fe(III) (top); strip curves, 0.50 CV/min., 7.5 N H_2SO_4 (bottom). 75
Figure 52. BPAP-CF 041504-DN, final strip profile data, 0.50 CV/min. (strip percentage). 76
Figure 53. BPAP-CF 041504-DN; breakthrough curves for precision study, 0.50 CV/min., pH 1.0, 2.7 g/L Eu(III) (top); average breakthrough curve with standard deviation, 50 mg/g $\pm$ 2 mg/g Eu(III) (bottom). 77
Figure 54. BPAP-CF 041504-DN load/strip cycles #1 and #2; breakthrough curves, 0.50 CV/min., pH 1.0, 7.9 g/L Eu(III) (top); strip profiles, 0.50 CV/min., 1.0 M EDTA (pH 10.6) (bottom). 78
Figure 55. BPAP-CF 041504-DN, stripping study #2, 0.050 CV/min. 79
Figure 56. BPAP-CF 041504-DN synthetic Cu(II) electrowinning solution; breakthrough curves, 0.50 CV/min., 4.0 N H_2SO_4, 30 mg/g Fe(III) (top); strip fractions, 0.050 CV/min., 1.5 M EDTA (pH 10.6), 99% stripped (bottom). 81
Figure 57. Ga(III) batch testing; BPAP-CF 041504-DN, BP-5-CF 120804-DN, BP-6-CF 021505-DN, BP-7-CF 022305-DN. 82

Figure 58. BPAP-CF 041504-DN; Ga(III)/Al(III) breakthrough curves, 0.50 CV/min., pH 1.0, (top); strip fractions, 0.50 CV/min., 1.0 M EDTA (pH 10.6) 92% Ga(III) purity (bottom). 83
Figure 59. BP-5-CF 120804-DN; breakthrough curve, 0.50 CV/min., pH 5.5, 2.0 g/L Eu(III), 55 mg/g capacity (top); strip fractions, 0.50 CV/min., 9.0 N H_2SO_4, 24% stripped (bottom). 85
Figure 60. ^{1}H, ^{13}C, and ^{31}P NMR spectra of Dimethyl (3-bromopropyl) phosphonate isolate. 87
Figure 61. Schematic structure of BP-6 (and BP-7). 88
Figure 62. ^{13}C (left) and ^{31}P (right) solid state NMR of BP-6. 89
Figure 63. ^{13}C (left) and ^{31}P (right) solid state NMR of BP-7. 90
Figure 64. Pilot scale column design for testing BPAP-QH 1201403-DN. 92
Figure 65. BPAP-QH 121403-DN pilot scale testing over 30 load/strip cycles; breakthrough curves, 0.32 CV/min., pH 1.5, 3.1 g/L Fe(III) (top); strip curves, 0.42 – 0.27 CV/min., (70 psi), 9.0 N H_2SO_4 (bottom). 93
Figure 66. BPAP-QH 121403-DN pilot scale flowthrough and strip capacities over 30 load/strip cycles. 94
Figure 67. Rare earth element purification results using WP-4-CF 101205-DN and BPAP-CF 041504-DN. 96
Figure 68. WP-4-CF 101205-DN load/strip cycle #1 and #2 by flame AAS; breakthrough curves, 0.50 CV/min., pH 1.3, 1.0 g/L Eu(III) (top); strip profiles, 0.50 CV/min., 9.0 N H_2SO_4, 26 mg/g capacity, ~100% stripped (bottom). 97
Figure 69. WP-4-CF 101205-DN breakthrough test #1 (top) and #2 (bottom) by ICP analysis (high conc. metals), 0.50 CV/min., pH 1.3. 98
Figure 70. WP-4-CF 101205-DN breakthrough test #1 (top) and #2 (bottom) by ICP analysis (low level metals), 0.50 CV/min., pH 1.3. 99
Figure 71. WP-4-CF 101205-DN strip profiles #1 (top) and #2 (bottom) by ICP analysis, 0.50 CV/min., 9.0 N H_2SO_4. 100
Figure 72. BPAP-CF 041504-DN breakthrough curves for REE recovery, load cycle #1 (top), #2 (bottom), 0.50 CV/min., pH 1.3. 101
Figure 73. BPAP-CF 041504-DN strip profiles for REE recovery, strip cycle #1 (top), #2 (bottom), 0.50 CV/min., 2.0 M H_3PO_3, 56 mg/g Ln(III) capacity, 99% Ln(III) purity [1% Al(III), <<1% Ca(II), Fe(III) Ti(IV)] 102
Figure 74. pH profile Th(IV) batch capacities for various composites. 103
Figure 75. BPSU-CF 080404-DN, BP-7-CF 022305-DN, BPAP-CF 041504-DN, BP-5-CF 120804-DN; Th(IV) breakthrough curves, 0.50 CV/min., pH 2.9 (top); strip profiles, 0.20 CV/min., 2.0 M H_3PO_3 (bottom). 104
Figure 76. Sampling Berkeley Pit Lake water, February 2002. 107
Figure 77. BPAP-CF 041504-DN Berkeley Pit Lake treatment; breakthrough curves, 0.50 CV/min., feed pH 2.2 (top); strip fractions, 0.10 CV/min., 13 N H_2SO_4, 85% Fe(III) purity (bottom). 108
Figure 78. WP-4-CF 101205-DN Berkeley Pit Lake treatment; breakthrough curves, 0.50 CV/min., pH 2.2 (top); strip fractions, 0.50 CV/min., 9.0 N H_2SO_4, 81% Fe(III) purity (bottom). 110
Figure 79. Cartoon of Berkeley Pit Lake treatment process. 112
Figure 80. CuWRAM-CF 022602-DN Berkeley Pit Lake treatment; breakthrough curves, 0.50 CV/min., pH 2.2 (top); strip fractions, 0.50 CV/min., 9.0 N H_2SO_4, 97% Cu(II) purity (bottom). 113

Figure 81. Berkeley Pit Lake water metal concentrations as a function of pH. 114
Figure 82. WP-2-CF 013002-BF; Zn(II)/Mn(II) breakthrough curves, 0.50 CV/min., pH 5.3 (top); strip fractions, 0.50 CV/min., 9.0 N H_2SO_4, 99.98% Zn(II) purity (bottom). 115
Figure 83. BP-2-CF 051903-CH; Mn(II)/Ca(II)/Mg(II) breakthrough curves, 0.50 CV/min., pH 4.9 (top); strip fractions, 0.50 CV/min., 9.0 N H_2SO_4, 83% Mn(II) purity (bottom). 117
Figure 84. BPAP-CF 041504-DN; Al(III)/Zn(II)/Mn(II) breakthrough curves, 0.50 CV/min., pH 1.6 (top); strip fractions, 0.50 CV/min., 9.0 N H_2SO_4, 95% A1(III) purity (bottom). 118
Figure 85. BP-1-CF 040804-DN; Al(III)/Mn(II)/Zn(II) breakthrough curves, 0.50 CV/min., pH 2.2 (top); strip fractions, 0.50 CV/min., 9.0 N H_2SO_4, 96% Al(III) purity (bottom). 120
Figure 86. WP-4-CF 101205-DN; Al(III)/Zn(II)/Mn(II) breakthrough curves, 0.50 CV/min., pH 1.6 (top); strip fractions, 0.50 CV/min, 9.0 N H_2SO_4, (bottom). 121
Figure 87. BPAP-CF 041504-DN; Al(III)/Zn(II)/Mn(II) breakthrough curves, 0.50 CV/min. feed pH = 1.6 (top); strip fractions, 0.50 CV/min., 9.0 N H_2SO_4 (bottom). 122
Figure 88. WP-4-CF 101204-DN; Zn(II)/Mn(II) breakthrough curves, 0.50 CV/min., pH 5.2 (top); strip fractions, 0.50 CV/min., 9.0 N H_2SO_4, 99.98% Zn(II) purity (bottom). 123
Figure 89. WP-4-CF 101204-DN; Zn(II)/Mn(II) breakthrough curves, 0.50 CV/min., pH 5.2 (top); strip fractions, 0.50 CV/min., 9.0 N H_2SO_4, 92% Zn(II) purity (bottom). 124
Figure 90. WP-2-CF 013002-BF; Zn(II)/Mn(II) breakthrough curves, 0.50 CV/min., pH 5.2 (top); strip fractions, 0.50 CV/min., 9.0 N H_2SO_4, 99.99% Zn(II) purity (bottom). 125
Figure 91. WP-2-CF 013002-BF; Zn(II)/Mn(II) breakthrough curves, 0.50 CV/min., pH 5.2 (top); strip fractions, 0.50 CV/min., 9.0 N H_2SO_4, 99.93% Zn(II) purity (bottom). 126
Figure 92. Montana state's 294 priority cleanup sites. 128
Figure 93. Metal concentration of Philipsburg Mining District sediments/tailings as a function of pH. 128
Figure 94. Experimental set-up for: degassing (top, left), nitrogen head-space (top, right), reflux (bottom, left), vacuum filtration (bottom, right). 134
Figure 95. Round bottom flask rotary stirrer. 143

Index of Reaction Schemes

Scheme 1. Synthesis of CP Gel (d). 8
Scheme 2. Synthesis of BP-2. 10
Scheme 3. Synthesis of BP-1. 32
Scheme 4. Synthesis of CP/M Gel. 39
Scheme 5. Synthesis of BPSU. 47
Scheme 6. Synthesis of BPDT. 50
Scheme 7. Synthesis of BPMA. 52
Scheme 8. Synthesis of BPCD (using t-butanol). 53
Scheme 9. Synthesis of BPCD (using methanol). 54
Scheme 10. Synthesis of BPAP. 56
Scheme 11. Acid-catalyzed Mannich reaction utilizing phosphorous acid. 57
Scheme 12. Synthesis of BP-1-t. 72
Scheme 13. Synthetic scheme of diphenyl phosphinic acid composite. 84
Scheme 14. Synthesis of BP-5. 84
Scheme 15. Synthesis of dimethyl (3-bromopropyl) phosphonate. 86
Scheme 16. Synthesis of BP-6. 88
Scheme 17. Synthesis of BP-7. 90

Index of Equations

Equation 1. Batch capacity formula. 25
Equation 2. Cu(II) standard addition calculation in Berkeley Pit Lake matrix. 30
Equation 3. Available amines calculation. 43
Equation 4. Rearranged Langmuir equation. 67

Index of Acronyms

8-HQ – 8-Hydroxyquinoline
AAS – Atomic Absorption Spectroscopy
AMD – Acid Mine Drainage
ARCO – Atlantic Richfield Company
BD/MAS – Bloch Decay Magic Angle Spinning
BP-1 – Silica Polyallylamine Composite
BP-2 – Silica Polyallylamine Acetate Composite
BPAP – Silica Polyallylamine Phosphonic Acid Composite
BPCD – Phosphonic Acid Polyallylamine Composite via Chloromethylphosphonic Dichloride
BPDT – Tetra Acetate Polyallylamine Composite
BPMA - Amino-δ-keto Phosphonic Polyallylamine Composite
BPSU – Silica-Polyallylamine Succinamic acid Composite
BV – Bed Volume
CF – Crosfield Silica Gel (INEOS, Inc.)
CMPD – Chloromethylphosphonic dichloride
CP/MAS – Cross Polarization Magic Angle Spinning
CPTCS – Chloropropyltrichlorosilane
CP Gel – Chloropropyl Gel
CP/M Gel - Chloropropyl
CuWRAM – Silica Poly(allylamine) Picolyl Composite (Copper Waste Recovery from an Aqueous Medium)
CV – Column Volume
DI – De-Ionized
DMSO – Dimethylsulfoxide
DTPA – Diethylenetriaminepentaacetic Acid Dianhydride
EMEW – Electrometals Electrowinning
EMSL – Environmental Molecular Science Laboratory
EPA – Environmental Protection Agency
HETCOR – Heteronuclear Chemical Shift Correlation NMR Experiment
HPLC – High Performance (or Pressure) Liquid Chromatography
MCL – Maximum Contaminant Level
MSR – Microbial Sulfate Reduction
MTCS - Methyltrichlorosilane
NJ – Nanjing (Silica Gel Supplier)
NMR – Nuclear Magnetic Resonance
NSF – National Science Foundation
NT – Nanjing Tianyi (Silica Gel Supplier)
PAA – Polyallylamine
PEI – Polyethyleneimine
PNNL – Pacific Northwest National Laboratory
PTCS – Propyltrichlorosilane
PVA – Polyvinylamine
QH – Qingdao Haiyang (Silica Gel Supplier)
QM – Qingdao Meigao (Silica Gel Supplier)
REE – Rare Earth Element

SAMMS - Self-Assembled Monolayers on Mesoporous Supports
SRB – Sulfate Reducing Bacteria
SWL – Safe Water Level
TEA – Triethylamine
THF – Tetrahydrofuran
TMAH – Tetramethylammonium hydroxide
TMDL – Total Maximum Daily Load
VA-CP/MAS – Variable Amplitude – Cross Polarization / Magic Angle Spinning
VP-1 – Silica Poly(vinylamine) Composite
WP-1 – Silica Poly(ethyleneimine) Composite
WP-2 – Silica Poly(ethyleneimine) Acetate Composite
WP-3 – Silica Poly(ethyleneimine) Dithiocarbamate Composite
WP-4 – Silica Poly(allylamine) 8-HQ Composite
WPAP – Silica Poly(ethyleneimine) Phosphonic Acid Composite
WPSU – Silica Poly(ethyleneimine) Succinamic Acid Composite
WQB-7 – Water Quality Bureau–7

1 INTRODUCTION

Toxic metal contamination from numerous industries is spread throughout the earth. As of 1999 mining efforts alone had disturbed roughly 250,000 km^2 of land (about the size of Oregon).[1] Milling and smelting currently have released on the order of 70,000 metric tons of metals to the aquatic environment to date. Management of metal laden hazardous waste is costly in regard to human health, the environment, and often to the taxpayer's pocketbook. The Environmental Protection Agency (EPA) has identified over 31,000 hazardous waste sites, and hundreds of superfund sites that amass the national priority list. Americas largest complex of superfund sites is located in the Clark Fork River Basin, Montana.

Metal laden liquid and solid wastes are either: contained in perpetuity exceeding volumes of 30 billion liters, and 200 million yds^3, respectively; discharged into riverian systems (treated or untreated); or relocated (sediments/tailings). The remediation of heavy metal-containing waste streams is of great importance to many industries additional to metal extraction and processing such as metal plating sites, pickling, pigment industries, tanneries, and paper mills. Municipal power generation plants, landfills, and water and wastewater treatment facilities have required the removal of metals.[2,3] Environmentally damaging effluents continually flow from thousands of acid mine drainage sites around the world.[4,5] Increasing regulation on natural resource extraction and industrial wastewater discharge has heightened the need for removal and recovery of metal ions from these effluents.[6] The need for "green" ore processing and the recovery of metals is vital with respect to our health, sustainability, and future supply of valuable metals.

A plethora of metal treatment processes have been in the research and development phases for several years now. The most simplistic, effective and economical process is the addition of lime [e.g., quick-lime (CaO) or limestone ($CaCO_3$)] to neutralize the pH and induce precipitation,[3,7] followed by addition of acid prior to discharge. However, this process does not capitalize on the recovery of salable metals. Other processes that have been investigated include bioremediation, chelation affinity chromatography, chemical precipitation, freeze crystallization, ion exchange, membrane filtration,[8] solvent extraction,[9] high-density sludge formation,[10] sulfide-precipitation, wetland treatment, turbidity removal,[11] and sulfate-reducing bacteria (SRB) treatment.[12,13]

In response to the need for high-flow, economical treatment of metal laden liquids a rigorous investigation of silica-polyamine composites commenced in 1993 at the University of Montana. The research has been directed by Professor Ed Rosenberg (University of Montana) in collaboration with Purity Systems, Inc. (Missoula, Montana). Over the past decade research and development has led to a series of patented materials which exhibit superior characteristics relative to other high-flow metal recovery technologies.

The goals of this thesis are to: develop novel silica composite materials for the recovery of manganese, ferric iron, gallium, lanthanide and actinide cations; construct a series of composites utilizing phosphorous based functional groups; characterize selected gels and composites at various stages of synthesis by the use of solid state nuclear magnetic resonance (NMR) spectroscopy; investigate the surface structure, kinetics, and capacity of composite materials incorporating mixtures of silanes in the lateral polymerization synthetic step of composite synthesis; generate and test separation strategies for the extraction of salable metals from contaminated waters and sediment;

engineer a single column system that allows for accurate assessment of pilot scale flow treatment.

Selected composites will be employed for the capture and recovery of selected metals from synthetic solutions as well as from genuine solutions such as The Berkeley Pit Lake (Butte, Montana), Mt. Weld Leachate (Laverton, Australia), and contaminated sediments/tailings from the Philipsburg District, Montana. Bench-scale testing of these materials will provide the necessary physiochemical information for the implementation of future pilot-scale operations at these and other similar sites.

Reported within this thesis is the further development of silica polyamine composite technology. The research pursued improving the density of lateral polymerization prior to the addition of polyamine in composite synthesis. Other efforts were directed at adding functional groups for modification of the parent composites (WP-1 and BP-1) and include succinamic acid, diethyltriamine tetra-acetate, phosphinic acid, phosphonic acid and phosphonate esters.

The succinamic acid and tetra-acetate composites were made in an effort initially aimed at Mn(II) recovery. Both of these composites exhibited decent Mn(II) capacities following base regeneration of the functional group. The succinamic acid composite showed affinity towards Eu(III) and Th(IV) above pH 1. The tetra-acetate ligand was very expensive limiting quantities available for testing, and similarly for industrial applications.

Interest in the selective recovery of lanthanide and actinide ions led to the development of a series of composites utilizing the phosphorous based ligands mentioned above.[14] Initially, three synthetic routes were considered. The first approach utilized the chloromethylphosphonic dichloride reagent to form the diester, preceding attachment to

the polyamine, and hydrolysis. A second route utilized the Michaelis-Arbuzov rearrangement.[15] A third approach employed the Mannich reaction to produce both the phosphonic and phosphinic acid functionalities.[16] Usage of a linker group connecting the functional group to the polyamine which preceded the Mannich reaction was also pursued. Phosphorous based ligand composites have been investigated for recovery of a host of tri- and tetravalent metals such as Fe(III), Al(III), Ga(III), Ln(III), and Th(IV).

Design and performance testing of a pilot scale column provided Fe(III) load/strip cycling data, backpressure information, and can be used for investigation of future pilot scale endeavors. Bench scale development of metal recovery strategies from actual mine waste sources and ore leaches have also been investigated. These studies include recovery of rare earth elements (REEs) from an acid leach solution, purification of Cu(II), Zn(II) and Mn(II) from an acid-mine drainage (AMD) lake solution, and similar recovery of Cu(II), Zn(II) and Mn(II) from solid "tailings" mine waste.

2 BACKGROUND

2.1 Silica Gel

Wide pore amorphous silica gel is produced via the controlled precipitation of sodium silicate with mineral acids. Depending on the method of production, silica gel may be manufactured in spherical and/or irregular shapes with moderate control over particle and pore sizes. The data in Table 1 show mercury porosimetry characterization (Delta Analytical Instruments, Inc.) of purchased silica gels from various suppliers. The micrograph in Figure 1 displays spherical and irregular shaped Qingdao Haiyang silica gel. Silica gel starting materials are available from a wide range of suppliers in particle diameters ranging from 30 – 1000 μm, with average pore diameters in the range of 80 – 300 Å (~0.01% particle diameter), pore volumes of 0.80 – 3.0 mL/g, porosities of 80 – 90%, and surface areas in the range of 250 – 600 m^2/g. Hence, 97 – 99% of the materials surface area is found on the walls of the interior pore volume.

Table 1. Physical characteristics of various silica gels.

Supplier	Diameter	Pore Diameter	Pore Volume	Porosity	Surface Area
	μm	Å	mL/g	%	m^2/g
Crosfield	90 - 105	267	2.82	84.7	422
Qingdao Haiyang	150 - 250	194	2.39	85.0	493
Qingdao Meigao	180 - 250	378	2.86	85.3	303
Nanjing	180 - 250	164	2.30	85.8	561
Nanjing Tianyi	80 - 250	150	2.28	85.6	526

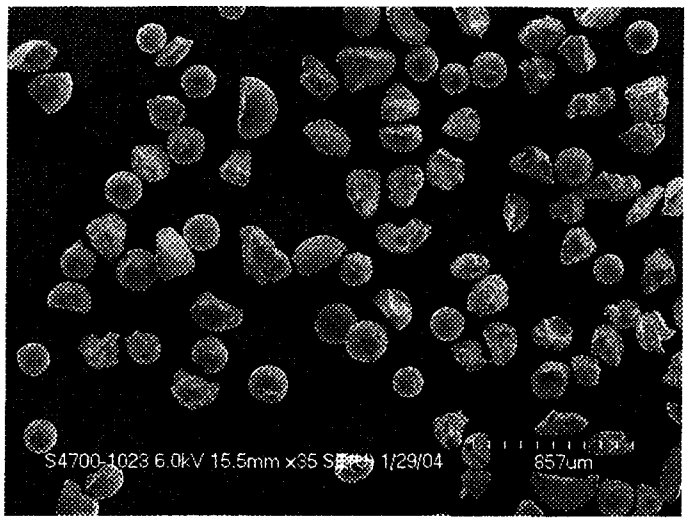

Figure 1. Micrograph of Qingdao Haiyang silica gel.

Silica gels used in these studies are non-crystalline but have partially ordered structures consisting of networks of inter-connective pores which house 99% of the gel's surface area. Pore characteristics greatly affect diffusion limited access to the functionalized surface area. Larger polymers covalently anchored to the gel will obstruct smaller pores, decreasing the material's metal capture and stripping kinetics, especially when hydrophobic functional groups are present.

The data in Table 1 show mercury porosimetry results (Micromeritics Autopore IV 9500, Delta Analytical Instruments, Inc.). Pore characteristic information is obtained by forcing liquid mercury into pores by increasing the external pressure. As the pressure is incrementally increased, the amount of mercury required to fill the pores is recorded. Mercury intrusion analyses (Figure 2) illustrate the variation in pore characteristics

between Crosfield and Qingdao Haiyang silica gels. The plots on the left hand side of Figure 2 show differential intrusion as a function of pore diameter. It is evident that Qingdao Haiyang silica gel exhibits a relatively broad range of pore diameters, where as Crosfield silica gel contains proportionally fewer small pores. The graphs on the right hand side of Figure 2 display incremental pore area versus pore diameter. Crosfield silica gel contains little accessible surface area by means of the smaller pores. Qingdao Haiyang silica gel not only has smaller pore diameters but also larger average particle diameter than Crosfield. These two factors play a major role in the relative kinetic performance of composites produced from these gels.

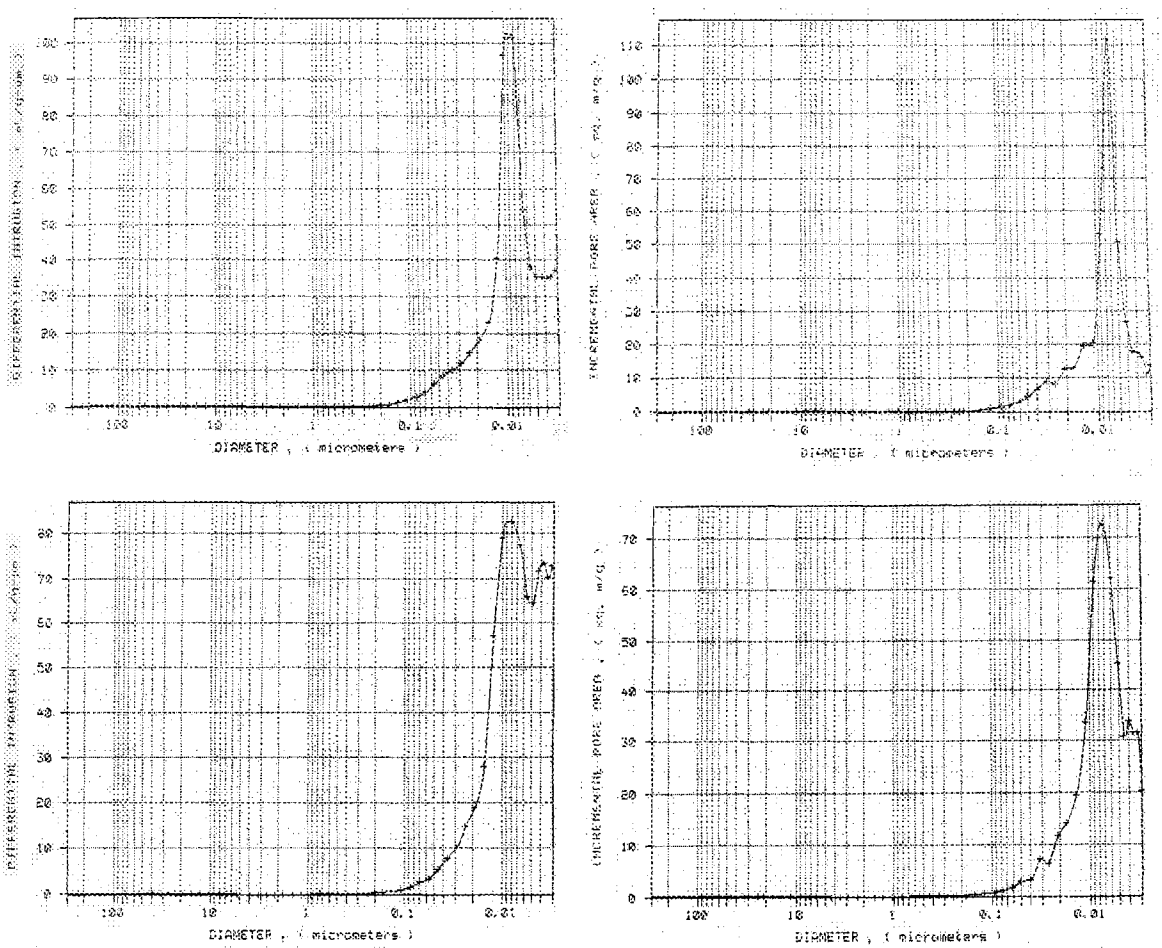

Figure 2. Mercury porosimetry analyses for Crosfield (top) and Qingdao Haiyang silica gels (bottom).

2.2 Chloropropyl Gel

Chloropropyl gel (CP Gel) is produced from acid washed hydrated silica gel (Scheme 1). A monolayer of water is introduced to the surface of the cleaned silica gel and is subsequently polymerized with a trifunctional silane (e.g., 3-chloropropyltrichlorosilane). This process is referred to as lateral polymerization, and incorporates the chloropropyl group onto the silica gel's surface for amendment of the selected polyamine. Incorporation of a mixed methyl/chloropropyl surface using methyltrichlorosilane has been investigated to allow for maximum coverage of the polymeric silane layer.

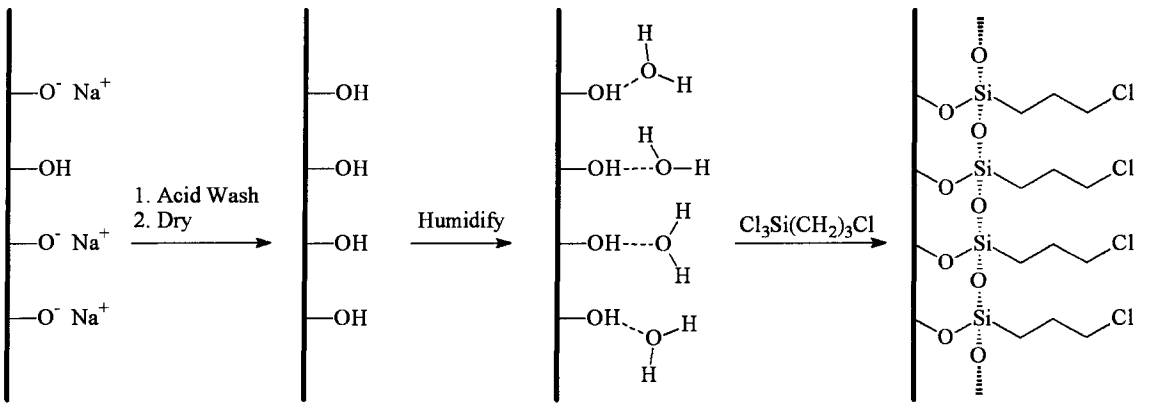

Scheme 1. Synthesis of CP Gel (d).

2.3 Polyamine Composites (WP-1, BP-1, VP-1)

Synthesis of WP-1, BP-1 and VP-1 utilize poly(ethyleneimine) (PEI), poly(allylamine) (PAA), and poly(vinylamine) (PVA) respectively to produce the composites shown in Figure 3. The three composites have been named to simplify the manner in which they are referenced. The trade names WP, BP, and VP are acronyms for working product, better product, and vinyl product. PEI 1,200 Daltons has been used exclusively within this thesis in the synthesis of WP-1. PEI is a highly branched water

soluble polymer containing 1°, 2° and 3° amino groups in a ratio of 0.35:0.35:0.30, respectively. PAA is a straight chain polyamine containing only primary amines which have been covalently linked to the silica support to create BP-1. PAA does come at an increased price in comparison to PEI (used in WP-1). BP-1 composites found within this thesis have incorporated PAA 15,000 Daltons. PVA was limited in availability during this thesis, and is briefly mentioned.

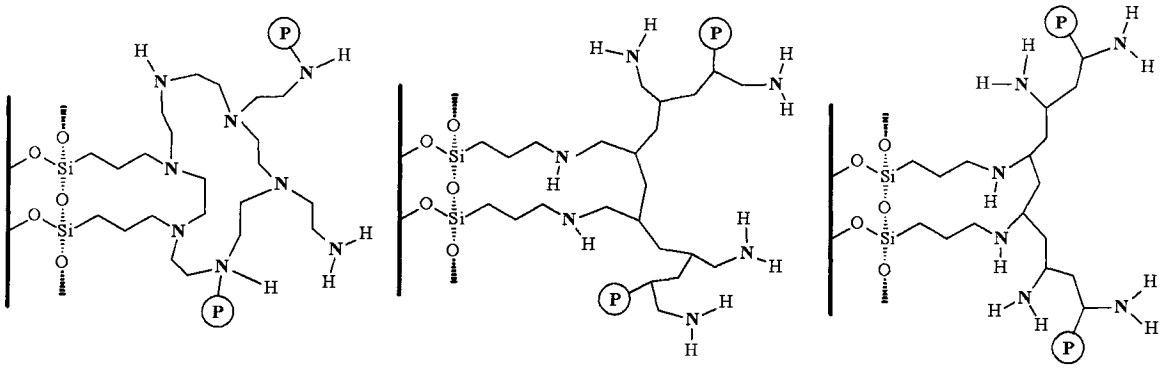

(a) (b) (c)

Figure 3. (a) WP-1 silica poly(ethyleneimine) composite, (b) BP-1 silica poly(allylamine) composite, (c) VP-1 silica poly(vinylamine) composite.

WP-1 and BP-1 parent composites can be utilized for certain metal separations though are not ideal for a number of reasons. Base regeneration of the amino ligand is essential for transition metal coordination requiring additional complexity to separation protocols. At pH < 3 WP-1 and BP-1 capacity diminishes for transition metals. The base form of the amine has little selectivity for metals of interest such as Cu(II) over Zn(II), nor for Fe(III) or Al(III) selectivity over Cu(II) as shown and discussed further in section 34.4. The parent silica poly(ethyleneimine) composite (WP-1) and silica poly(allylamine) composite (BP-1) are readily modified through their amines with ligating groups. Modification of the parent composites lead to specific metal selectivity over a wide range of pH values, and avoid the use of base regeneration.

2.4 Acetate Polyamine Composites (WP-2, BP-2)

The synthesis of BP-2 is shown in Scheme 2, and the schematic structure in Figure 4 (right). WP-2 is produced in the same fashion as BP-2, employing WP-1 as the parent composite (Figure 4, left). The acetate functional group imparts affinity towards Cu(II), Ni(II), Zn(II), and Co(II) at lower pH values than the parent composites (WP-1 and BP-1), and without base regeneration of the ligand.[17] Zinc was extracted utilizing WP-2 as discussed in section 34.4. Mn(II) capture was accomplished using the base form of BP-2 (Section 34.4).

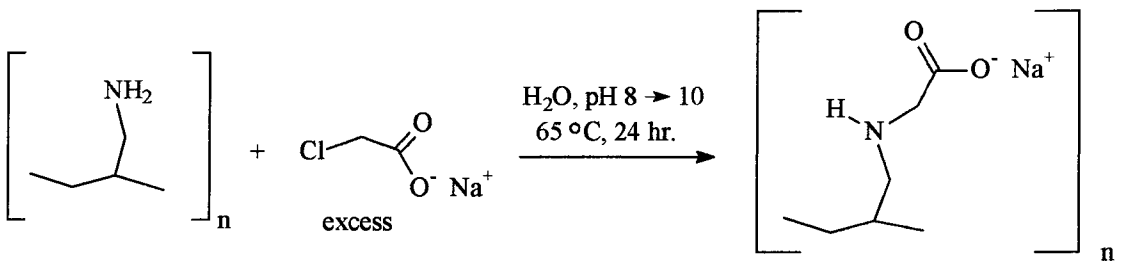

Scheme 2. Synthesis of BP-2.

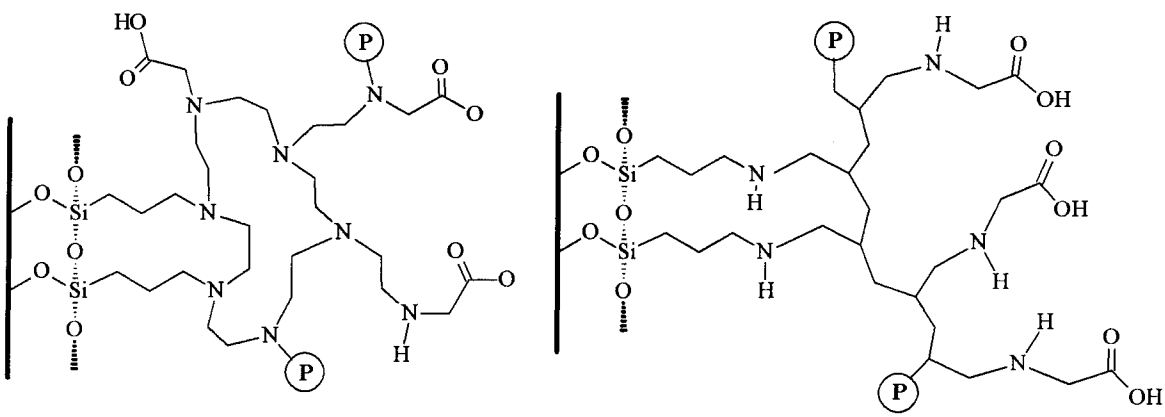

Figure 4. Schematic structure of WP-2 (left), and BP-2 (right).

2.5 Picolylamine Composite (CuWRAM)

The material coined "Copper Waste Recovery from an Aqueous Medium" (CuWRAM) was developed in pursuit of a material that could selectively remove copper(II) in the presence of other metal ions, specifically iron(III).[18] Figure 5 illustrates

a schematic structure of CuWRAM chelating a copper(II) ion. Section 34.4 includes data reporting CuWRAM's ability to selectively remove copper(II) in the presence of iron(III) and zinc(II) in Berkeley Pit Lake water. This material has successfully removed copper from other feed solutions as well.[17] CuWRAM is currently in production on an industrial scale. Unfortunately synthetic routes are expensive and currently require chloroform as the solvent for the modifying ligand. However, cheaper and more environmentally benign routes to produce this remarkable material are presently under investigation involving synthesis of the 2-picolylchloride hydrochloride reagent.

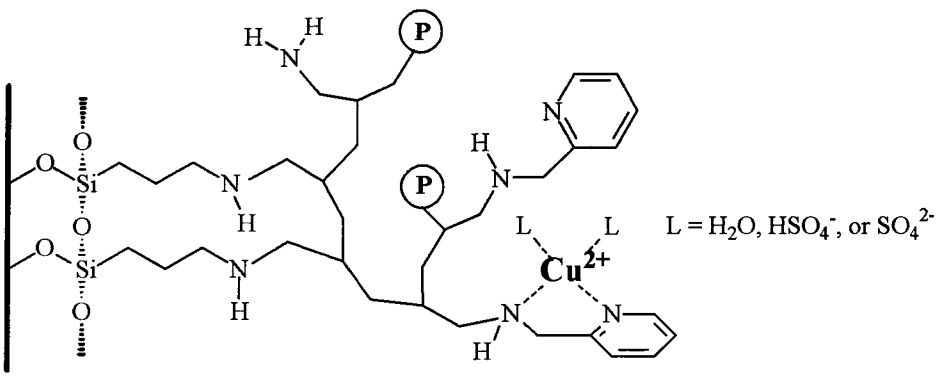

Figure 5. Schematic structure of CuWRAM chelating a copper ion.

2.6 Metal Selectivity

Ligands incorporated into composite materials can provide for selective binding of a metal of interest. Competition for metals is based primarily upon charge to radius ratios of the metals present. Higher valency metals such as tri-valent Fe(III) and tetra-valent Th(IV) commonly exhibit the strongest metal ligand interactions. Divalent species exhibit higher affinity to a given ligand relative to alkali metals. Competition between metals of the same charge can be predicted from critical stability constants and published experimental results with similar ligands. Relative affinity of like charged metals has been assessed when relevant for various composites within this thesis such as for

Fe(III)/Eu(III) and Cu(II)/Zn(II) separations. Empirical trends such as the Irving-Williams series have also been referenced for multi-element extraction strategies.[19]

The Irving-Williams series of increasing stability from Ba^{2+} to Cu^{2+} is a measure of increasing inherent Lewis acidity of the metal (largely due to decreasing size). Superimposed upon this is a hardness-softness factor in which the softer species coming later in the series (greater number of *d* electrons) favor ligands S > N > O.[20] The equilibrium constants for Mn(II) complexes in aqueous solution are not high compared to those for Fe^{2+} - Cu^{2+} because the Mn^{2+} ion is the largest of these, and it has no ligand field stabilization energy in its complexes, except in those that induce a low spin configuration (e.g., CN).[21]

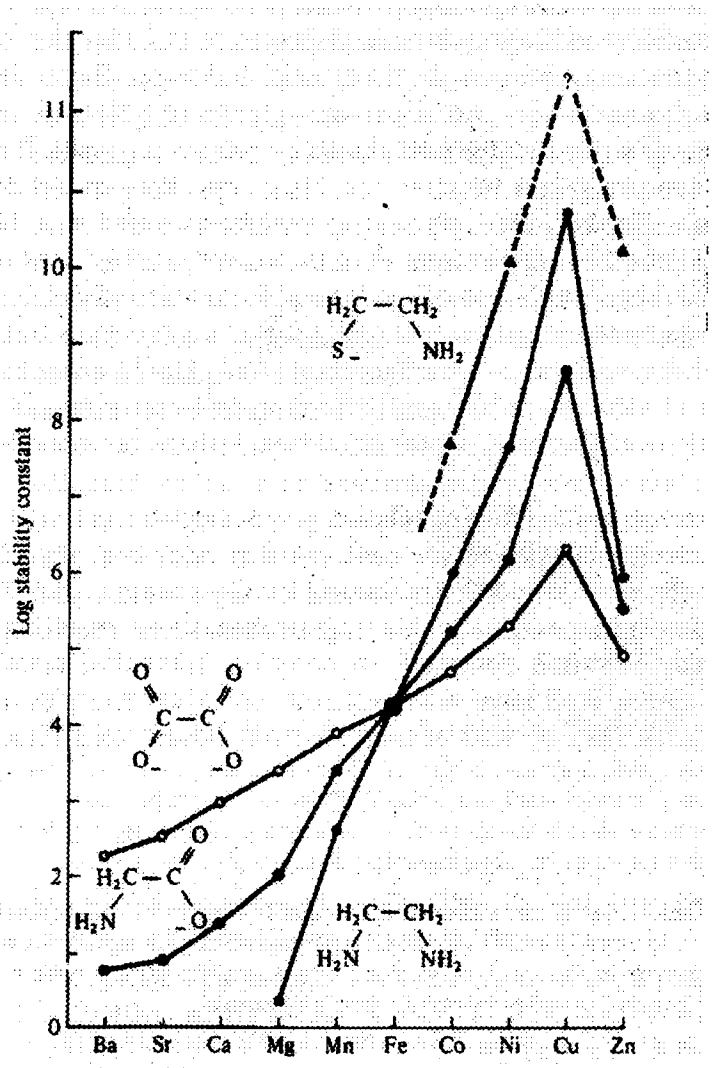

Figure 6. The Irving-Williams effect.

2.7 Multi-Column Continuous Treatment Systems

ISEP (Calgon Carbon Corporation)[22] and SepTor (SepTor Technologies)[23] are two patented multi-column continuous treatment systems. Figure 7 shows the 30 column arrays for the ISEP and SepTor systems. Treatment protocols depend on target metal concentrations and composite performance kinetics. The extreme height to diameter ratio of these columns allow for maximum separation of target metals. However, flow rates can be limited due to backpressure induced by column dimensions, composite particle size, and feed solution viscosity (especially strip solutions). Bench-scale testing is used to

determine the relative time required for metal loading, rinsing, stripping and regeneration, each potentially at a different flow rate. The 30 columns in the array can then be separated into groups or zones designated for loading, rinsing, stripping, and regeneration to be continuously cycled.

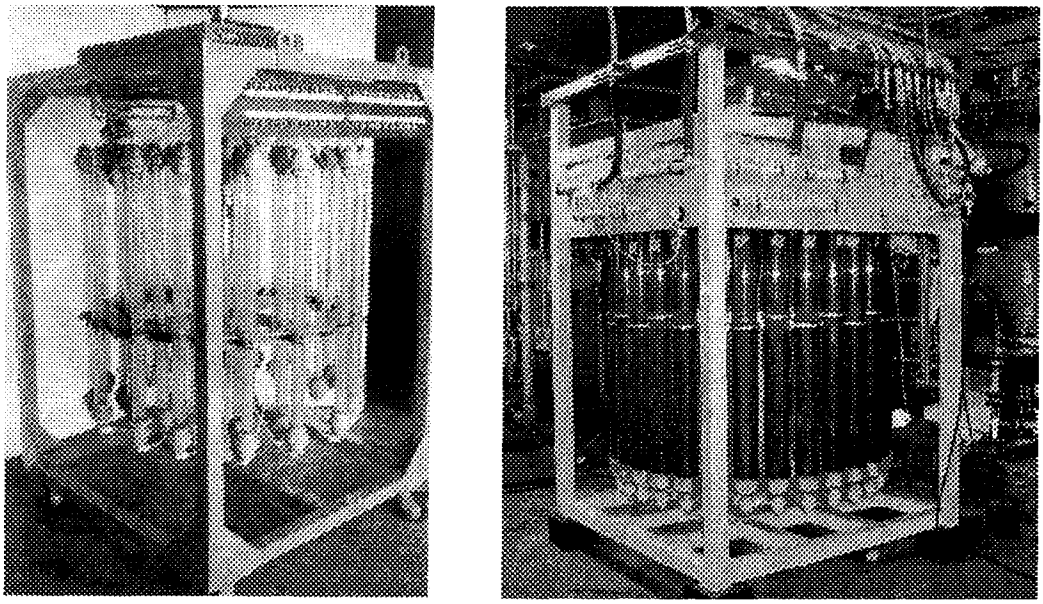

Figure 7. Multi-column continuous treatment systems; ISEP (left), SepTor (right).

2.8 Comparison with Other Metal Recovery Technologies

2.8.1 Electrowinning

Electrowinning is the process of reducing a metal cation to its elemental form. By applying a specific voltage (or electrical potential) an electrolysis reaction ensues reducing the metal and oxidizing the water solvent to oxygen gas. Solutions containing hydrochloric acid or the chlorine ion in general, are usually not processed using electrowinning since electrolysis of these fluids can result in the evolution of chlorine gas.[24] Sulfuric acid is the solvent of choice.

Figure 8 illustrates conventional and state of the art electrowinning processes. Traditional cells can be produced at minimal cost, however may not be cost effective. As the target metal ion is depleted from solution, the efficiency of the process can become

quite poor. Low quality electrowinning processes require liquor concentrations to be above 30 g/L. The EMEW® (Electrometals Electrowinning) electrolytic cell maximizes efficiency due to the rapid mixing of liquor solution between a pair of tubular (versus planar) shaped.

EMEW cells have been used to recover gold, silver, cadmium, cobalt, copper, manganese, nickel, platinum, tin, and zinc.[25] EMEW cells can treat low level copper (0.10 – 1.0 g/L), but not efficiently when in the presence of iron(III). Cost effective liquors require above 5 g/L copper (II) and less than 1 g/L iron (III).[26] Electrowinning is a competitive technology. However, the versatility and performance obtainable with silica composites for multi-element solutions of low concentration requiring high flow rate treatment is not achievable using EMEW technology. However, electrowinning is suitable for the final recovery of metal from sulfate strip solution produced using silica composite treatment. Correspondingly the silica composite BPAP offers efficient Fe(III) removal from divalent metal electrowinning solutions as discussed in section 3.12.

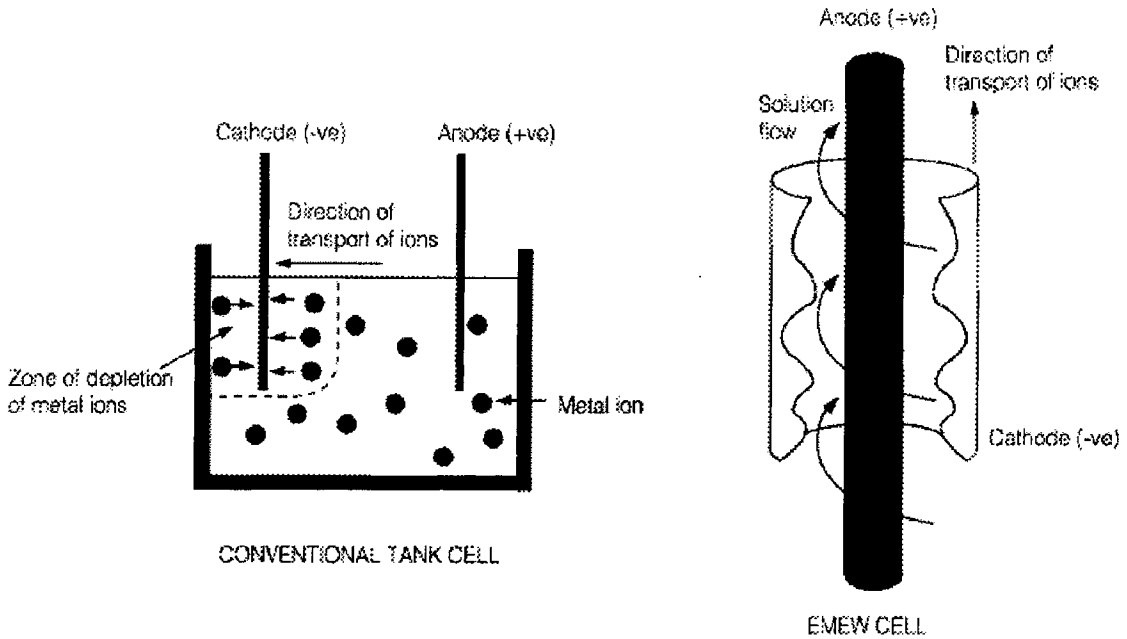

Figure 8. Conventional electrowinning (left), and EMEW® electrowinning cell (right).[27]

2.8.2 Polystyrene Ion-Exchange Resins

Polystyrene based resins can be produced cheaply on an industrial scale. However, the cost advantage may not be realized competing against silica composites due to material performance. Figure 9 illustrates a leading polystyrene resin Diphonix®.[28] Surface coverage of functional phosphonic acid is shared with a bulky sulfonated styrene-divinylbenzene matrix. The resins surface is also shared by functional carboxylate groups. Carboxylate groups have affinity towards copper(II) except under very acidic conditions limiting a wide range of applications. Most importantly the working lifetime of polystyrene resins can not compete with silica composites. Maximum Fe(III) batch capacities for Diphonix are 30 mg/g compared to 60 mg/g for the silica poly(allylamine) phosphonic acid composite (BPAP) reported within this thesis. Capacities are however quite competitive when described as mass per volume of material, due to differences in densities. In other words, per cycle capacities would be equal if Diphonix resin utilized columns 10% larger in volume (than for BPAP).

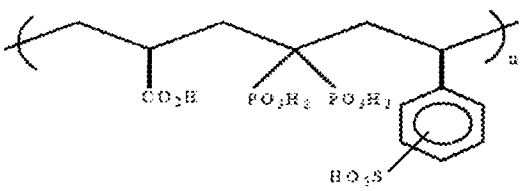

Figure 9. Diphonix resin polymer matrix.

The relative hydrophobicity of the multi-functional styrene resins do not allow for rapid capture kinetics under flow conditions. Figure 10 illustrates the relative deficiency of Diphonix to remove iron(III) to low levels under flow conditions. The flow rate is of most importance but is omitted from the documented performance evaluation of Diphonix.[28] The stripping performance of Diphonix is also described as a sulfite strip solution (to reduce ferric iron to ferrous), and can be performed for at least 10 cycles

yielding consistent loading and strip capacities (Figure 11, left). However, the flow rates and strip profiles have been omitted from the documented evaluation. Stripping BPAP proved to be difficult with reducing sulfite solutions as discussed in section 3.12. The BPAP longevity study shown in Figure 11 (right) far exceeded that done for Diphonix. Metal loading and stripping was consistent for over 600 cycles using BPAP using 9 N H_2SO_4 as the strip solution, which did inhibit 100% stripping each cycle (further discussed in section 3.12).

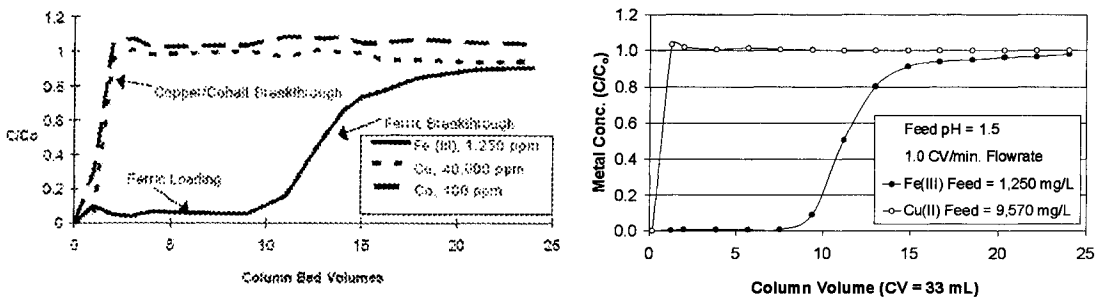

Figure 10. Breakthrough curves comparing Diphonix resin (left) to BPAP-CF composite (right).

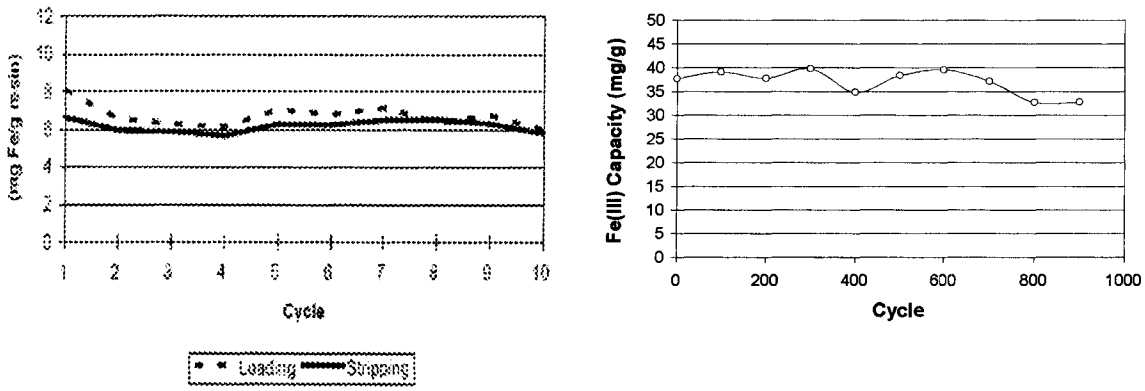

Figure 11. Longevity testing comparing Diphonix resin (left) to BPAP-CF composite (right).

Previous studies performed at the University of Montana have evaluated the performance of WP-1 (primary and secondary amine functionality) against the polystyrene based resin Amberlite IRC-718 (acetic acid functionality).[29,17] Testing

involved an acid strip (2 M H_2SO_4) and base regeneration (4 M NH_4OH) of WP-1 and IRC-718. These conditions led to a marked difference in material lifetimes. The multifunctional polystyrene support was subject to considerable shrink and swelling effects upon extreme swings in pH. Silica gel provides a rigid support eliminating these problems and allowing for considerably longer material lifetimes. Polystyrene supports are also relatively short-lived under thermal conditions.[29]

2.8.3 Competitive Silica Based Ion-Exchange Materials

Numerous research groups around the world have investigated ion-exchange using a silica gel support. These gels do not incorporate a polyamine which limits metal capacities due to relatively low coverage of the functional group compared to silica composite technology.[30] A leading research group has reported a new modified silica gel material with chemically bound phosphonic acid for use with lanthanide ion adsorption.[31] This phosphonic acid modified inorganic chemically active bead (ICAB) was used to extract Nd(III) as shown in Figure 12. Feed concentration of Nd(III) was only 200 ppb at pH 4.0, and showed breakthrough after just five column volumes to give a total Nd(III) capacity of 0.08 – 0.1 mg/g. BPAP exhibits Ln(III) capacities two to three orders of magnitude greater mainly due to the superior coverage of ligand per gram of material (and additional concentration dependent effects).

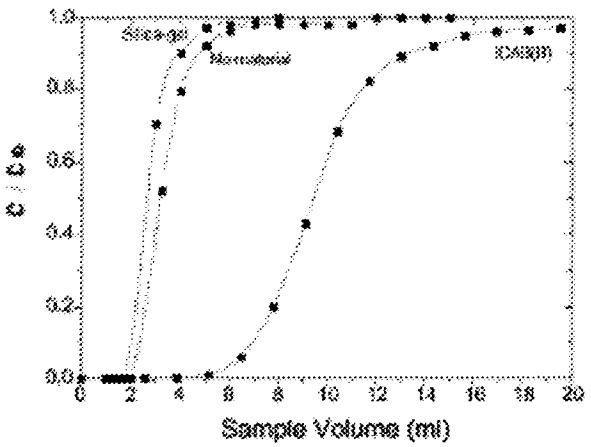

Figure 12. Breakthrough curves for Nd(III) using phosphonic acid ICAB.

Researchers at the Pacific Northwest National Laboratory (Richland, WA) have developed self-assembled monolayers on mesoporous supports (SAMMS) for sequestration of heavy metals, tetrahedral oxometalate anions (e.g., TcO_4^-), and radionuclides (Figure 13).[32] SAMMS materials have superior solid adsorbent properties: they do not suffer from solvent swelling; their rigid, open pore structure allows rapid sorption kinetics; their extremely high surface area enables the installation of high functional density; and being silica based, they are compatible with vitrification into a final vitreous waste form. These mentioned attributes are exhibited by silica polyamine composites such as BPAP found within this thesis. SAMMS technology utilizes mesoporous ceramics which are very expensive relative to composite technology and does not employ a polymer which limits the functional density.

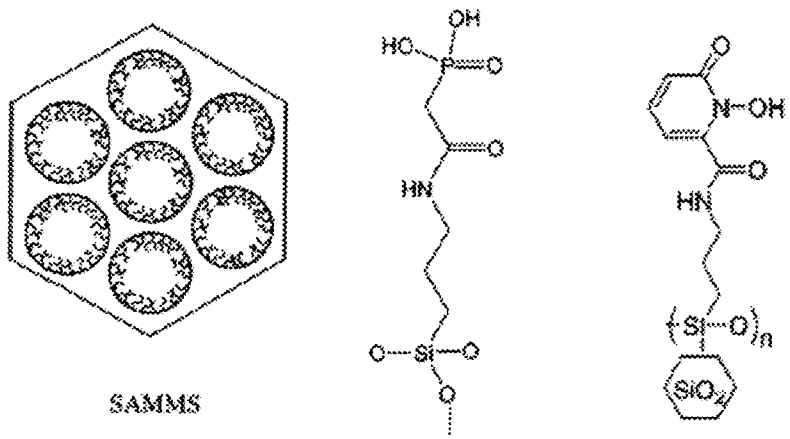

Figure 13. Molecular diagram of SAMMS technology and example functionalities.

2.8.4 Lime Treatment for Acid Mine Drainage (The Berkeley Pit Lake)

The Berkeley Pit and Lake (Figure 14) currently contains over 100 billion liters of water at pH 2.5 – 2.7 (depending on depth and time of year). This water contains over a million tons of dissolved metals, and is located at the headwaters of the Clark Fork River Basin in Butte, Montana. The hydrological components controlling the present Berkeley Pit water balance are net evaporation, surface water inflows (formerly from Silver Bow Creek and presently from Horseshoe Bend), and ground water inflows. In October 1987, the static water level in the Pit was approximately 200 m below the upper rim of the Pit, and was rising at a rate of 22 m per year.[33] Currently, the rate has slowed to approximately 5.4 m per year. As the water continues to rise, the contaminated water will eventually begin discharging into the surrounding alluvial aquifers south of the pit and The Clark Fork River Basin via Silver Bow Creek. Water levels in the East Camp/Berkeley Pit system will not be allowed to exceed the established Safe Water Level (SWL) of 1,710 meters. Presently the Pit's water level is approximately 1,680 meters.[34]

British Petroleum (BP) and its sister corporation The Atlantic Richfield Company (ARCO) are the primary funding sources contributing to the construction of a two-stage

lime treatment facility located at The Berkeley Pit superfund site. This multi-million dollar facility must be able to effectively treat ~20,000 L/min. The Berkeley Pit lake overflow will soon be treated by the addition of quick- lime (CaO) to neutralize the pH and induce precipitation, followed by addition of acid prior to discharge.[7] A notable concern is that lime (CaO) addition results in high levels of calcium sulfate (because the Berkeley Pit water contains high sulfate concentrations). The insoluble compound $CaSO_4$ (gypsum) is slow to precipitate, potentially following discharge causing cementation of the downstream river bed. Cadmium levels may also be above the allowed discharge levels of 1.0 ppm.

Lime treatment does not capitalize in the recovery of valuable metals which would offset the cost of remediation. Silica polyamine composite technology would also reduce the amount of added species to the waste stream (e.g., calcium(II)), and reduce the amount of waste sludge produced. Furthermore, a silica polyamine composite containing a dithiocarbamate functional group (WP-3) has the ability to remove cadmium, but can not be stripped of the material for reuse.[5] One of the major goals of this thesis was to develop a process whereby the valuable metals Cu(II), Zn(II), and Mn(II) could be separated and concentrated from the Berkeley Pit Lake while at the same time remediating this waste stream.

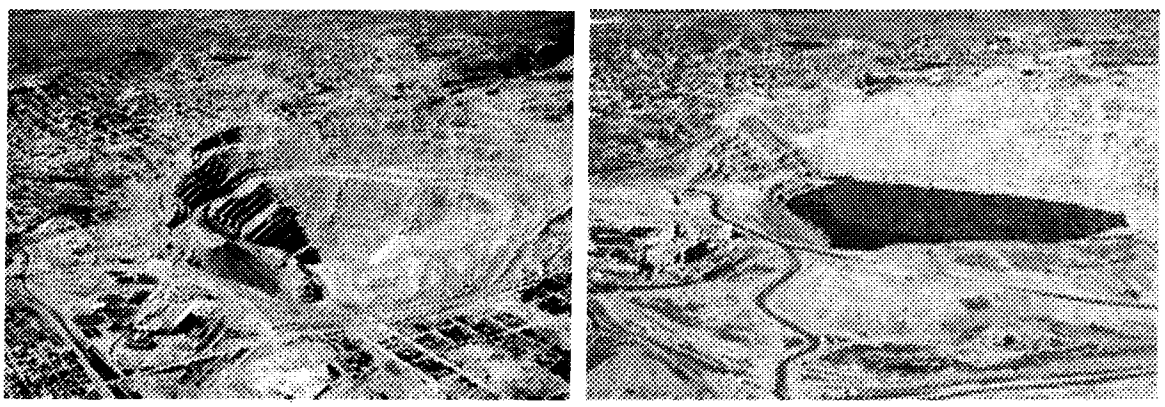

Figure 14. The Berkeley Pit, 1981 (left) & Lake, 1999 (right), Butte, Montana.

2.8.5 Sulfate Reducing Bacteria Treatment

Sulfate reducing bacteria (SRB) treatment makes use of sulfide produced via the reduction of sulfate in an anoxic environment.[35] Carbon is traditionally the bacterium's food source and serves as the electron donor. Studies have shown that improved sulfate reduction can be realized by augmenting the organic acid substrates with certain polymers. These hydrolytically degradable polymers provide low molecular weight organics as a food supplement in a time-released manner. Metal extraction via bacteria sulfide production is a slow process and produces a large volume, high mass, non-recoverable metal laden waste. Furthermore, this technology is presently suitable for non-selective metal polishing, not metal recovery.[13]

3 RESULTS AND DISCUSSION – COMPOSITE MATERIALS

3.1 Composite Characterization

Composites are characterized in a variety of ways. Initially a mass gain during each synthetic step provides information about the extent of reaction. The mass gain is simply the percent increase in mass of a dry product gel (or composite) relative to the starting mass of the dry gel (or composite). Care must be taken to wash the gel (or composite) of excess reagents and byproducts. Mass gains are typically in the range of 20-30% and can be estimated based on the molecular mass of the group amended. All gels are white in color; composites can vary in color (e.g., white, yellow and orange). Composites often change in color when loaded with metal, or when stripped of metal typically using a strong acid.

Elemental analysis (Schwarzkopf Microanalytical Laboratory) was utilized to more accurately define element ratios and surface coverage. Elemental analysis results are reported in their respective sections and are all collected together in Appendix A. The data in Table 1 show mercury porosimetry results. Solid-state NMR is an additional tool valuable for characterizing surface structure. The Pacific Northwest National Laboratory (PNNL) has provided use of their Varian/Chemagnetics Infinity 500 MHz NMR spectrometer at the Environmental Molecular Science Laboratory (EMSL). A number of spectra were obtained on a 270 MHz instrument at The University of Turin, Italy. Additionally a couple spectra have been included from Bruker, Inc. on a 500 MHz instrument. ^{13}C, ^{29}Si, and ^{31}P spectra have been collected for various gels and composites. Magic angle spinning is used in solid state NMR to eliminate the peak broadening caused by chemical shift anisotropy and dipolar coupling.[36] This is achieved by spinning the sample tipped at an angle of 54.7 ±1°, and spinning at 3,000 – 12,000 Hz. Proton

decoupling was also used in the analysis sequence to suppress proton dipolar broadening and the interaction between nuclear spins.

Most NMR experiments utilized cross polarization magic angle spinning (CP/MAS). Cross polarization enhances the sensitivity by using the proton's large magnetization to polarize the observed nuclei allowing for rapid relaxation.[36] CP/MAS experiments allow for pulse delays to be on the order of seconds (or less) allowing for acceptable spectral resolution in only a matter of hours. However, CP/MAS experiments are not quantitative biasing nuclei with nearby protons, therefore providing only qualitative structural information. Quantitative ^{29}Si NMR analyses were pursued utilizing Bloch decay magic angle spinning (BD/MAS). These traditional experiments require very long pulse delays (at least 2 minutes) for silicon nuclei necessitating days of acquisition to give acceptable signal to noise.

3.2 Performance Testing of Composites

The performance of composites is evaluated by determining metal ion capacity at various pH values, loading and stripping kinetics, metal selectivity, and composite longevity upon load/strip cycling. Initially single element batch capacities at various pH values provide a profile of the working pH range. Challenge solution is prepared at a concentration that will allow for about 25% of the metal to be extracted to provide for accurate maximum capacities. Challenge solution can be acidified (using either H_2SO_4, HNO_3, or HCl) to a desired pH, or typically to a range of pH values leaving one solution at its intrinsic pH. Typically, all batch capacities are evaluated in triplicate. 0.2000 ± 0.0010 g composite are massed into a 25 mL glass scintillation vial, adding 20 ± 0.1 mL metal challenge solution, shaking on an automated shaker for 24 hours, sampling the metal extracted solution, and determining composite capacity based on Equation 1:

$$C = \frac{v\,([c] - [e])}{m}$$

Equation 1. Batch capacity formula.

The composite capacity (C) is a function of the volume of the challenge solution (v) multiplied by the difference in concentration of the challenge solution [c] mg/L and the extracted solution [e] mg/L, and dividing by the composite mass (m). Relative standard deviations for triplicate batch tests are typically in the range of 0.5 – 2.0%. Comparative testing between different composites is stated as significantly different when composite capacities differ by more than 10%. Batch testing can be utilized to investigate thermodynamic metal selectivity using multi-element solutions. Applications for actinide sequestration could involve batch separation prior to vitrification of the silica composite.

Breakthrough testing provides a more detailed evaluation of composite performance under flow conditions. Single element solutions of a target metal at a desired pH are first investigated providing clear kinetic information. Synthetic and genuine multi-element solutions are next tested providing vital information with regard to selectivity for the target metal. Metal concentrations in the feed solution vary depending on the target application. Composites are loaded to capacity employing an appropriate volume of feed solution depending on feed concentration, feed pH, and composite capacity. Breakthrough testing also examines metal stripping kinetics that is of critical importance for industrial scale applications. Bench-scale testing typically utilizes a plastic 5 cc syringe, with porous frit discs on each end to contain the composite. Column volume (CV) is defined as the geometric volume containing the composite (synonymous with bed volume (BV)) equal to the inner cross sectional area of the column in cm^2 multiplied by the length of the packed part of the column in centimeters.

Effluent is collected in fractions typically equal to one or two column volume(s) using a graduated cylinder (Figure 15). Flow rates are adjusted in column volumes per minute units to allow for reproducibility at different scales. Flow rates for metal loading and stripping are in the range of 0.10 – 1.0 CV/min., typically employing a 0.50 CV/min. flow rate. A variable flow FMI Lab Pump, Model QG150 (Fluid Metering Inc.) was used for bench-scale flow testing.

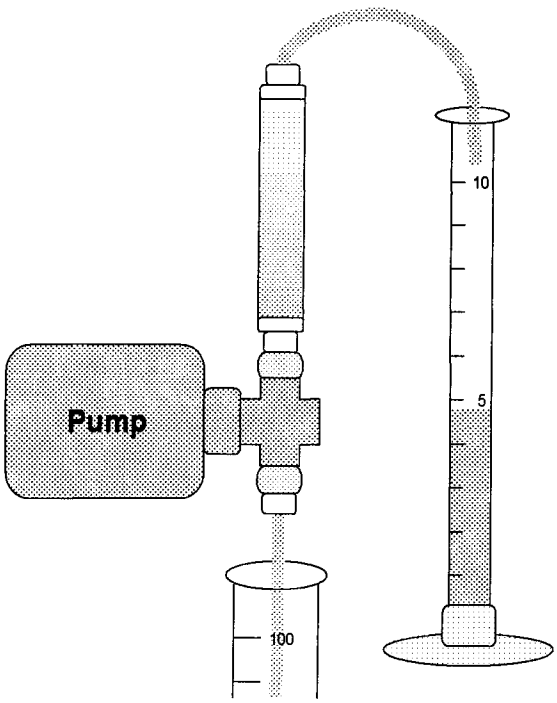

Figure 15. Breakthrough testing cartoon.

Metal concentrations of the effluent fractions are plotted as a function of column volumes in order to be independent of column size (Figure 16). This plot has taken the average of three replicate trials to provide standard deviation bars for each point in both the x and y direction. The potential error shown for each column volume (x-axis) is 0.1% due to human error in collection of the 10 mL fraction. Error in the y-direction varies for each point due to three major systematic errors: dilution error (tolerance of the pipettes), analysis error (accuracy of instrument, AAS in this case) and method errors arising from

non-reproducible behavior due to channeling, diffusion and extra column effects. The challenge solution was analyzed in triplicate for each of the three runs to give an average Eu(III) challenge concentration of 2,870 ± 2.1% mg/L (pool size = 9). The flowthrough capacity was calculated for each trial to give 50.4 ± 3.5% mg/g. Most data presented within this thesis do not include error bars due to having only one set of data. Research efforts prioritized novel investigations versus running these time consuming performance tests in triplicate. However, replicate studies such as that shown in Figure 16 confirm precision to be within 5% standard deviation. Comparative testing between different composites is stated as significantly different when composite capacities differ by more than 10%.

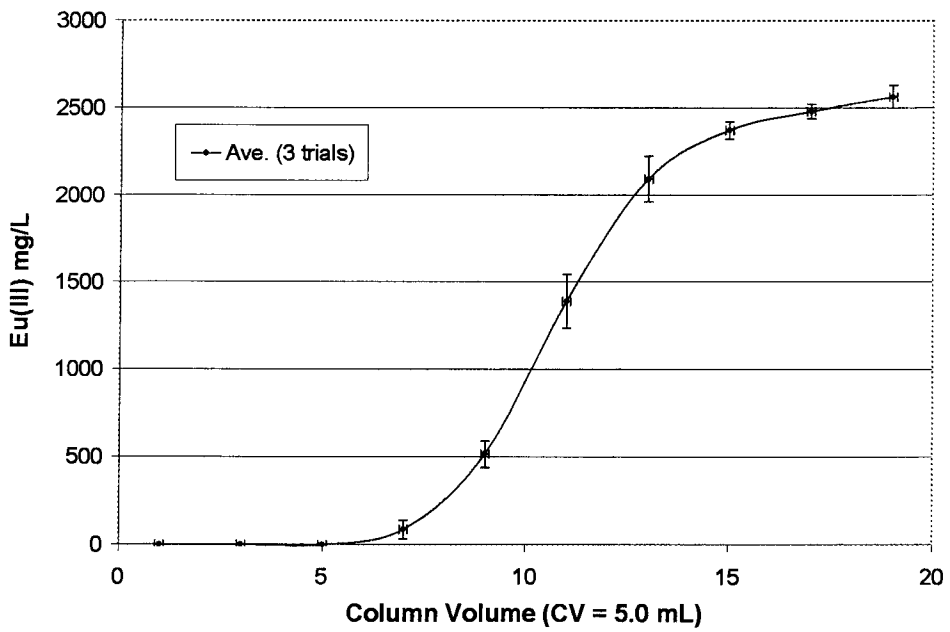

Figure 16. BPAP-CF 041504-DN, Eu(III) average breakthrough curve with standard deviation of three trials, 0.50 CV/min., pH 1.0, 50 mg/g Eu(III) capacity.

Prior to breakthrough performance testing the composite material is conditioned for use. Base regeneration of the functional group is utilized for specific metal extraction situations [e.g., Mn(II) separation from Ca(II) and Mg(II)]. This is carried out by first

"wetting" the column with 4 column volumes (CV) water, then 6 CV 9.0 N H_2SO_4 (or the strip conditions to follow metal loading), then 4 CV water, then 4 CV 0.5 M NaOH, followed by 10 CV water to flush out the entrained base prior to metal loading. Typically base regeneration is avoided due to increased cost and complexity, and reduced selectivity. "Water regeneration" is therefore desirable eliminating the base (and following water flush) from the conditioning protocol.

Flowthrough performance testing has been utilized on occasion and is similar to a breakthrough performance test. In this case the composite material is evaluated under flow conditions, although the effluent is collected as one fraction versus many fractions as with a breakthrough test. Flowthrough testing saves much time and effort, but compromises kinetic information provided by a breakthrough test.

Analysis of metal solutions used either a Model S2 (Thermo Electron Corporation) Flame Atomic Absorption Spectrometer (AAS) in the Department of Chemistry, or a Model IRIS (Thermo Jarrell Ash) Inductively Coupled Plasma Atomic Emission Spectrometer (ICP-AES) in the Environmental Biogeochemistry Laboratory, Department of Geology. Samples were acidified to pH < 2 using one drop HNO_3 (conc.) if necessary. Samples outside the analytical linear range were diluted using 2% HNO_3 for air/acetylene AAS, and with 2% HNO_3/2% KCl (5.0 g/L KCl; from a 250 g/L near saturated KCl solution) for nitrous/acetylene AAS. Samples not diluted for nitrous/acetylene analyses were spiked to give 2% KCl. To avoid precipitation the EDTA (pH 10.5) strip fractions were diluted without acid using either DI H_2O (air/acetylene) or 2% KCl (nitrous/acetylene). In the case of ICP-AES analysis samples were diluted using 5% HNO_3/5% HCl. Inter-element interferences were corrected for during ICP-AES method development. AAS and ICP-AES quality control consisted of running a standard every

ten samples and insuring experimental values to be within 10% (5% for AAS) of the known concentration, as well as duplicate samples (±10% difference), spike samples (±30% recovery), and blank samples (<0.1 mg/L). Standard additions were carried out for matrices suspect to interferences for AAS, which showed no significant interferences. Shown below in Figure 17 is a standard addition for Cu(II) in the Berkeley Pit Lake matrix. The calculation derived from Equation 2 shows an acceptable 2.5% difference between the standard addition and raw sample values; where A_s is the sample absorbance, ε is the molar absorptivity coefficient, b is the instrument's path length, V_s is the volume of a standard spike solution, c_s is the concentration of the standard spike solution, V_t is the total sample volume (spike and analyte matrix solutions), V_x is the volume of the analyte matrix solution, and c_x is the metal concentration of the analyte matrix solution. The actual metal concentration (c_x) of the matrix solution can then be obtained.

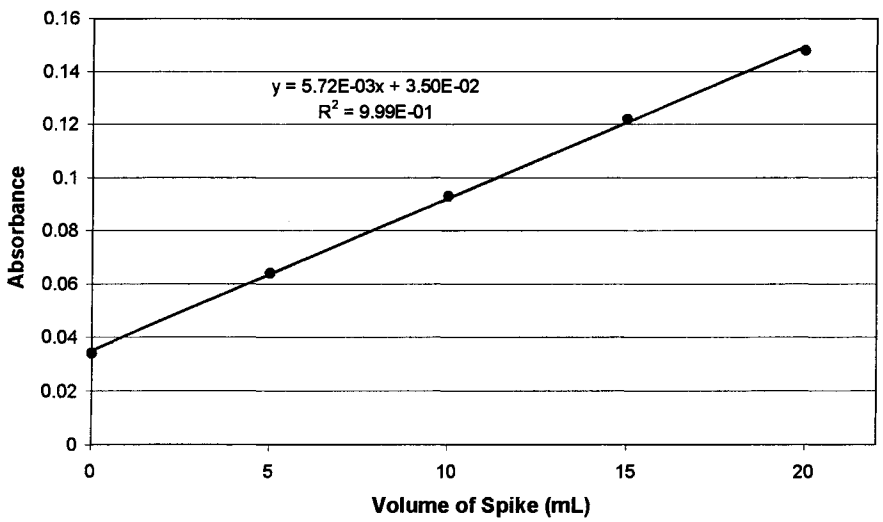

Figure 17. Standard addition for Cu(II) in Berkeley Pit Lake matrix.

$$A_s = \frac{\varepsilon\, b\, V_s\, c_s}{V_t} + \frac{\varepsilon\, b\, V_x\, c_x}{V_t}$$

$$= k\, V_s\, c_s + k\, V_x\, c_x$$

$= m V_s + b$ where: $m = k c_s$

$b = k V_x c_x$

$k = \varepsilon b / V_t$

$\therefore m / b = c_s / V_x c_x$

$\Rightarrow c_x = c_s b / V_x m$

= [20 (ppm) * 3.50 E-2 (ppm)] / [1.0 (mL) * 5.72 E-3 (ppm / mL)]

= 122 ppm

0 mL spike showed $[Cu^{2+}]$ = 119 ppm (2.5% difference)

Equation 2. Cu(II) standard addition calculation in Berkeley Pit Lake matrix.

3.3 Impact of Silica Gel on Composite Performance

Figure 2 shows the distribution of pore sizes of Crosfield and Qingdao Haiyang silica gels. Crosfield gel exhibits a greater distribution of larger pore diameters than Qingdao Haiyang gel. Particle diameter also plays an important role in the kinetic performance of the produced composite. Larger particle silica gels have deeper pores limiting access to these surfaces in addition to greater channeling effects. Crosfield silica gel having a smaller particle size combined with larger pore sizes allows for superior kinetics. However, column backpressure is inversely proportional to particle size. Breakthrough curves shown in Figure 18 reveal the kinetic effects of variable silica gels. Metal capacities are similar for these two composites having comparable surface area per gram characteristics. Optimal silica gel would be spherical in shape, 150 – 250 μm particle diameter, exhibit pore diameters of 200 – 300 Å, with 400 – 500 m^2/g surface area, supplied for around $5.00/kg. These silica gel characteristics would provide for maximum kinetic performance and metal capacity with an allowable column backpressure.

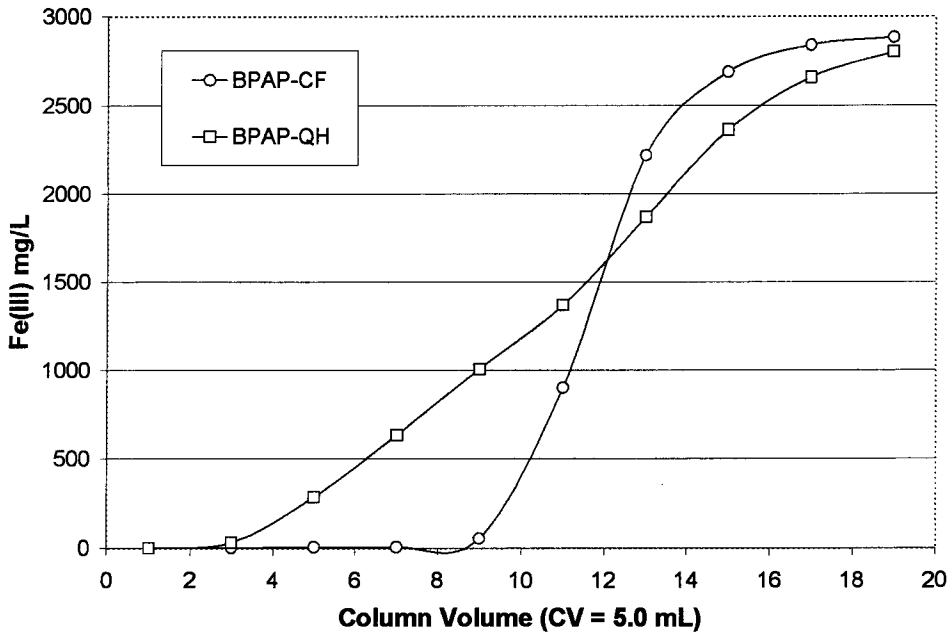

Figure 18. BPAP-CF 041504-DN and BPAP-QH 082503-DN, Fe(III) breakthrough curves, 0.50 CV/min., pH 1.5, 2.9 g/L Fe(III).

3.4 Chloropropyl Gel

Acid washed silica gel exhibits 8.0 ± 1.2 μmol/m^2 of available silanols, and is a physiochemical constant of amorphous silica gel (Scheme 3a,b).[37] The addition of a monolayer of water will subsequently form a polymeric phase with reagent trifunctional (e.g., trichloro or trimethoxy) silanes (Scheme 3c,d). It is critical that hydration is uniform throughout the hydration column to allow for a complete and consistent monolayer of water on the silica gel (Figure 19). Time of hydration is variable dependent upon flow rate and percent humidity of the hydration air. Hydration air humidity was between 60 – 80% (over 90% humidity must be avoided).

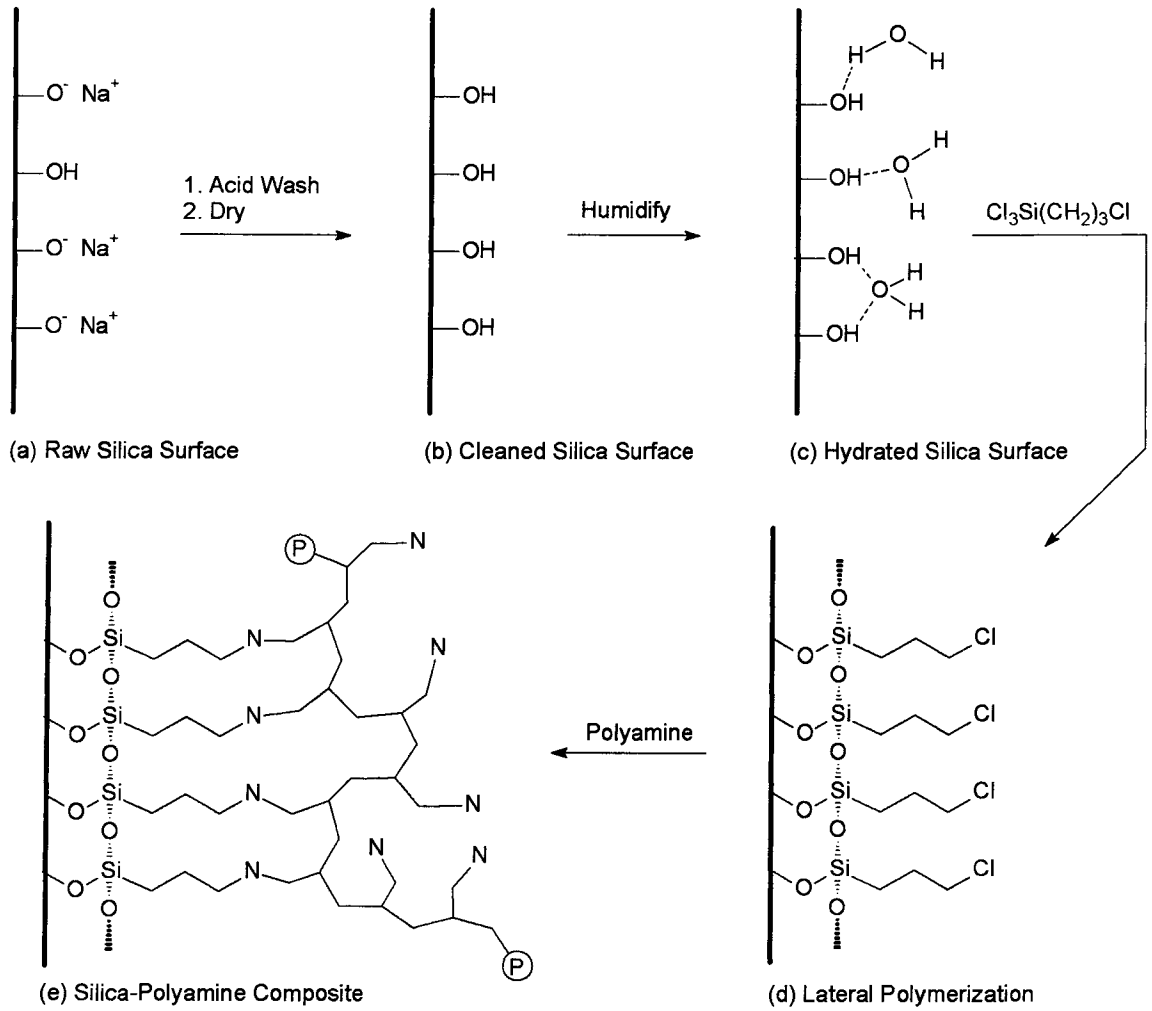

Scheme 3. Synthesis of BP-1.

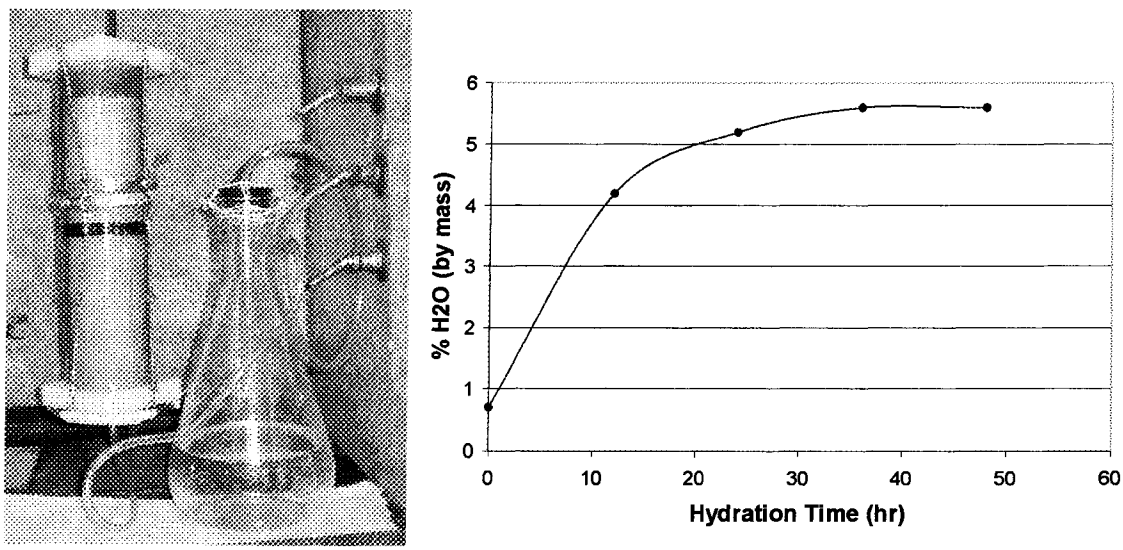

Figure 19. Hydration apparatus for silica gel and typical hydration curve.

Bulk water will allow for undesired vertical polymerization of reagent tangential to the surface as illustrated in Figure 20. Bulk water can also lead to siloxane ether by-products which are difficult to remove from the pores due to their low vapor pressures. Figure 21 displays two hydration experiments using Crosfield silica gel, showing variable time of hydration. Both trials utilized a three foot hydration column as shown in Figure 19. These data show the mass increase due to hydration and also the molar ratio of water to silanol sites. This is calculated from the surface area per gram (422 m^2/g) of Crosfield silica gel, assuming 8.0 $\mu mol/m^2$ silanol groups. It is evident that hydration slows as the molar ratio of water to silanol groups approaches 1.0. However, time of hydration to achieve the surface monolayer of water varies. Unfortunately, the humidity and flow rate were not monitored throughout hydration.

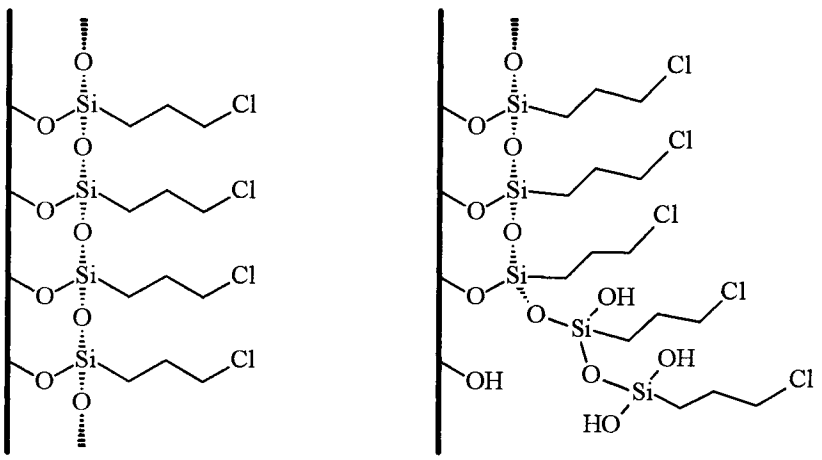

Figure 20. Lateral (left) and vertical (right) polymerization on hydrated silica gel.

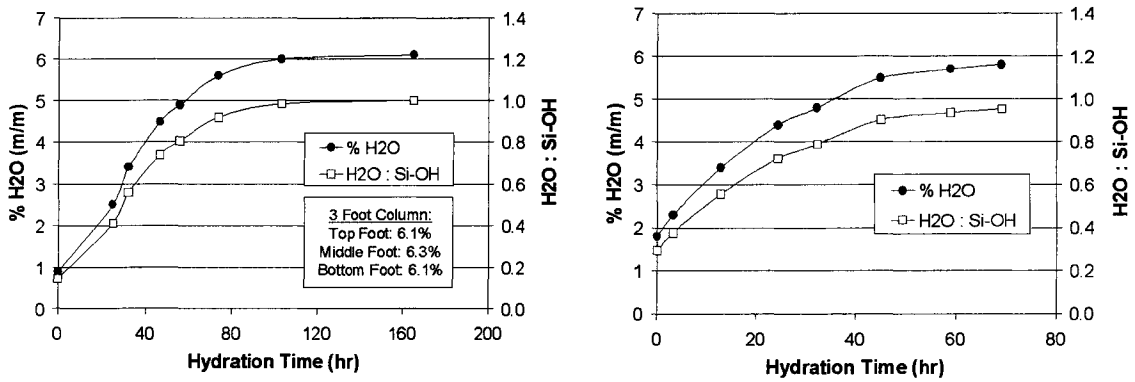

Figure 21. Two hydration experiments on Crosfield silica gel (% H_2O and H_2O:Si-OH).

The desired process is commonly referred to as horizontal,[38] or lateral polymerization.[39] A silicon-oxide framework is thereby incorporated onto the gels surface creating multiple bonding sites for each trifunctional silane. Trichlorosilanes have been chosen over trimethoxysilanes due to the increased rate and completion the reaction undergoes, by removing the produced HCl gas, driving the reaction.

Consistent and complete lateral polymerization is desired. CP Gel is washed and dried using methanol potentially leading to methanolysis of any unreacted chlorosilane. Figure 22 illustrates that hydration of the silica gel allows for an increase in the number of reacted chlorine atoms as methanolysis products are almost eliminated.[4]

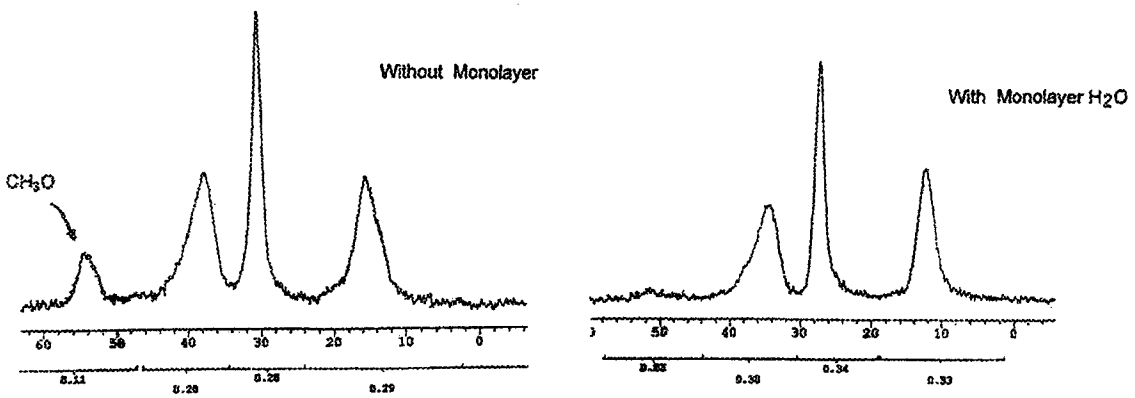

Figure 22. ^{13}C NMR CP/MAS of the non-hydrated CP Gel (left), and hydrated CP Gel (right).

Elemental analyses of CP Gels are given in Table 2. Table 3 displays surface coverage density of the chloropropyl groups on the silica gel surface for both Crosfield and Qingdao Haiyang gels. Coverage densities are very similar as would be expected and further discussed in section 3.5. The mass increase is needed in this calculation as mercury porosimetry information is based on the raw silica gel. A density increase is observed in production of CP Gel thereby lowering the surface area per gram relative to the raw silica gel.

Table 2. Elemental analyses of CP Gels.

Entry	Sample Name	Comp. Ref. #	C	H	Cl	C	H	Cl
			%	%	%	mmol/g	mmol/g	mmol/g
1	CP Gel-QH	091703-DN	6.71	1.11	6.35	5.6	11	1.8
2	CP Gel-QH (2)	092003-CH	6.07	1.35	6.05	5.1	13	1.7
3	CP Gel-QH (3)	092103-CH	7.17	1.47	5.65	6.0	15	1.6
4	CP Gel-QH (A)	022904-DN	6.54	1.25	6.00	5.4	12	1.7
5	CP/M Gel-QH (B)	030104-DN	5.59	0.93	4.19	4.7	9.2	1.2
6	CP/M Gel-QH (C)	030204-DN	4.49	0.75	2.24	3.7	7.4	0.63
7	M Gel-QH (D)	030304-DN	3.33	0.63	0.00	2.8	6.3	0.00
8	CP Gel-CF	040604-DN	7.02	1.46	6.24	5.8	14	1.8

Table 3. CP Gel-CF and QH surface coverage of chloropropyl anchor.

	Surface Area	Mass Inc.	Carbon	Carbon	CP Coverage
	m^2/g	%	%	mmol/g	$\mu mol/m^2$
CP Gel-CF	422	125	7.0	5.8	5.8 ± 1.0
CP Gel-QH	493	127	6.8	5.7	4.9 ± 0.9

Figure 23 displays the spectrum of CP Gel-CF obtained at PNNL (further reported in Experimental section 6.3). Both the downfield (chlorine bound), and upfield (silicon bound) carbon peaks are broader than the centered propyl carbon and its corresponding centered peak. Peak broadening is induced by the neighboring quadrupolar silicon and chlorine atoms.

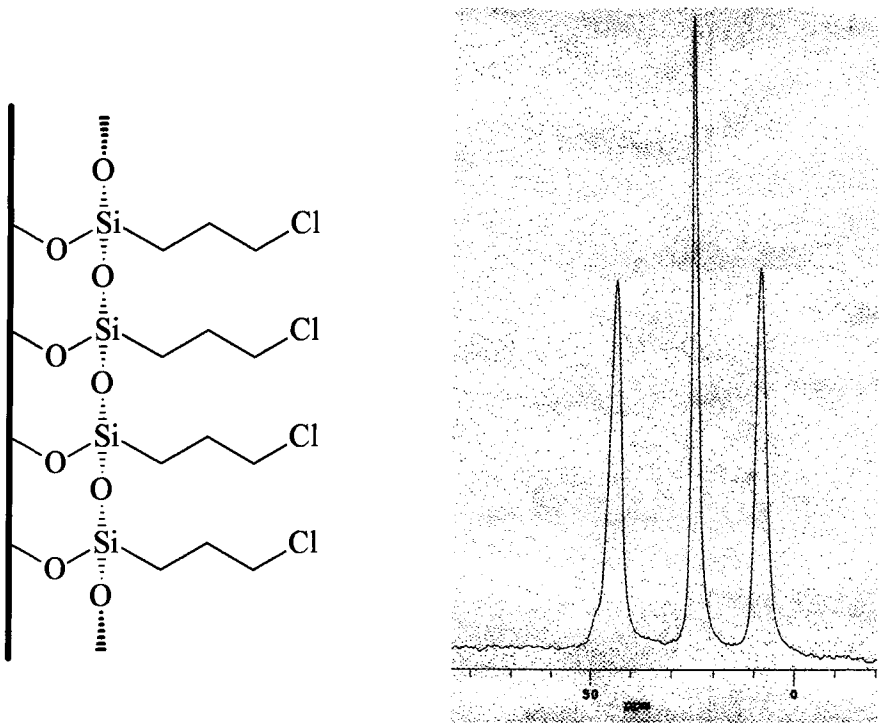

Figure 23. Schematic structure (left) and ^{13}C NMR spectra of CP Gel (right).

An investigation of the CP Gel surface was pursued via ^{29}Si NMR. CP Gel was characterized for ^{29}Si using both BD/MAS and CP/MAS experiments. Assignments of all six silicon atoms were able to be made as shown in Figure 24 from the CP/MAS spectrum.[40] Peak resolution is superior utilizing the CP/MAS experiment allowing for partial resolution of the bulk siloxane from overlapping silanol peaks. However, integration of these assigned peaks would not be quantitative because cross polarization efficiency is dependent on the Si-H internuclear distances. There are three types of silicon atoms in the lateral polymerization layer. Each laterally polymerized silane has one to three bonds to the silica gel's surface silanol sites $(SiO)_{1\text{-}3}$. The three laterally polymerized silicon atom types are reagent geminal silanol $[(SiO)\text{-}Si\text{-}(OH)_2CP]$, reagent isolated silanol $[(SiO)_2\text{-}Si\text{-}(OH)CP]$ and reagent siloxane $[(SiO)_3\text{-}Si\text{-}CP]$. Three additional silicon atoms are found; surface geminal silanol $[(SiO)_2\text{-}Si\text{-}(OH)_2]$, surface isolated silanol $[(SiO)_3\text{-}Si\text{-}OH]$ and bulk siloxane $[(SiO)_4\text{-}Si]$. The Bloch decay

experiment provides quantitative information although requires days of acquisition collection to achieve decent spectral resolution in order for peak integration to be accurate. Deconvolution analysis of the reagent isolated silanol is shown in the Bloch decay spectum (Figure 24, right), and was discussed further in section 3.5.

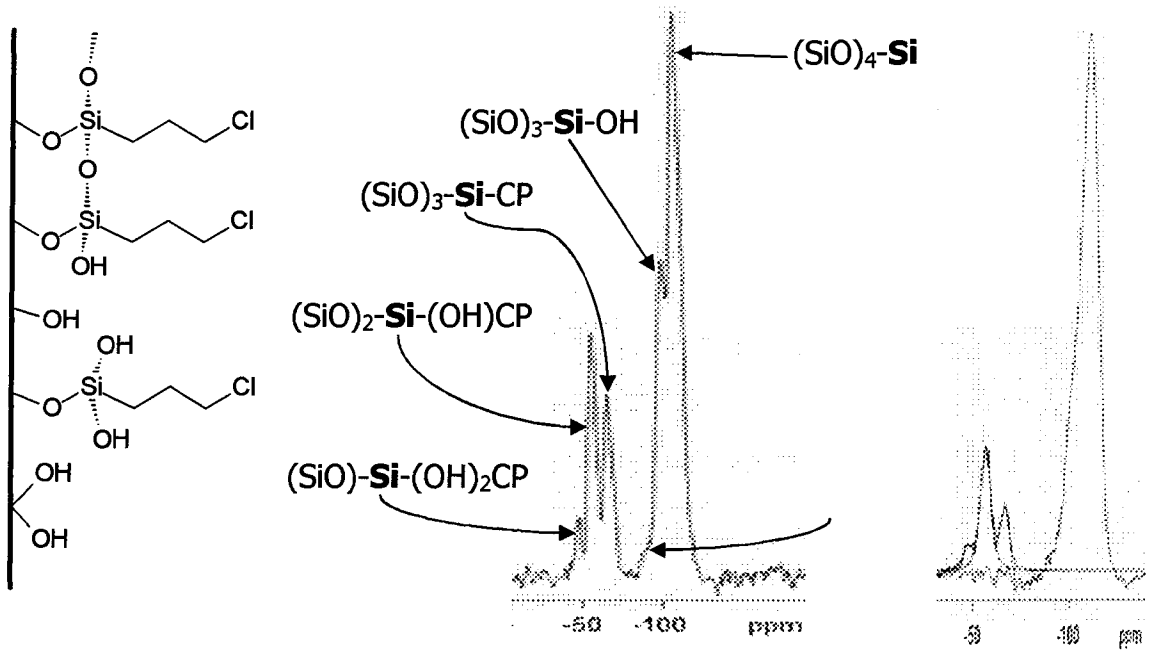

Figure 24. Schematic structure CP Gel (left), ^{29}Si CP/MAS NMR spectrum of CP Gel (middle), ^{29}Si BD/MS spectrum of CP Gel (right).

3.5 Lateral Polymerization of Mixed Trifunctional Silanes

The surface density of available silanols is 8.0 ± 1.2 μmol/m^2, and is considered a physiochemical constant of amorphous silica gel.[37] The incorporation of a hydration layer to form a polymeric phase with trifunctional silanes is commonly referred to as horizontal,[38] or lateral polymerization (Figure 20),[39] and self assembly when the functional groups are close packed (approximately 8 μmol/m^2).[41] Surface coverage of a mixed C_3/C_{18} monolayer has been reported to be 8.0 μmol/m^2, but only about 37% of the groups are reagent siloxane groups, leaving 55% as reagent isolated silanols and 8% as reagent geminal silanols (refer to Figure 24).[42]

The silica gels used in this study were characterized via mercury porosimetry analysis (Table 1). CP Gel produced from Crosfield (CP Gel-CF) and Qingdao Haiyang (CP Gel-QH) silica gel was characterized via elemental analysis (Table 3). Wirth and coworkers more sterically hindered C_3/C_{18} modified gel (relative to the Cl-C_3 phase of CP Gel) utilized about eight times more excess reagent silanes per gram of hydrated silica gel.[41] The C_3/C_{18} phase was reported to exhibit a close packed surface of 8.0 μmol/m^2, where as CP Gel achieved only 4.9 – 5.8 μmol/m^2 (Table 3). Relative hydration of the two gels could not be evaluated as was not reported in the synthesis of the C_3/C_{18} gel.

A separate study investigated the flow performance of BPAP made from different CP Gel in an effort to reduce cost. One CP gel utilized 2 mmol/g (33% less) the reagent quantity of CPTCS yielding 93% (7% decrease) in coverage density of the chloropropyl anchor (Table 2 – Entries 2, 3). These CP Gel's were further modified to BPAP to be tested for relative performance. BPAP produced on the CP Gel made with less CPTCS did not compromise the composite performance with respect to kinetics and capacity. It was then proposed that the use of a mixed trifunctional silane phase may allow for complete protective coverage of the silica gels surface without compromising composite performance, and may even enhance composite performance.

Methyltrichlorosilane (MTCS) was utilized to produce a mixed trifunctional silanes reagent in an effort to obtain better coverage density of the laterally polymerized silane layer (Scheme 4). A pure methyltrichlorosilane reagent was also used to determine the maximum density of reagent siloxanes. A series of four gels were produced from Qingdao Haiyang silica gel using variable ratios of chloropropyltrichlorosilane and methyltrichlorosilane. Each gel was prepared using 3.00 mmol of total silane per gram of hydrated gel with ratios of CPTCS:MTCS of 3:0, 2:1, 1:2, and 0:3, referred to

respectively as CP Gel (A), CP/M Gel (B), CP/M Gel (C), and M Gel (D). It was calculated from elemental analysis (Table 2: Entries 4 – 7) that the laterally polymerized silane layer incorporated CPTCS:MTCS in ratios of ∞:0, 1.3:1, 1:2.6, and 0:∞. The less sterically hindered MTCS was able to polymerize to a greater extent than its original reagent ratio prepared.

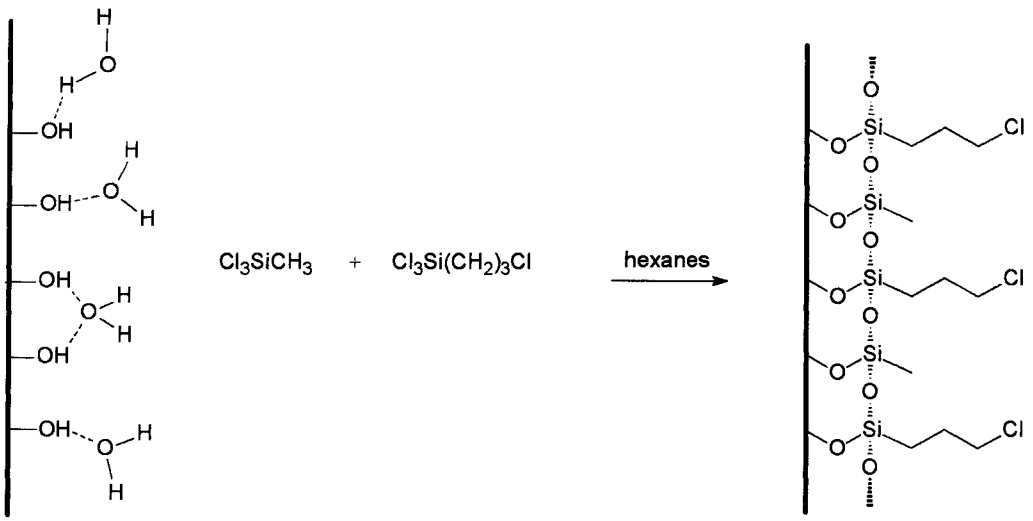

Scheme 4. Synthesis of CP/M Gel.

Quantitative BD/MAS spectra of the series of gels were obtained with a 120 second relaxation delay (Figure 25). Spectral deconvolution was then used to integrate the relative peak areas for the three silane types in the laterally polymerized layer. Deconvolution of the reagent isolated silanol is shown in Figure 25 (bottom, right). Using deconvolution techniques and elemental analysis the percent reagent silane type and total reagent silane coverage density was determined (Table 4). The coverage data has 15% error due to presence of the mercury porosimetry and elemental analysis. Deconvolution analysis contains 20% error in addition to these mentioned errors giving 25% error in the percentage silane type data.

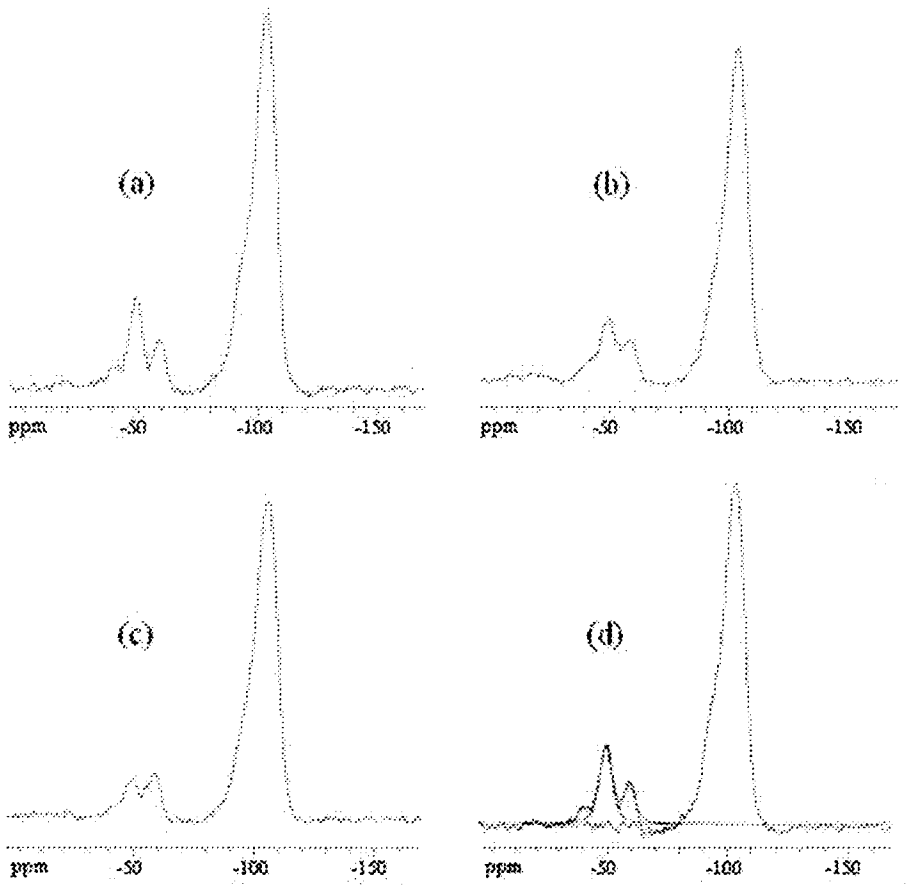

Figure 25. BD/MAS ^{29}Si NMR spectra; CP Gel (A) (top, left), 1.3:1 CP/M Gel (B) (top, right), M Gel (D) (bottom, left), deconvolution CP Gel (A) (bottom, right).

Table 4. Mixed silane gel coverage density results.

Gel	CP:M	Silane Coverage (mmol/g)	Silane Coverage (umol/m^2)	O_3SiR (%)	$O_2Si(OH)R$ (%)	$OSi(OH)_2R$ (%)
A	∞:0	1.8	4.5	28	59	13
B	1.3:1	2.1	5.1	30	56	14
C	1:2.6	2.4	6.1	-	-	-
D	0:∞	2.8	6.6	48	44	7.3

In comparison to the CPTCS only product, the MTCS only product has a 47% increase in surface silane coverage density. The MTCS only product has surface silane coverage of 6.6 ± 1.1 μmol/m^2 (2.8 ± 0.5 mmol/g). The physiochemical constant for

surface silanol concentration is 8.0 ± 1.1 μmol/m^2 indicating that the majority of silanols have been reacted.[15,16] Achieving 8.0 μmol/m^2 silane coverage should be possible if each MTCS binds once to each surface silanol and twice to neighboring reagent silanes. Vertical polymerization could allow for greater than 8.0 μmol/m^2 silane coverage. The percent reagent siloxane increases while the percent reagent isolated (and geminal) silanol decrease (Table 4). For the 1:1 MTCS:CPTCS mixture surface silane coverage (μmol/m^2) is also improved relative to the CPTCS only composite, however not to the same extent as the MTCS only silica gel (~16% increase compared to ~50%). CP-Gel's surface structure is very similar to the reported C_3/C_{18} self-assembled monolayer, containing 30% reagent siloxane groups, 56% reagent isolated silanols, and 14% reagent geminal silanols.

The traditional CP Gel (A) and mixed CP/M Gel (B) and (C) were further modified to produce BPAP. Consistent with the initial study mentioned above composite performance was not compromised due to incorporation of the mixed silane phase. Figure 26 shows a slight improvement in capacity (8% increase) and kinetic performance by use of the mixed silane reagent phase, although modest. Stripping performance was limited due to the use of sulfuric acid, later improved using other stripping agents (Section 3.12).

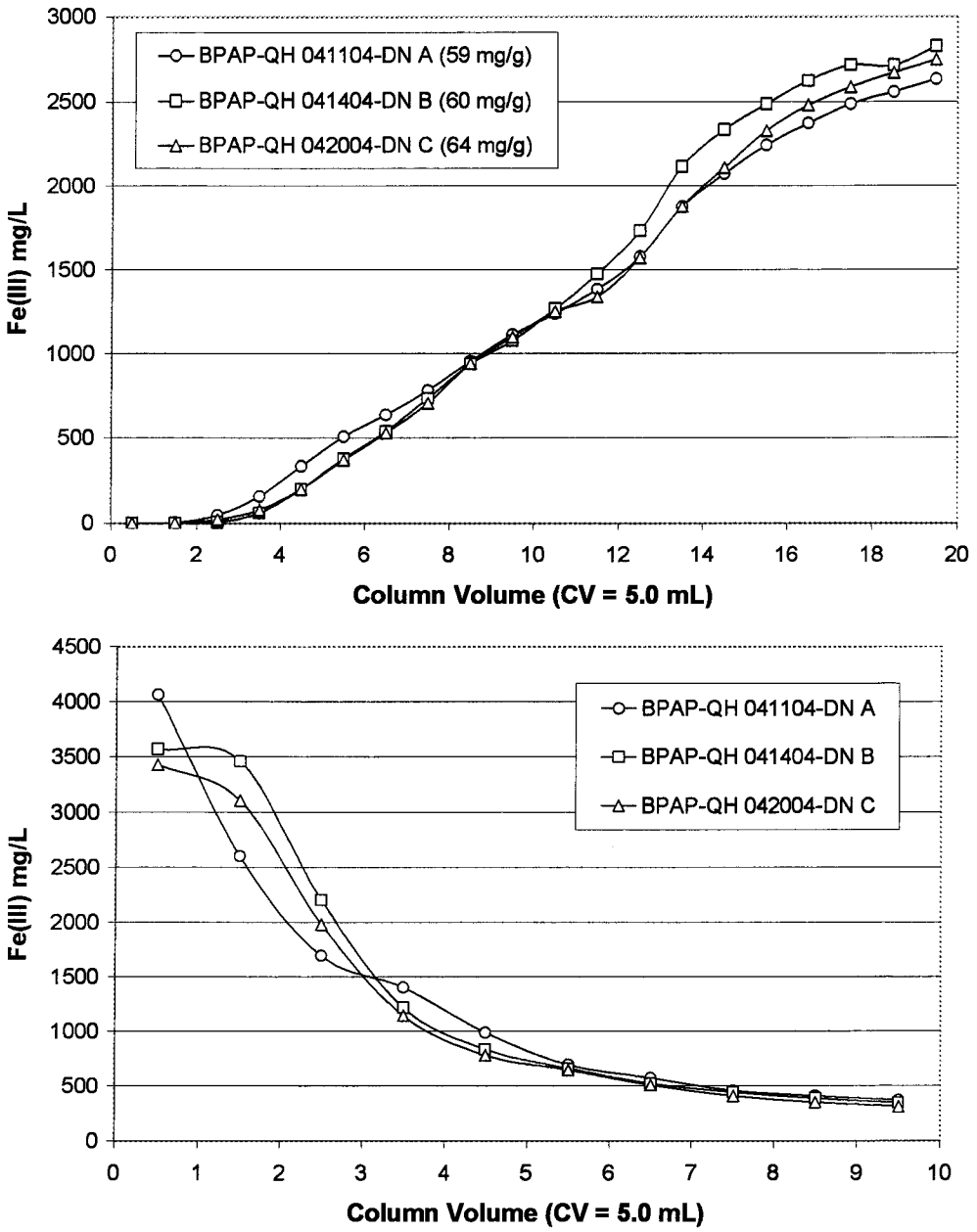

Figure 26. BPAP-QH mixed silane study: Fe(III) breakthrough curves, 0.50 CV/min., pH 1.5, 3.1 g/L Fe(III) (top); strip curves, 0.50 CV/min., 9.0 N H_2SO_4 (bottom).

3.6 Polyamine Composites (WP-1, BP-1)

The selected polyamine is covalently bound to the silica gel surface via the chloropropyl linker group (Scheme 3d,e). Synthesis of the composites WP-1 and BP-1

utilize PEI and PAA respectively (Figure 3). Elemental analysis of the parent composites WP-1 and BP-1 are given in Table 5.

Table 5. Elemental analyses of polyamine composites WP-1 and BP-1.

Entry	Sample Name	Comp. Ref. #	C %	H %	N %	Cl %	C mmol/g	H mmol/g	N mmol/g	Cl mmol/g
9	WP-1-NJ	012702-DN	11.22	2.47	4.77	-	9.3	25	-	-
10	BP-1-QH	120903-DN	16.18	3.54	3.96	1.61	13	35	2.8	0.45
11	BP-1-CF	040804-DN	16.05	3.14	3.97	0.98	13	31	2.8	0.28

A fraction of the amines on the polyamine become "bound," and these amines are less likely to undergo modification due to steric hindrance. Additional inertness of the bound amines may come from the loss of rotational flexibility in going from primary to secondary (or secondary to tertiary). Non-bound or "available" nitrogen atoms (N*) are those on the polyamine that are not directly bound to the silica gel's surface via a propyl linker group. The percent of available nitrogen atoms in BP-1 can be calculated from elemental analysis (Table 5) by Equation 3 (using units of mmol/g). BP-1 contains 40 – 50% anchored amines, leaving 50 – 60% available amines readily modified with ligating groups.

$$N^* (\%) = 100 - 100[(C - 3N)/3 - Cl) / N]$$

Equation 3. Available amines calculation.

WP-1 would use a similar formula using 2N in place of 3N due to having 2 carbon atoms per nitrogen atom on the polymer backbone. WP-1 contains approximately 75% available amines, therefore anchoring 25% via the chloropropyl group. PEI used to make WP-1 contains only 35% primary amines (35% secondary and 30% tertiary) in comparison to PAA having 100% primary amines. Presently the ratio of 1° : 2° : 3° amines on WP-1 is not well understood as the more basic, but more sterically hindered secondary amines of PEI may be binding to the propyl linker instead of the primary amines found on the polymer. It is likely that both the primary and secondary amines of

PEI take part in binding the polymer to the silica gel's surface through the propyl linker. Therefore WP-1 contains 10 – 35% primary amines, 10 – 35% secondary amines and 30% tertiary amines. Solid state ^{15}N NMR could elucidate this question though would require a strong field instrument and many days of acquisition collection for adequate spectral resolution and intensity. Utilization of ^{15}N labeled PEI would greatly enhance the signal to noise, although this would be an expensive investigation.

BP-1 was characterized by ^{13}C NMR as shown in Figure 27. Superimposed upon the three propyl carbon peaks (Figure 23) are the three carbon types found within polyallylamine. These are the secondary (nitrogen bound), secondary (polyamine backbone), and tertiary carbons. Variable local environments among these three carbon types lead to broad NMR peaks.

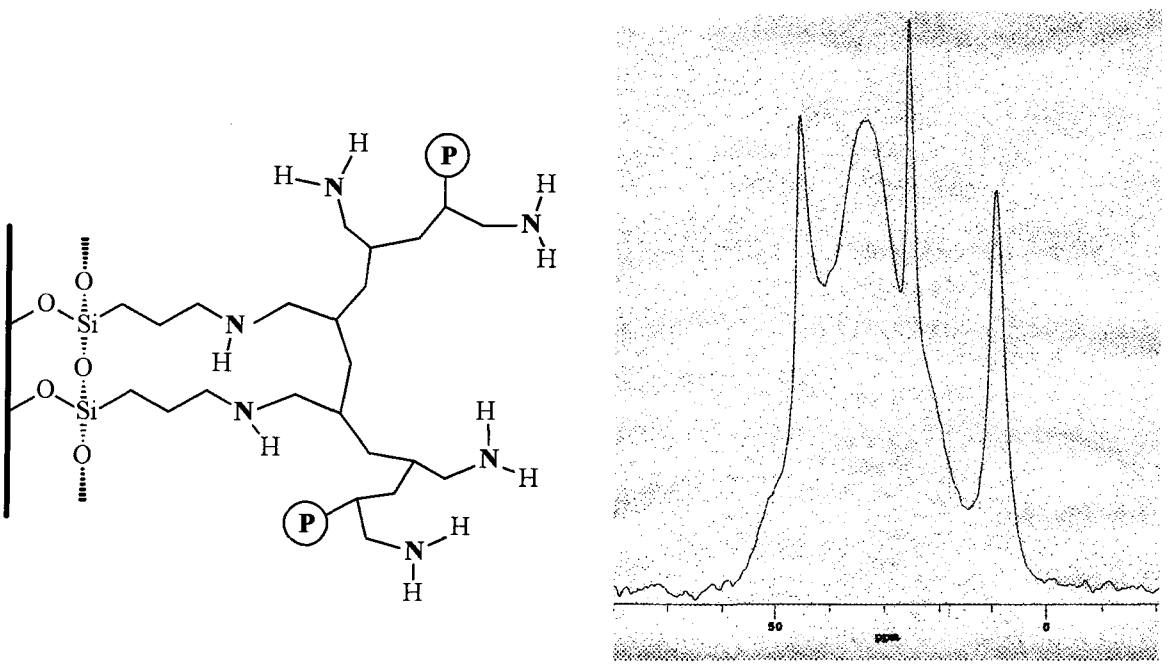

Figure 27. Schematic structure (left) and ^{13}C NMR spectra of BP-1 (right).

WP-1's carbon peaks are relatively broad (Figure 28) in comparison to BP-1's carbon peaks (Figure 27). Increased broadness of WP-1's carbon peaks is most likely due

to the relative rigidity of the polymer's structure. WP-1's nitrogen atoms are interwoven throughout the polymer, leading to a more rigid composite. Another contributor is the increased carbon microenvironments that WP-1 exhibits, when compared to BP-1's carbon atoms.[17]

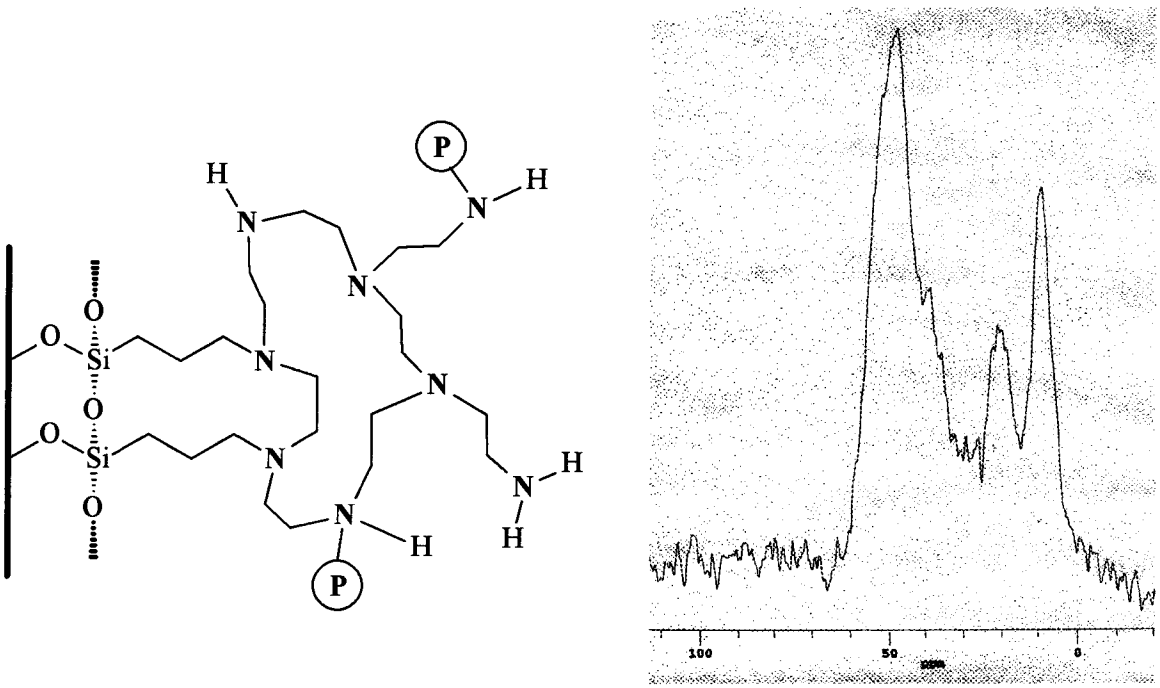

Figure 28. Schematic structure (left) and ^{13}C NMR spectra of WP-1 (right).

3.7 Oxine Polyethyleneimine Composite (WP-4)

The ligand 8-hydroxyquinoline (oxine) has been amended to BP-1 to produce the oxine poly(ethyleneimine) composite (WP-4) shown in Figure 29.[68] The trade name WP-4 has been adopted for the oxine composite although BP-1 is used as the parent composite for best results. Elemental analysis is given in Table 6. This composite has been utilized for recovery of Ga(III), and separation of Fe(III) from divalent metals such as Ni(II), and also from Ln(III) ions as discussed in section 34.2. Unfortunately, WP-4 exhibits affinity towards Cu(II) as discussed in section 34.4. WP-4 was characterized via solid state NMR at the Pacific Northwest National Laboratory (Figure 29).

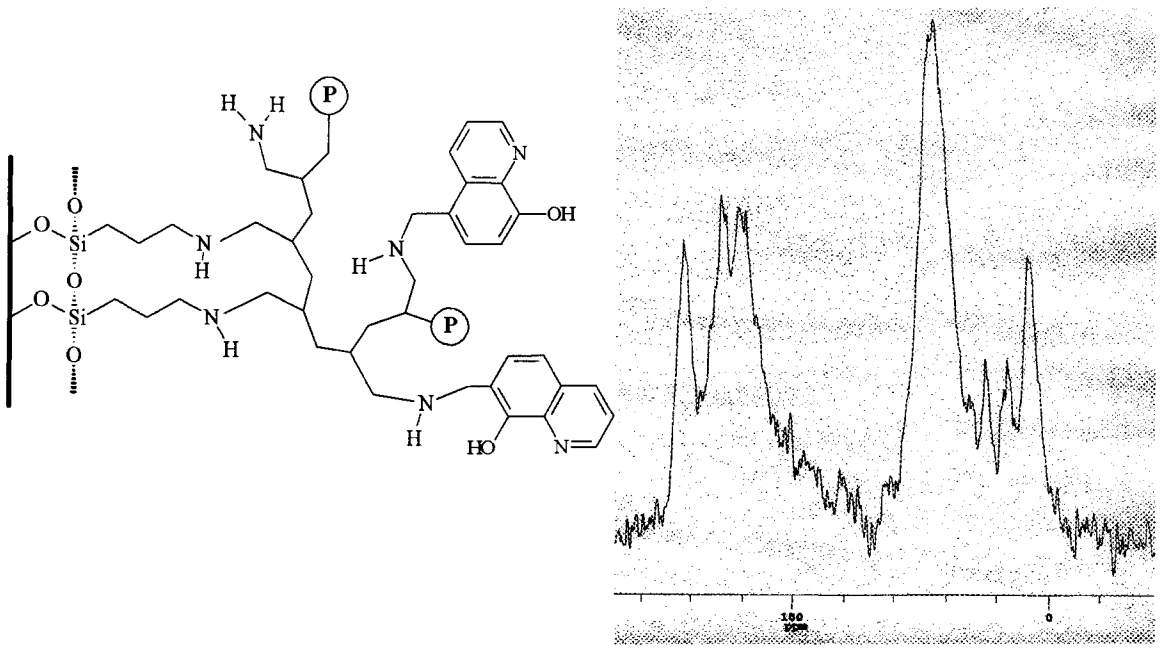

Figure 29. Schematic structure (left) and ^{13}C NMR spectra of WP-4 (right).

Table 6. Elemental analysis of WP-4.

Entry	Sample Name	Comp. Ref. #	C %	H %	N %	C mmol/g	H mmol/g	N mmol/g
12	WP-4-CF	101205-DN	22.53	3.49	3.99	19	35	2.8

3.8 Succinamic Acid Polyallylamine Composite (BPSU)

Aqueous manganese(II) is commonly found in acid mine drainage (AMD). In pursuit of a manganese(II) selective composite, critical stability constants for manganese complexes available in the literature were examined.[43] Many ligands showing moderate to high logarithms of the equilibrium quotients (log K values) contained the carboxylic acid functionality. Modification of BP-1 to produce the succinamic acid functionality was pursued based on the referenced stability constants. Manganese capture and selectivity over its neighbors on the periodic table were anticipated to be difficult as described by the Irving-Williams effect (Section 2.6).

The succinic anhydride reaction was carried out initially utilizing WP-1 to give very low Mn(II) batch capacities, and was not pursued thereafter. Succinic anhydride

dissolved in THF readily reacted with BP-1 to give BPSU (Scheme 5 and Figure 30). Succinic anhydride was not readily soluble in more environmentally benign solvents such as 1,4-dioxane and ethylene glycol dimethyl ether (glyme). Elemental analysis (Table 7) confirms excellent reaction efficiency showing modification at each available nitrogen site in a one to one ratio. Characterization of BPSU was also carried out via solid state NMR (Figure 31).

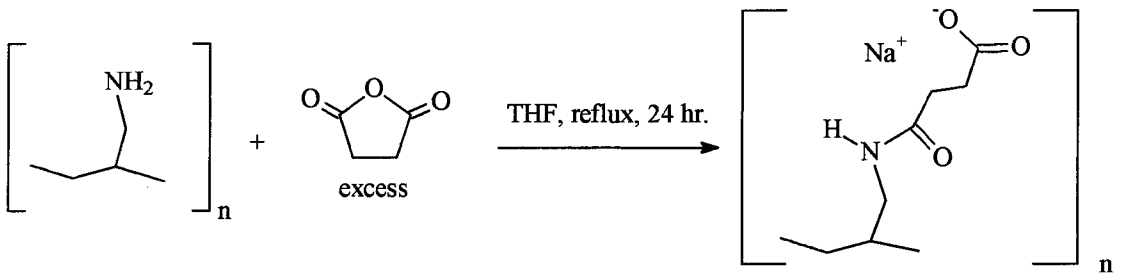

Scheme 5. Synthesis of BPSU.

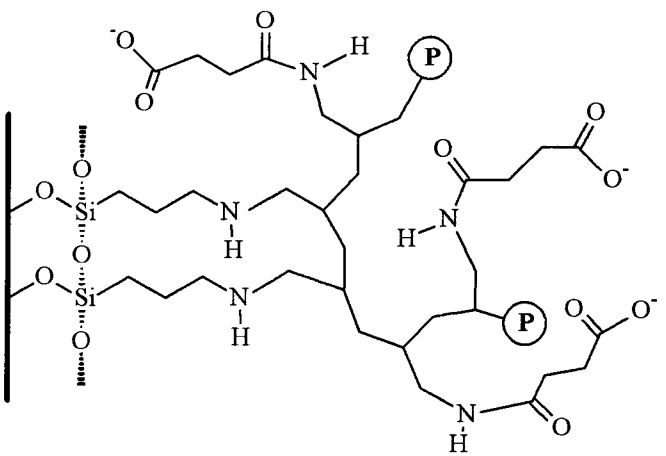

Figure 30. Molecular structure of BPSU.

Table 7. Elemental analysis of BPSU.

Entry	Sample Name	Comp. Ref. #	C %	H %	N %	C mmol/g	H mmol/g	N mmol/g
13	BPSU-CF	080404-DN	21.28	3.15	3.43	18	31	2.4

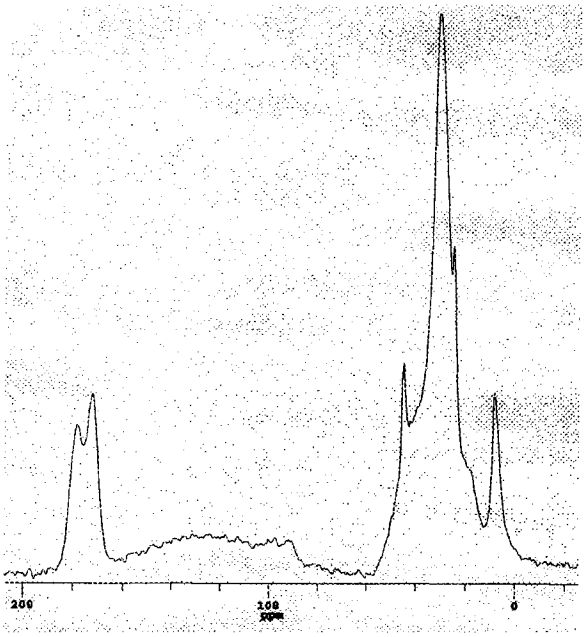

Figure 31. 500 MHz CP/MAS ^{13}C NMR spectrum of BPSU.

Initial batch testing showed promising results for Mn(II) capture exhibiting a 29.1 ± 1.9 mg/g capacity in the base regenerated sodium ion form. Low Mn(II) capacity was exhibited by BPSU in the acid form without the use of base regeneration. Breakthrough testing was then pursued utilizing base regeneration (refer to section 3.2). Breakthrough testing at pH 3.0 (Figure 32, left) allowed for Mn(II) extraction for nearly 50 CV at 253 mg/L (similar to that found in the Berkeley Pit Lake). The strip profile shown in Figure 32 (right) illustrates modest Mn(II) capacity (22 mg/g), but poor strip kinetics. Later studies investigated Mn(II) capture at pH 1.5 as shown in Figure 33. The acidity of the feed led to meager Mn(II) capacities.

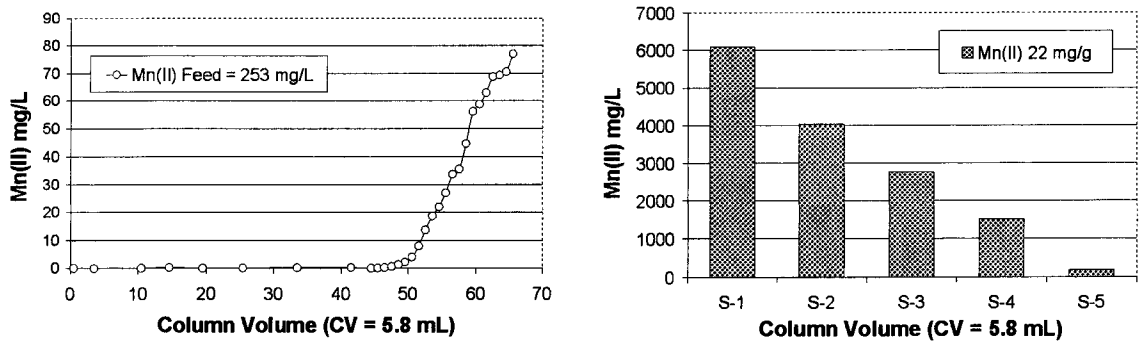

Figure 32. BPSU-CF 032202-DN; breakthrough curve, 0.50 CV/min., pH 3.0 (left); strip profile, 0.50 CV/min., 8.0 N H_2SO_4, 92 % stripped (right).

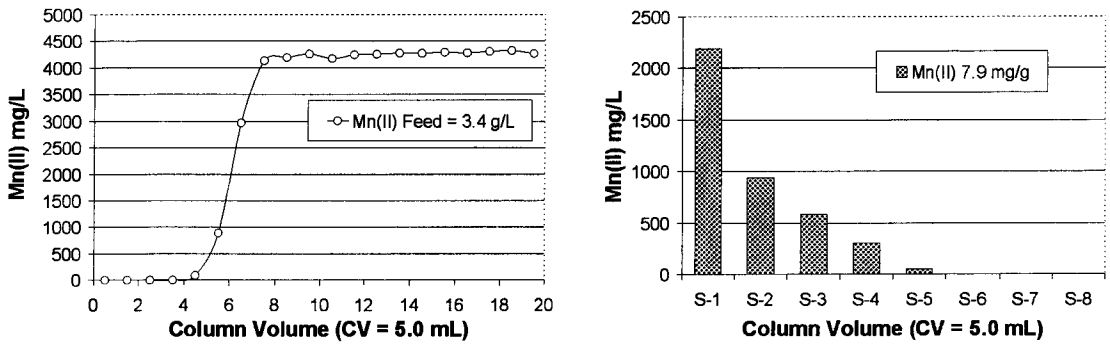

Figure 33. BPSU-CF 080404-DN; breakthrough curve, 0.50 CV/min., pH 1.5 (left); strip profile, 0.50 CV/min., 9.0 N H_2SO_4, 84 % stripped (right).

In response to a need for separation of rare earth elements (Section 34.2), BPSU was tested for Eu(III) batch capacity. Unfortunately BPSU did not coordinate Eu(III) at the target pH of 1. However Eu(III) capacity was significant at higher pH (Table 8).

Table 8. Eu(III) batch testing on BPSU.

pH	Eu(III) mg/g
1.1	0
3.2	28
4.4	34

Further work investigated the use of BPSU for Th(IV) recovery as discussed in section 34.3. BPSU did not show significant affinity towards Zn(II) without the use of base regeneration. Additional testing confirmed relative affinity towards Al(III) over Mn(II) relevant to acid mine drainage treatment strategies.

3.9 Tetra-Acetate Polyallyamine Composite (BPDT)

Investigation of the tetra-acetate composite was subsequent to the fabrication of the succinamic acid composite BPSU. Diethylenetriamine pentaacetic dianhydride (DTPA) reagent was expensive, restricting the production and testing of BPDT. Limited solubility of DTPA led to utilization of DMSO as a solvent. BP-1 was reacted with DTPA to produce BPDT as shown in Scheme 6 and Figure 34.

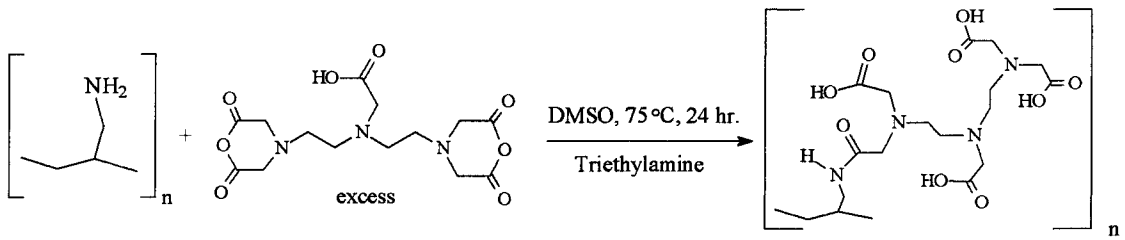

Scheme 6. Synthesis of BPDT.

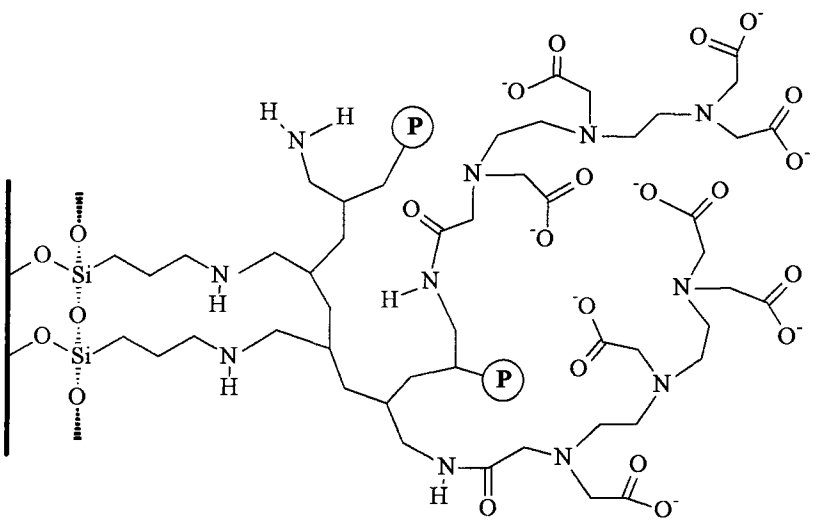

Figure 34. Schematic structure of BPDT.

Initial batch testing showed a 23.8 ± 1.3 mg/g Mn(II) capacity following base regeneration of BPDT. Separate testing evidenced little affinity toward rare earth elements. BPDT batch capacities were in the range of 4 – 6 mg/g for Ce(III), Gd(III) and

Yb(III). A preliminary breakthrough curve shown in Figure 35 illustrates similar performance in comparison to BPSU under identical conditions.

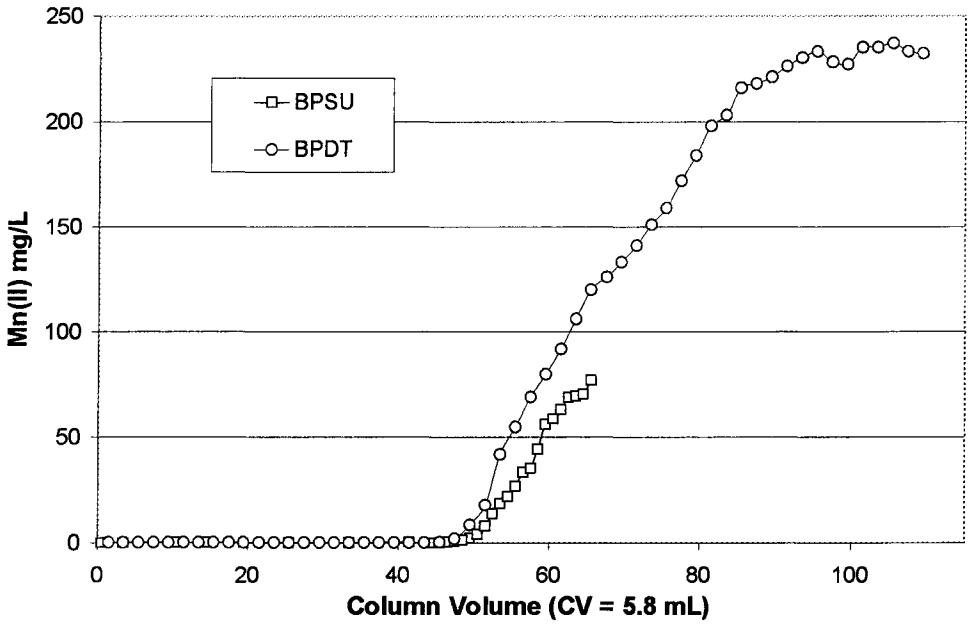

Figure 35. BPSU-CF 082202-DN, BPDT-CF 033002-DN; Mn(II) breakthrough curves, 0.50 CV/min., pH 3.0, 200 mg/L Mn(II).

Synthesis of a mixed succinamic acid and tetra-acetate functional composite was produced on BP-1 similar to BPSU and BPDT. Batch testing revealed slightly lower capacities (relative to BPSU and BPDT) for Mn(II) (18.9 ± 0.3 mg/g), and Ce(III), Gd(III) and Yb(III) in the range 4 – 5 mg/g. Futher testing was not pursued due to cost, solvent toxicity, and performance relative to BP-2 (Section 34.4).

3.10 Amino-δ-Keto Phosphonic Acid Polyallylamine Composite (BPMA)

The Michaelis-Arbuzov rearrangement, also known as the Arbuzov rearrangement, Arbuzov reaction, or Arbuzov transformations, is one of the most versatile pathways for the formation of carbon-phosphorous bonds and involves the reaction of an ester of trivalent phosphorous with acyl or alkyl halides.[44] In this study, initial pathways focused upon the more reactive acyl halide, 4-butyryl chloride (Scheme 7). Future work may

include the much lesser reactive, but potentially more stable linkage by utilizing primary alkyl halides. Initially both 3-chloropropionyl chloride and 4-butyryl chloride were chosen to react with trimethylphosphite to make the halogenoacylphosphonates. The 3-chloropropionyl-phosphonate yielded unstable and impure products by nuclear magnetic resonance (NMR), in agreement with the literature.[45] Using 4-butyryl chloride reagent led to only one in every seven nitrogen atoms on the polyallyl amine to be functionalized with the phosphorous containing ligand (Table 9). Due to mediocre loading of the functional group combined with the expensive and hazardous reagents, further optimization and performance testing was terminated.

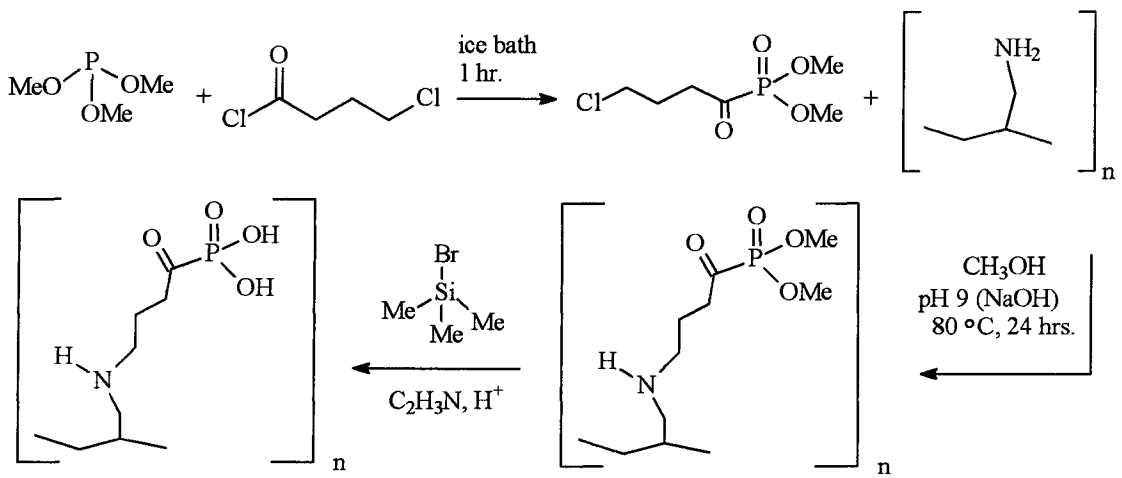

Scheme 7. Synthesis of BPMA.

Table 9. Elemental analysis of BPMA.

Entry	Sample Name	Comp. Ref. #	C %	H %	N %	P %	C mmol/g	H mmol/g	N mmol/g	P mmol/g	N/P	N*/P
14	BPMA-CF	111702-DN	16.56	3.02	2.87	0.57	14	30	2.0	0.18	11	5.9

3.11 Phosphonic Acid Polyallylamine Composite via CMPD (BPCD)

The chloromethylphosphonic dichloride (CMPD) route was initially chosen for its simplicity and versatility for variable phosphonate synthesis (Scheme 8).[46,47] The choice of alcohol would allow for control over the bulkiness of the ester group. Chloromethylphosphonic dichloride was initially reacted with tertiary butanol to make

the dialkyl phosphonate. The phosphonate was then attached to the silica-polyamine using a tetrahydrofuran (THF) solvent ~0.5% dimethylsulfoxide (DMSO), followed by acid hydrolysis. At best this pathway showed one in ten available nitrogen atoms to attach the alkyl phosphonate (Table 10 – Entry 15).

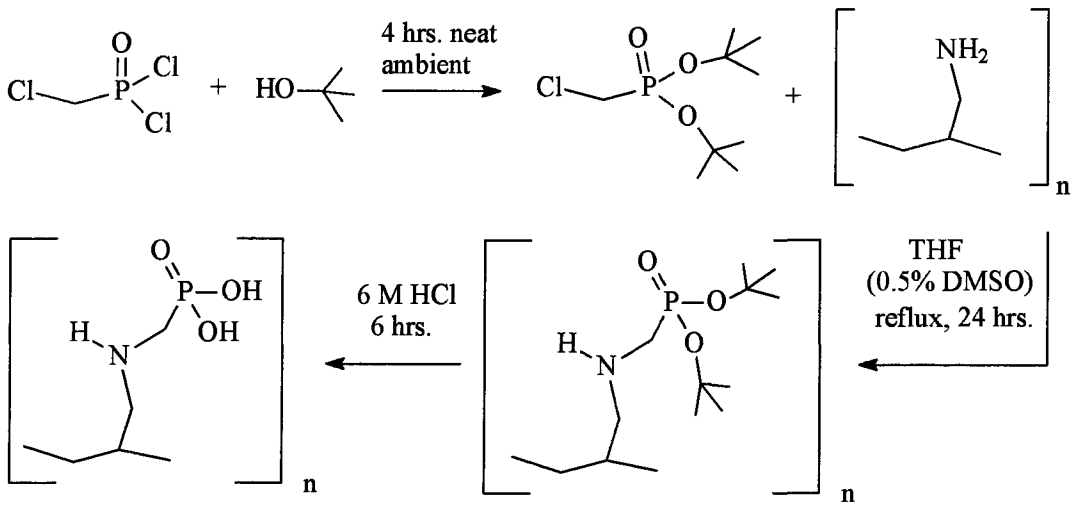

Scheme 8. Synthesis of BPCD (using t-butanol).

Table 10. Elemental analysis of BPCD.

Entry	Sample Name	Comp. Ref. #	C %	H %	N %	P %	C mmol/g	H mmol/g	N mmol/g	P mmol/g	N/P	N*/P
15	BPCD-CF	101602-DN	12.64	2.65	3.00	0.35	11	26	2.1	0.11	19	10
16	BPCD-CF	100404-DN	16.99	3.87	3.15	0.02	14	38	2.2	0.01	387	203

Other attempts were made using this synthetic pathway utilizing methanol in the formation of the phosphonate, followed by addition to BP-1 using NaOH instead of TEA to drive the reaction (Scheme 9). This led to even lower reaction efficiency as evident from minimal phosphorous loading (Table 10 – Entry 16). The first methoxyl formation is extremely exothermic, but the second methoxy formation was not complete. This product was initially mistaken for the hydrolysis product and the reaction was stopped prematurely. Further time and possibly heating should allow for complete formation of the dimethylphosphonate. This synthetic approach was not continued due to better

success via the cheaper, simpler and more environmentally benign routes utilizing the Michaelis-Arbuzov and Mannich reactions.

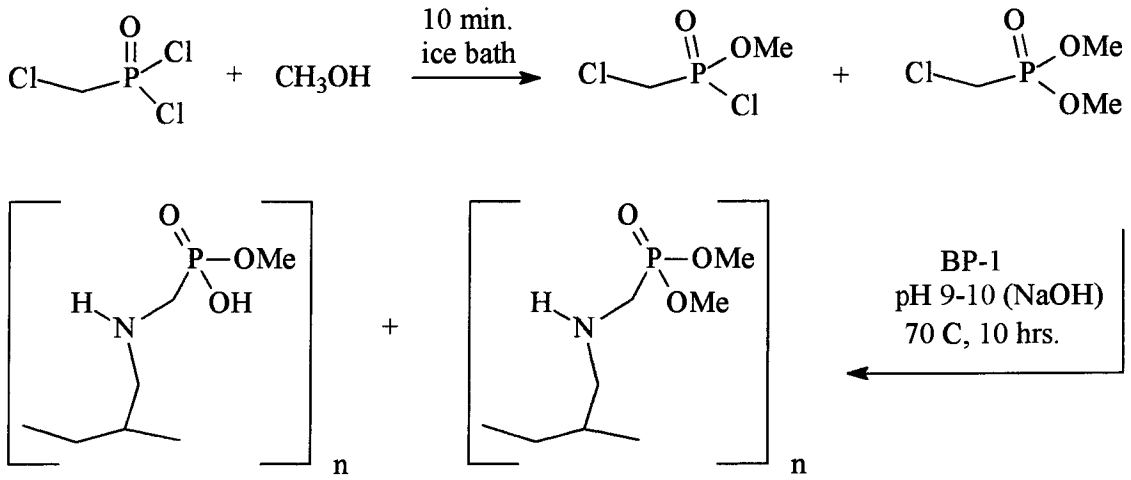

Scheme 9. Synthesis of BPCD (using methanol).

3.12 Phosphonic Acid Polyallylamine Composite by Mannich (BPAP)

In the Mannich reaction an aldehyde such as formaldehyde is condensed with ammonia or a primary or secondary amine as the free amine or its salt, and a compound containing an active hydrogen.[48,49] The product is referred to as a Mannich base. A literature investigation of the Mannich reaction led to two main approaches. One route would be to pursue the base-catalyzed reaction using the free amine.[69] The other approach followed the acid-catalyzed Mannich, investigated as both the one and two-step reaction. Phosphorous acid was chosen as the nucleophile to construct the phosphonic acid functional group via the Mannich reaction.

The base-catalyzed pathway showed no phosphorous loading by elemental analysis when sodium hydroxide was utilized as the base (Table 11 - Entry 17). Tetramethylammonium hydroxide allowed the base-catalyzed reaction to lead to stable products, but with only 1 in 26 available nitrogen atoms to be functionalized (Table 11 –

Entry 18). Further studies were interrupted by the high degree of functionalization exhibited via the less expensive and simpler route via the acid-catalyzed reaction.

Table 11. Elemental analysis of WPAP, BPAP, and BPAP-t.

Entry	Sample Name	Comp. Ref. #	C	H	N	Cl	P	C	H	N	Cl	P	N/P	N*/P
			%	%	%	%	%	mmol/g	mmol/g	mmol/g	mmol/g	mmol/g		
17	BPAP-CF	081902-DN	12.92	3.24	4.45	-	<0.10	11	32	3.2	-	-	-	-
18	WPAP-NJ	072902-DN	12.57	2.69	4.44	-	0.20	10	27	3.2	-	0.06	49	26
19	WPAP-NJ	073002-DN	11.59	2.00	4.08	-	0.11	9.7	20	2.9	-	0.04	82	43
20	WPAP-NJ	082202-DN	11.75	2.84	3.87	-	0.88	9.8	28	2.8	-	0.28	9.7	5.1
21	WPAP-CF	090803-DN	11.49	2.74	3.39	-	1.45	9.6	27	2.4	-	0.47	5	2.7
22	BPAP-CF	111302-DN	16.18	3.10	2.89	-	4.05	13	31	2.1	-	1.3	1.6	0.83
23	BPAP-CF	120902-DN	15.00	2.92	2.65	-	4.26	12	29	1.9	-	1.4	1.4	0.72
24	BPAP-CF	041504-DN	15.87	3.40	2.95	0.68	4.71	13	34	2.1	0.19	1.5	1.4	0.73
25	BPAP-QH	121403-DN	15.35	3.64	2.90	1.42	4.98	13	36	2.1	0.40	1.6	1.3	0.68
26	BPAP-CF	100203-DN	14.45	2.99	2.52	-	3.11	12	30	1.8	-	1.0	1.8	0.94
27	BPAP-CF	082003-DN 3	13.59	3.04	2.39	-	4.01	11	30	1.7	-	1.3	1.3	0.69
28	BPAP-CF	082003-DN 13	14.05	3.20	2.34	-	4.60	12	32	1.7	-	1.5	1.1	0.59
29	BPAP-CF	082003-DN 24	14.12	3.07	2.30	-	4.32	12	30	1.6	-	1.4	1.2	0.62
30	BPAP-t-CF	071504-DN	16.71	3.44	3.39	-	5.37	14	34	2.4	-	1.7	1.4	0.73
31	BPAP-CF	042704-DN	16.93	3.44	2.87	-	5.26	14	34	2.0	-	1.7	1.2	0.63
32	BPAP-CF	042804-DN	15.55	3.29	2.75	-	4.21	13	33	2.0	-	1.4	1.4	0.76
33	BPAP-CF	042904-DN	16.88	3.19	2.89	-	4.71	14	32	2.1	-	1.5	1.4	0.71
34	BPAP-CF	043004-DN	15.79	3.33	2.77	-	4.66	13	33	2.0	-	1.5	1.3	0.69

The two-step acid-catalyzed reaction pathway resulted in low functionalization of the polyamines. The two-step reaction involves the addition of the silica-polyamine to formaldehyde, isolation of the imine followed by a nucleophilic substitution. The two-step acid-catalyzed route showed to have poor results. Elemental analysis showed only 1 in 43 available (non-anchored) nitrogen atoms to be functionalized (Table 11 – Entry 19).

From numerous small scale reactions the pathway that exhibited the highest phosphorous content followed the one-pot acid-catalyzed reaction (Scheme 10).[50] Initially a water solvent was used allowing the excess phosphorous acid to catalyze the reaction to yield good coverage of the ligand with modification of 1 in 5 available amines (Table 1 – Entry 20). Scheme 11 presents the acid catalyzed reaction mechanism. Studies showed that use of a 2.0 M HCl solvent was advantageous in comparison to a water solvent, presumably assisting in the condensation (Table 11 – Entry 21). The acid catalyzed Mannich reaction using BP-1 employed 10 mmol/g formaldehyde and phosphorous acid, a 3.6 molar excess with respect to total amines, or a 6.8 molar excess

with respect to the primary "available" amines. This excess allowed for 15% of the employed reagents to be reacted leading to the phosphonic acid functionality. The available nitrogen to phosphorous ratio for BPAP is in the range of 0.6 – 0.9 (Table 11: Entries 22 – 34), suggesting difunctionalization of about one-third of the available amines when using BP-1. Fortuitously, this pathway is the simplest, cheapest and is environmentally benign, all important with regard to industrial scale production. Other work investigated reaction kinetics to show near completion in only 3 hours under reflux conditions, where samples were taken at 3, 13 and 24 hours (Table 11: Entry 27 – 29). BPAP performance testing also showed that the addition of formaldehyde before heating, or once at reflux made no disparity. Base washing of BPAP following synthesis was shown to improve the breakthrough performance. Other washing protocols investigated 0.1 M NaOH, and omitting base altogether both of which showed compromised kinetic performance compared to base washing with 1.0 M NaOH.

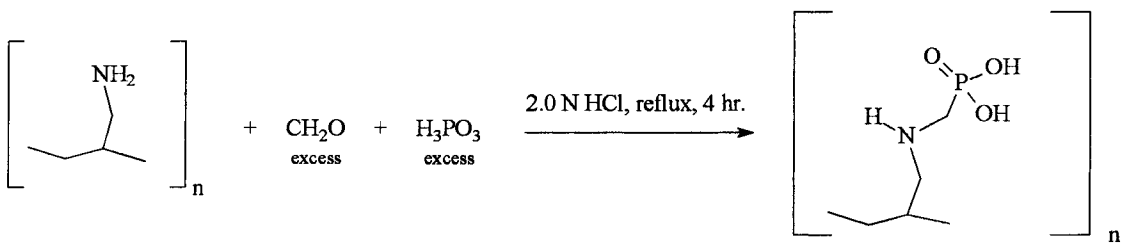

Scheme 10. Synthesis of BPAP.

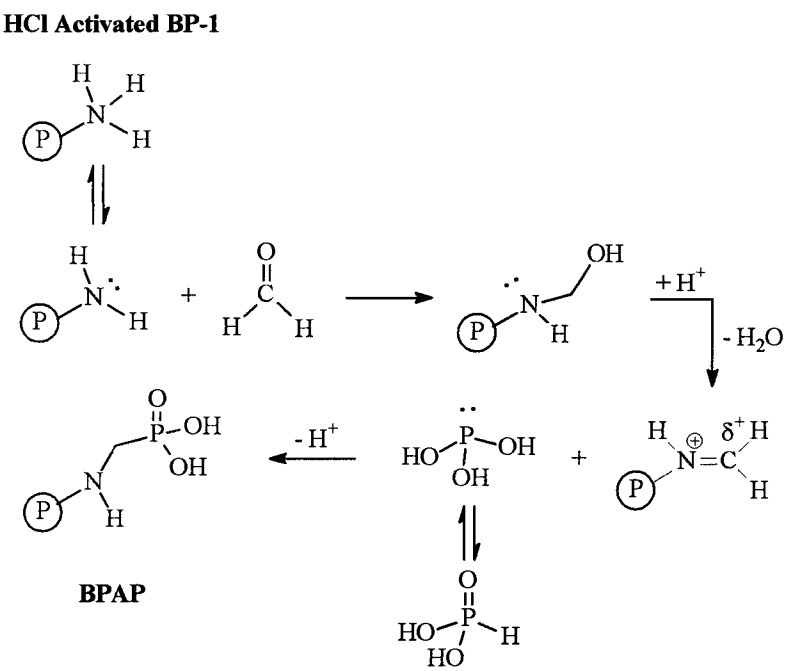

Scheme 11. Acid-catalyzed Mannich reaction utilizing phosphorous acid.

The phosphonic acid functionalized silica composite (BPAP) was characterized by solid state NMR for carbon and phosphorous in Figure 36. Figure 36 displays the three propyl carbon peaks amidst the envelope of polyallylamine carbons, and the small peak at 39 ppm may be the formaldehyde carbon linking the nitrogen to the phosphorous atom. Disregarding the spinning sidebands in the ^{31}P NMR (Figure 36) the main peak centered at 25 ppm is the mono-substituted phosphonic acid groups of BPAP. The left shoulder at 34 ppm is the di-substituted phosphonic acid groups of BPAP as discussed below. Figure 37 shows a $^{1}H - ^{31}P$ heteronuclear correlation (HETCOR) NMR experiment for BPAP. The F1-axis contains the proton NMR spectrum showing a broad envelope of methylene (and methine) protons centered at 3.0 ppm. The broad peak centered at 6.3 ppm (F1-axis) contains the secondary amine protons in BPAP. The F2-axis shows the phosphorous NMR spectrum analogous to that in Figure 36 showing a shoulder at 15 ppm and the major peak centered at 5 ppm (the ^{31}P shifts are not calibrated using a reference standard). Correlation is shown between the methylene protons and both the mono- and

di-substitued phosphonic acid peaks. Correlation is also observed between the secondary amines and the mono-substituted phosphonic acid groups. No correlation is seen between the secondary amines to the di-functionalized phosphonic acid groups as would be expected due to the absence of amino protons. These studies strongly support that di-substitution of the polyamine by the phosphonic acid does occur, supported further by elemental analysis results. However, Alexandratos and coworkers have suggested that the downfield shoulder could arise from sites in which the phosphoryl oxygen is interacting with the acidic proton of another phosphonic acid group.[51] This suggested interaction may in fact be contributing to the downfield shift observed in the difunctionalized polyamines.

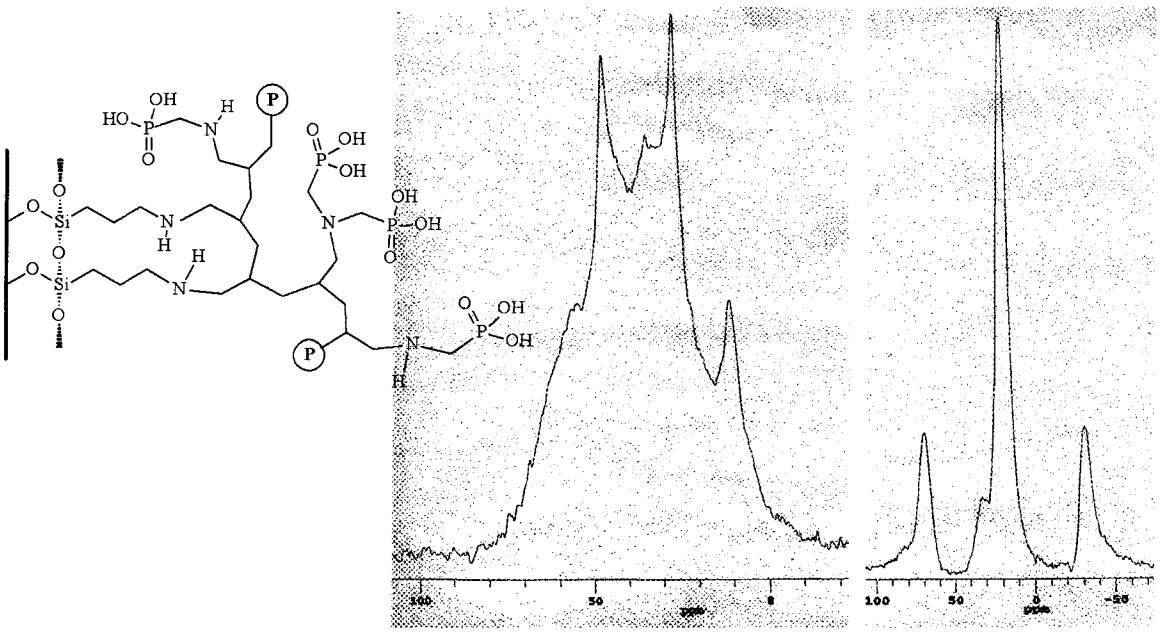

Figure 36. Schematic structure (left), ^{13}C (center) and ^{31}P (right) NMR spectra of BPAP.

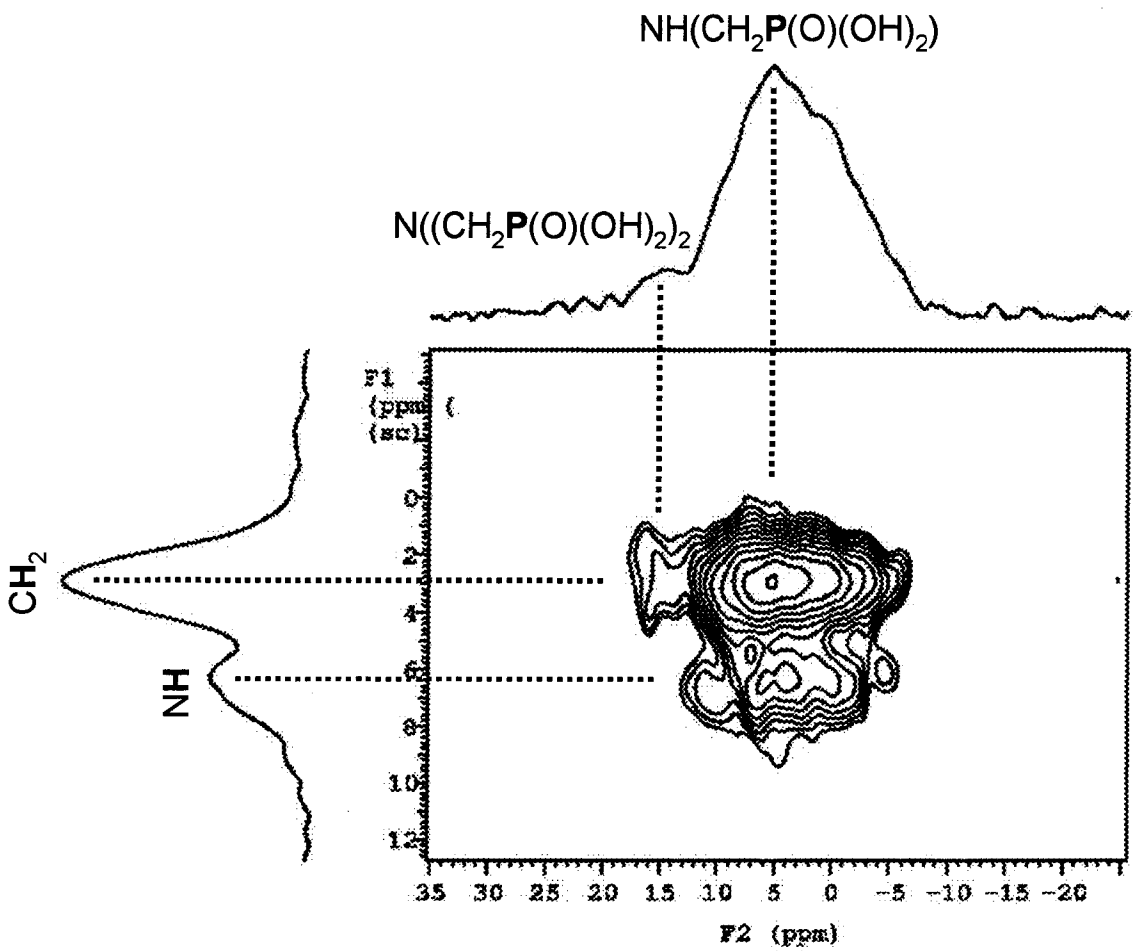

Figure 37. $^{1}H - ^{31}P$ HETCOR NMR spectrum of BPAP.

BPAP has a marked ability to extract tri- and tetra-valent species such as Al(III), Fe(III), Ga(III), Ln(III), and Th(IV). Little affinity is displayed for divalent metals such as Cu(II), Ni(II), Zn(II) and Co(II). Selectivity between trivalent species has been explored for relevant applications such as with sources of AMD (Section 34.4) and REEs (Section 34.2).

Presently optimal particle sizes of silica composite materials are in the range of 150 – 250 μm. Crosfield (CF) silica gel leads to unacceptably high backpressures for industrial scale applications. Qingdao Haiyang (QH) offers larger particle diameter (Table 1) and correspondingly lower back pressures. Crosfield silica gel comes at a price

many times that of Qingdao Haiyang silica gel. However, academic and other smaller scale applications preserve interest in Crosfield silica gel. The kinetic superiority of BPAP-CF relative to BPAP-QH can be attributed to its smaller average particle size and larger average pore diameter. Unfortunately, column permeability is proportional to the square of the particle diameter.[52] Since the back pressure is inversely proportional to the column permeability, applications involving columns in series leads to unacceptable pressure requirements (for current treatment systems).

BPAP-CF exhibits similar batch capacities to BPAP-QH both 64 (±1%) mg/g. BPAP-CF performs better under flow conditions compared to BPAP-QH. BPAP-CF exhibited superior exchange kinetics due to smaller particle size and larger average pore diameter (Figure 38, top). Strip kinetics were however comparable for the two composites as shown in Figure 38 (bottom). The major limitation of strip kinetics was due to the use of sulfuric acid outweighing the effects due to particle and pore sizes. Roughly 99% of the surface area is found on the walls of the interior pores of the composite where the metal exchange takes place. Although the two materials have very similar porosities and coverage of the ligand (due to equal batch capacities), diffusion is relatively limited in BPAP-QH. This is partially due to the smaller average pore diameter of about 73% the diameter of BPAP-CF, limiting diffusion into and out from the pores. Crosfield silica gel exhibits greater pore volume per gram, and its pores diameters are wider and shallower with respect to Qingdao Haiyang as evident from mercury porosimetry analysis (Figure 2).

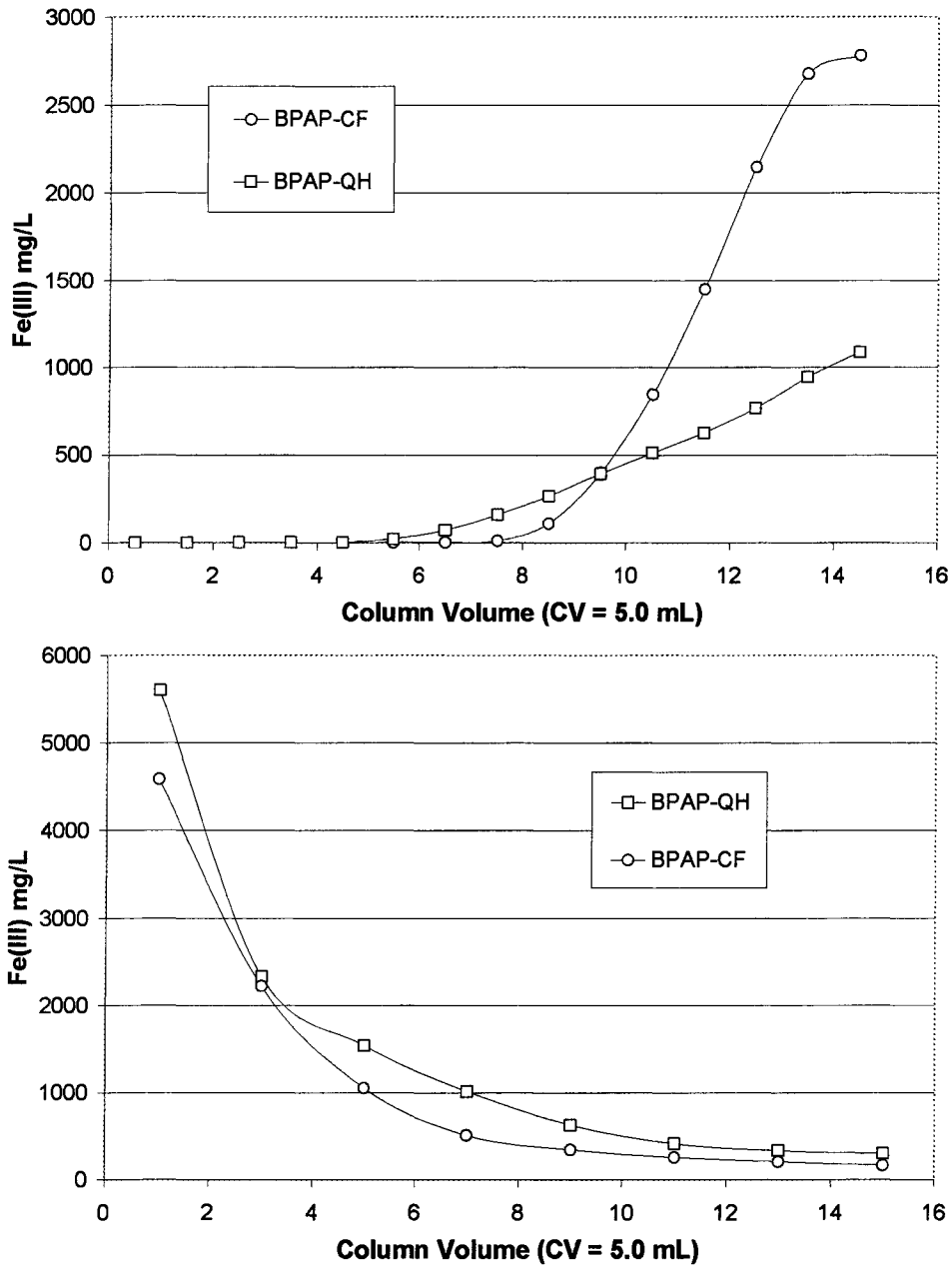

Figure 38. BPAP-CF 082003-DN, BPAP-QH 082503-DN; Fe(III) breakthrough curves, 0.50 CV/min., pH 1.5, 2.9 g/L Fe(III) (top); strip curves, 0.50 CV/min., 7.5 N H_2SO_4 (bottom).

Qingdao Haiyang, Qingdao Meigao, Nanjing and Nanjing Tianyi silica gels were transformed into BPAP (Table 1). These BPAP composites were then tested under batch conditions as shown in Figure 39. 0.2 g composite was exposed to 20 mL of 2.8 g/L Fe(III) or 290 mg Fe(III) per gram composite at pH 1.5. Fe(III) batch capacities were

highest using Qingdao Haiyang silica gel, and relative kinetic performance was similar amongst the tested BPAP composites. The parent BP-1 composites were tested similarly for Qingdao Meigao and Nanjing Tianyi silica gels for baseline information. Base regeneration of the BP-1 composites having a pKa of about 9.3 led to partial precipitation of Fe(III). Precipitation is apparent from the rapid approach to constant Fe(III) capacity (Figure 39), supported by BP-1 flowthrough Fe(III) capacity of only 3 mg/g.

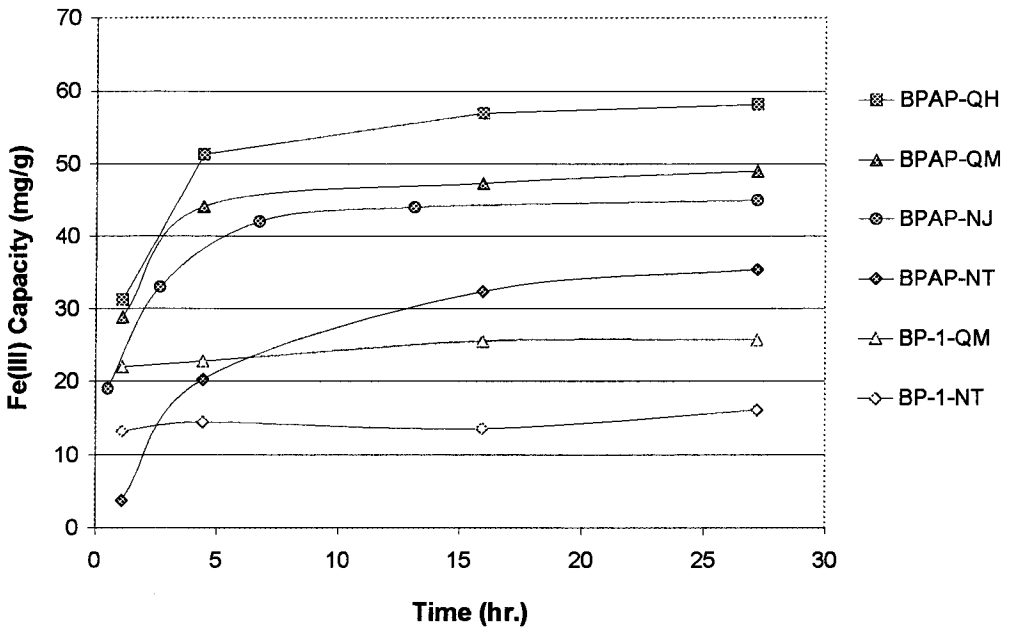

Figure 39. Batch profile silica gel study using BPAP, pH 1.5.

BPAP composites were tested on five silica gels as reported in Figure 40. The four gels produced from Chinese silica gels were tested at 0.50 CV/min. Earlier testing with BPAP made on Crosfield silica gel used a 1.0 CV/min. flow rate. Crosfield silica gel allowed for superior kinetic performance even at twice the flow rate. This is due to both particle and pore diameter characteristics (Table 1). Both the Nanjing Tianyi and Nanjing silica gels exhibited very poor kinetic performance under flow conditions. The batch profiles shown in Figure 39 do not clearly predict the poor flow performance of these silica gel types.

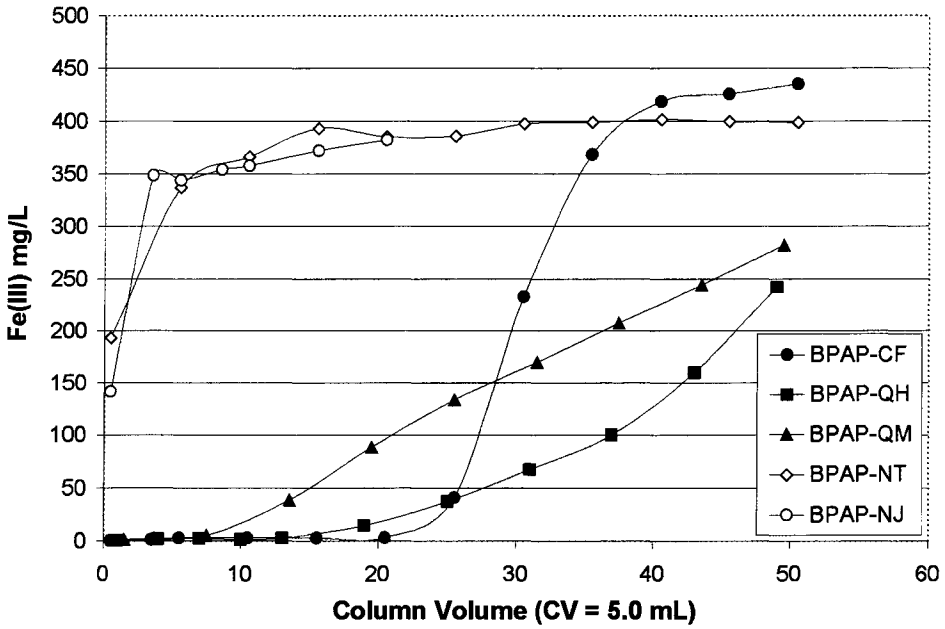

Figure 40. Silica gel study using BPAP breakthrough curves, 0.50 CV/min. (1.0 CV/min. BPAP-CF), pH 1.5, 459 mg/L Fe(III).

Utilization of polyallylamine in BPAP yields higher capacities with respect to polyethyleneimine utilized in the production of WPAP. A comparison between WPAP-CF and BPAP-CF for loading and stripping Fe(III) in the presence of Cu(II) is shown in Figure 41. All of the unanchored amines on BPAP are primary, where as WPAP contains only 35% primary amines (35% secondary, 30% tertiary) in the free polymer, and fewer once anchored to the silica substrate. The flow through capacities (adsorption capacity) for BPAP-CF and WPAP-CF are 54 and 36 mg/g respectively. Batch capacities were 64 and 39 mg/g for BPAP-CF and WPAP-CF, respectively. Therefore, WPAP-CF exhibited 67% flowthrough capacity and 61% batch capacity with respect to BPAP-CF. Elemental analysis shows that WPAP-CF contains only 47% of the ligand than BPAP-CF per gram of material (Table 11 – Entries 21, 26).

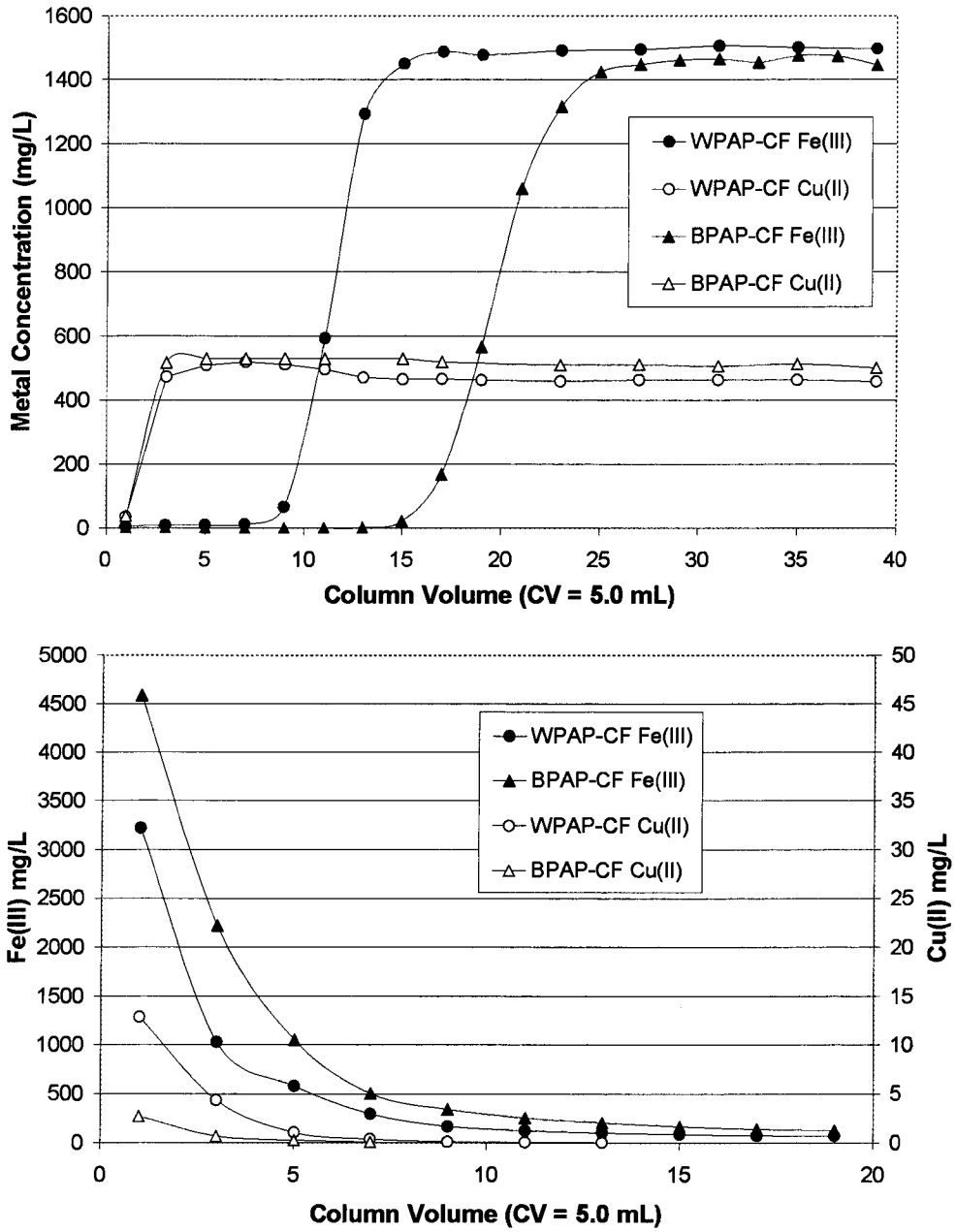

Figure 41. WPAP-CF 090803-DN, BPAP-CF 100203-DN; Fe(III) breakthrough curves, 0.50 CV/min., pH 1.5, 1.5 g/L Fe(III)/0.50 g/L Cu(II) (top); strip curves, 0.50 CV/min., 7.5 N H_2SO_4 (bottom).

BPAP was tested for removal of Fe(III) in the presence of Cu(II) as commonly found in electrowinning solutions (Figure 10). Longevity studies were pursued using 9 N H_2SO_4 prior to the discovery of improved stripping solutions discussed below. Removal of Fe(III) at pH 1.5 to below detection limit (<100 ppb) with concurrent elution of Cu(II)

at the feed concentration supports applications for Fe(III)/Cu(II) separations such as Cu(II) electrowinning solutions. However Cu(II) electrowinning solutions are most commonly 100 – 200 g/L (1 – 2 mol/L) H_2SO_4, having a negative pH value.[26]

A batch capacity pH profile from intrinsic to very acidic pH values was constructed for Fe(III) and Eu(III) using BPAP-CF (Figure 42). The Fe(III) and Eu(III) solutions were prepared at 2.0 g/L and 1.5 g/L, respectively, at various pH values using sulfuric acid. This study confirms the remarkable ability for BPAP to extract these trivalent metals from extremely acidic media. Each data point was carried out in triplicate for this study with relative standard deviations of 2%. Surprisingly, BPAP extracted Fe(III) and Eu(III) from a 10 N H_2SO_4 solution (pH = -1).

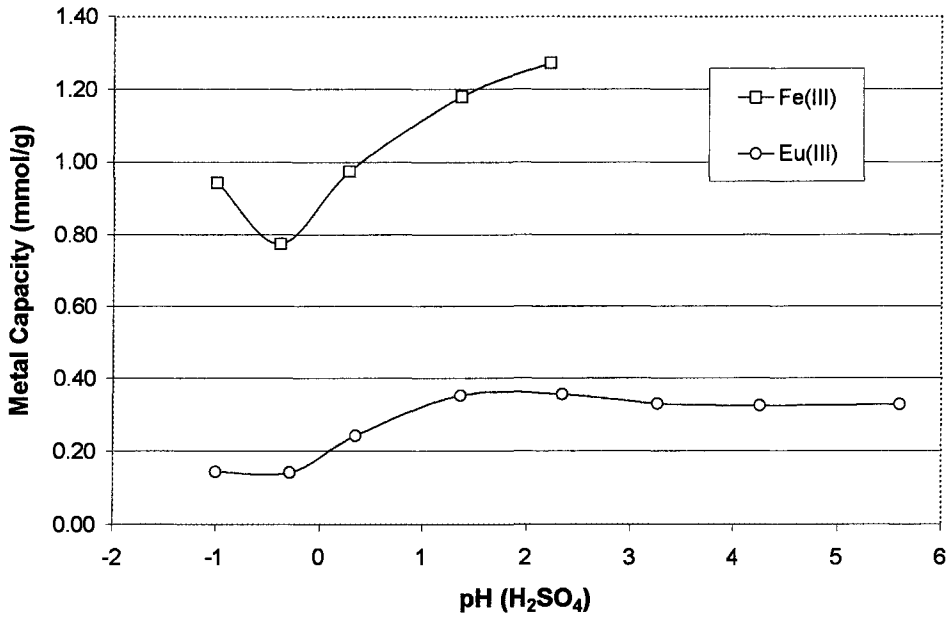

Figure 42. Fe(III) and Eu(III) batch capacity pH profile for BPAP.

The phosphonic acid pK_1 has been reported to be in the range of 2.9 – 6.2,[53] and suggested that predominate complexation occurs through the phosphoryl oxygen.[54] However, it is quite feasible that coordination occurs by proton exchange, or even possibly chelation involving both the acid and phosphoryl oxygens. The increased Fe(III)

capacity at pH -1 with respect to pH -0.4 may be due to increasing sulfate concentration leading to stabilization of the coordinated metal, outweighing converse effects due to the analogous increase in proton concentration. Similar effects may explain the slight decrease in Eu(III) capacity above pH 2.3. The final equilibrated pH of the Eu(III) batch test solutions were 2.3 for the four Eu(III) solutions initially at or above pH 2.3 due to the phosphonic acid functional group. To reiterate, the final equilibrated pH values of the Eu(III) solutions initially at, or above 2.3 were all equal (at pH 2.3), but the increasing sulfate concentration may have led to increased Eu(III) capacity.

A separate batch test study evaluated the Fe(III) capacity at pH 1.7 using initial Fe(III) concentrations of 3.6, 1.8, 0.87, 0.43 and 0.21 g/L (Figure 43). A Langmuir plot (Figure 44) was constructed from these data using the rearranged Langmuir equation (Equation 4) where Q_e is the amount of metal ions adsorbed onto the composite (mmol/g), Q_m is the theoretical quantity of coordination sites, b is the intensity of the adsorption constant, and C_e is the concentration of metal ions in solution (non-coordinated) at equilibrium (mmol/L).[55] Non-cooperative monolayer adsorption is suggested due to an R^2 value of 0.99. Q_m is equal to 1.89 mmol/g (105 mg/g). Using elemental analysis and maximum batch capacities, the ligand to coordinated metal ratio can be found. Maximum coordination numbers (ligand to metal ratio) approach 1 for Fe(III) adsorption. The theoretical Q_m value suggests that maximum coordination would result in an Fe(III) monolayer with a 1:1 ratio of phosphonic acid groups to Fe(III). Although a concentration dependent isotherm was not constructed for Eu(III) the maximum capacity (0.37 mmol/g, 57 mg/g) exposing 297 mg/g of Eu(III) at the intrinsic pH of 5.4 results in a ligand to metal ratio of 4. This ratio value may approach three if higher feed concentrations were employed, or by determining a Q_m value. Wee and

coworkers recently suggested that a phosphonic acid ester ligand coordinates rare earth elements (RE) in an octahedral geometry where both the phosphoryl and phosphonic acid partake in chelation of the metal as shown in Figure 45.[56] It is clear that BPAP does not afford six ligands per metal atom utilizing other ligands such as H_2O and SO_4^{2-}. Furthermore, it is unclear if phosphoryl and/or phosphonic acid ligands partake in coordination as a proton exchanger.

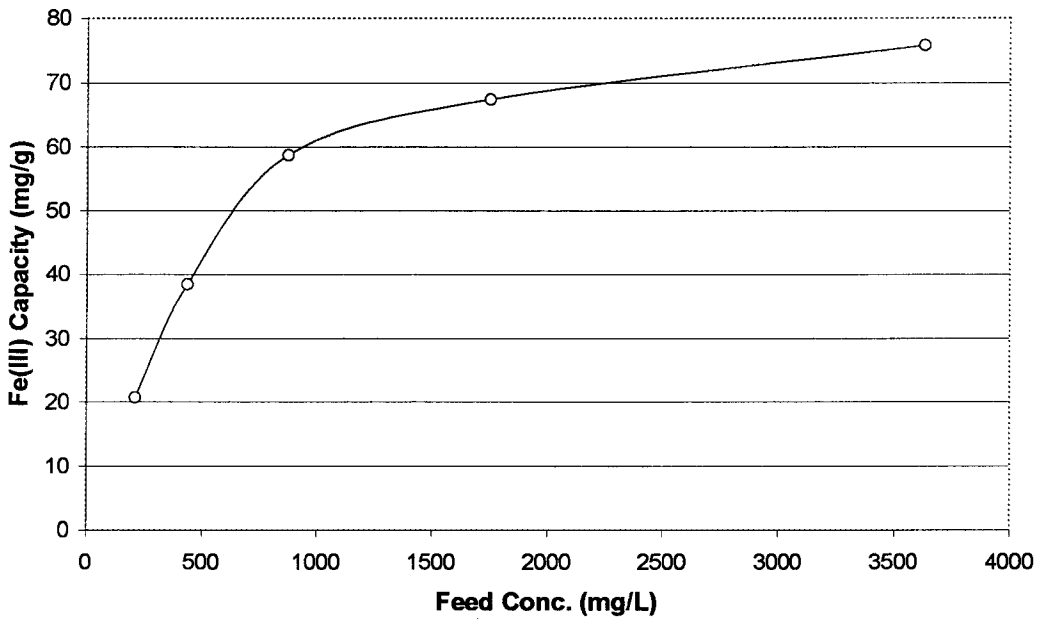

Figure 43. BPAP-CF 041504-DN, Fe(III) concentration dependent adsorption isotherm, pH 1.7.

$$\frac{1}{Q_e} = \frac{1}{Q_m b C_e} + \frac{1}{Q_m}$$

Equation 4. Rearranged Langmuir equation.

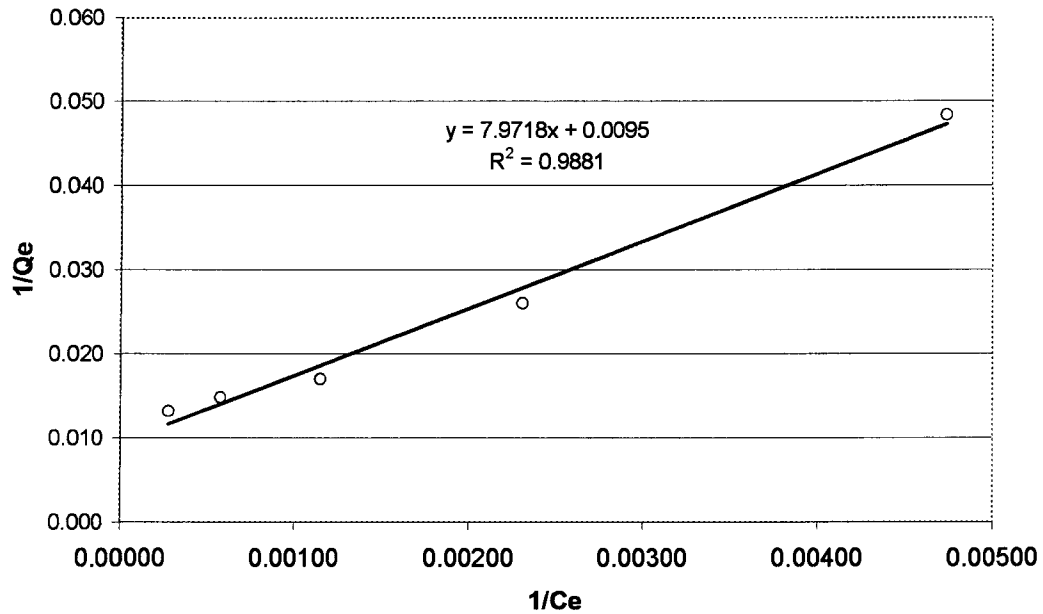

Figure 44. BPAP-CF 041504-DN, Fe(III) Langmuir plot.

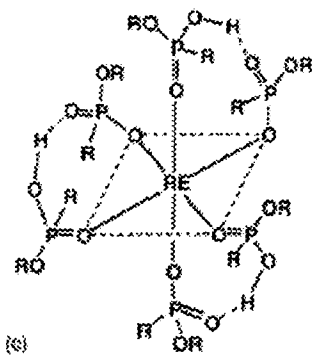

Figure 45. Rare earth element (RE) coordination by phosphonic acid ester ligand.

BPAP has a higher affinity towards Fe(III) than Eu(III) as displayed in Figure 46, and presumably the other lanthanide elements. Poor Fe(III) loading is due to the low feed concentration [0.46 g/L Fe(III)], larger particle silica gel (Qingdao Haiyang), and low ligand coverage (0.50 mmol P/g) thereafter improved to 1.5 mmol P/g with an enhanced available (non-anchored) nitrogen to phosphorous ratio of 0.83. The relatively high affinity towards Fe(III) over Eu(III) was pursued in hopes of a one-step extraction of REEs from an Fe(III) sulfate leach solution.

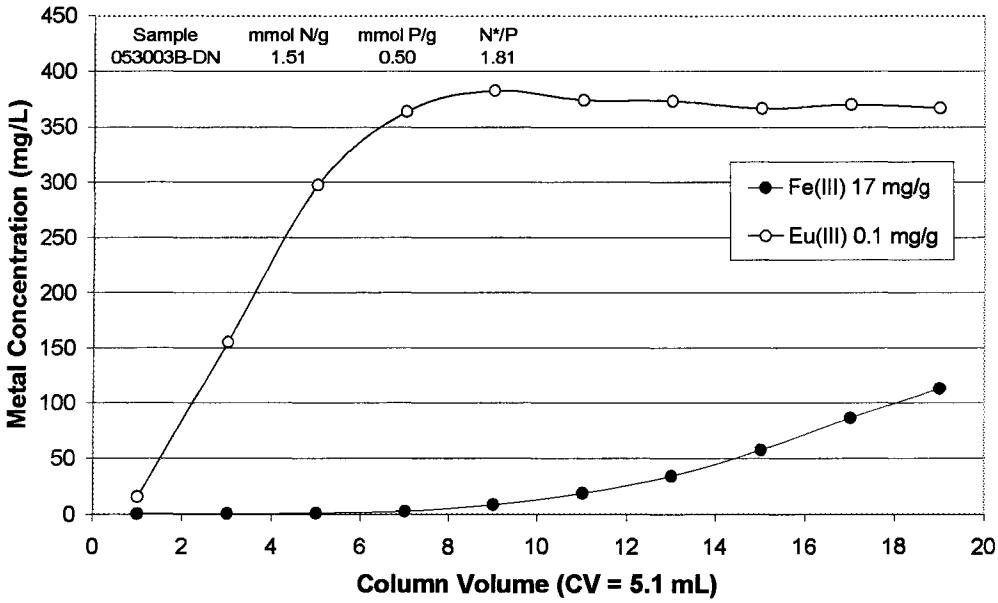

Figure 46. BPAP-QH 053003B-DN, breakthrough curves, 0.50 CV/min., pH 1.5, 456 mg.L Fe(III), 339 mg/L Eu(III).

Once Fe(III) binds to the phosphonic acid modified composites discussed above, it does not easily elute. BPAP-CF and WPAP-CF only stripped 69 and 75% of the loaded iron after eluting with 20 column volumes of 7.5 N (20%) H_2SO_4 at 22°C (Figure 41). Reducing the flow rate to 0.25 CV/min. showed to have no significant effect upon strip performance as shown in Figure 47.

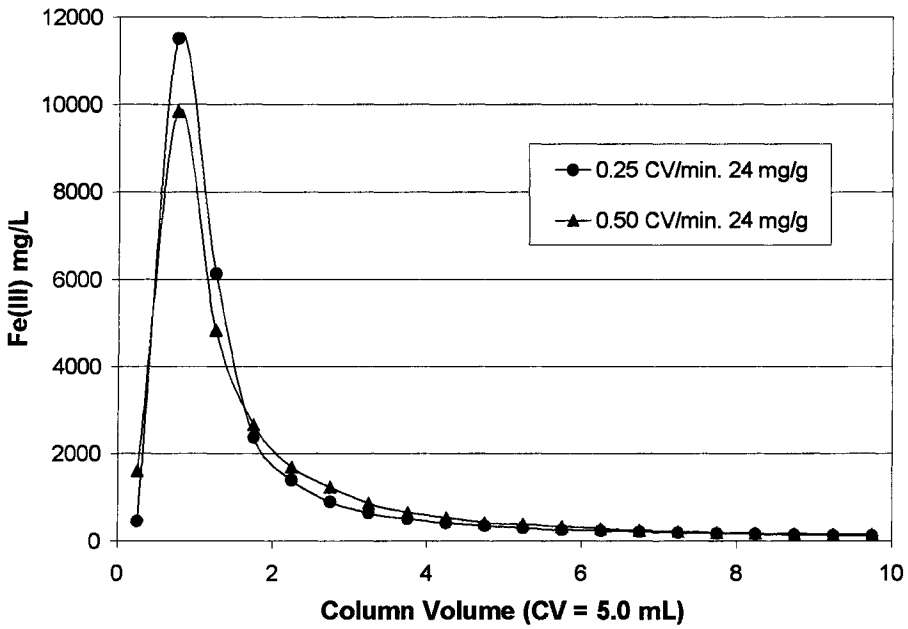

Figure 47. BPAP-QH 053003B-DN, Fe(III) strip curves, 0.25 and 0.50 CV/min., 7.5 N H_2SO_4.

Lowering the density coverage of the functional group (phosphonic acid) was investigated in hopes to increase stripping kinetics due to lowering coordination number and stability. Synthesis employed 30% (0.3 g H_3PO_3/g composite) of the reagent quantities to produce lower coverage of the phosphonic acid functional group of BPAP. Flow testing resulted in almost identical performance to that of WPAP, coincidentally (Figure 48).

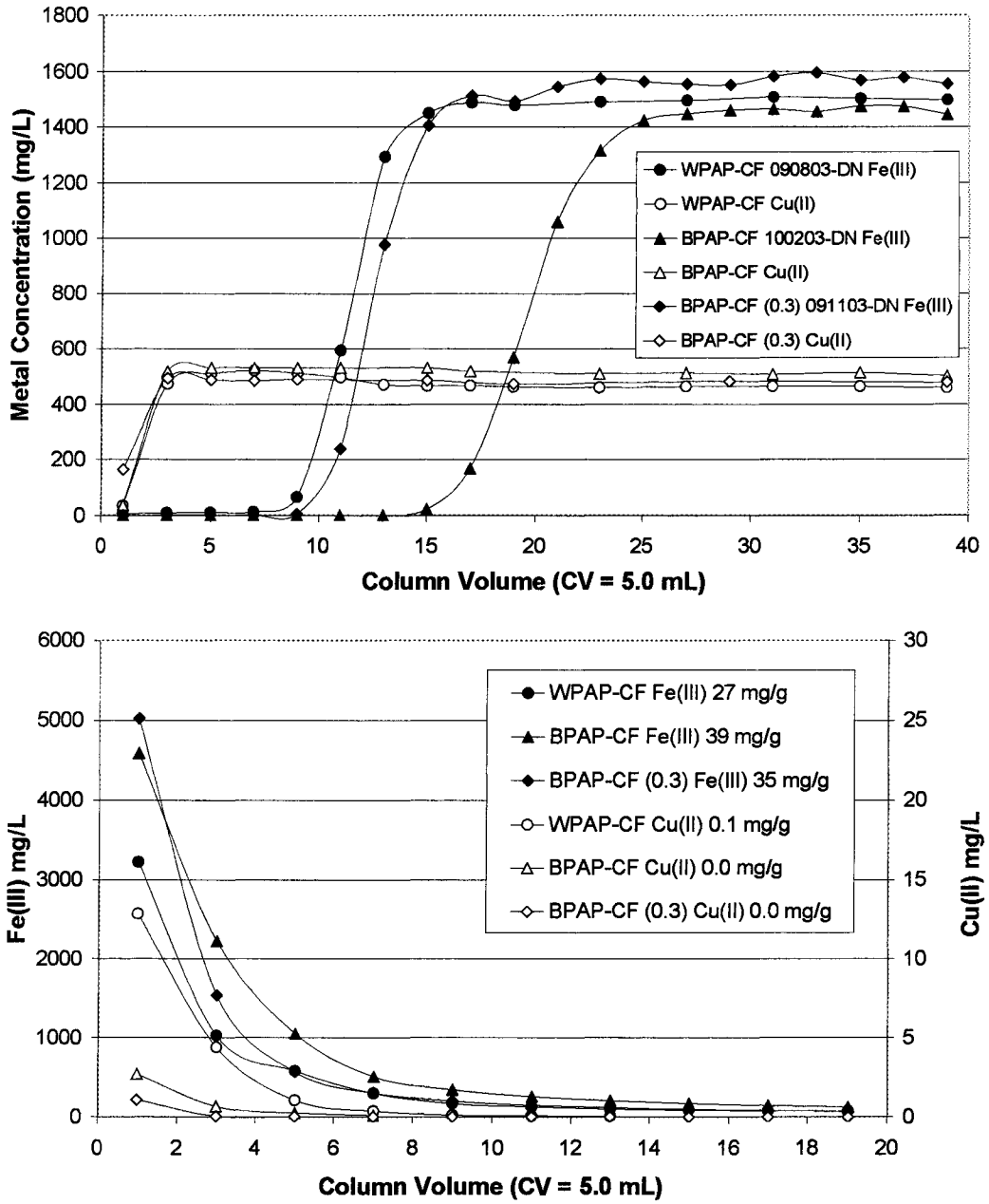

Figure 48. WPAP-CF 090803-DN, BPAP-CF 100203-DN, BPAP-CF 091103-DN (0.3 g H_3PO_3/g); breakthrough curves, 0.50 CV/min., pH 1.5, 1.5 g/L Fe(III), 0.50 g/L Cu(II) (top); strip curves, 0.50 CV/min., 7.5 N H_2SO_4 (bottom).

Another study explored the use of a 2-bromoethylamine to extend the functional group from the polyamine (Scheme 12). The phosphonic acid functional group was then amended via the Mannich reaction. Kinetic performance of BPAP was then investigated using a 3.0 g/L Fe(III), pH 1.5 (H_2SO_4) challenge solution fed at a 0.50 CV/min. flow

rate (Figure 49). Elemental analysis is given in Table 11 - Entry 30. BPAP-t exhibited a 13% increase in capacity over BPAP. The flowthrough capacities were 71 and 63 mg/g for BPAP-t and BPAP composite respectively (Figure 49). Stripping was incomplete even with the tether at 45%.

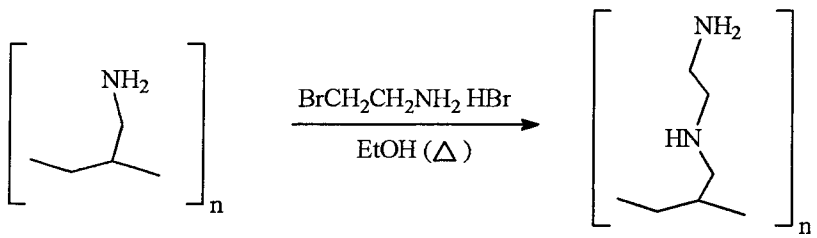

Scheme 12. Synthesis of BP-1-t.

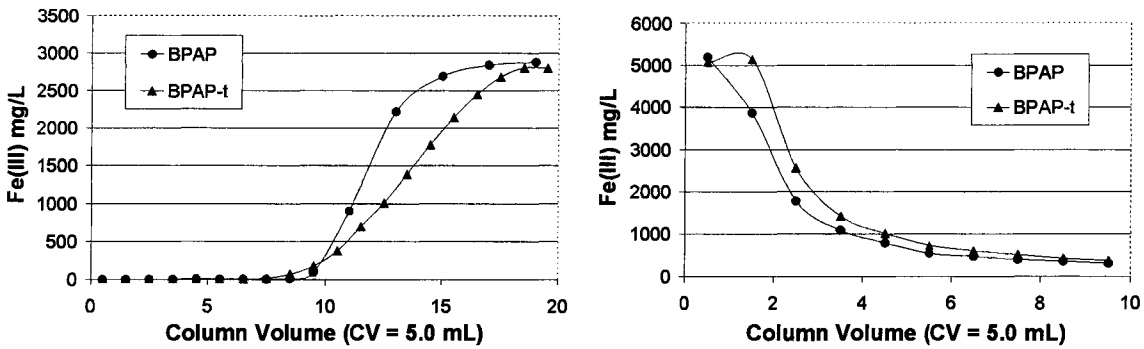

Figure 49. BPAP-CF 041504-DN, BPAP-t-CF 071504-DN; breakthrough curves, 0.50 CV/min., pH 1.5, 3.1 g/L Fe(III) (left); strip curves, 0.50 CV/min., 9.0 N H_2SO_4 (right).

Complete stripping of the loaded metal has been achieved using 25 column volumes of 10 N (81%) HCl heated to 50°C at a reduced flow rate of 0.20 CV/min. (Figure 50). However, industry can not use HCl to strip iron due to environmental considerations and corrosiveness towards stainless steel equipment. Another approach investigated sulfite strip solutions aimed at reducing Fe^{3+} to Fe^{2+} in order to improve strip kinetics as mentioned in section 2.8.2.[28]

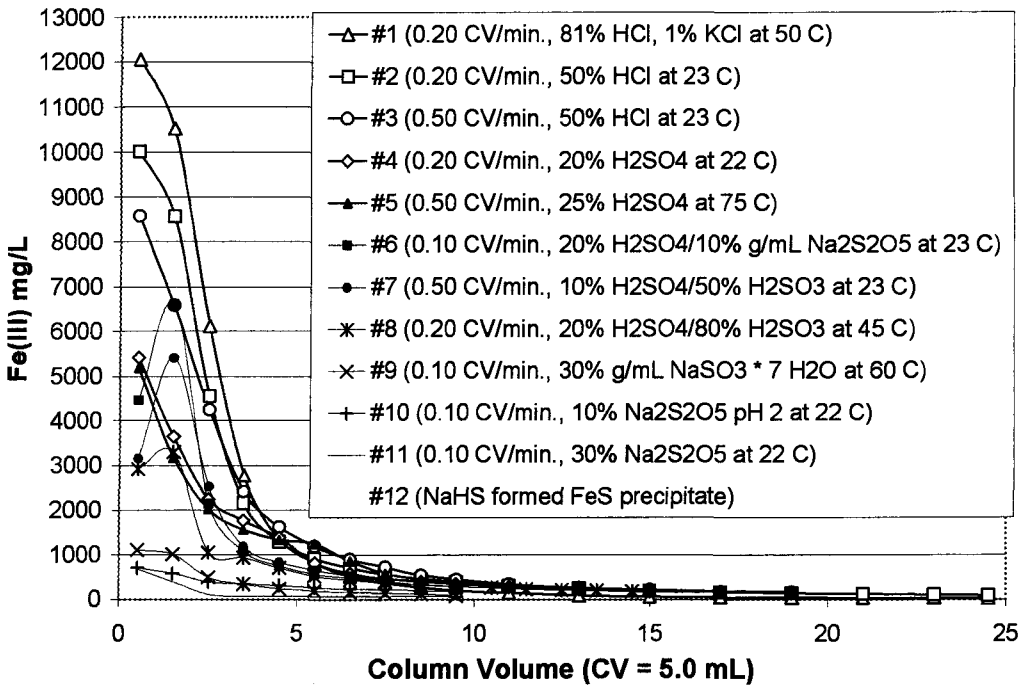

Figure 50. BPAP-QH 081303-MT, initial stripping study.

Changing the phosphonic acid of BPAP to a phosphonate was then pursued in the hope of decreasing the binding constant with Fe^{3+} and improving stripping kinetics. Methylation of the phosphonic acid composite BPAP proved to be difficult as discussed below. In addition to the methylation of BPAP a number of other synthetic schemes were investigated in pursuit of the phosphonate functionality discussed later in sections 3.13 and 3.15 in addition to the unsuccessful Mannich reaction using diphenylphosphinic acid (Scheme 13). Thereafter the phosphinic acid composite (BP-5) was produced exhibiting similar performance to BPAP, disappointing with respect to stripping kinetics (discussed later in section 3.13). More ideal stripping kinetics was eventually attained using EDTA and phosphorous acid stripping agents Figure 52.

As mentioned above attempts were made to methylate the phosphonic acid composite BPAP in hopes of producing the phosphonate functionality. Four reactions were pursued using BPAP. The first methylation utilized dimethylsulfate added to BPAP,

and stirred at ambient temperature to produce BPAP-CF 042704-DN. A second attempt used dimethylsulfate, and was refluxed in ethanol to produce BPAP-CF 042804-DN. In a third study iodomethane was added to BPAP, refluxed neat to produce BPAP-CF 042904-DN. A fourth attempt utilized iodomethane and refluxed in THF to produce BPAP-CF 043004-DN. Elemental analysis (Table 11: Entries 31 – 34) also show limited methylation, although the potential increase in carbon content is small in comparison to the polymer carbon content. Figure 51 show no improvement in loading or stripping kinetics as sought in this investigation. Solid-state NMR was not pursued for these composites.

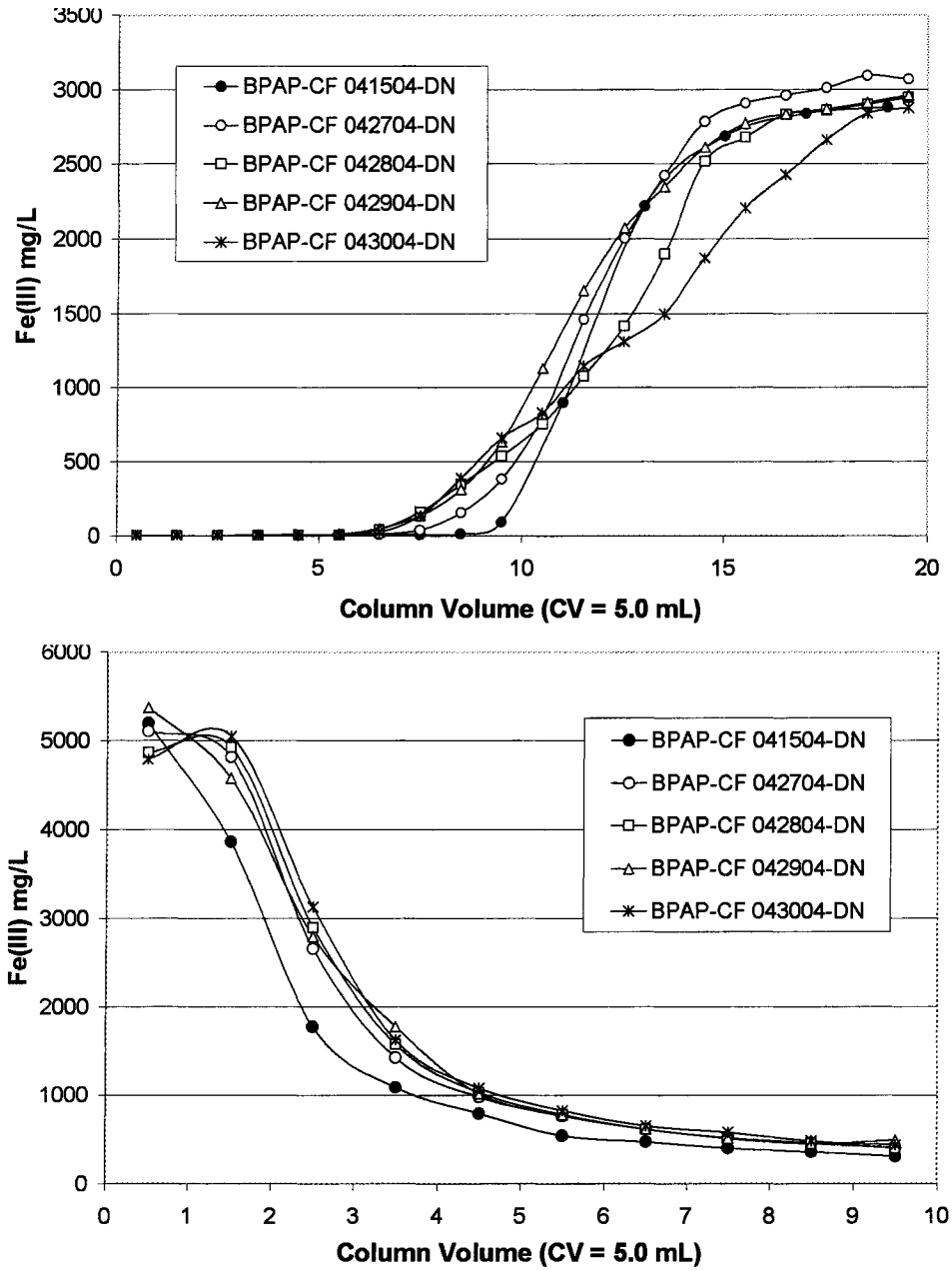

Figure 51. BPAP-CF methylation study; breakthrough curves, 0.50 CV/min, pH 1.5, 3.0 g/L Fe(III) (top); strip curves, 0.50 CV/min., 7.5 N H_2SO_4 (bottom).

More recent studies with Eu(III) discovered greater success with the use of 1 M EDTA (pH 10.5), 10 N H_3PO_3, and 10 N H_3PO_4 to achieve complete stripping in comparison to when using 4 N HNO_3, 18 N H_2SO_4 and 10 N HCl (Figure 52). The di-sodium salt of EDTA is inexpensive, but only soluble to 0.1 M. The pK_4 of EDTA is

10.3, and adjusting the pH to 10.5 using NaOH provides for the formation of the tetra-sodium salt of EDTA, and is soluble at 1 M concentration. Introduction of a basic stripping agent such as EDTA has disadvantages due to pH swings, and potential degradation of the composite. Further studies would investigate minimization of the concentration of EDTA and utilization of the tri-sodium form of EDTA at lower pH regimes (e.g., 8-10). However, final recovery of metal from the EDTA strip solution may be advantageous. This would be accomplished by acidifying the strip solution to free the target metal, precipitating the EDTA, thereafter filtered and adjusted to 10.5 for reuse. Phosphorous acid (H_3PO_3) is another inexpensive stripping agent that is a solid. Phosphoric acid (H_3PO_4) is relatively expensive and is a liquid.

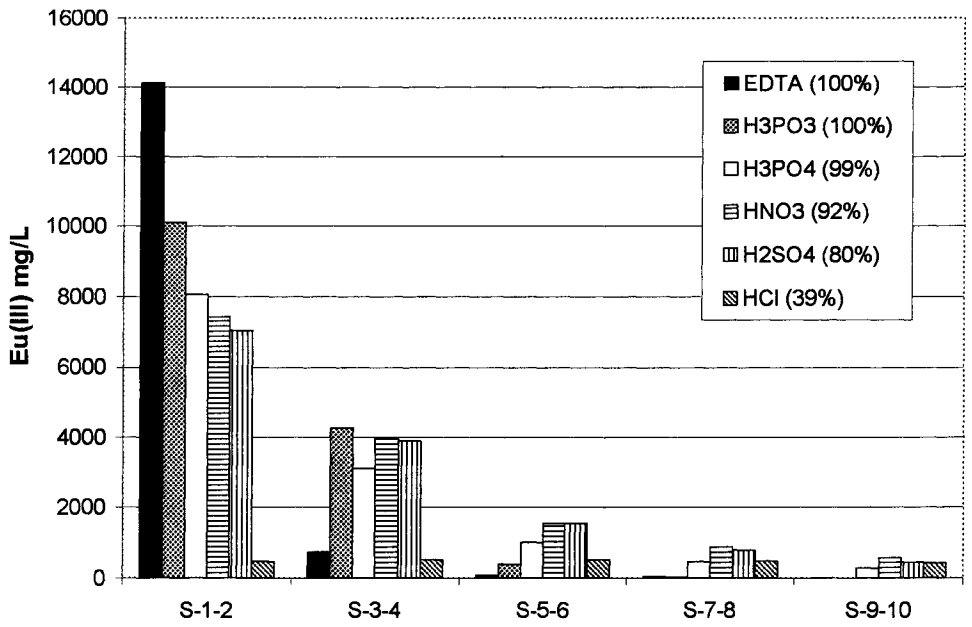

Figure 52. BPAP-CF 041504-DN, final strip profile data, 0.50 CV/min. (strip percentage).

A follow up study investigated the reproducibility of three loading cycles on separate columns of BPAP (same batch) using the various strip solutions shown above in

Figure 52. The three breakthrough curves are shown in Figure 53 (top), with the average breakthrough curve with standard deviation in Figure 53 (bottom).

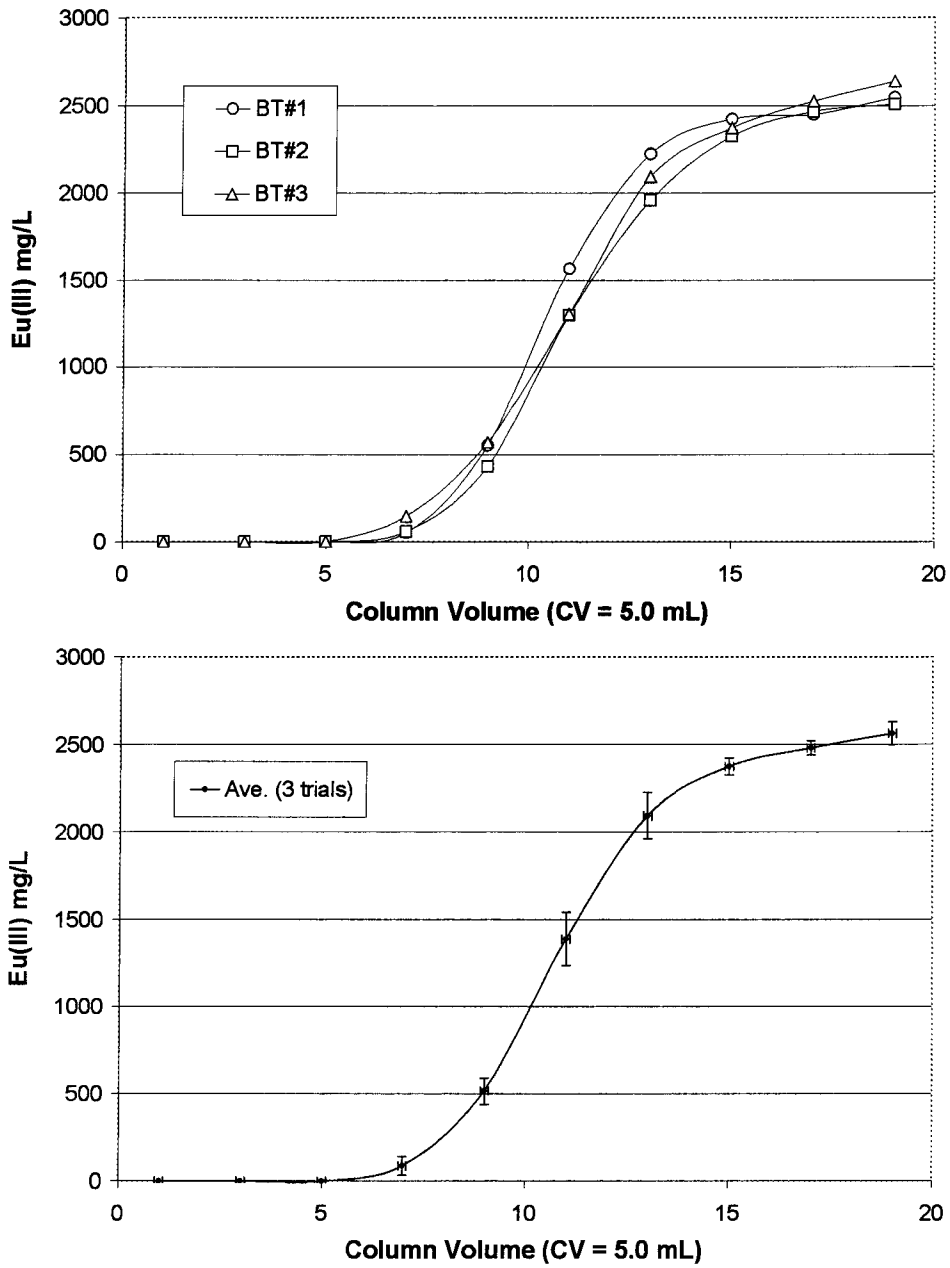

Figure 53. BPAP-CF 041504-DN; breakthrough curves for precision study, 0.50 CV/min., pH 1.0, 2.7 g/L Eu(III) (top); average breakthrough curve with standard deviation, 50 mg/g ± 2 mg/g Eu(III) (bottom).

The column of BPAP that was used with the EDTA stripping agent (1 M, pH 10.5) was reloaded and stripped under identical conditions to investigate the reproducibility.

The breakthrough curves in Figure 54 show the ability to reload BPAP following complete stripping, as also achieved using phosphorous acid.

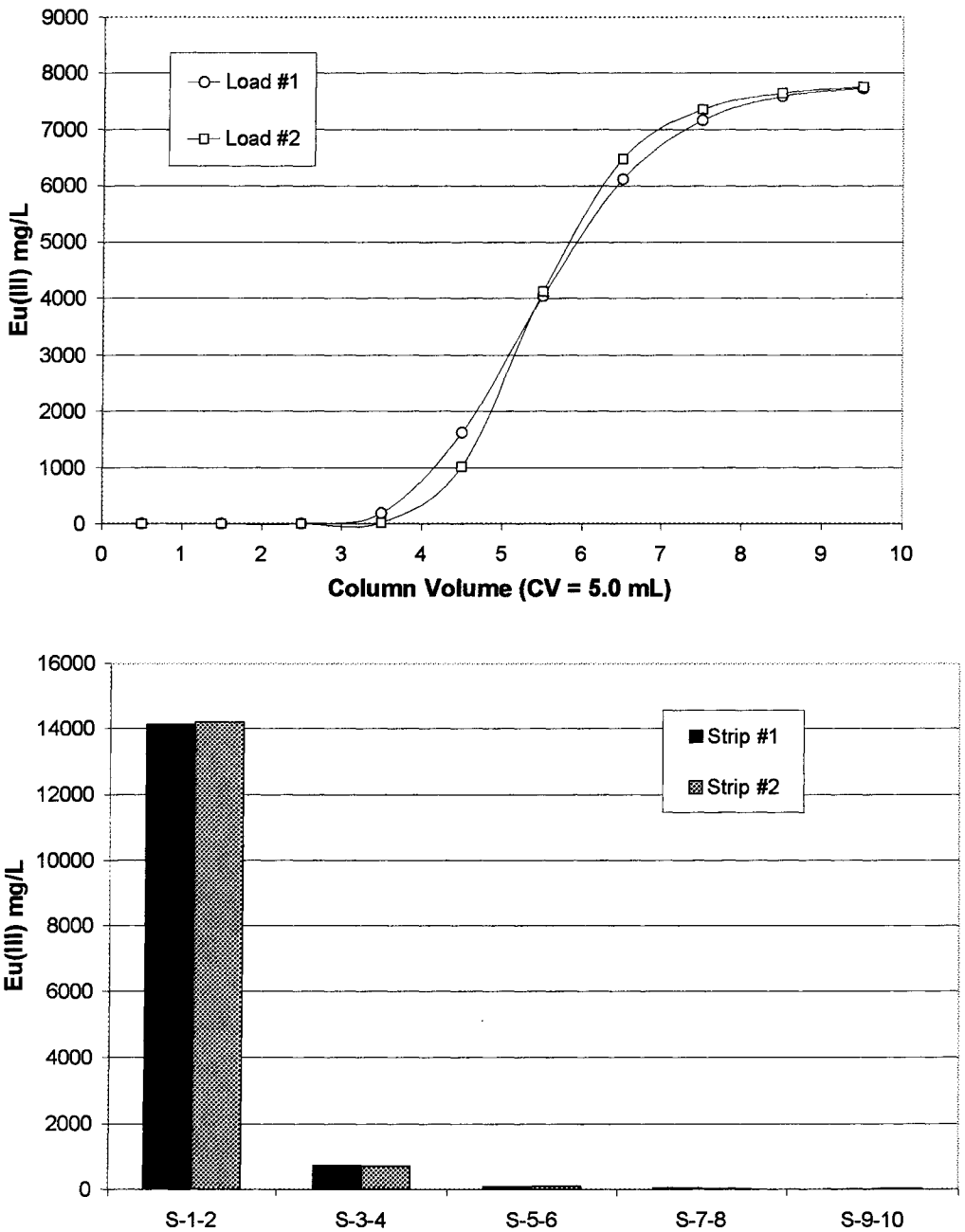

Figure 54. BPAP-CF 041504-DN load/strip cycles #1 and #2; breakthrough curves, 0.50 CV/min., pH 1.0, 7.9 g/L Eu(III) (top); strip profiles, 0.50 CV/min., 1.0 M EDTA (pH 10.6) (bottom).

Successful results with stripping Eu(III) led to revisiting problems associated with stripping Fe(III). A follow up study for Cu(II) electrowinning solutions contaminated with Fe(III) was investigated using BPAP under flow conditions. As previously mentioned typical electrowinning solutions are 2 – 4 N sulfuric acid, although can range from pH 4 (0.1 mN H_2SO_4) to pH -1 (10 N H_2SO_4).[26] The feed solution was prepared in 4.0 N sulfuric acid, which afforded the smallest batch capacity (Figure 42). Three separate columns of BPAP were loaded with the synthetic Cu(II) electrowinning solution contaminated with Fe(III), rinsed with 10 CV of DI water, and stripped using 1.5 M EDTA (pH 10.6), 5.0 M H_3PO_3, and 5.0 M H_3PO_4, all at 0.05 CV/min. utilizing countercurrent (reverse flow) stripping protocol (Figure 55). EDTA afforded the best stripping results with 98% strip in ten column volumes, and over 90% strip in the first four column volumes. Trace levels of Cu(II) were detected only in the first strip fraction for all three strip solutions.

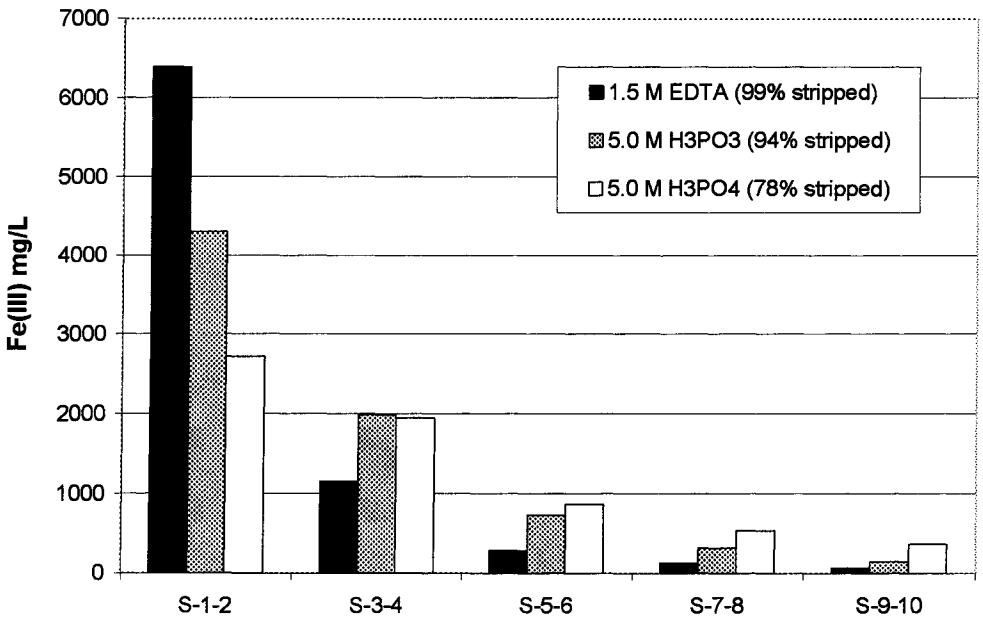

Figure 55. BPAP-CF 041504-DN, stripping study #2, 0.050 CV/min.

Reloading Fe(III) following the EDTA strip was next investigated. BPAP was capable of removing Fe(III) to less than 0.5 mg/L at 0.50 CV/min. flowrate, affording 30 mg/g Fe(III) capacity (Figure 56, top). After loading BPAP with Fe(III) a 10 CV rinse (DI water) was used to flush out the entrained Cu(II) from within the pores. The strip solution contained only trace levels of Cu(II), and eluted 99% of the loaded Fe(III) in 12 – 14 CV using 1.5 M EDTA (pH 10.6) at 0.050 CV/min., utilizing countercurrent stripping protocol (Figure 56, bottom). A second load/strip cycle paralleled the first cycle, indicative of complete stripping. A preliminary study for the recovery of EDTA showed promising results. To the first strip fraction (S-1-2, 10 mL) was added 50 mL of 3 M H_2SO_4. The clear wine red solution immediately precipitated the EDTA as a white powder, resulting in a clear pale yellow solution. The solution was filtered using a glass fritted Buchner funnel, and the precipitate dried at 120 °C. The dried precipitate was massed resulting in an 87% recovery of the EDTA. The filtrate was analyzed by AAS resulting in an 93% recovery of the Fe(III) in the S-1-2 fraction.

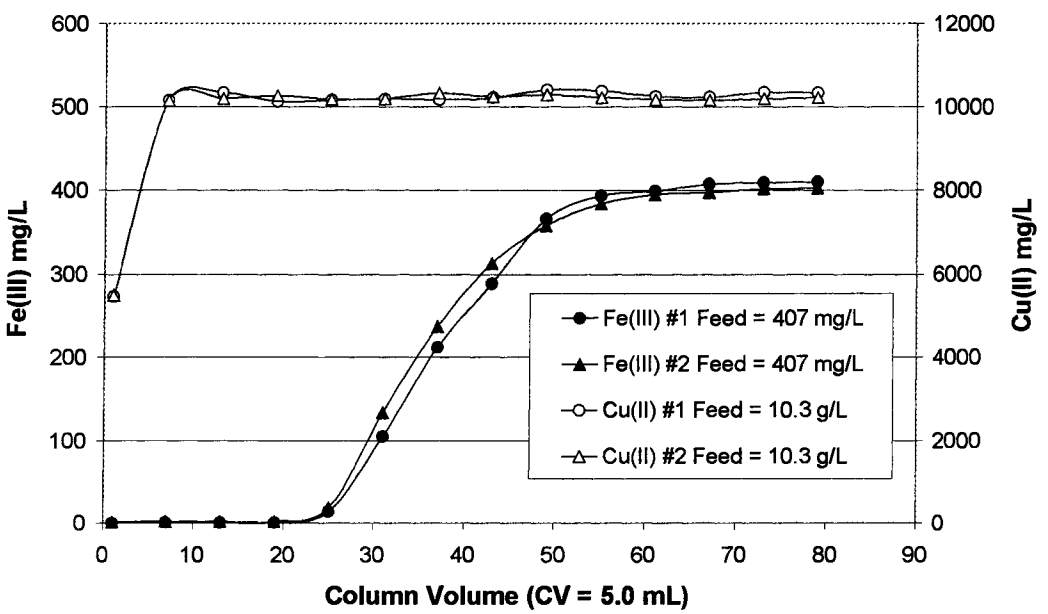

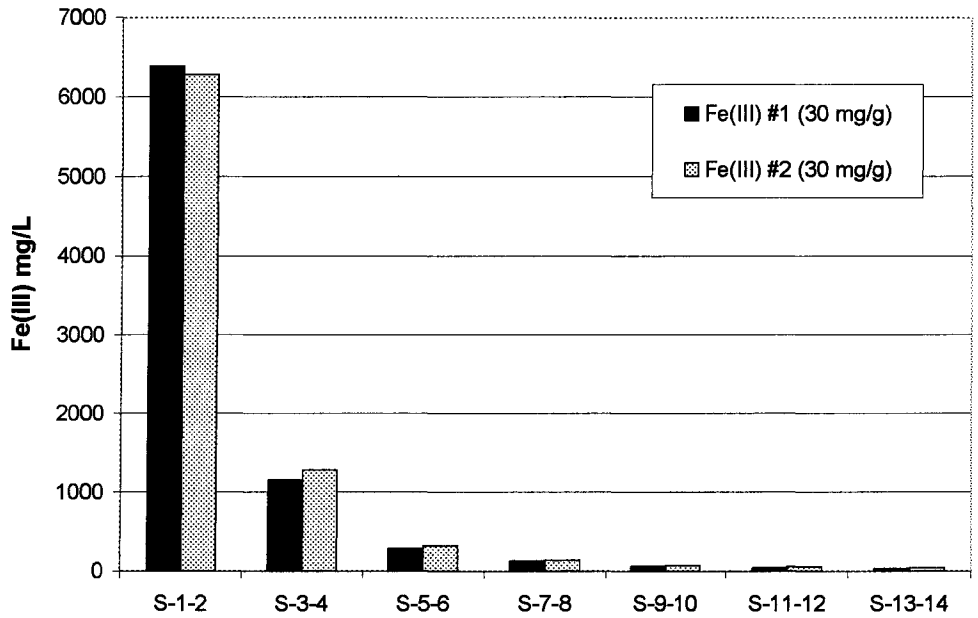

Figure 56. BPAP-CF 041504-DN synthetic Cu(II) electrowinning solution; breakthrough curves, 0.50 CV/min., 4.0 N H_2SO_4, 30 mg/g Fe(III) (top); strip fractions, 0.050 CV/min., 1.5 M EDTA (pH 10.6), 99% stripped (bottom).

Ga(III) separation from Al(III) was investigated at feed concentrations and pH similar to that found for a known mining solution. Ga(III) batch testing was initially carried out for BPAP, BP-5 (phosphinic acid), BP-6 (phosphonate) and BP-7 (phosphonate) discussed later in sections 3.13,3.14, and 3.15. BPAP exhibited the highest Ga(III) batch capacities of 42 and 56 mg/g at pH 1.0 and 2.1, respectively (Figure 57). Figure 58 shows the selectivity for Ga(III) over Al(III). Although capacity is moderate, favorable stripping kinetics were observed in the purification of Ga(III) to 92% purity (Figure 58).

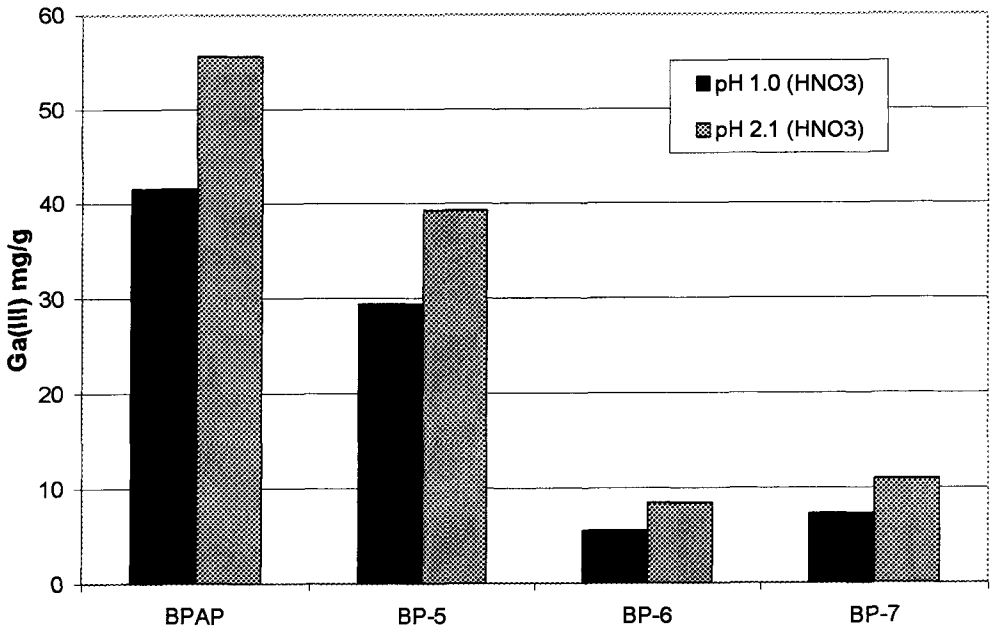

Figure 57. Ga(III) batch testing; BPAP-CF 041504-DN, BP-5-CF 120804-DN, BP-6-CF 021505-DN, BP-7-CF 022305-DN.

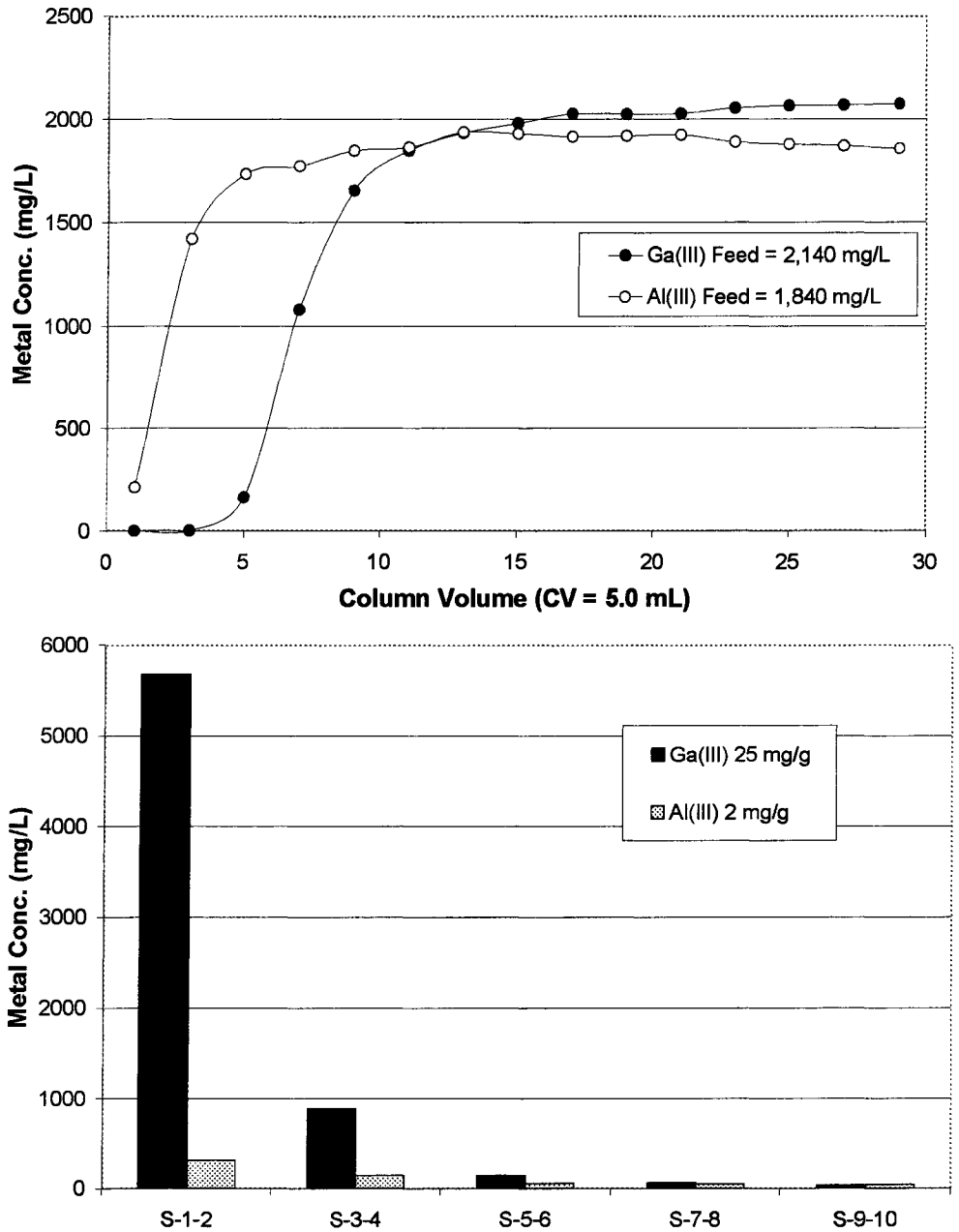

Figure 58. BPAP-CF 041504-DN; Ga(III)/Al(III) breakthrough curves, 0.50 CV/min., pH 1.0, (top); strip fractions, 0.50 CV/min., 1.0 M EDTA (pH 10.6) 92% Ga(III) purity (bottom).

Synthesis of diphenyl phosphinic polyallylamine composite via the Mannich reaction was pursued using the two-step synthesis as solubility of the reactant ligand was limited to these basic conditions (Scheme 13). This reaction pathway resulted in no mass gain to the starting composite BP-1, and was not further pursued.

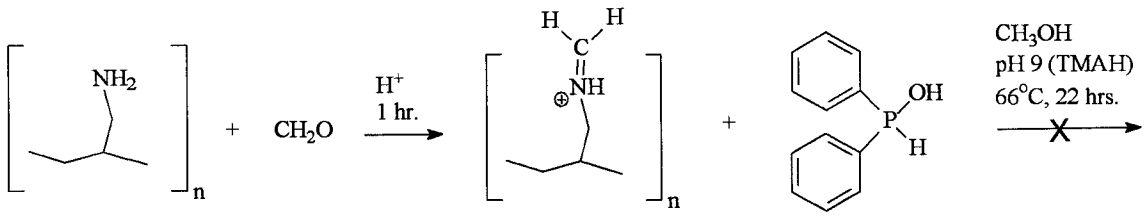

Scheme 13. Synthetic scheme of diphenyl phosphinic acid composite.

3.13 Phosphinic Acid Polyallylamine Composite (BP-5)

The phosphinic acid functionality was pursued aiming to improve stripping kinetics of rare earth elements. Scheme 14 illustrates the synthesis of BP-5 utilizing BP-1 via the Mannich reaction utilizing hypophosphorous acid.[57] Elemental analysis shows an available nitrogen to phosphorous ratio of 0.58 (Table 12). This composite exhibits the greatest functional group coverage density of any composite in this research group to date (2.1 mmol P/g). Eu(III) extraction was excellent (55 mg/g), as well as metal loading kinetics as shown in Figure 59 (top). Disappointingly only 26% of the loaded metal stripped when using sulfuric acid, similar to the performance of BPAP (Figure 59). Comparative testing with BPAP showed BP-5 to exhibit inferior Ga(III) (Figure 57) and Th(IV) (shown later in Figure 74 and **Error! Reference source not found.**) capacity even though BP-5 contains about 40% more functional group per gram of composite.

Table 12. Elemental analysis of BP-5.

Entry	Sample Name	Comp. Ref. #	C %	H %	N %	Cl %	P %	C mmol/g	H mmol/g	N mmol/g	Cl mmol/g	P mmol/g	N/P	N*/P
35	BP-5-CF	120804-DN	16.55	3.30	3.15	-	6.36	14	33	2.2	-	2.1	1.1	0.58

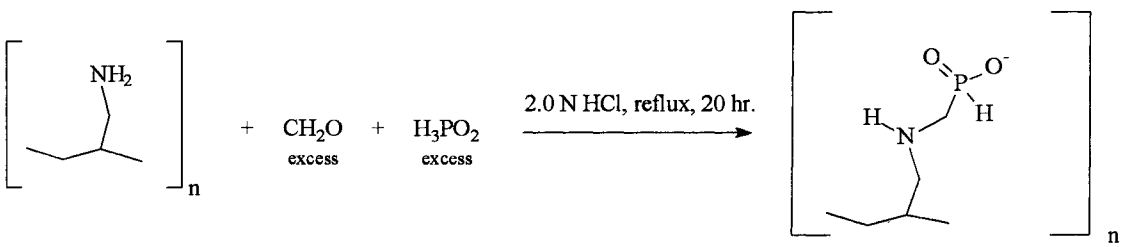

Scheme 14. Synthesis of BP-5.

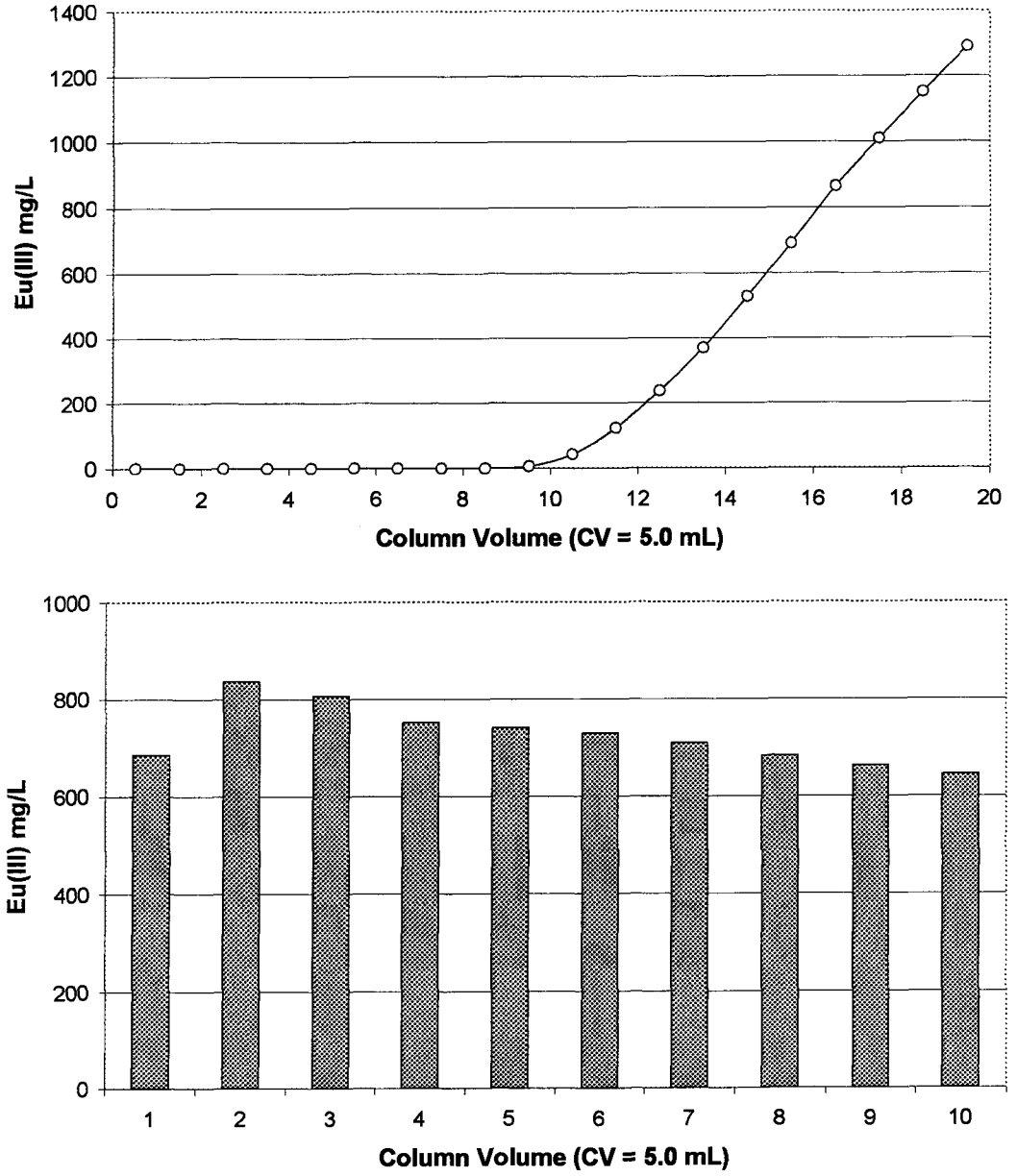

Figure 59. BP-5-CF 120804-DN; breakthrough curve, 0.50 CV/min., pH 5.5, 2.0 g/L Eu(III), 55 mg/g capacity (top); strip fractions, 0.50 CV/min., 9.0 N H_2SO_4, 24% stripped (bottom).

3.14 Methyl/Dimethyl Phosphonate Polyallylamine Composite (BP-6)

The phosphonate functionality was pursued in hope of achieving complete stripping of trivalent metals such as Fe(III) and Eu(III). Attempts to produce the phosphonate functionality via methylation of BPAP were unsuccessful as discussed in

section 54 (Figure 51). Dimethyl (3-bromopropyl) phosphonate was produced via the Michaelis-Arbuzov rearrangement as shown in Scheme 15. Figure 60 shows NMR spectra of the 82% pure product solution containing dimethyl (3-bromopropyl) phosphonate.

Table 13. Elemental analysis of BP-6.

Entry	Sample Name	Comp. Ref. #	C %	H %	N %	Cl %	P %	C mmol/g	H mmol/g	N mmol/g	Cl mmol/g	P mmol/g	N/P	N*/P
36	BP-6-CF	021505-DN	19.54	3.11	4.39	-	3.33	16	31	3.1	-	1.1	2.9	1.5

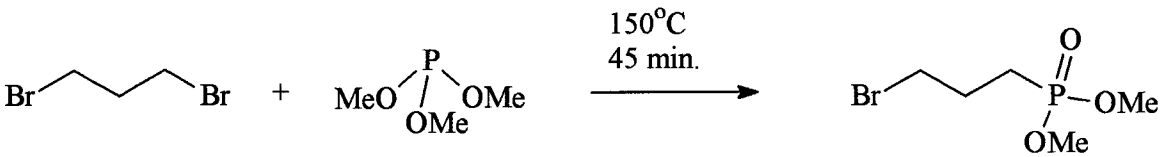

4 eq. eq.

Scheme 15. Synthesis of dimethyl (3-bromopropyl) phosphonate.

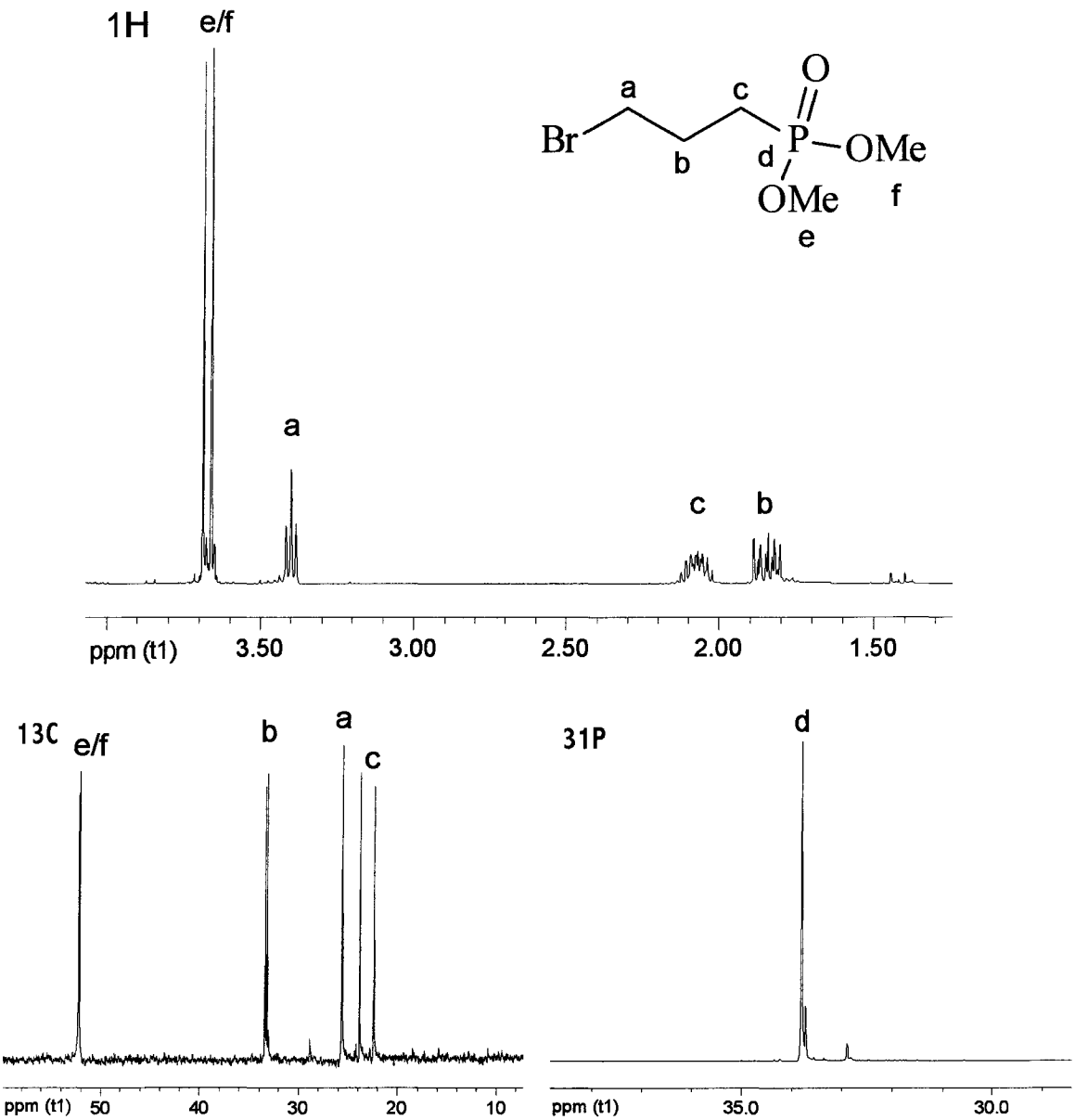

Figure 60. ^{1}H, ^{13}C, and ^{31}P NMR spectra of Dimethyl (3-bromopropyl) phosphonate isolate.

Scheme 16 illustrates the synthesis of BP-6 by means of a nucleophilic substitution utilizing BP-1. The general schematic structure of both BP-6 and BP-7 is shown in Figure 61. Elemental analysis shows good coverage of the ligand with an available nitrogen to phosphorous ratio of 1.5 (Table 13). ^{13}C and ^{31}P solid state NMR spectra for BP-6 are included in Figure 62. The mono and dimethoxy substituents are suggested by the broad

packet between 50 and 65 ppm (Figure 62, left), and more convincingly by the presence of two ^{31}P peaks seen in Figure 62 (right). Phosphorous analysis by NMR was used to characterize the ratio of dimethyl to methyl phosphonate groups.[58,59] Integration of the deconvoluted ^{31}P spectrum gives a phosphonate diester to monoester ratio of 1.9:1 (65% : 35%).

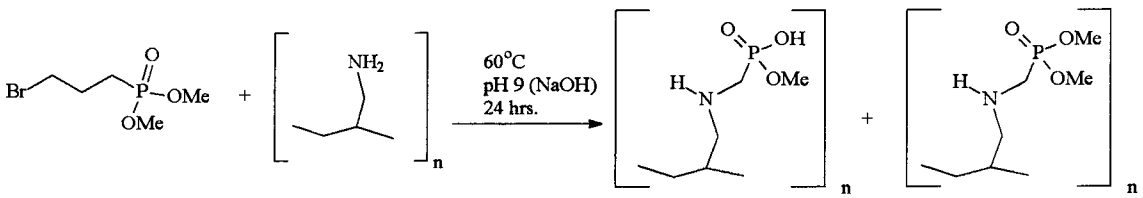

Scheme 16. Synthesis of BP-6.

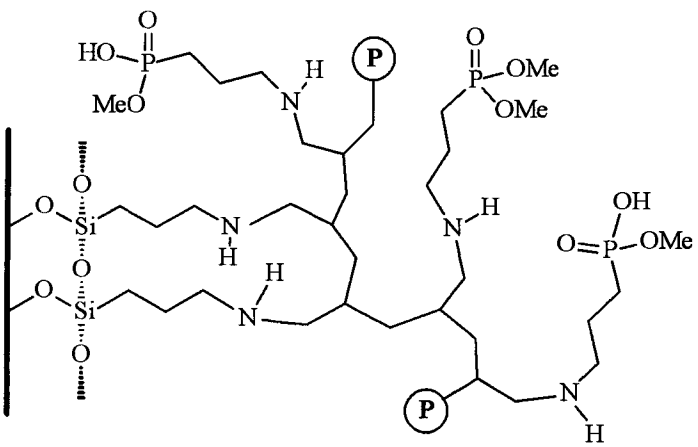

Figure 61. Schematic structure of BP-6 (and BP-7).

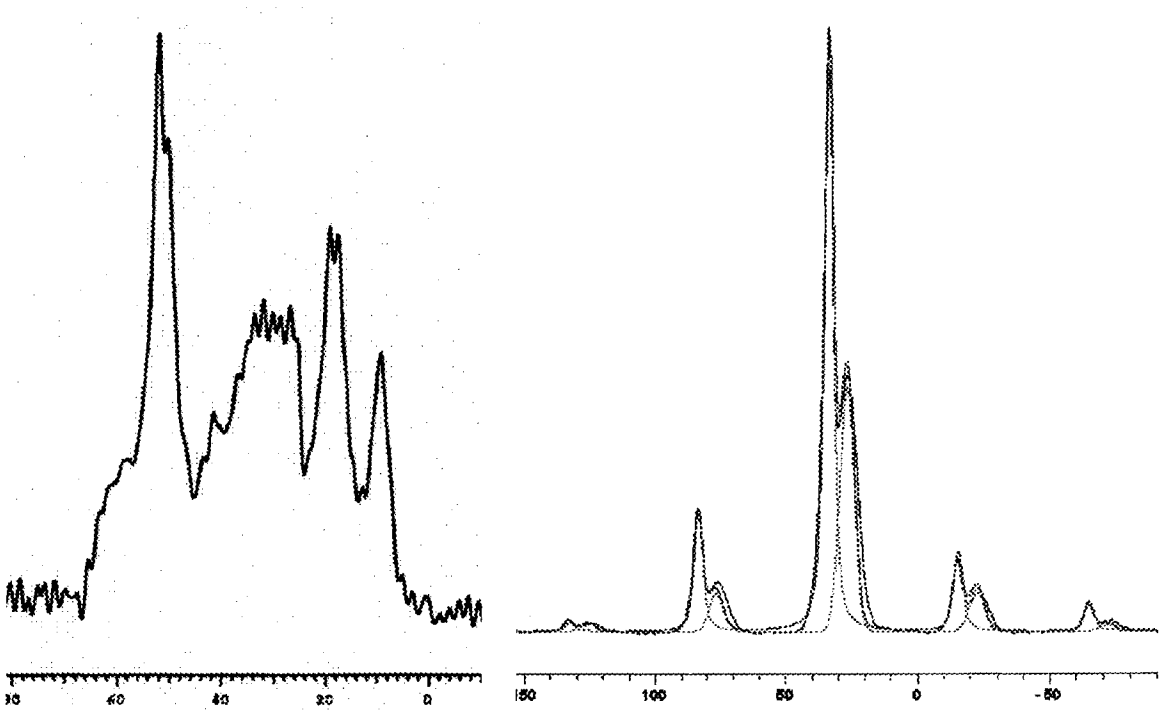

Figure 62. ^{13}C (left) and ^{31}P (right) solid state NMR of BP-6.

3.15 Methyl/Dimethyl Phosphonate Polyallylamine Composite (BP-7)

The synthesis of BP-7 was pursued in conjunction with BP-6 utilizing the reagent ligand dimethyl (3-bromopropyl) phosphonate (Scheme 15 and Figure 60). Scheme 17 illustrates the synthesis of BP-7 by means of a nucleophilic substitution utilizing BP-1. Triethylamine (TEA) was used as a proton scavenger instead of sodium hydroxide in hopes of minimizing hydrolysis of the diester. Elemental analysis shows good coverage of the ligand with an available nitrogen to phosphorous ratio of 1.7 (Table 14). ^{13}C and ^{31}P solid state NMR spectra for BP-6 are included in Figure 63. Integration of the deconvoluted ^{31}P spectrum gives a phosphonate diester to monoester ratio of 1:1.5 (41% : 59%). Unexpectedly increased hydrolysis was observed with respect to BP-6 (35% as monoester).

Table 14. Elemental analysis of BP-7.

Entry	Sample Name	Comp. Ref. #	C %	H %	N %	Cl %	P %	C mmol/g	H mmol/g	N mmol/g	Cl mmol/g	P mmol/g	N/P	N*/P
37	BP-7-CF	022305-DN	18.49	3.55	4.70	-	3.17	15	35	3.4	-	1.0	3.3	1.7

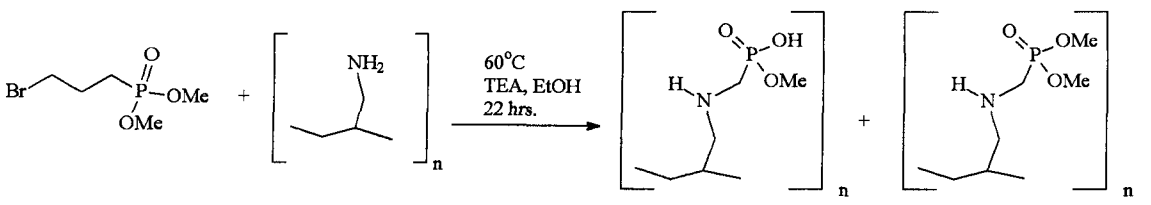

Scheme 17. Synthesis of BP-7.

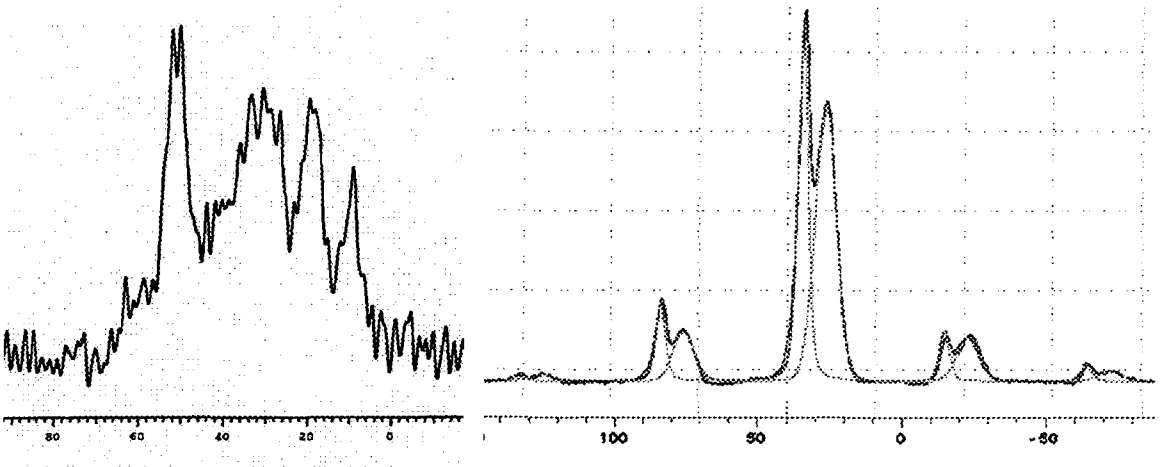

Figure 63. ^{13}C (left) and ^{31}P (right) solid state NMR of BP-7.

4 RESULTS AND DISCUSSION – ADDITIONAL APPLICATIONS

4.1 Pilot Scale Column Testing

Design of a pilot scale column was pursued to obtain backpressure and performance data to scale. Figure 64 shows the set-up using a high-flow pump (Micropump, model 405), backpressure gauge and four T-valves to allow for top or bottom feed capability. The columns end-caps were drilled to $3/8^{th}$ inch diameter, and screens were replaced with a large and rigid 500 μm screen supporting an inside 46 μm screen. A blue translucent 4" tube was used as a shatter guard as the maximum backpressure of the column was rated at 70 psi. All valves and fittings should be made from an acid resistant material such as Teflon® or Kynar®.

BPAP was produced from Qingdao Haiyang silica gel due to larger particle diameter of 150-250 micron. Fe(III) was tested for loading and stripping performance over 30 load/strip cycles. A 3.1 g/L Fe(III) solution was prepared as the metal loading solution, and adjusted to pH 1.5 using sulfuric acid. Rinse and regeneration solution was pH 2.0 (H_2SO_4) water, and strip solution used was 9.0 N H_2SO_4. Flowrates and backpressures in parenthesis were as follows: loading 0.32 CV/min. (33 psi), rinsing 0.15 CV/min. (16 psi), stripping 0.4-0.3 CV/min. (70 psi), regeneration 0.15 (0.4-0.2 psi). Breakthrough testing was carried out for cycle 1, 2, 10, 20 and 30 (Figure 65). Flowthrough testing was done for the remaining cycles, and the load and strip capacities are shown in Figure 66. Flowthrough capacities quickly decline due to incomplete stripping of Fe(III) from BPAP initially stripping only 32% of loaded iron, initially loading 47 mg/g Fe(III). Strip capacities were steady between 15-20 mg/g (strip problem resolved in section 3.12).

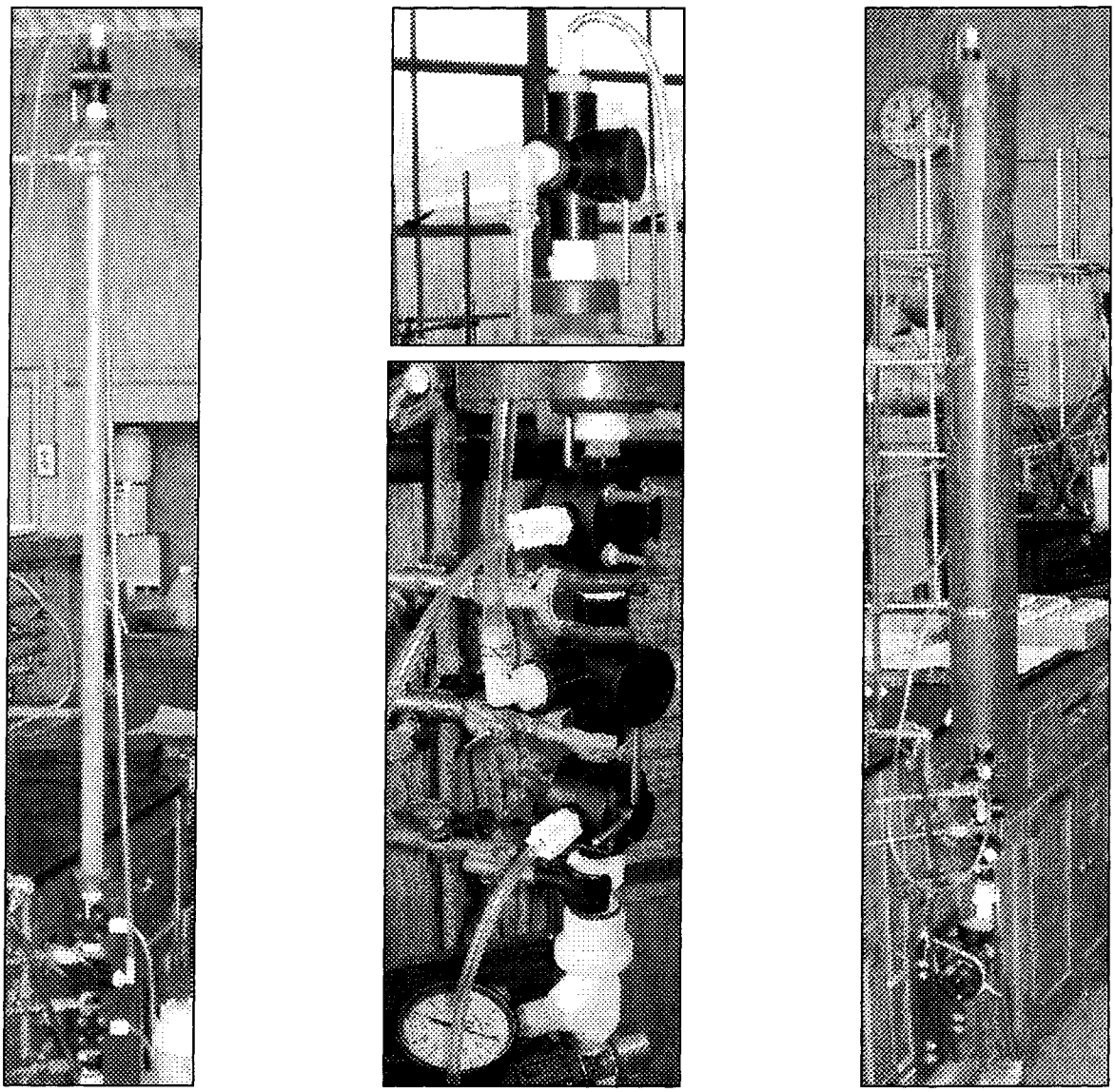

Figure 64. Pilot scale column design for testing BPAP-QH 1201403-DN.

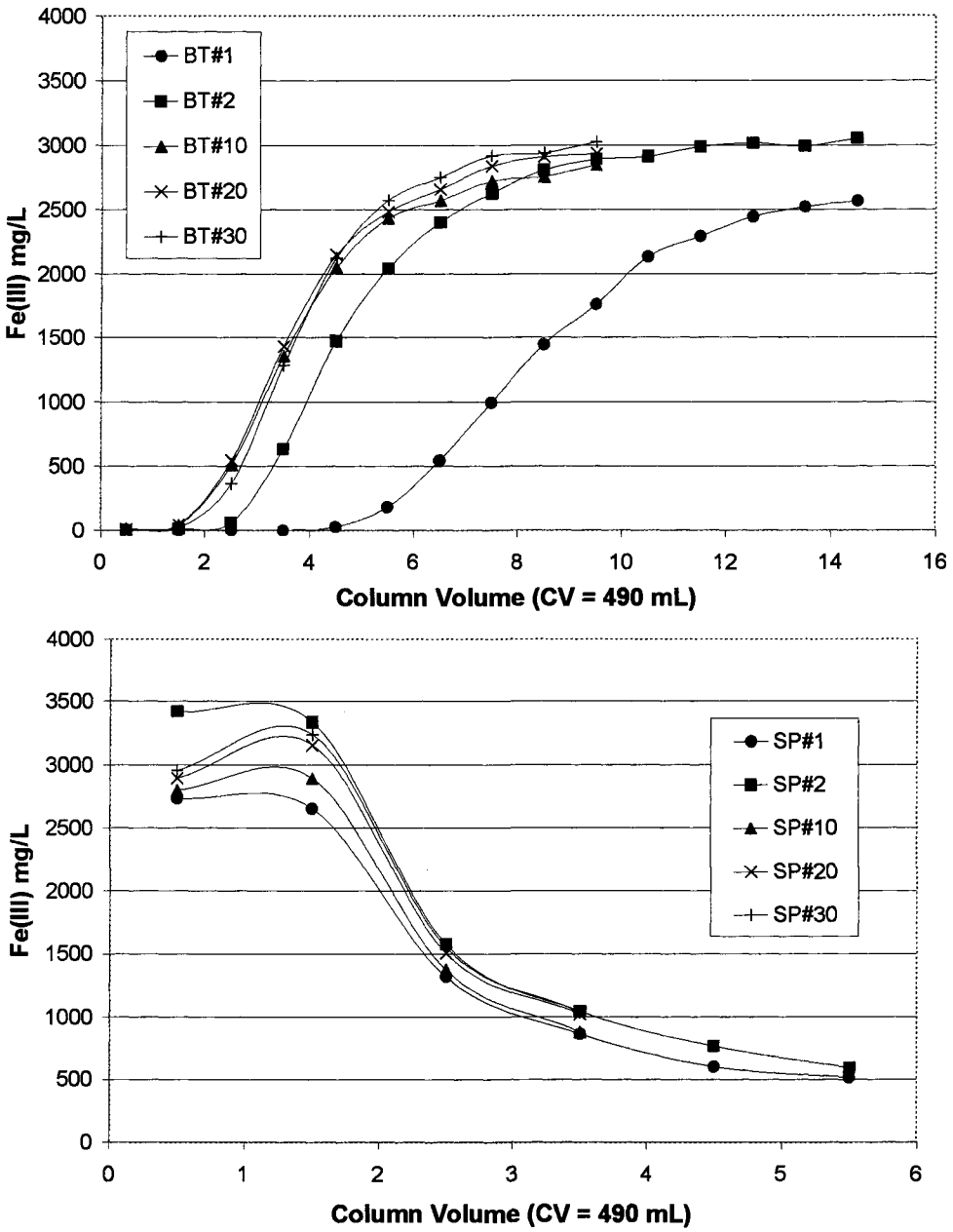

Figure 65. BPAP-QH 121403-DN pilot scale testing over 30 load/strip cycles; breakthrough curves, 0.32 CV/min., pH 1.5, 3.1 g/L Fe(III) (top); strip curves, 0.42 – 0.27 CV/min., (70 psi), 9.0 N H_2SO_4 (bottom).

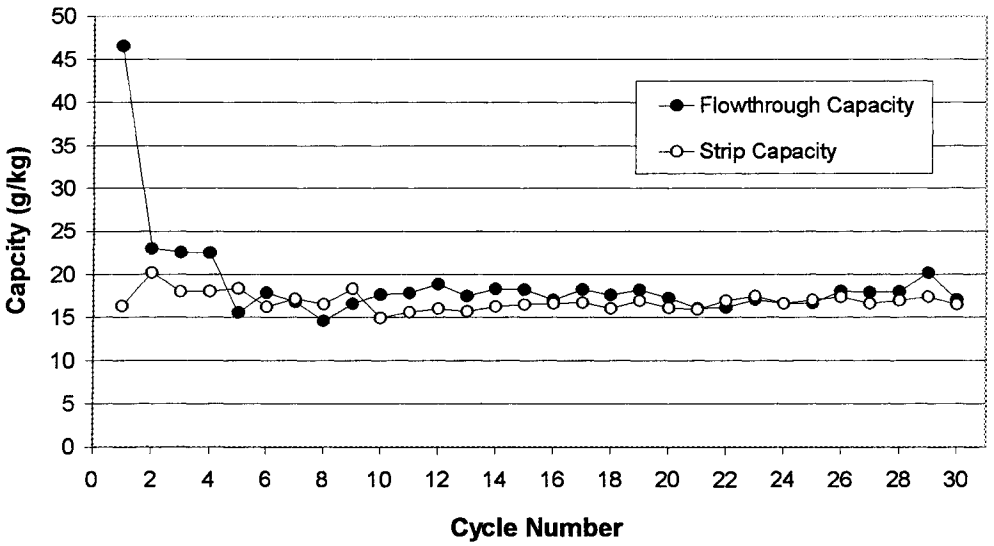

Figure 66. BPAP-QH 121403-DN pilot scale flowthrough and strip capacities over 30 load/strip cycles.

4.2 Rare Earth Element Separation

This study evaluated the recovery of rare earth elements (REE) from the Mt. Weld (Laverton, Australia) REE sulfate leach solution pH 1.0. The projects goal was to separate the rare earth elements Ce(III), La(III), Nd(III), Sm(III), and Pr(III) from the solution matrix which contains Fe(III), Mn(II), Ca(II), Mg(II), Al(III), Zn(II), Ti(IV), and other lower concentration trace metals. WP-4 and BPAP were produced on Crosfield silica gel for Fe(III) and REE extraction, respectively. Single element Fe(III) and Eu(III) testing was first accomplished to determine approximate target metal capacities. The two step lanthanide separation initially used 9.0 N sulfuric acid as the strip solution for both WP-4 and BPAP. These results are not included within this thesis as were repeated below with an improved stripping agent. Single element Eu(III) testing of BPAP showed improved results using 2 M phosphorous acid. An additional and separate study using a 1.0 M EDTA strip solution showed similarly reproducible results for Eu(III) extraction (Section 3.12), and could be used for the lanthanide separation process reported below.

The REE leach solution contains over 24 g/L in total Ln(III) ions. Dilution to 50% concentration using water was used to prevent REE precipitation as observed in the minus Fe(III) effluent from WP-4 in the initial trial (results not shown). Precipitation was almost eliminated after dilution of the feed solution, but was slightly evident in CV 3 of WP-4 treatment due to matrix effects. Dilution also resulted in increased resolution for the REE extraction using BPAP, as REE breakthrough is extremely rapid at these very high feed concentrations.

Figure 67 displays the overall results from the two step purification of REEs discussed in greater detail in the following paragraphs. This graph displays the initial REE feed solution metal concentrations, WP-4 treated effluent, and BPAP recovery solution. The feed solution concentrations are shown at 50% dilution thereby increasing the REE leach solution pH from 1.0 to 1.3. The WP-4 flowthrough solution contained low levels of both Fe(III) and Ti(IV) due to extraction, and remained at pH 1.3. WP-4 flowthrough solution was subsequently treated using BPAP. Figure 67 shows the 2 M H_3PO_4 strip solution containing REEs at 99% purity [>1% Al(III), >>1% Ca(II), Fe(III), Ti(IV)], originally at 87% purity predominately due to Fe(III), Mn(II), and Ca(II) ions.

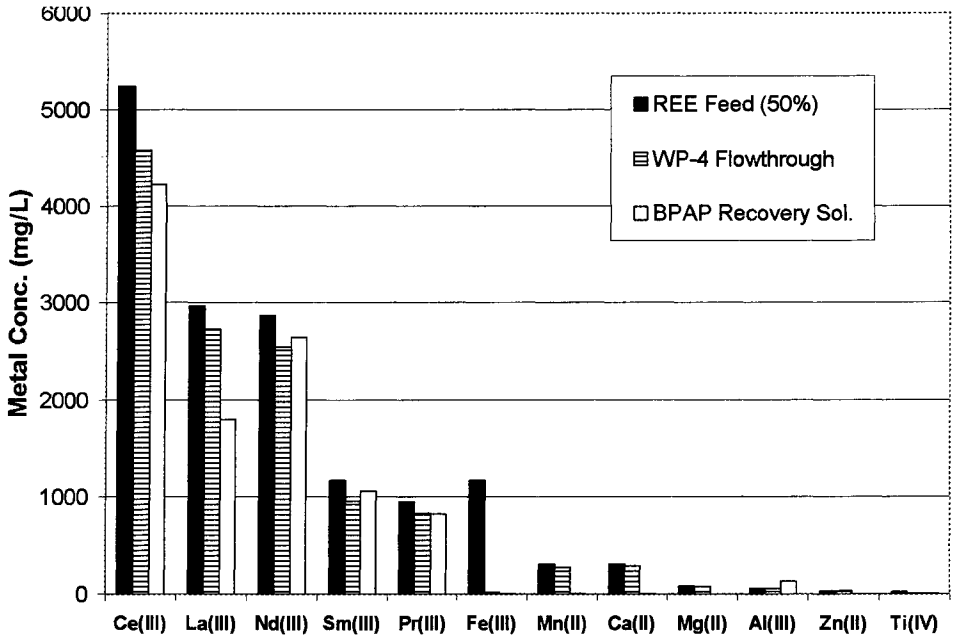

Figure 67. Rare earth element purification results using WP-4-CF 101205-DN and BPAP-CF 041504-DN.

A 10 cc syringe was packed with 12 mL (7.0 g) of WP-4. Figure 68 shows the breakthrough curve for Fe(III) removal using WP-4 obtained by flame AAS, and the corresponding strip profile in Figure 68. The first 10 CV of flow through were sampled for ICP analysis, and then combined for subsequent REE recovery via BPAP. Excellent separation of Fe(III) from REEs is evident from the breakthrough curves shown in Figure 69. Figure 70 displays the lower level metals all showing low affinity with the exception of Ti(IV) co-loading with Fe(III). ICP analysis of the WP-4 strip solution shows an 11 fold concentration of both Fe(III) and Ti(IV) and virtually no affinity towards the REEs.

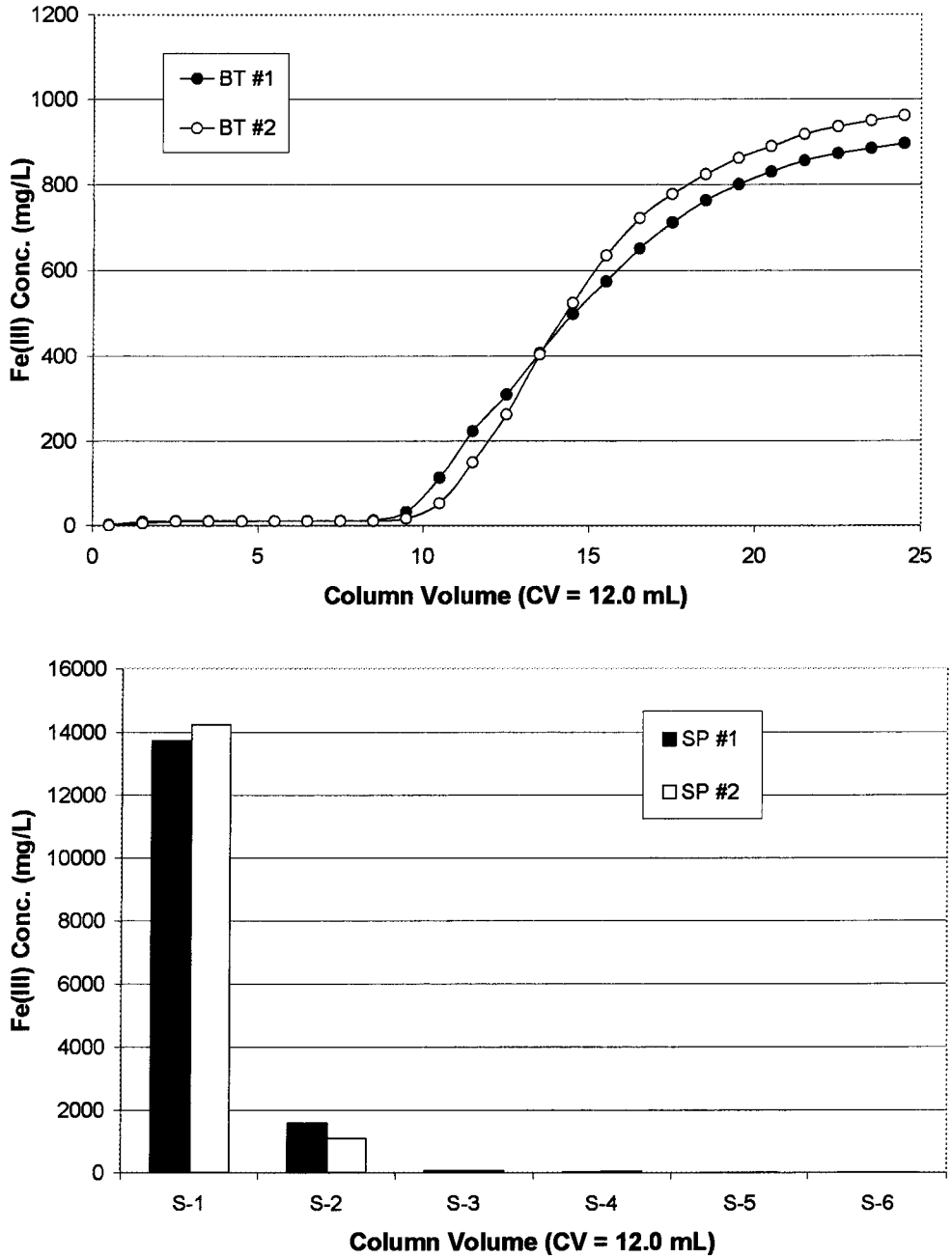

Figure 68. WP-4-CF 101205-DN load/strip cycle #1 and #2 by flame AAS; breakthrough curves, 0.50 CV/min., pH 1.3, 1.0 g/L Eu(III) (top); strip profiles, 0.50 CV/min., 9.0 N H_2SO_4, 26 mg/g capacity, ~100% stripped (bottom).

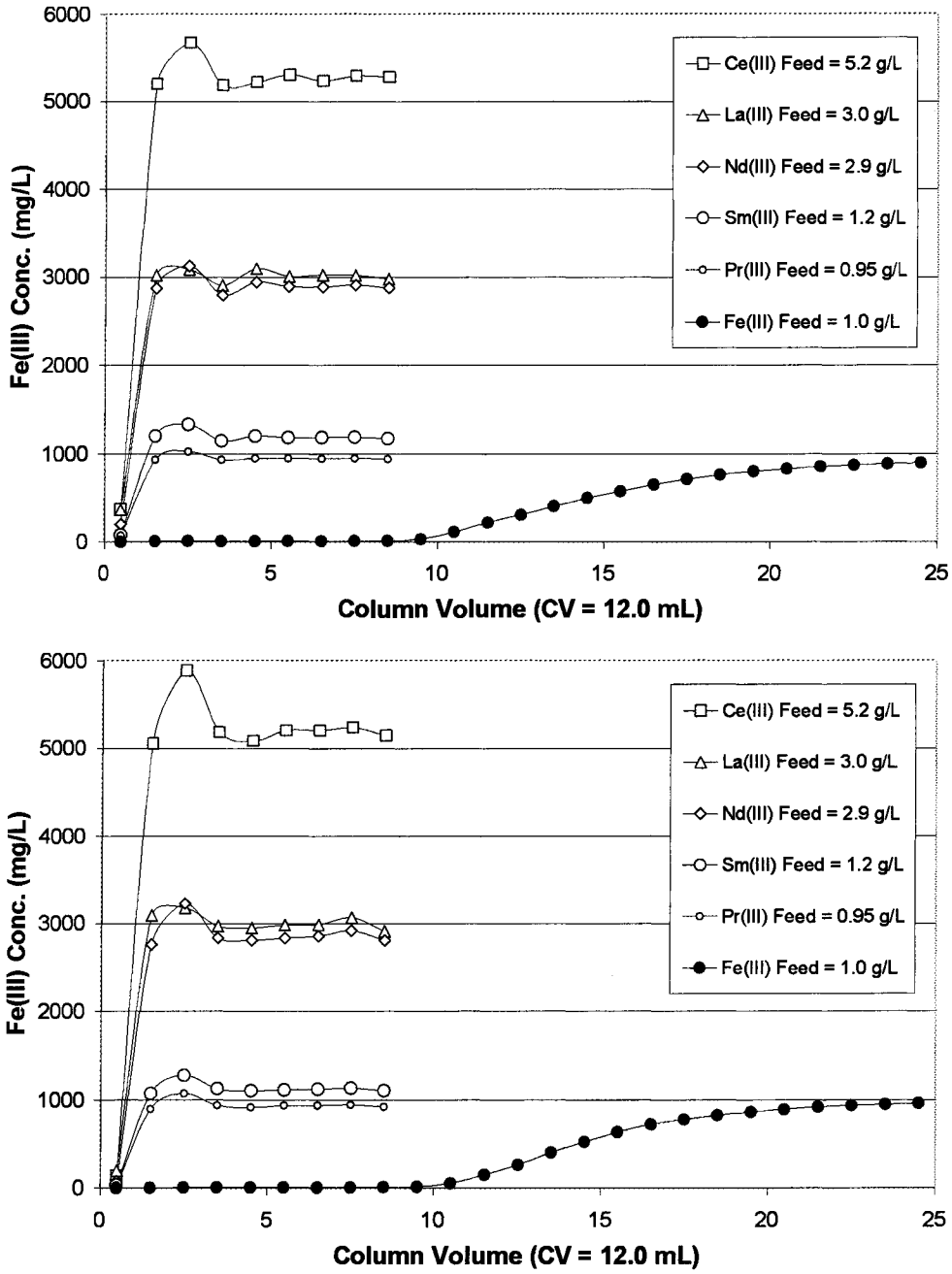

Figure 69. WP-4-CF 101205-DN breakthrough test #1 (top) and #2 (bottom) by ICP analysis (high conc. metals), 0.50 CV/min., pH 1.3.

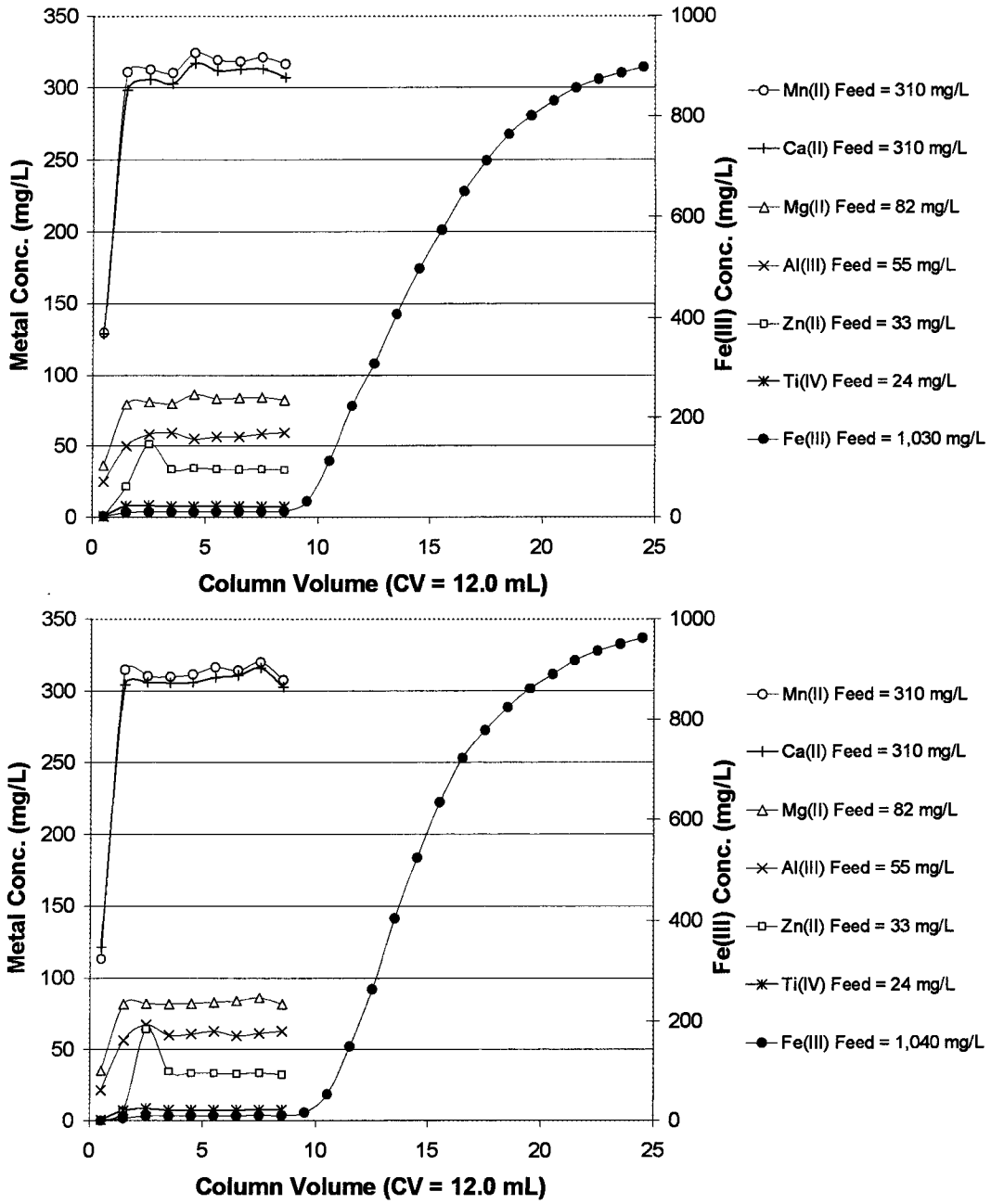

Figure 70. WP-4-CF 101205-DN breakthrough test #1 (top) and #2 (bottom) by ICP analysis (low level metals), 0.50 CV/min., pH 1.3.

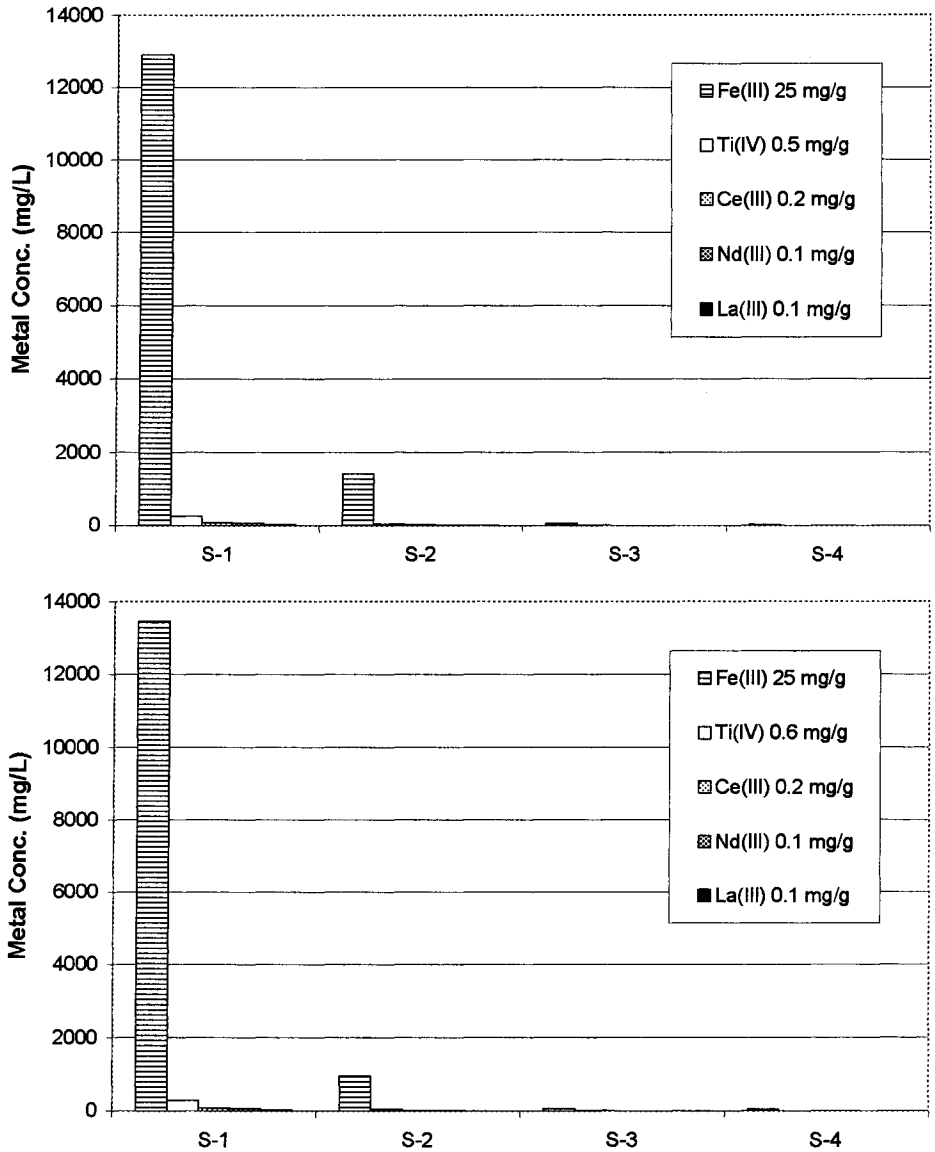

Figure 71. WP-4-CF 101205-DN strip profiles #1 (top) and #2 (bottom) by ICP analysis, 0.50 CV/min., 9.0 N H_2SO_4.

Loading and stripping were reproduced on the same column (9.0 mL, 4.9 g) as shown in Figure 72 and Figure 73. Reproducibility confirms complete stripping, which was not achieved when using sulfuric acid as the strip solution. The recovery solution was 99% pure in REEs showing 1% Al(III) and only trace levels of Ca(II), Fe(III) and Ti(IV) (Figure 73).

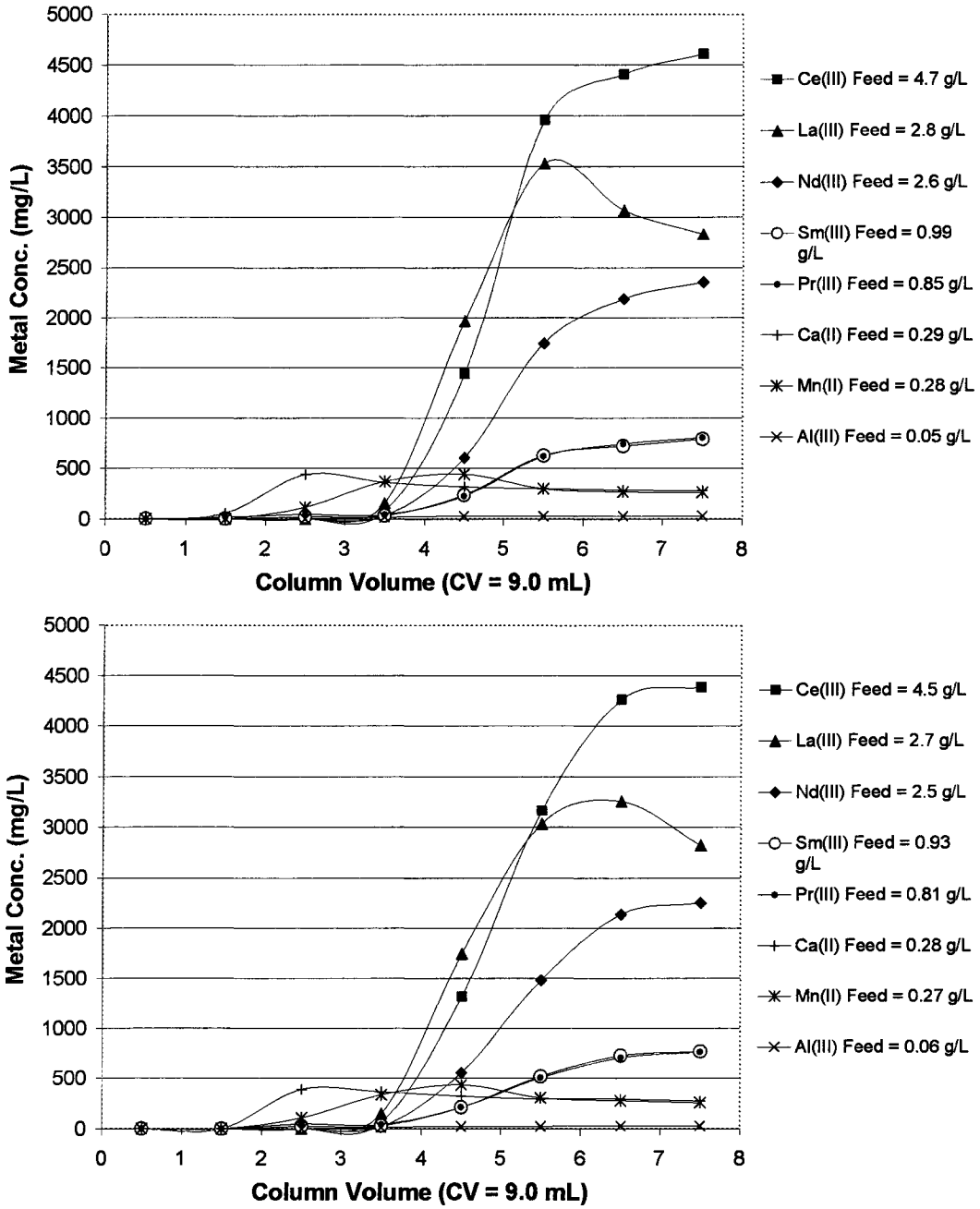

Figure 72. BPAP-CF 041504-DN breakthrough curves for REE recovery, load cycle #1 (top), #2 (bottom), 0.50 CV/min., pH 1.3.

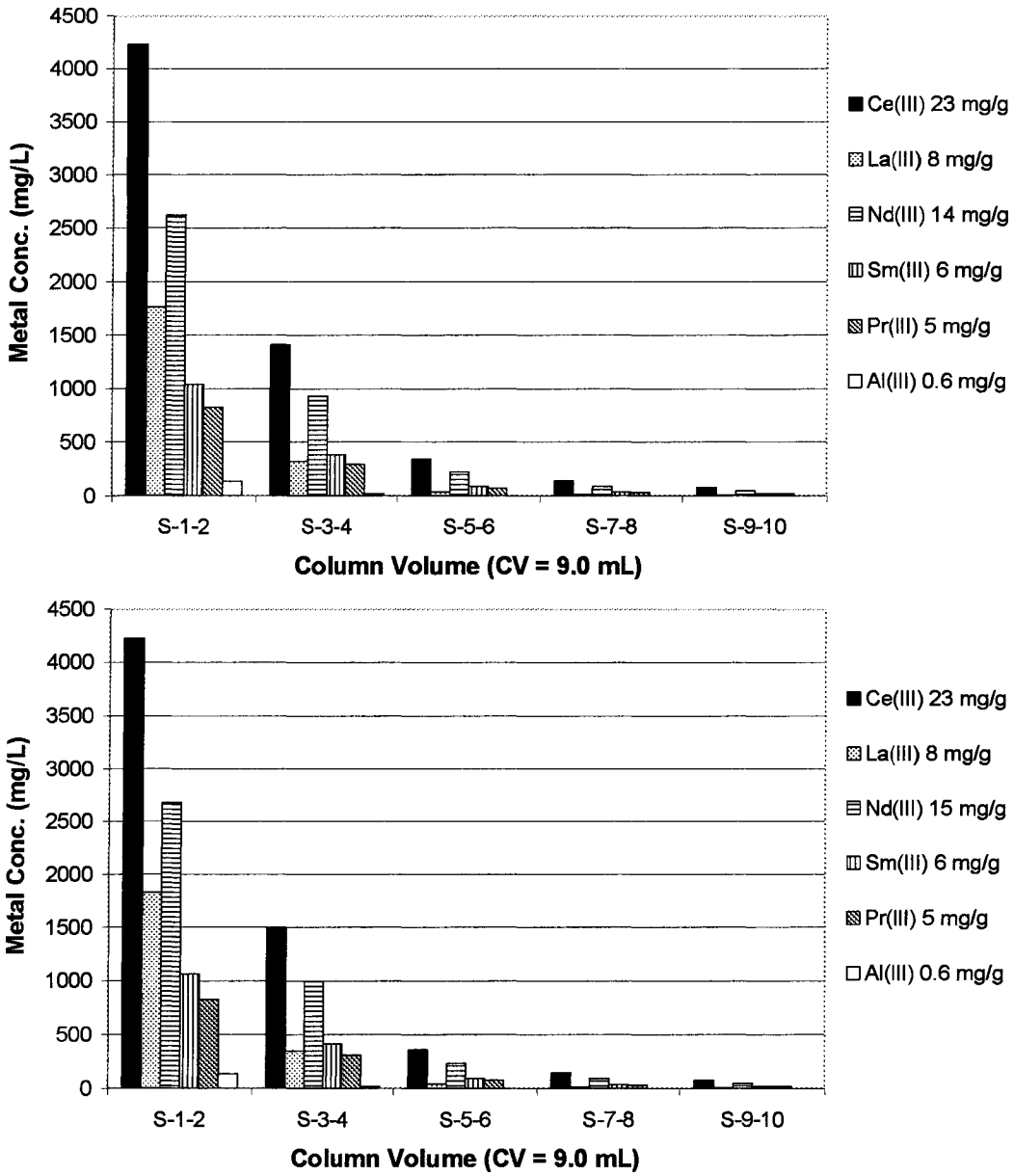

Figure 73. BPAP-CF 041504-DN strip profiles for REE recovery, strip cycle #1 (top), #2 (bottom), 0.50 CV/min., 2.0 M H_3PO_3, 56 mg/g Ln(III) capacity, 99% Ln(III) purity [1% Al(III), <<1% Ca(II), Fe(III) Ti(IV)]

4.3 Actinide Element Separation

Interest in recovery of actinide elements led to a preliminary investigation of Th(IV) batch capacities on eight selected composites. A pH profile was constructed for Th(IV) batch capacity at pH 1.0, 1.9 and 2.9 for each composite. BPAP and BP-5 showed the highest capacities with very little pH dependence. BPSU showed the next highest

Th(IV) capacity, although diminishes rapidly with decreasing pH. BP-1 follows similarly with an even greater loss in capacity with decreasing pH. Phosphonate composites BP-7 and BP-6 exhibit mediocre capacities, but do not have significant dependence upon pH.

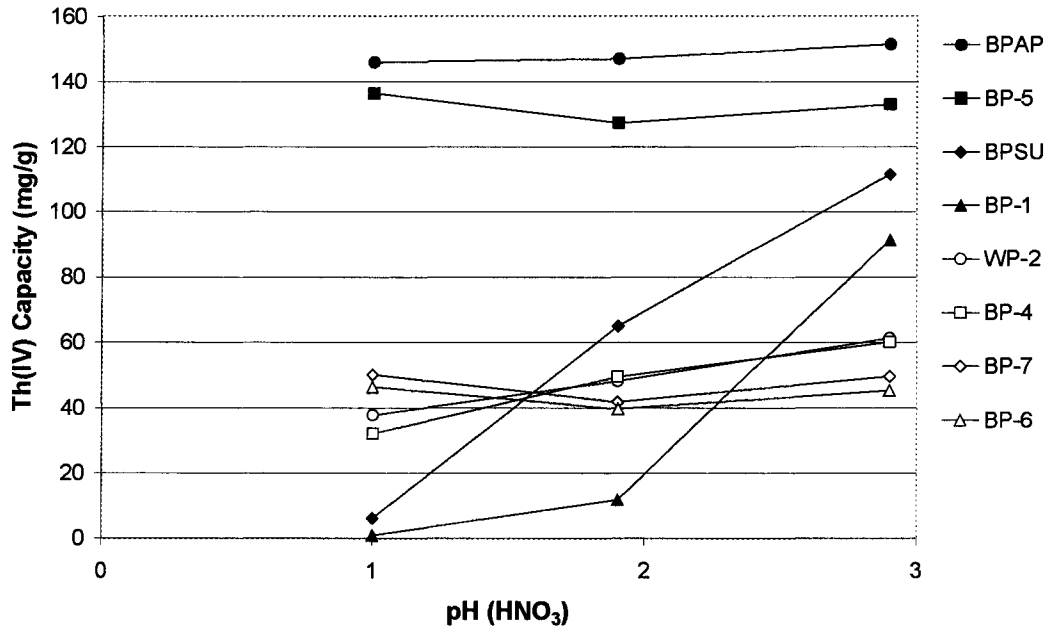

Figure 74. pH profile Th(IV) batch capacities for various composites.

BPAP, BP-5, BP-7 and BPSU were then tested for breakthrough performance under flow conditions. The 4.2 g/L Th(IV) feed solution was used at the intrinsic pH of 2.9. BPAP and BP-5 demonstrate ideal loading kinetics and marked extraction capacity towards Th(IV) as evident in Figure 75 (top). BP-7 exhibits similar kinetic qualities although mediocre capacity relative to BPAP and BP-5. Conversely BPSU has poor kinetic qualities but excellent Th(IV) capacity. In congruence with the pH dependency of BPSU and the poor kinetic affinity toward Th(IV), the stripping kinetics are very good as shown in Figure 75 (bottom). Stripping of BPAP, BP-5 and BP-7 proved unsuccessful using 2 M H_3PO_3, as strip percentages were 34, 7 and 3% respectively.

Poor stripping of BPAP may in turn be an attribute for certain applications. Th(IV) was used as a model actinide, potentially radioactive waste material. Vitrification of the

loaded composite for burial in a designated waste repository would benefit from the non-leaching characteristics.

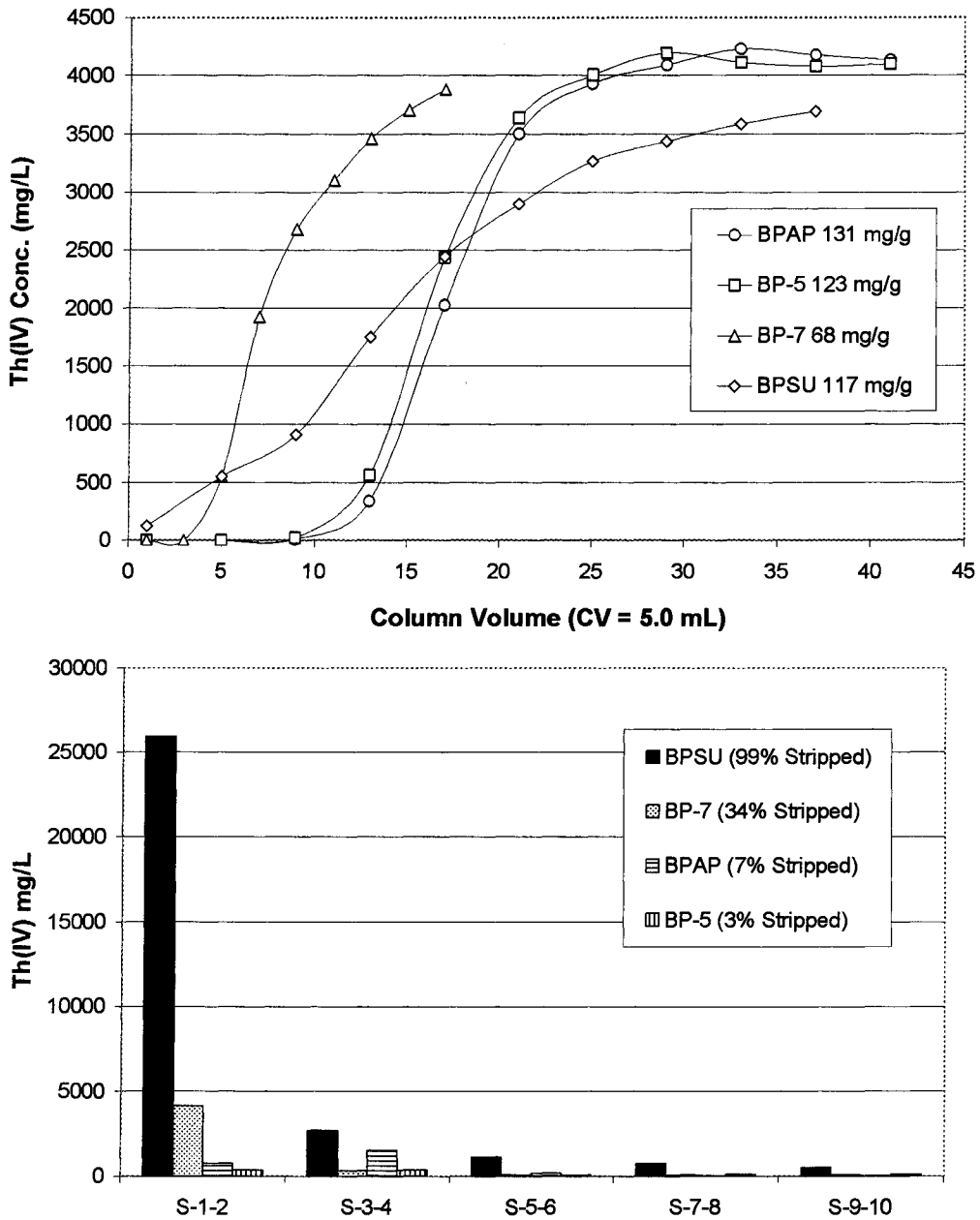

Figure 75. BPSU-CF 080404-DN, BP-7-CF 022305-DN, BPAP-CF 041504-DN, BP-5-CF 120804-DN; Th(IV) breakthrough curves, 0.50 CV/min., pH 2.9 (top); strip profiles, 0.20 CV/min., 2.0 M H_3PO_3 (bottom).

4.4 Acid Mine Drainage Treatment

The lake that now occupies the Berkeley Pit at Butte, MT, is a well-known example of a highly acidic pit lake with high levels of metals and sulfate. It has a pH value near 2.6 and contains high concentrations of iron, zinc, magnesium, calcium, aluminum, manganese, and copper as revealed in Table 15.[60,61] The Pit's water chemistry has varied over the past twenty years due to natural and anthropogenic perturbations (and analytical variances). The maximum contaminant level (MCL) or secondary maximum contaminant level was included in Table 15 to give reference to the magnitudes of the listed metal concentrations. The maximum contaminant level is the highest level of a contaminant that is allowed in drinking water. Secondary levels are non-enforceable guidelines regulating contaminants that may cause cosmetic effects (such as skin or tooth discoloration) or aesthetic effects (such as taste, odor, or color) in drinking water. A more appropriate standard is the total maximum daily load (TMDL). A TMDL is the sum of the allowable loads of a single pollutant from all contributing point and nonpoint sources that a water body can receive to meet water quality standards. Anticipated TMDL submittals are set for December 31st, 2007.

Table 15. Metal concentrations (mg/L) of Berkeley Pit Lake water (at various depths), and Montana water quality standards.

	SO_4	Fe	Zn	Mg	Ca	Al	Mn	Cu	Cd	As
Berkeley Pit Water (mg/L)										
Depth (ft)										
0	6345	270	378	430	512	195	179	86.8	1.84	<0.22
50	8994	892	578	538	494	281	212	145	2.39	0.34
500	9105	986	580	536	494	281	209	177	2.43	0.78
Montana Water Quality Standards (mg/L)										
ALS-A	***	***	0.067	***	***	0.750	***	0.007	0.001	0.340
ALS-C	***	1.000	0.067	***	***	0.087	***	0.005	<0.001	0.150
HHS-SW	***	***	2.00	***	***	***	***	1.30	0.005	0.018
HHS-GW	***	***	2.00	***	***	***	***	1.30	0.005	0.020
MCL	250*	0.3*	5.0*	***	***	0.05-0.2*	0.05*	1.30	0.005	0.010**

Aquatic Life Standards - Acute (ALS-A)
Aquatic Life Standards - Chronic (ALS-C)
Human Health Standards - Surface Water (HHS-SW)
Human Health Standards - Groundwater (HHS-GW)
Maximum Contaminant Level (MCL)
*** Secondary maximum contaminant level**
**** Effective Oct. 31, 2001; Mandated Jan. 2006**
***** Not determined**

In February of 2002 fifty-five gallons of Berkeley Pit water was collected (Figure 76) from Butte, Montana and brought to The University of Montana (Missoula, Montana). Oxidation of Fe(II) was anticipated to occur following sampling. The barrel was pressurized with nitrogen which was displaced by the sampled water. In Missoula (two hours after sampling) the barrel's headspace was again pressurized with nitrogen. In spite of the mentioned efforts the Fe(II) did rapidly oxidize to Fe(III) before any studies commenced.

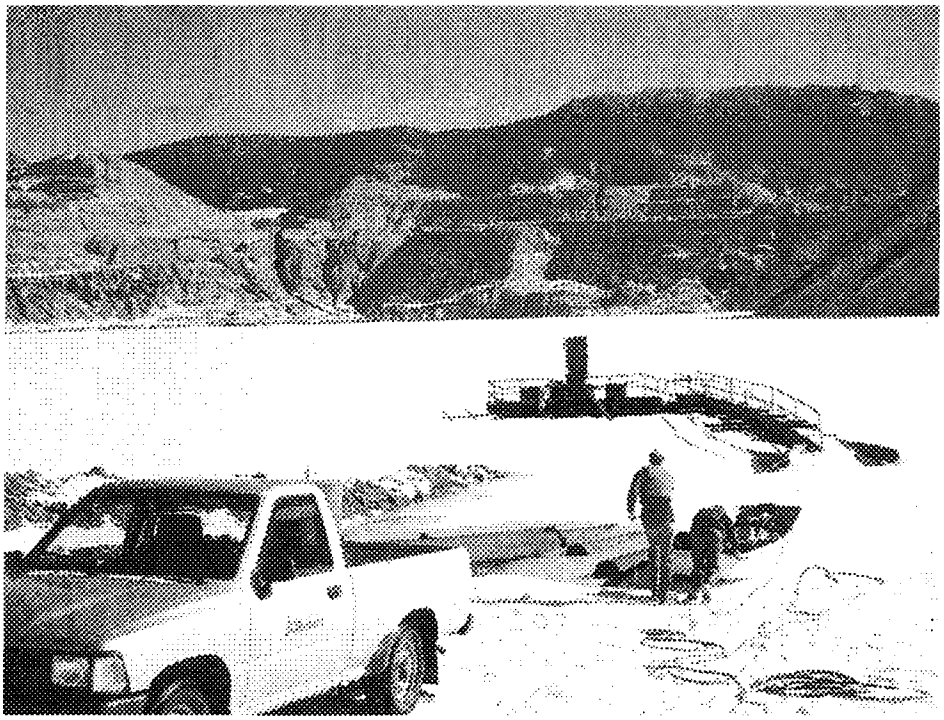

Figure 76. Sampling Berkeley Pit Lake water, February 2002.

Numerous treatment pathways have been investigated aiming to recover copper(II), zinc(II), and manganese(II) from the Berkeley Pit Lake. All strategies first target Cu(II), followed by Zn(II), and then Mn(II). This order of metal recovery is explained by the Irving-Williams effect or series (Figure 6).[20] Fe(III) and Al(III) interfere in the separation and recovery of the mentioned target metals. One treatment strategy involves removing Fe(III) before Cu(II) recovery. BPAP successfully separated Fe(III) from the three target metals as illustrated in Figure 77. On this first load cycle Fe(III) levels were reduced to less than 100 ppb for 10 CV, less than 1 ppm until 20 CV of treatment, and exhibited a flowthrough capacity of 40 mg/g. Co-loading of aluminum afforded a 7 mg/g Al(III) flowthrough capacity. Elution of Fe(III) has proven difficult using BPAP as revealed in Figure 77. After stripping with ten column volumes of 12.6 N (35%) H_2SO_4 at a 0.10 CV/min. flowrate, only 59% of the loaded Fe(III) eluted from the column. In similar

fashion just 52% of the loaded Al(III) eluted. For this reason selective removal of Fe(III) using BPAP is not ideal.

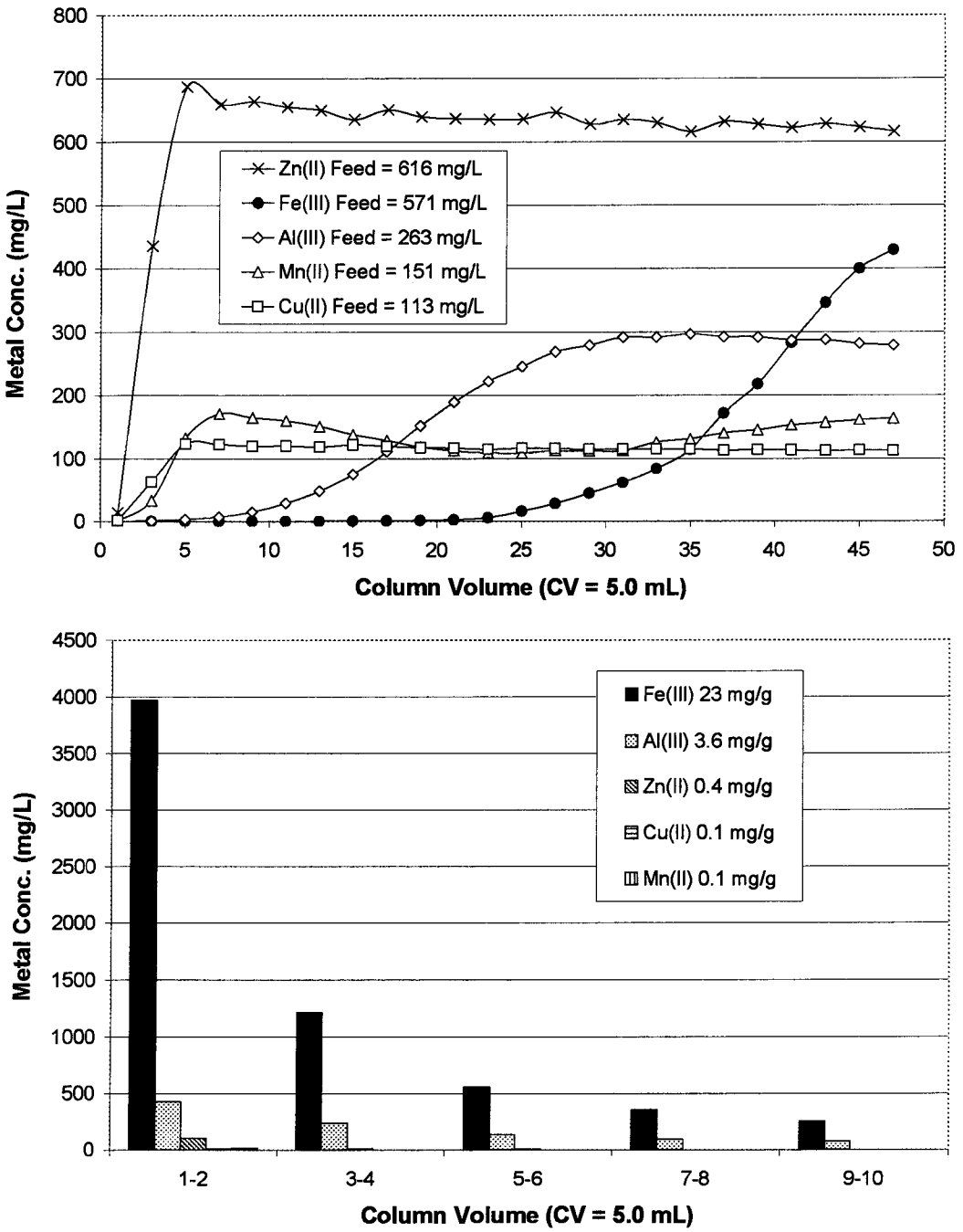

Figure 77. BPAP-CF 041504-DN Berkeley Pit Lake treatment; breakthrough curves, 0.50 CV/min., feed pH 2.2 (top); strip fractions, 0.10 CV/min., 13 N H_2SO_4, 85% Fe(III) purity (bottom).

WP-4 was also investigated for selective Fe(III) removal to precede Cu(II) recovery. Affinity towards Cu(II) shown in Figure 78 (top) limits WP-4 to other applications [e.g., Fe(III) separation from Zn(II), Ni(II), Co(II), and Mn(II)]. Figure 78 (bottom) shows the strip fractions, exhibiting excellent elution kinetics for Fe(III) [and Cu(II)].

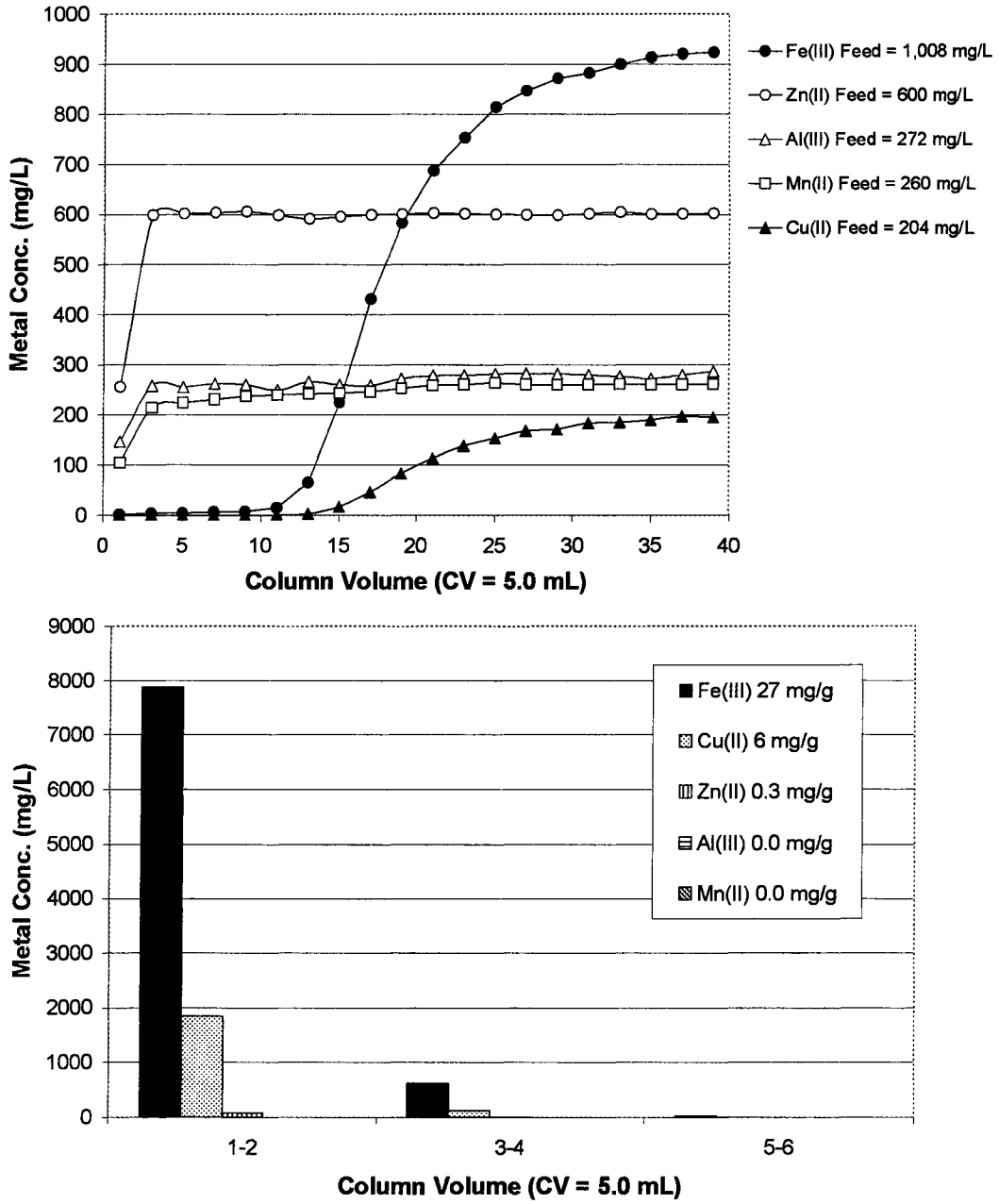

Figure 78. WP-4-CF 101205-DN Berkeley Pit Lake treatment; breakthrough curves, 0.50 CV/min., pH 2.2 (top); strip fractions, 0.50 CV/min., 9.0 N H_2SO_4, 81% Fe(III) purity (bottom).

Although Fe(III) removal as the initial target metal was not accomplished in an industrially feasible fashion, another approach succeeded targeting Fe(III)/Al(III) removal following Cu(II) recovery. Bench-scale separation of Cu(II), Zn(II), and Mn(II) was also achieved producing high purity, highly concentrated recovery solutions of each

target metal ion (Table 16). The cartoon illustrated in Figure 79 displays the treatment pathway investigated to produce the results in Table 16. Berkeley Pit water pumped from depth (to obtain higher metal concentrations) is collected in a holding tank. Oxidation of Fe(II) can be accelerated by spraying the water up into the air upon collection, and/or by bubbling compressed air throughout the collection reservoir. The solution is then pumped to an array of columns (refer to section 2.7) packed with CuWRAM. CuWRAM exhibits a remarkable ability to extract copper in the presence of high levels of ferric iron and other metals as shown by the breakthrough curve in Figure 80. After loading a CuWRAM column with copper to capacity the column is rinsed with pH 2 (H_2SO_4) water to flush out the entrained metals not captured. The column is then stripped using 9 N H_2SO_4 (Figure 80). The strip solution meets criteria to recover the copper by means of electrowinning technology.[26] After stripping the column it is regenerated by passing water through the column.

Table 16. Berkeley Pit Lake metal ion recovery data.

	Cu(II)	Zn(II)	Mn(II)
Berkeley Pit (% purity)	5.0	18	6.0
Recovery (% purity)	97	99.98	83
Berkeley Pit (g/L)	0.17	0.58	0.21
Recovery (g/L)	10	6.5	9.0

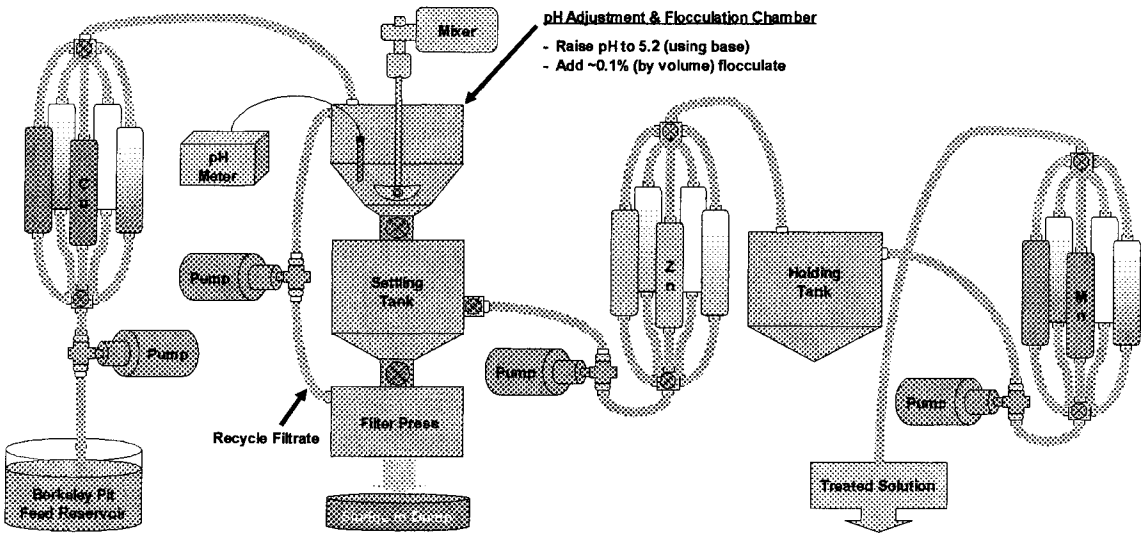

Figure 79. Cartoon of Berkeley Pit Lake treatment process.

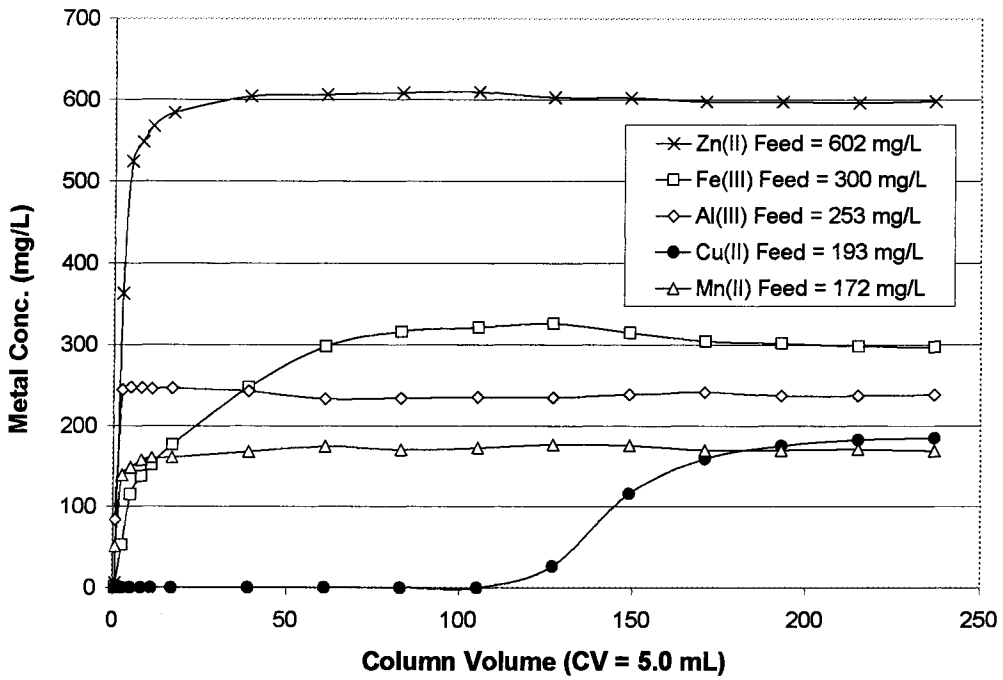

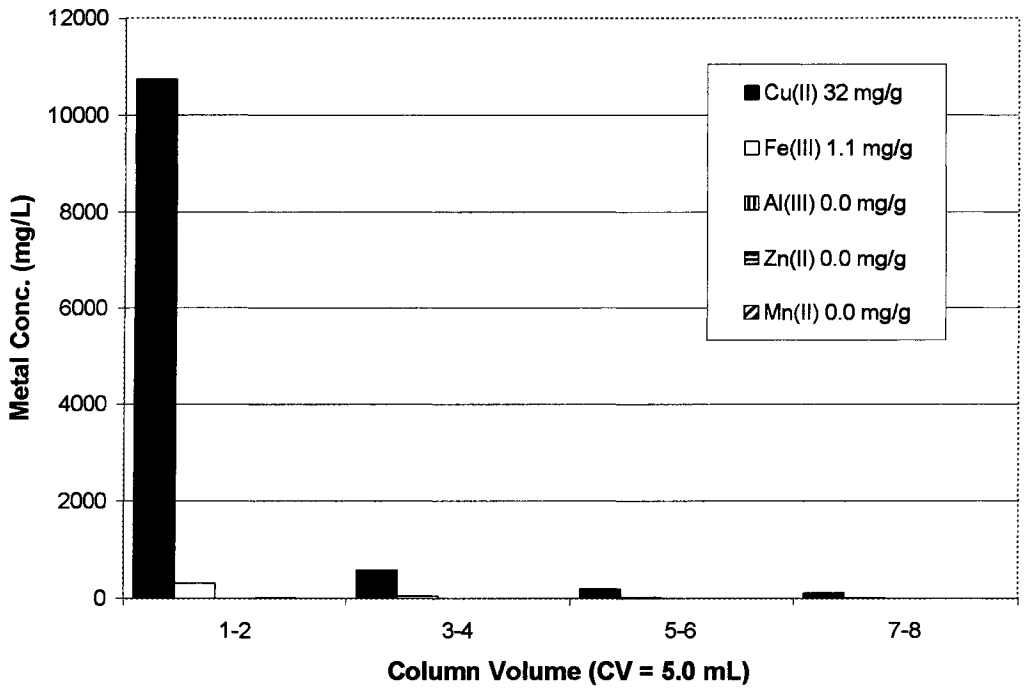

Figure 80. CuWRAM-CF 022602-DN Berkeley Pit Lake treatment; breakthrough curves, 0.50 CV/min., pH 2.2 (top); strip fractions, 0.50 CV/min., 9.0 N H_2SO_4, 97% Cu(II) purity (bottom).

CuWRAM's effluent is then adjusted to pH 5.2 with NaOH (or other base). This induces precipitation of the iron (co-precipitating the arsenic, unfortunately diluted to below the detection limit), and aluminum, as the metal hydroxides (Figure 81). A flocculate can be added to assist settling of the precipitate which is then filter pressed (recycling the filtrate) and disposed of at an appropriate repository (e.g., Opportunity Ponds, Opportunity, MT).

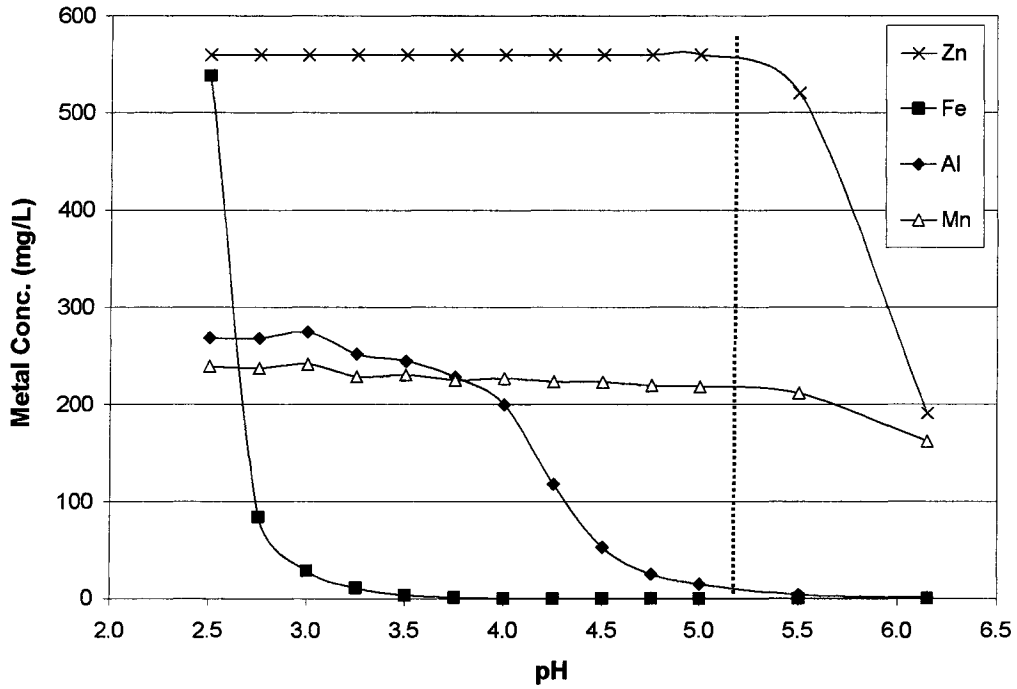

Figure 81. Berkeley Pit Lake water metal concentrations as a function of pH.

Zinc(II) is then separated from manganese(II) utilizing the amino acetate composite WP-2. The synthetic feed used did not contain magnesium or calcium as these elements are lower in the Irving-William series with respect to Mn(II). WP-2 was regenerated using 4 CV 0.01 N NaOH (followed by 4 CV DI H_2O) to increase the capacity towards Zn(II), but not compromising the selectivity over Mn(II). Figure 82 (top) illustrates WP-2's affinity towards Zn(II), while Mn(II) quickly breaks through the column. WP-2 was rinsed with 4 CV pH 2 (H_2SO_4) water before stripping with 9 N H_2SO_4 (Figure 82, bottom).

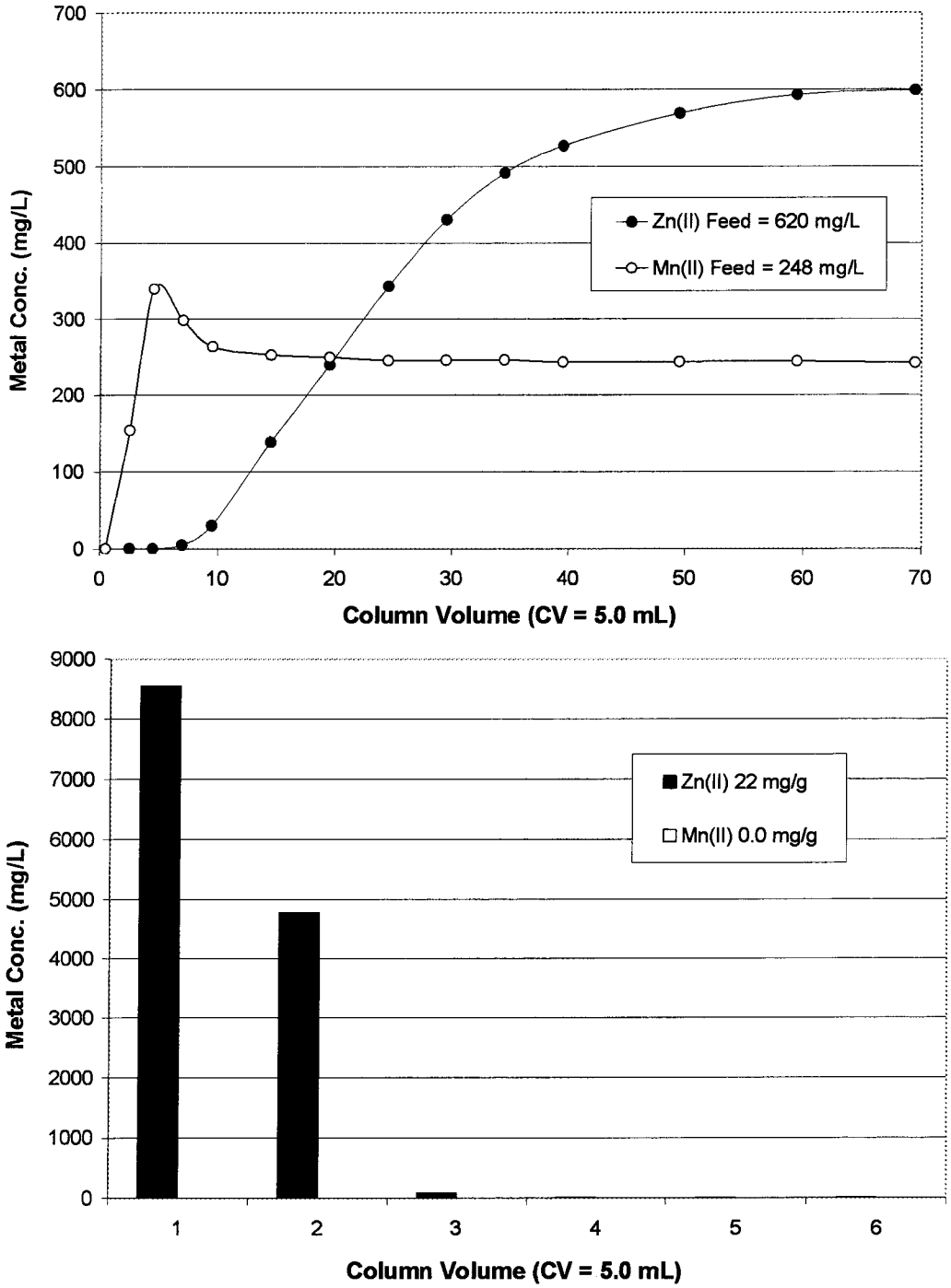

Figure 82. WP-2-CF 013002-BF; Zn(II)/Mn(II) breakthrough curves, 0.50 CV/min., pH 5.3 (top); strip fractions, 0.50 CV/min., 9.0 N H_2SO_4, 99.98% Zn(II) purity (bottom).

Manganese(II) was separated from calcium(II) and magnesium(II) using BP-2. BP-2 was base regenerated using 13 CV of 0.10 N NaOH, followed by 4 CV water. The

breakthrough curve in Figure 83 (top) shows Mn(II) loading onto BP-2. Mg(II) and Ca(II) are slightly retained, but are replaced by Mn(II) having greater affinity with the acetate ligand. After loading Mn(II) to capacity, BP-2 was rinsed with 4 CV DI H_2O before stripping with 9 N H_2SO_4 (Figure 83, bottom).

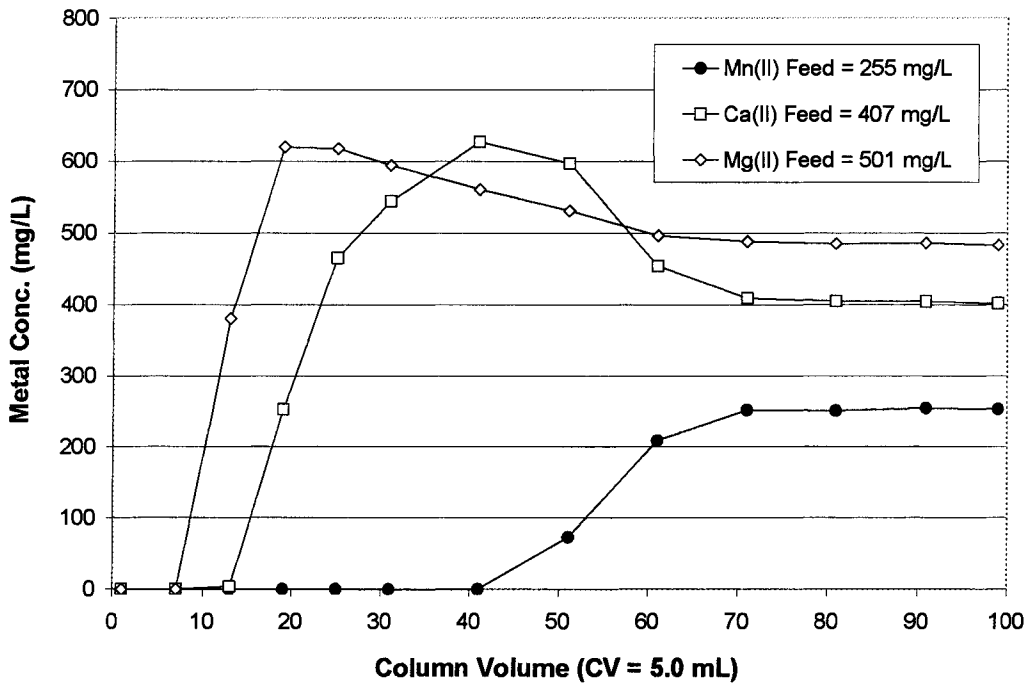

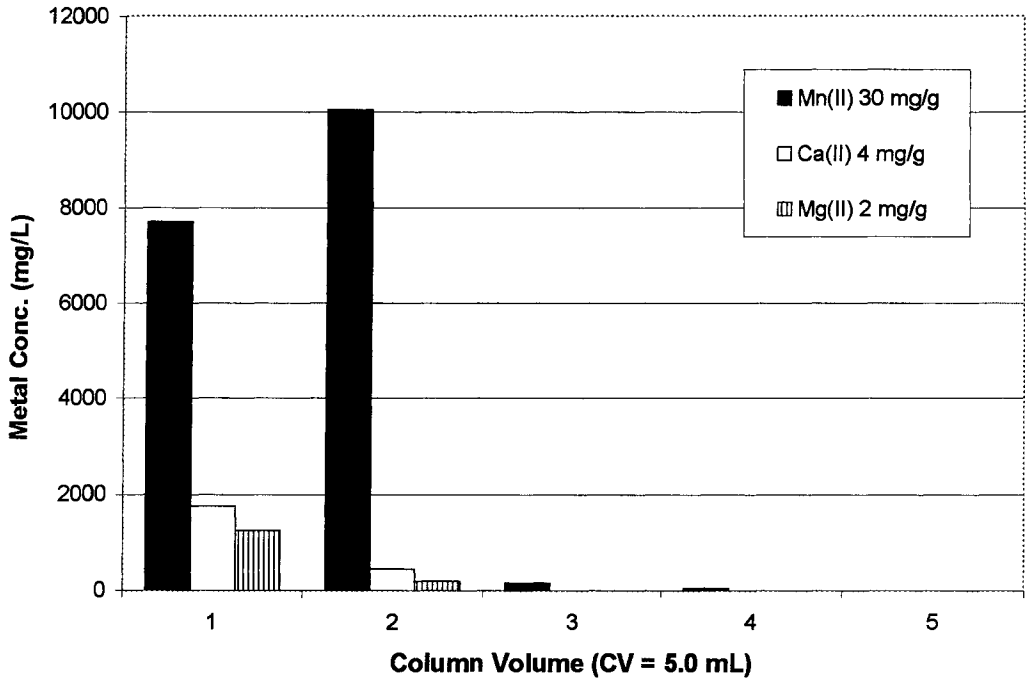

Figure 83. BP-2-CF 051903-CH; Mn(II)/Ca(II)/Mg(II) breakthrough curves, 0.50 CV/min., pH 4.9 (top); strip fractions, 0.50 CV/min., 9.0 N H_2SO_4, 83% Mn(II) purity (bottom).

Summarized in the following paragraphs are additional approaches to treatment pathways that were found to be inadequate but worthy of mention. Selective removal of Al(III) in the presence of Zn(II) and Mn(II) was achieved using BPAP as shown in Figure 84 (top). This investigation was pursued as a treatment strategy to follow Fe(III) and Cu(II) removal. Poor stripping of Al(III) from BPAP was again observed (Figure 84, bottom).

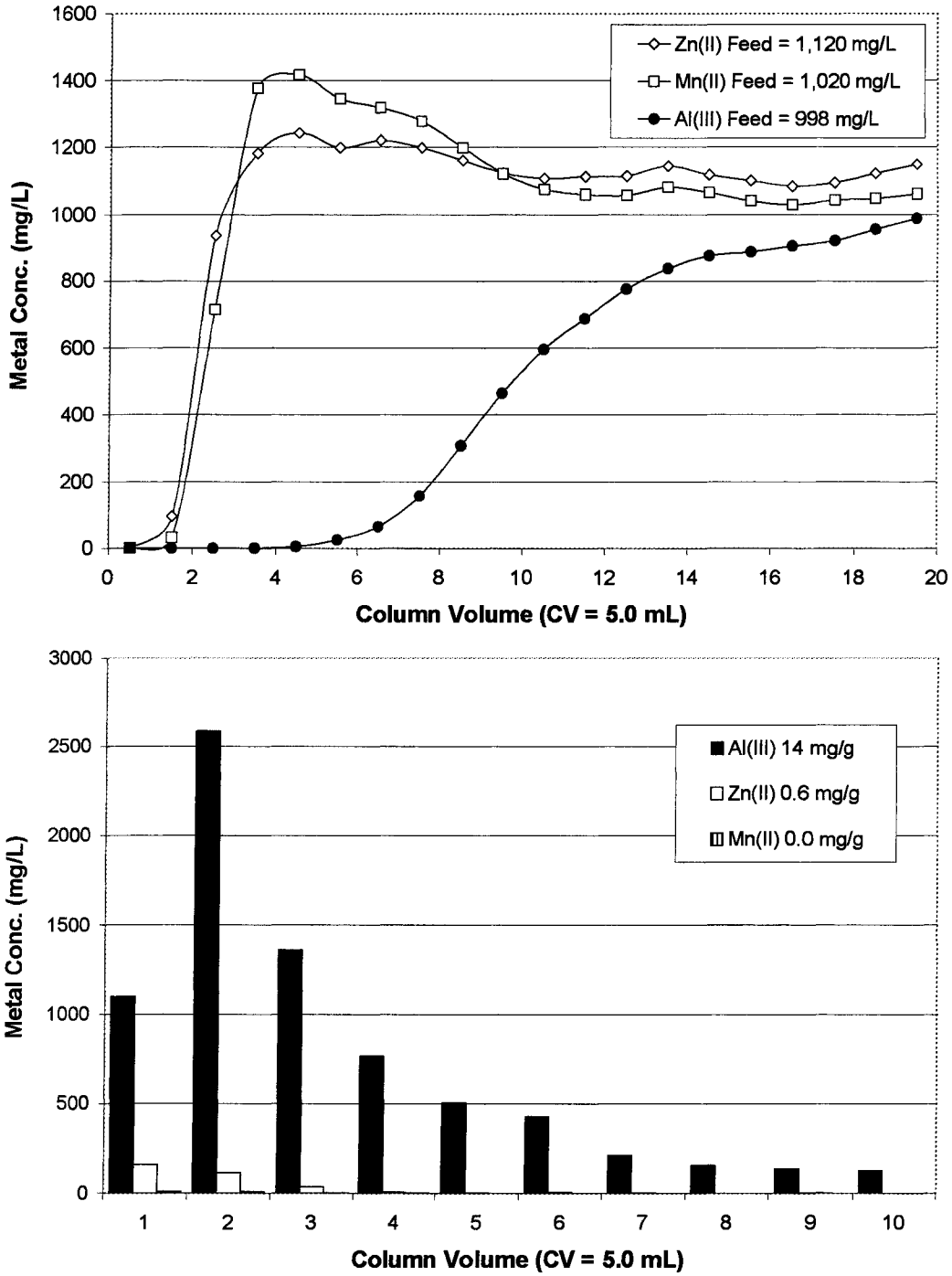

Figure 84. BPAP-CF 041504-DN; Al(III)/Zn(II)/Mn(II) breakthrough curves, 0.50 CV/min., pH 1.6 (top); strip fractions, 0.50 CV/min., 9.0 N H_2SO_4, 95% Al(III) purity (bottom).

Selective removal of Al(III) was also investigated using the amino functionalized composites WP-1 and BP-1. Neither of these two materials provided sufficient separation

of Al(III) from Zn(II). Significant affinity towards Zn(II) does not result in a flowthrough solution void of Al(III) and containing feed concentrations of Zn(II). Figure 85 (top) shows the breakthrough curve from base regenerated BP-1. Corresponding strip fractions in Figure 85 (bottom) illustrate the primary amines affinity towards Al(III) in the presence of Zn(II) and Mn(II) exhibiting 96% Al(III) purity, though only a 7 mg/g Al(III) capacity.

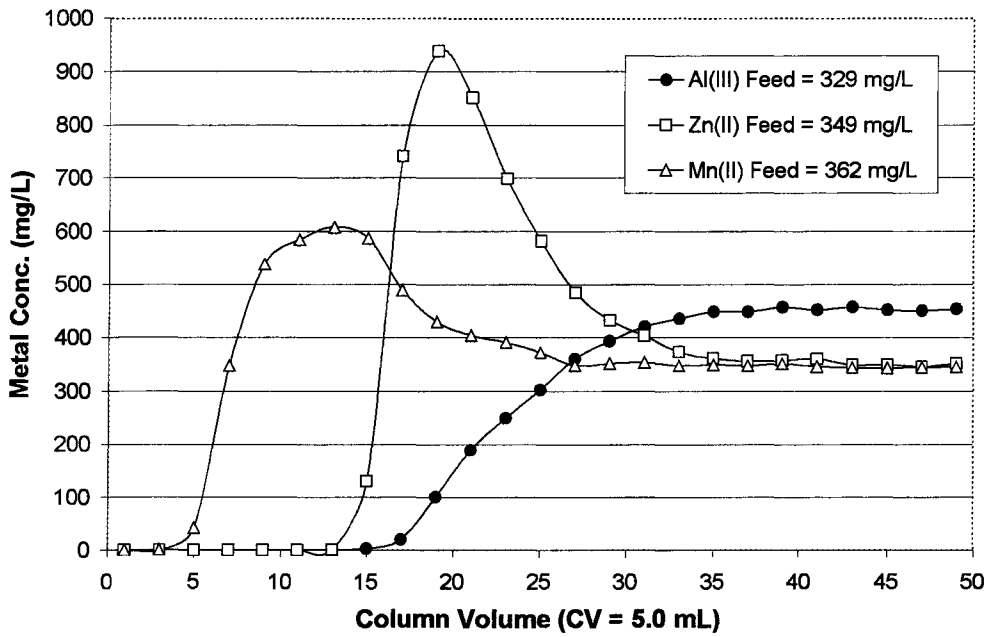

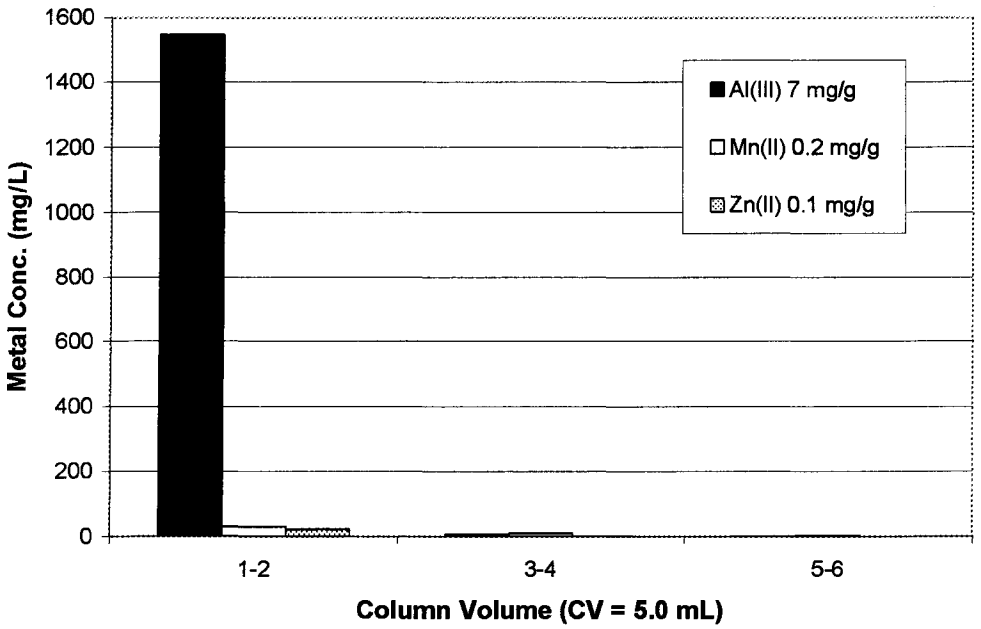

Figure 85. BP-1-CF 040804-DN; Al(III)/Mn(II)/Zn(II) breakthrough curves, 0.50 CV/min., pH 2.2 (top); strip fractions, 0.50 CV/min., 9.0 N H_2SO_4, 96% Al(III) purity (bottom).

BP-2 and WP-4 did not exhibit significant Al(III) capacity at a feed pH of 1.7. Both Zn(II) and Al(III) were slightly retained by BP-2 and WP-4, though were not captured due to the low feed pH of 1.7. Base regeneration of WP-4 afforded a 4 mg/g Al(III) capacity, with no selectivity over Zn(II) which loaded 6 mg/g.

Base regeneration of BP-4 led to co-loading of Zn(II) and Al(III), while increasing the retention of Mn(II) as shown in Figure 86 (top). The high acidity of the feed solution increased the proton exchange to the oxine ligands, illustrated by the flowthrough concentrations exceeding feed levels. Rapid elution of Zn(II) and Al(III) from WP-4 provided for minimal strip capacities (Figure 86, bottom) due to limited metal coordination at this feed pH.

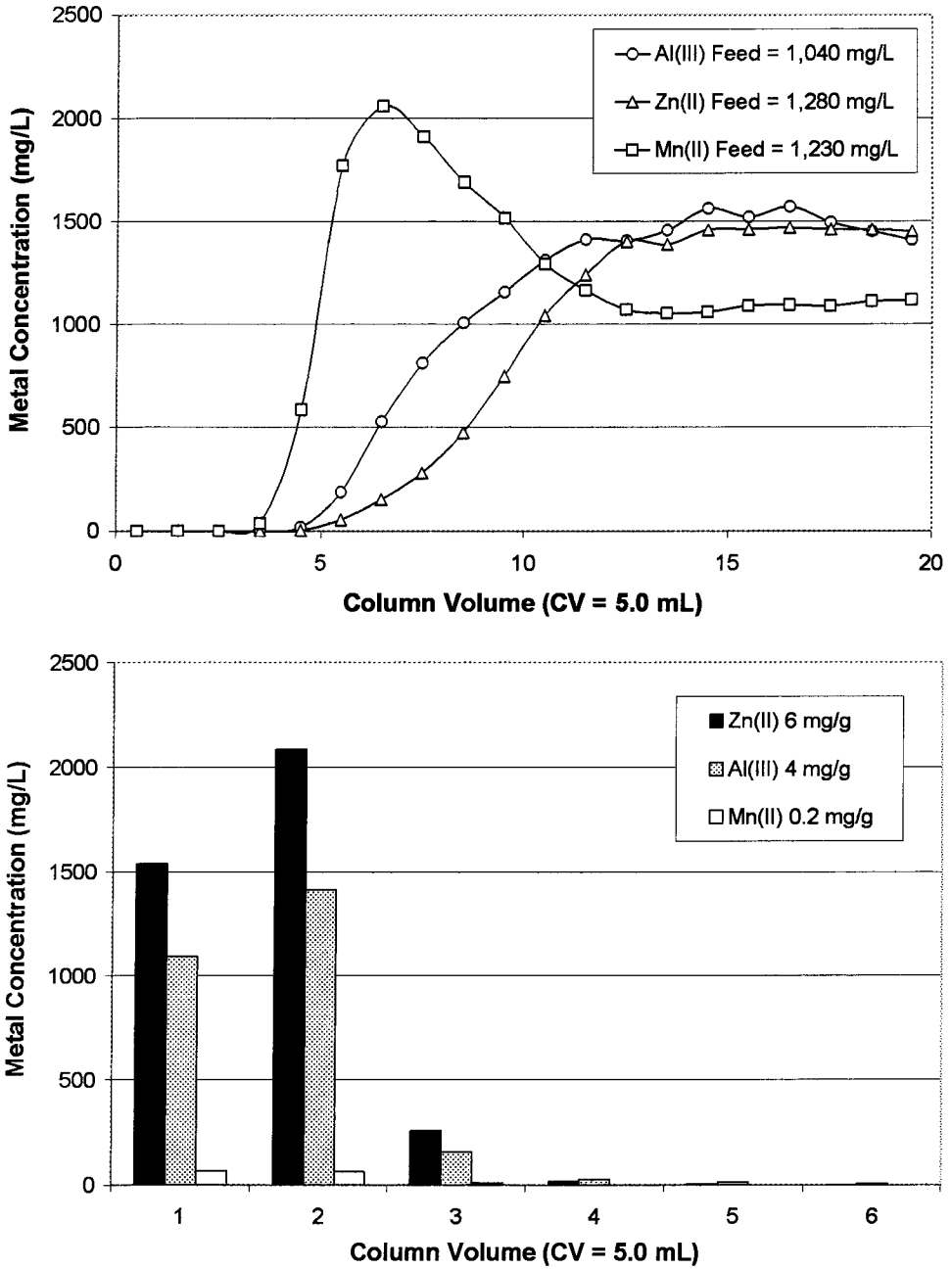

Figure 86. WP-4-CF 101205-DN; Al(III)/Zn(II)/Mn(II) breakthrough curves, 0.50 CV/min., pH 1.6 (top); strip fractions, 0.50 CV/min, 9.0 N H_2SO_4, (bottom).

Base regeneration of BPAP did not affect Al(III) capture relative to the acid form of the phosphonic acid ligand. However, Zn(II) and Mn(II) were retained with Al(III) co-loading significant levels of all three challenge metals (Figure 87).

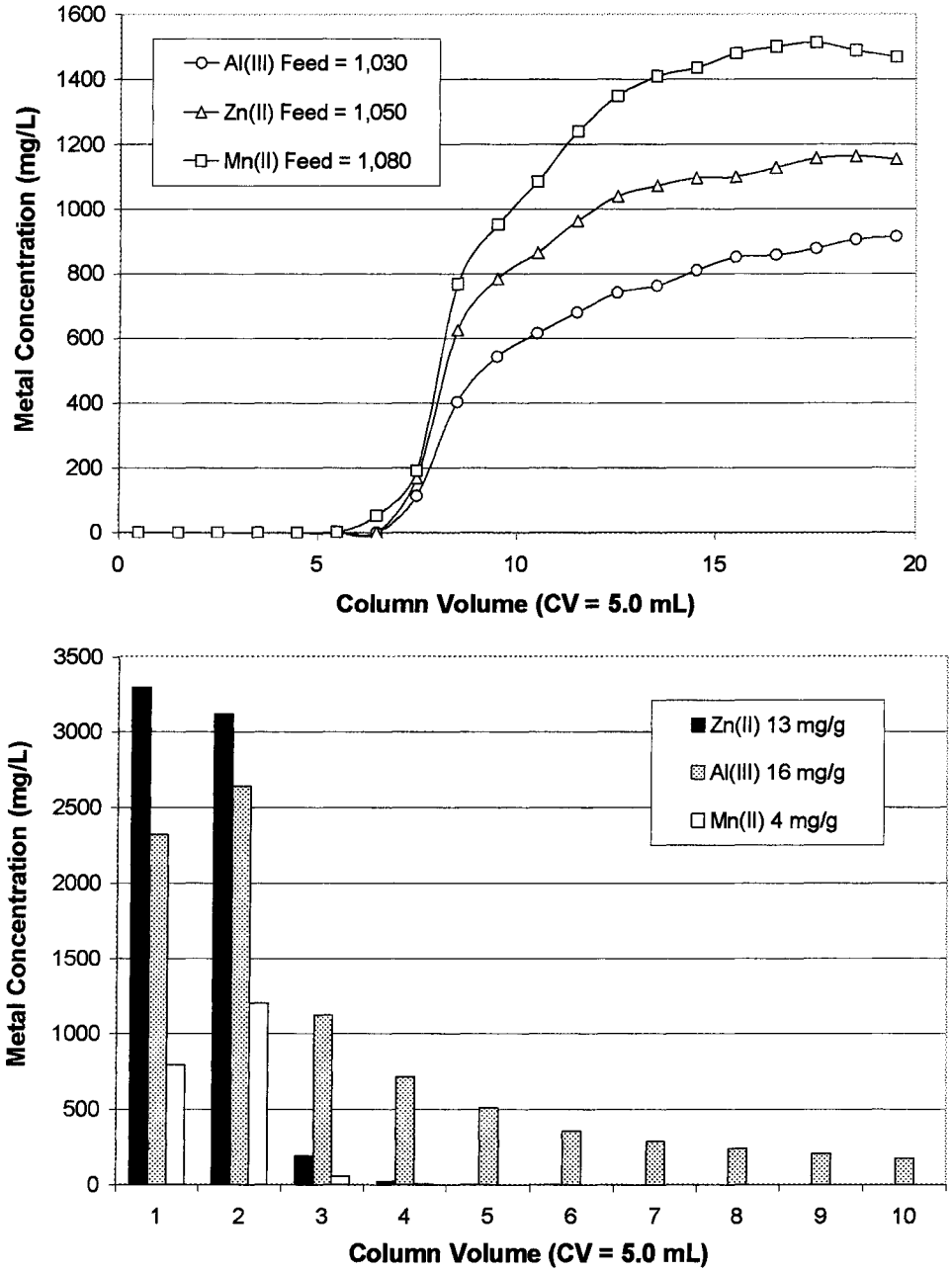

Figure 87. BPAP-CF 041504-DN; Al(III)/Zn(II)/Mn(II) breakthrough curves, 0.50 CV/min. feed pH = 1.6 (top); strip fractions, 0.50 CV/min., 9.0 N H_2SO_4 (bottom).

Selective Zn(II) capture in the presence of Mn(II) was successful using WP-4 in addition to WP-2 (reported above). WP-4 exhibited excellent selectivity for Zn(II) over Mn(II) combined with exceptional loading kinetics as shown in Figure 88. Low capacity of 8 mg/g is the limiting factor for Zn(II) recovery using WP-4 even at a favorable feed

pH of 5.2. However, the high selectivity for Zn(II) over Mn(II) in conjunction with fast loading kinetics permits for Zn(II) recovery using WP-4.

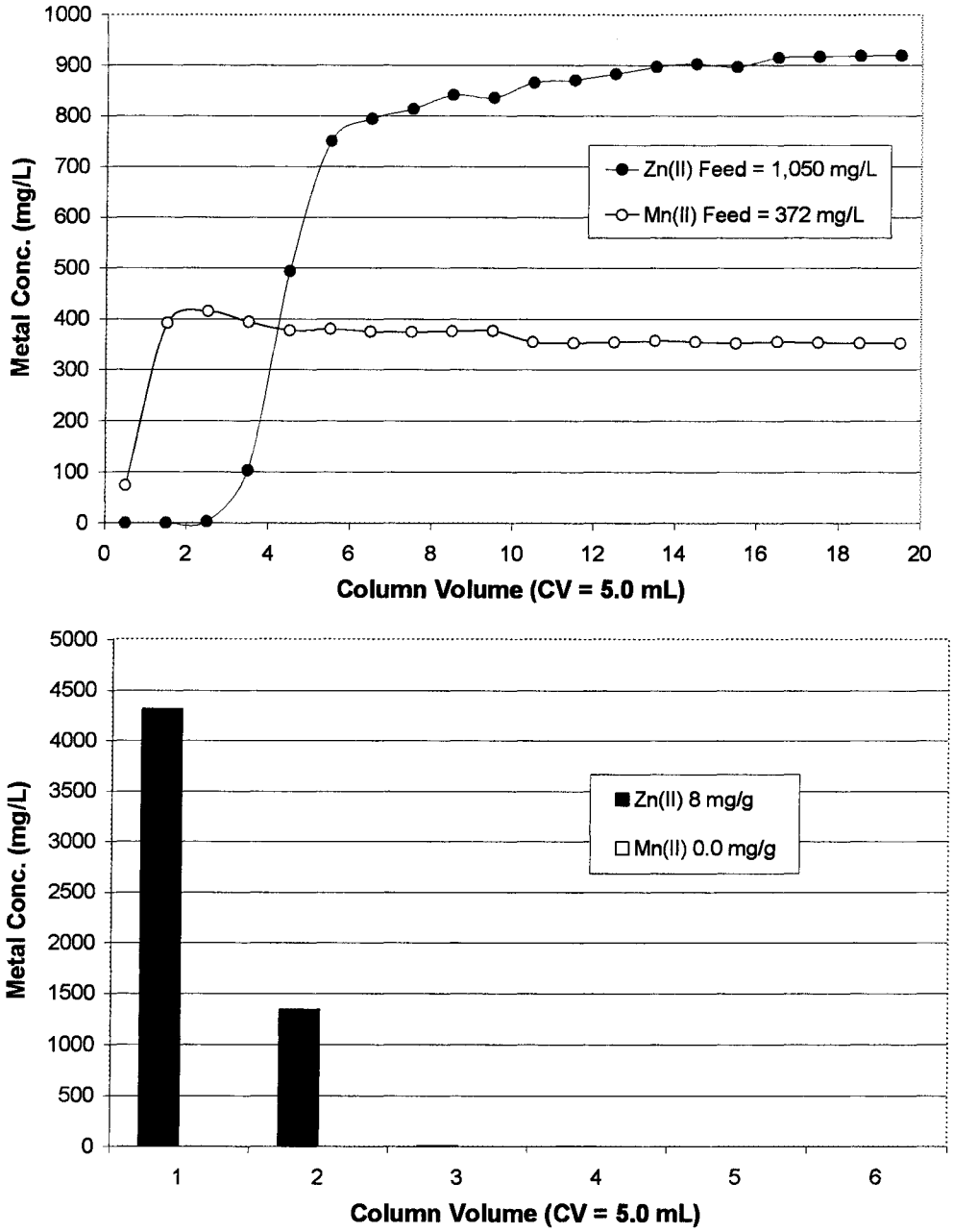

Figure 88. WP-4-CF 101204-DN; Zn(II)/Mn(II) breakthrough curves, 0.50 CV/min., pH 5.2 (top); strip fractions, 0.50 CV/min., 9.0 N H_2SO_4, 99.98% Zn(II) purity (bottom).

In an attempt to increase Zn(II) capacity, base regeneration of WP-4's oxine ligand was investigated using 0.10 M NaOH. Zn(II) capacity increased by more than three fold,

although the selectivity over Mn(II) was compromised as can be seen from the breakthrough curve and strip profile (Figure 89).

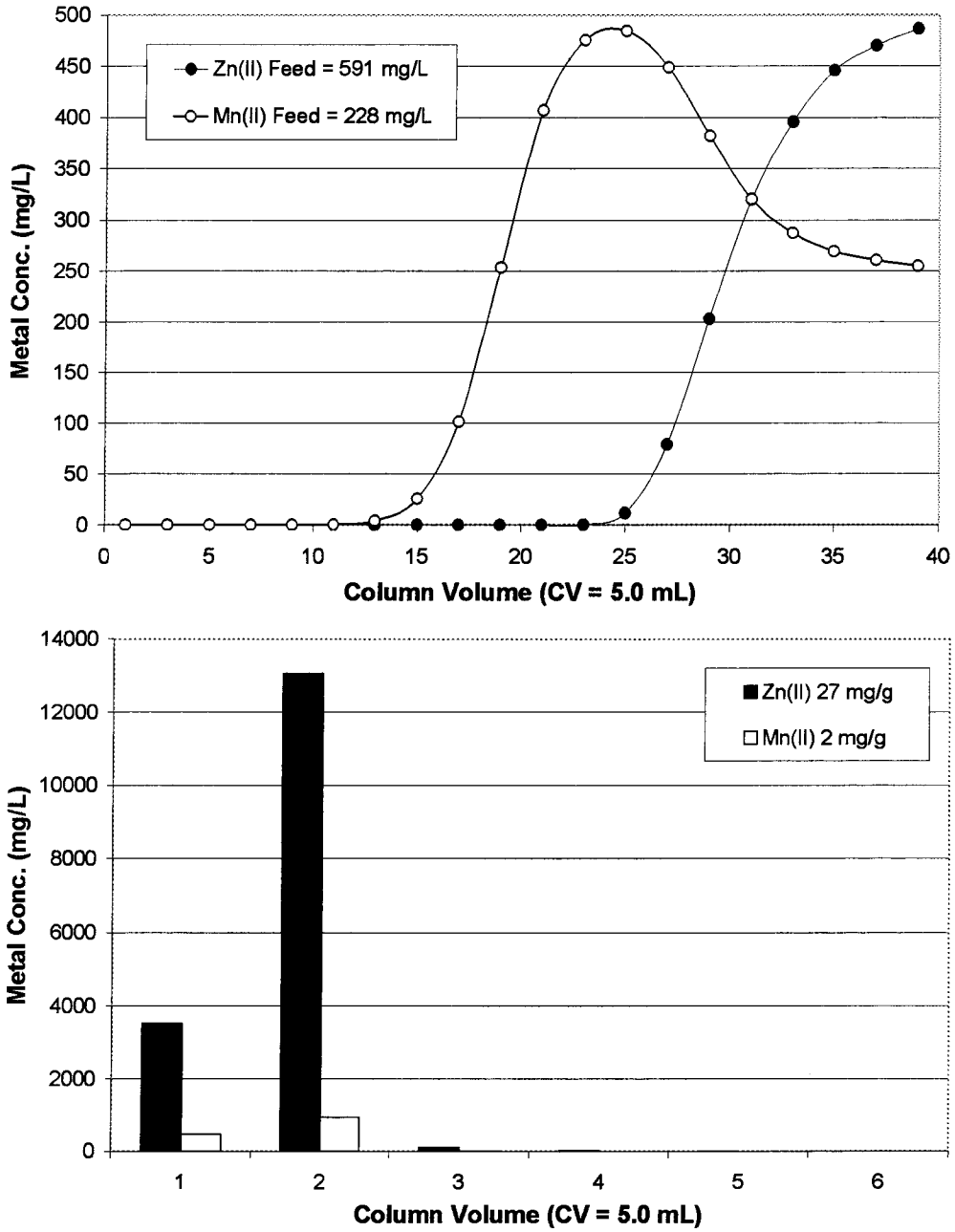

Figure 89. WP-4-CF 101204-DN; Zn(II)/Mn(II) breakthrough curves, 0.50 CV/min., pH 5.2 (top); strip fractions, 0.50 CV/min., 9.0 N H_2SO_4, 92% Zn(II) purity (bottom).

WP-2 was tested in the acid form in addition to the results mentioned above. Retention of Mn(II) is thereby minimized, although compromising Zn(II) capacity

compared to results using base regeneration. The breakthrough curve and strip fractions illustrate reasonable Zn(II) loading kinetics and capacity, with good selectivity over Mn(II) (Figure 90).

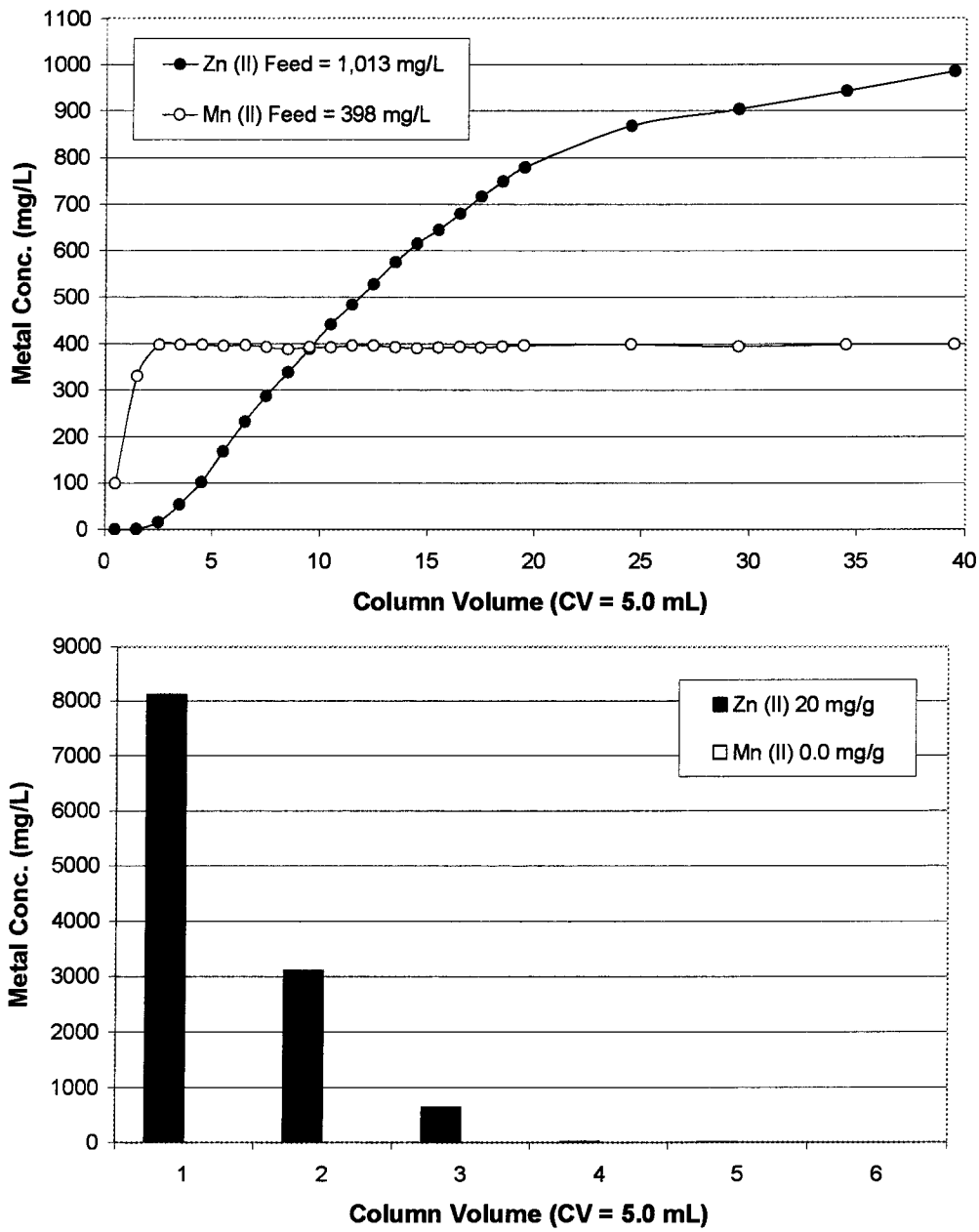

Figure 90. WP-2-CF 013002-BF; Zn(II)/Mn(II) breakthrough curves, 0.50 CV/min., pH 5.2 (top); strip fractions, 0.50 CV/min., 9.0 N H_2SO_4, 99.99% Zn(II) purity (bottom).

WP-2 was additionally tested using stronger base regeneration solutions leading to increased Zn(II) capacity (Figure 91). Undesirable retention of Mn(II) increases with increasing base regeneration as shown in Figure 91 (top).

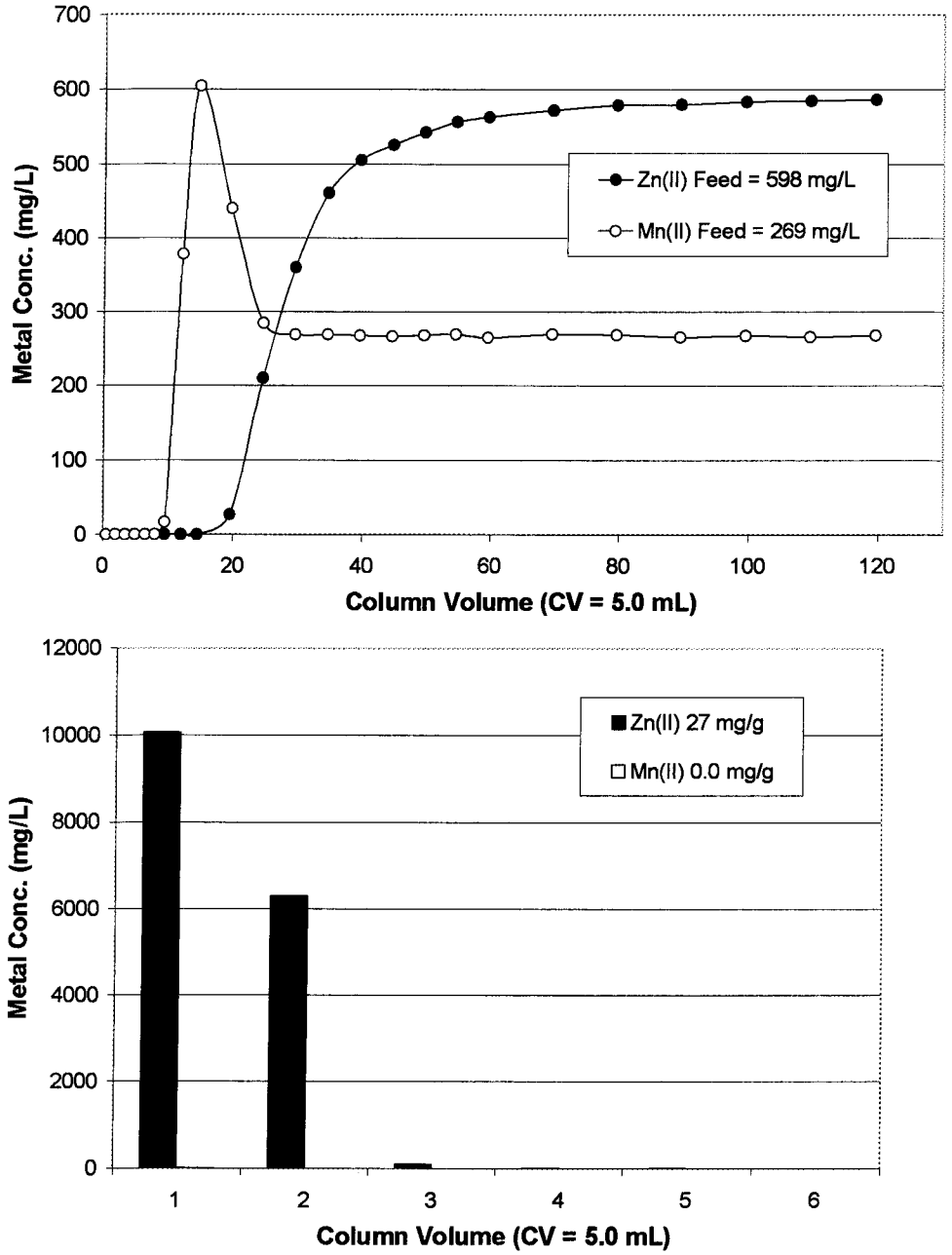

Figure 91. WP-2-CF 013002-BF; Zn(II)/Mn(II) breakthrough curves, 0.50 CV/min., pH 5.2 (top); strip fractions, 0.50 CV/min., 9.0 N H_2SO_4, 99.93% Zn(II) purity (bottom).

4.5 Metal Recovery from Mining Tailings

Metals can be found sequestered (generally as oxyhydroxides or sulfides) in sediments at or down stream of mining sites. Tertiary contamination (metal contaminated river sediments) was discovered at the Milltown Reservoir in the Clark Fork Complex, more than 200 km from the mines and smelters at Butte and Anaconda.[1] In 1999 the Federal Energy Regulatory Committee (FERC) reclassified Milltown Dam as a "Significant Hazard Potential" because of the tailings contained behind the Dam. Filled with contaminated sediment, the reservoir retains approximately 13,100 MT of copper, 19,000 MT of zinc, 9,200 MT of manganese, and 2,100 MT of arsenic.[62] Numerous scientific studies have been done in an attempt to better understand the geochemistry of the Milltown Reservoir.[63] This type of tertiary contamination may be found at or near large-scale metal extraction sites throughout the world. The proposed process is capable of recovering selected metals from the sediment and treating the sediment on-site, thus eliminating costly transportation of non-treated sediment to a waste repository.

Figure 92 displays Montana State's 294 priority cleanup sites that may contain acid mine drainage (AMD) and/or metal laden sediments/tailings. Figure 93 includes results from a digest study of sediments/tailings obtained in The Philipsburg District, Montana. This study illustrates the potential to mobilize metals by digesting the sediments/tailings for 1 hour in a dilute sulfuric acid solution at pH 2.3. The filtered acid digest solution does not contain unwanted ferric iron. However, copper, zinc and manganese are dissolved into the acidic solution. These three metals are ubiquitous among mining waste-sites and their recovery/resale could offset the cost of waste treatment considerably. The procedures discussed in the previous section (4.4) could be applied to the separation and recovery of Cu(II), Zn(II) and Mn(II) from mine tailings and

contaminated sediments. Metal extracted sediment could potentially be revegitated on-site, eliminating costly transportation of hazardous sediments to a designated waste repository.

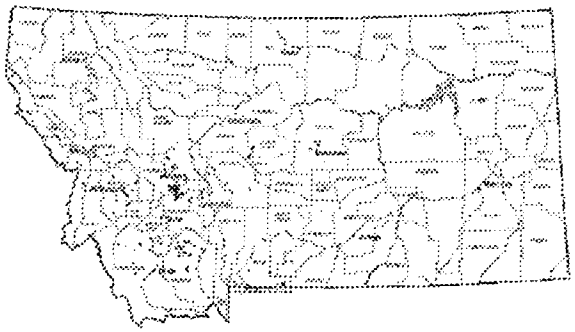

Figure 92. Montana state's 294 priority cleanup sites.

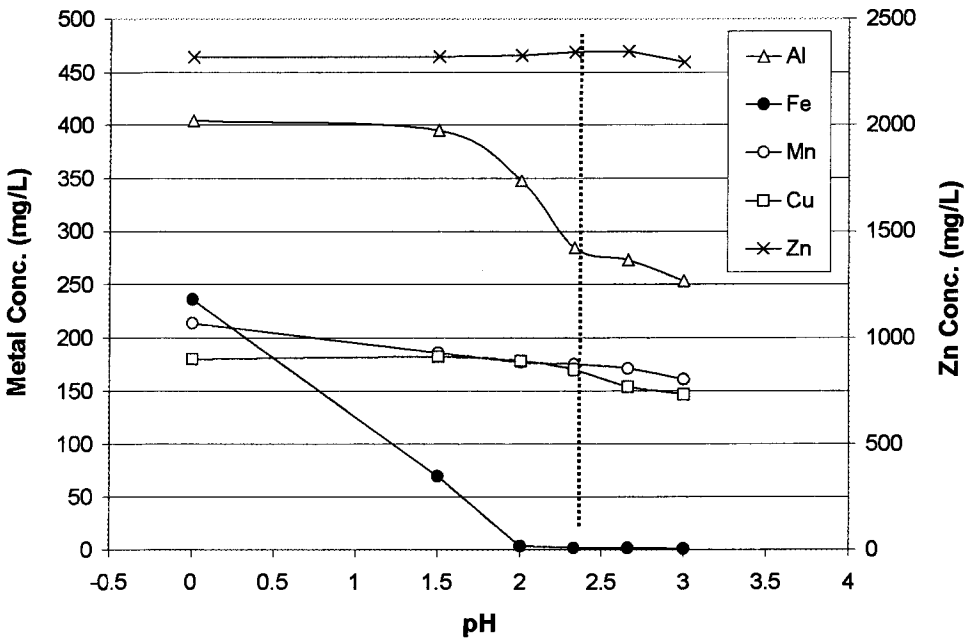

Figure 93. Metal concentration of Philipsburg Mining District sediments/tailings as a function of pH.

5 CONCLUSIONS AND FUTURE WORK

5.1 Lateral Polymerization of Mixed Trifunctional Silanes

Incorporation of a mixed silane reagent (CPTCS:MTCS) led to gels with increased coverage density of the laterally polymerized silane phase (Table 4). Structural improvement was shown by an increase in reagent siloxanes and a corresponding decrease in reagent silanols (Figure 25). BPAP made from these gels showed to have a slight improvement in performance with respect to capacity and kinetics. Future studies would investigate higher ratios of MTCS to CPTCS which could lead to improved kinetics and higher yields of ligand modified sites.

It can be calculated from elemental analysis that approximately 45% of the amines on BP-1's poly(allylamine) are bound to a propyl anchor group. Modification of BP-1 is often limited to the number of available amines (about 55%). Bulky reagent ligands such as 2-picolyl chloride have been shown to modify about 40% of the available amines (22% of total amines).[18] Reducing the number of anchored amines may result in more dramatic increases in composite capacities for bulky and/or hydrophobic ligands such as 2-picolyl chloride or 8-hydroxyquinoline.

Other applications involving base regeneration of the composite's functional group may benefit from a denser silane phase providing greater protection of the silica gel's surface. Treatment of solutions containing basic species such as fluoride may also benefit from incorporation of a mixed silane phase. This study has relevance to HPLC technology as well. HPLC columns commonly include components containing cationic amino sites that unfavorably interact with the anionic silanol sites at neutral to slightly basic pH. Reducing the number of silanol sites would lead an increase in column longevity with a corresponding improvement in reproducibility.

Propyltrichlorosilane (PTCS) was considered initially for this investigation. PTCS may provide for better protection of the silica gel's surface due to the relative non-polarity relative to methyltrichlorosilane (MTCS). However, MTCS was chosen over PTCS due to its minimal steric hinderance.

5.2 Phosphorous Based Silica Polyamine Composites

A series of composites was constructed all of which incorporated phosphorous based ligands. Synthetic routes developed varied significantly in cost, complexity and efficiency of yield. The Mannich reaction proved ideal in many regards. Simplicity of a one-pot reaction scheme is complemented by inexpensive reagents, an aqueous solvent, high rate of reaction, excellent efficiency of yield, under acidic conditions which do not degrade either BP-1 or BPAP. Utilization of phosphorous or hypophosphorous acid yielded the phosphonic and phosphinic acid functionalities, respectively. These materials have high metal capacities for trivalent and tetravalent metals such as Ga(III), Eu(III) and Th(IV) at very acidic pH values. BPAP revealed a remarkable ability to remove Fe(III) and Eu(III) from 10 N (pH -1) acid solutions.

BPAP has been used for biochemistry applications to selectively remove Fe(III) from bacterial (*Sulfolobus solfataricus*) growth media.[64] This elegant approach to Fe(III) removal eliminated the problems associated with precipitation of iron using hydrogen peroxide. Selective Fe(III) removal has a plethora of applications in the field of biochemistry similar to the mentioned investigation. These material's potential to polish copper electrowinning solutions that contain ~10 g/L copper and ~0.5 g/L iron should be tested at lower pH.

The mixed methyl/dimethyl phosphonate composites BP-6 and BP-7 exhibited mediocre Eu(III) and Th(IV) capacities. Production of the pure methylphosphonate may

allow for increased capacities. The phosphonate composites may be useful for Fe(III) separations such as with Cu(II) electrowinning solutions, providing for improved stripping kinetics. Synthetic routes utilizing chloromethylphosphonic acid could be revisited using various alcohols (e.g., MeOH, EtOH, *i*-PrOH) to produce the dialkyl and/or monoalkyl phosphonates.[65]

Fryxell and coworkers recently reported two materials incorporating the diethyl phosphonate functionality bound to a silica surface.[66] Their investigation utilized carboxylate activation using carbonyl diimidazole (CDI) coupled with a primary amine. This approach could be pursued using the silica polyamine composite BP-1.

5.3 Mining Waste Treatment

The Berkeley Pit Lake offered a real world source of AMD containing Cu(II), Zn(II) and Mn(II). Results in section 3.12 show successful recovery of these ions suitable for electrowinning. The use of CuWRAM for Cu(II) extraction presents a simple and effective step that could be used for certain applications where only copper recovery is of interest. Recovery of Zn(II) and Mn(II) present additional complexity to treatment strategies due to the separation from Fe(III) and Al(III). Presently treatment strategies involved neutralization of AMD, filtration of the precipitated Fe(III) and Al(III) hydroxides (following Cu(II) recovery using CuWRAM). Zn(II) and Mn(II) can then be recovered with high purity and cycle capacities.

Potentially, developing new composites may offer improvement over the reported treatment strategies. For example an ethylene diamine tri-acetate polyallylamine composite (BP-ED) made from EDTA anhydride has been shown to extract Zn(II) ions in the presence of Al(III).[67] However, Fe(III) would still need to be removed prior to Zn(II) recovery. Additionally the kinetics of this remarkable composite (BP-ED) are inferior to

WP-2, although capacities are superior. Furthermore, Al(III) would still pose separation problems for recovery of Mn(II). Precipitation of Fe(III) and Al(III) following Cu(II) extraction may ultimately be required for subsequent recovery of Zn(II) and Mn(II).

Treatment of AMD does not offer significant profits in the recovery of Cu(II), Zn(II), and Mn(II) as the metal salts, but may at least offset the cost of remediation. Reduction of the recovered metal ions to their elemental form via electrowinning technology generates added value, but at an additional cost. Superfund sites such as the Berkeley Pit demand immediate treatment with current yearly budgets of about $3 million. Composite technology can be competitive when metal recovery profits augment yearly wastewater treatment budgets.

6 EXPERIMENTAL

6.1 Reagents and Synthetic Procedures

Silica gel was first sieved to ensure particle diameters were within the desired range. The data in Table 1 show mercury porosimetry characterization (Delta Analytical Instruments, Inc.) of purchased silica gels from various suppliers. Poly(ethyleneimine) (PEI) $50\%_{aq}$ at pH 12.2 (base form), 1,200 Daltons, ~28 mers/polymer was purchased from Nippon Shokubei, Japan. Poly(allylamine) (PAA) $15\%_{aq}$ at pH 11.7 (base form), 11,400 Daltons, ~200 mers/polymer was purchased from Nitto Boseki Co., Ltd., Japan. Poly(vinylamine) (PVA) 5 – $10\%_{aq}$ at pH 10.0 (base form), 50,000 Daltons, ~900 mers/polymer was purchased from BASF, United States. All water was de-ionized (DI) by reverse osmosis. Chemicals were purchased from Aldrich Chemical Co., reagent grade (unless noted), and used without further purification (unless noted).

Elevated temperature pH measurements were made using a Thermo Orion 250 Aplus meter with a Thermo Orion Triode electrode. Ambient temperature pH measurements were made using a VWR SympHony SB20 meter with a VWR SympHony Posi-pHlo electrode. Elevated temperature reactions (Figure 94; bottom, left) were heated via a round bottom flask heating mantle (GLAS-COL Co.) controlled by a variable autotransformer (STACO, Inc.).

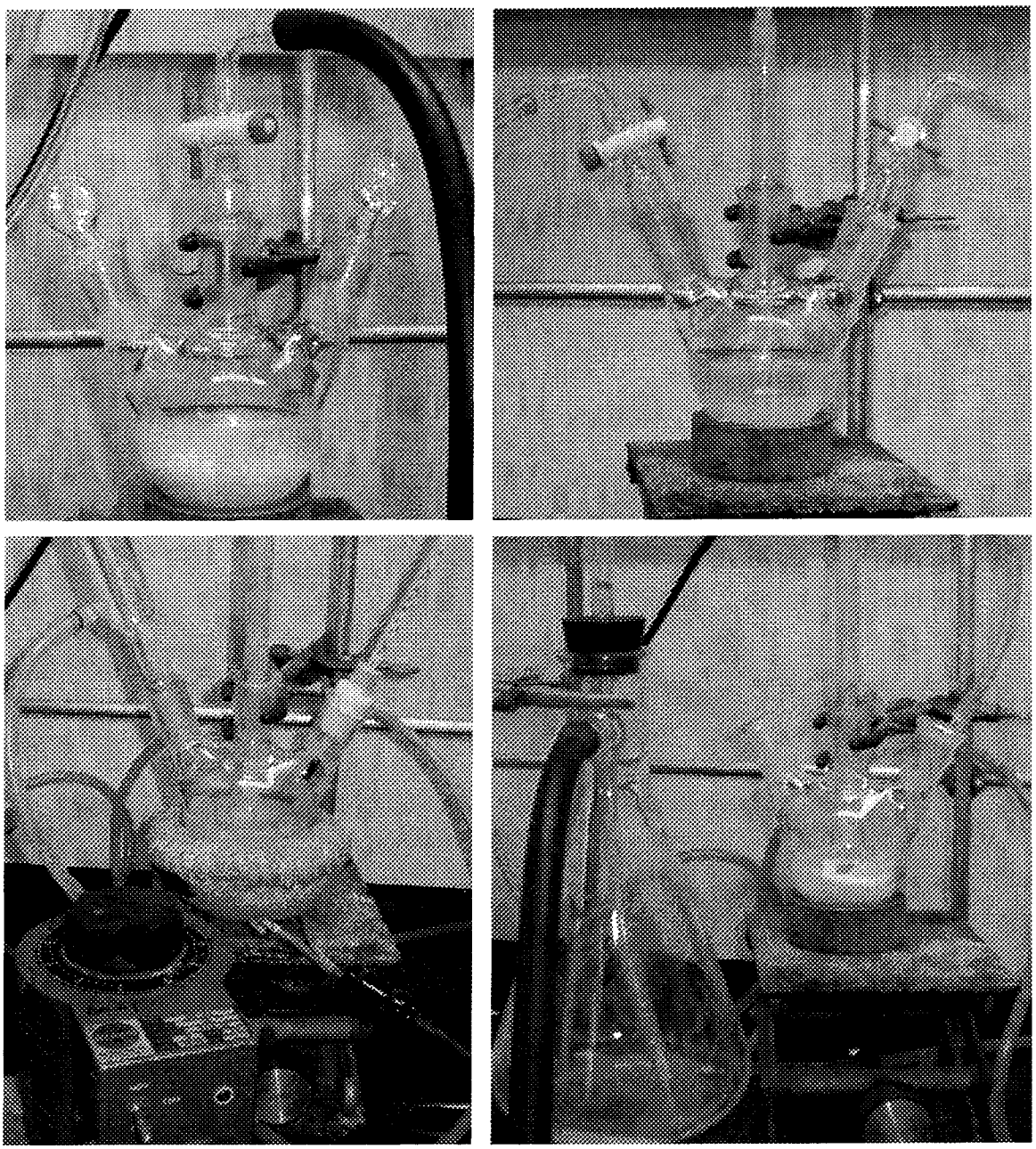

Figure 94. Experimental set-up for: degassing (top, left), nitrogen head-space (top, right), reflux (bottom, left), vacuum filtration (bottom, right).

Reaction scales varied from as small as 5 g (bench-scale), up to 10 kg (pilot-scale) quantities. Synthetic protocols are reported independent of scale using reagent ratios based upon X grams of silica gel (or composite), reported in grams for solid reagents and milliliters for liquid reagents and solvents. Reactions were carried out in round bottom

flasks of volume 10 – 15X mL (where X is the mass of gel or composite in grams). Reagent quantities have been calculated based on elemental analysis and empirical determination, typically employing a 3 – 5 fold molar excess.

Composites are produced by the controlled layering and modification of the raw silica gel's surface. Approximately 99% of the surface area is within the interior of the gel. Prior to each synthetic step the dry "gel" (or "composite" following polyamine amendment) was degassed to remove air from the pore volume to ensure efficient and reproducible synthesis. This is accomplished by applying a vacuum (~30 mm Hg) to the reaction flask containing gel (or composite) and the reagent solution for ~10 minutes (Figure 94; top, left) using an electric aspirator pump (Model WP-15, Oakton). Gel or composite was mixed into slurry by gently swirling the flask before degassing to allow the reagent solution to displace the air. When working with bench-scale reactions and volatile reagents or solvents, care must be taken not to remove significant amounts of these liquids during degassing. Strategies used to avoid the above mentioned problems include limiting degassing to 5 minutes, addition of volatile reagents after degassing, and addition of supplemental solvent after degassing. The degassed reaction flask is then restored to ambient pressure before proceeding with each reaction.

The substrate and reagents were mixed using an overhead Talboy laboratory stirrer (Model 134-1, Troemner, LLC). Mixing speed was in the range of 40 – 80 rpm, depending on the size of the paddle stirrer with respect to the flask size. Care must be taken not to crush the silica gel by having the paddle against the flask bottom. Mixing speed should be fast enough to suspend the substrate and no faster. Following completion of each reaction excess reagent is removed from the pore volume by washing the gel or composite. Figure 94 (bottom, right) shows the vacuum filtration setup utilizing a fritted

tube, side arm flask, and an electric aspirator pump (not shown, Model WP-15, Oakton). Wash solutions are then added to the reaction flask rinsing the fritted tube in order not to lose any gel or composite. Decantation is used when the reaction solution is too viscous to pass through the fritted tube; this is time consuming and gel or composite loss is inevitable. Wash solutions were 5X mL in volume where X grams of gel (or composite) were utilized. Mixing was accomplished using an overhead paddle stirrer and washes were 30 – 60 minutes in duration. Base washes were 1 hour exactly, and methanol washes were 30 minutes.

6.2 Synthesis of Cleaned Hydrated Gel

Scheme 3 illustrates the synthetic pathway utilized in the production of the various silica-polyamine composite materials. X grams of the sieved gel (Scheme 3a) was added to 4X mL 1.0 N HCl in a three necked round bottom flask (of volume 10 – 15X mL). The gel was then degassed (Figure 94; top, left). The flask was restored to ambient pressure and fitted with a condenser. The solution was then heated to 100°C using a heating mantle, stirred with an overhead paddle stirrer (Figure 94; bottom, left). After six hours at reflux, the solution was allowed to cool with stirring. The solution was removed by vacuum filtration (Figure 94; bottom, right), and washed five times using water, followed two more times using methanol. The cleaned silanol gel (Scheme 3b) was then dried to constant mass at 120°C in a ventilated oven.

Next a monolayer of water was introduced to the silica gel's surface using a side armed flask, a translucent column, and connective tubing as shown in Figure 19. This was accomplished by passing compressed air over the surface of water, and subsequently through a column containing dry (acid washed) silica gel. The hydration set-up allowed air humidity to be between 60 – 80% (over 90% humidity must be avoided).[40] The

hydration apparatus was sampled from the top periodically to record the silica gel's increasing water content. The column was periodically mixed by inverting and rotating by hand. Hydration was ceased when the increase in percent water was less than 10% over a 24 hour period, sampling every 12 hours. Water content in adequately hydrated gel (Scheme 3c) is about 6% (Figure 21) depending on the silica gel's surface area per gram. Following hydration of the silica gel samples were taken from the top, middle, and bottom of the hydration apparatus demonstrating homogeneous hydration due to equal percent hydration.

6.3 Synthesis of Chloropropyl Gel (CP Gel)

All glassware was dried for 10 minutes at 120°C. A reaction solution was prepared based upon X grams of hydrated silica gel. 3.00 mmol (0.484 mL) chloropropyltrichlorosilane (CPTCS) per gram of hydrated gel was added to a hexanes solution to yield a total volume of 4X mL. The reagent solution was added to a three necked round bottom flask (of volume 10 – 15X mL). The left neck of the reaction flask was fitted with a vacuum adapter fitting (with valve). Hydrated silica gel was slowly added through a funnel on the right neck and mixed into a suspension, producing copious amounts of gaseous hydrochloric acid. A gentle vacuum was applied between adding gel to remove the produced HCl gas. After adding all of the gel and thoroughly mixed (by swirling the flask) the silica gel was degassed (Figure 94; top, left). The flask was restored to ambient pressure, fitted with an overhead stirrer, and vacuum adapters (with valves) on both the left and right necks (Figure 94; top, right). Solution was stirred under N_2 gas (passed through molecular sieves), flushing the head space periodically. After 16 hours the solution was removed by vacuum filtration (Figure 94; bottom, right), and the

CP Gel (Scheme 3d) was washed five times with hexanes, and then washed two times with methanol (dried over molecular sieves), and dried to constant mass at 120°C.

Mass gain: 120 – 130%

Elemental Analysis Table 2 and Appendix A

^{13}C NMR (126 MHz, CP/MAS, 5 mm zirconia rotor spun at 10 kHz, 7912 transients, 5.0 s pulse delay, 3.0 ms contact time) δ 53 (s, 1C, C-Cl), 26 (s, 1C), 9 (s, 1C, C-Si). ^{29}Si NMR (99 MHz, CP/MAS 5 mm zirconia rotor spun at 10 kHz, 620 transients, 30 sec pulse delay, 5.0 ms contact time) δ -39 (s, (SiO)-Si-$(OH)_2$CP), -49 (s, $(SiO)_2$-Si-(OH)CP), -57 (s, $(SiO)_3$-Si-CP), -83 (s, (SiO)-Si-$(OH)_2$), -95 (s, $(SiO)_3$-Si-OH), -100 (s, 1Si, $(SiO)_4$-Si).

6.4 Synthesis of Mixed Silane Gel

Scheme 4 illustrates the generic reaction scheme to produce the mixed silane gel. All glassware was dried for 10 minutes at 120°C. A reaction solution was prepared based upon X grams of hydrated silica gel. Variable molar ratios of two silane reagents [CPTCS and methyltrichlorosilane (MTCS)] to total 3.0 mmol per gram of gel were added to a hexanes solution to yield a total volume of 4X mL. The reagent solution was added to a three necked round bottom flask (of volume 10 – 15X mL). The left neck of the reaction flask was fitted with a water aspirator vacuum adapter (with valve). Hydrated silica gel was slowly added through the right neck and swirled into a suspension, producing copious amounts of gaseous hydrochloric acid. A gentle vacuum was applied in between adding gel to remove the produced HCl gas. After adding all of the gel and thoroughly mixed (by swirling the flask) the silica gel was degassed (Figure 94; top, left). The flask was restored to ambient pressure, fitted with an overhead stirrer, and vacuum adapters (with valves) on left and right necks (Figure 94; top, right). Solution was stirred for 16

hours under N_2 gas (passed through molecular sieves), flushing the head space periodically. After 16 hours the solution was removed by vacuum filtration, and the mixed siloxane gel was washed for one hour with 4X mL hexanes, and repeated four more times (Figure 94; bottom, left). The CP Gel was then washed two times (30 minute washes) with 4X mL methanol (dried over molecular sieves), and dried to constant mass at 120°C.

Mass Gains: (1:2) CP/M Gel: 16 – 20%, (2:1) CP/M Gel: 24 – 28%, M Gel: 16 – 20%

Elemental Analysis Table 2 and Appendix A

^{29}Si NMR (99 MHz, BD/MAS, 6 mm zirconia rotor spun at 10 kHz, 1300 transients, 120 sec pulse delay) δ -40 (s, (SiO)-Si-$(OH)_2$CP), -49 (s, $(SiO)_2$-Si-(OH)CP), -58 (s, $(SiO)_3$-Si-CP), -85 (shoulder, (SiO)-Si-$(OH)_2$), -93 (shoulder, $(SiO)_3$-Si-OH), -102 (s, $(SiO)_4$-Si).

6.5 Synthesis of Polyamine Composites (WP-1, BP-1)

A reagent solution was prepared in a three necked round bottom flask (of volume 10 – 15X mL) based upon X grams of dry CP gel. The aqueous reaction solution used to make WP-1 was of volume 4X mL, 18.8% by volume poly(ethyleneimine), 10% methanol, at pH 11. CP Gel was slowly added to the appropriate reaction solution under slow mixing to prevent clumping of the gel in a three necked round bottom flask. Once the reaction solution was well mixed the gel was degassed (Figure 94; top, left). The reaction flask was restored to ambient pressure and fitted with a condenser. The solution was heated to 70°C using a heating mantle, and stirred with an overhead stirrer (Figure 94; bottom, left). After 72 hours the solution was allowed to cool, and then decanted, subsequent washes were removed by vacuum filtration (Figure 94; bottom, right). WP-1 was washed three times with water, one time with 1 N H_2SO_4, three times with water, one

time with 1 N NaOH, three times with water, and two times with methanol, and dried to constant mass at 70°C.

Mass gain: 110 – 116%

Elemental Analysis Table 5 and Appendix A

^{13}C NMR (126 MHz, CP/MAS, 5 mm zirconia rotor spun at 10 kHz, 2840 transients, 5.0 s pulse delay, 3.0 ms contact time) δ 48 (s, 1C, C-N), 38 (polyethyl), 21 (s, 1C), 9 (s, 1C, C-Si).

A reagent solution was prepared in a three necked round bottom flask (of volume 10 – 15X mL) based upon X grams of dry CP gel. The aqueous reaction solution used to make BP-1 was of volume 5X mL, 8% by volume poly(allylamine), 10% methanol (to retard foaming during degassing), at pH 11 due to the poly(allylamine) reagent in its base form. CP Gel was slowly added to the appropriate reaction solution under slow mixing to prevent clumping of the gel in a three necked round bottom flask. Once the reaction solution was well mixed the gel was degassed (Figure 94; top, left). The reaction flask was restored to ambient pressure and fitted with a condenser. The solution was heated to 70°C using a heating mantle, and stirred with an overhead stirrer (Figure 94; bottom, left). After 72 hours the solution was allowed to cool, and then decanted, subsequent washes were removed by vacuum filtration (Figure 94; bottom, right). BP-1 was washed five times with water, one time with 1 N NaOH, three times with water, two times with methanol, and dried to constant mass at 70°C.

Mass gain: 112 – 120%

Elemental Analysis Table 5 and Appendix A

^{13}C NMR (126 MHz, CP/MAS, 5 mm zirconia rotor spun at 10 kHz, 5964 transients, 10 s pulse delay, 3.0 ms contact time) δ 47 (s, 1C, C-N), 33 (~7C, polyallyl), 25 (s, 1C), 9 (s, 1C, C-Si).

6.6 Synthesis of Tethered Polyallylamine Composite (BP-1-t)

Synthesis of tethered polyamine can be produced on both WP-1 and BP-1 composites. The reaction shown in Scheme 3 is based upon X grams of BP-1, massed into a three necked round bottom flask (of volume 10 – 15X mL). 1.0X g 2-bromoethylamine hydrobromide was dissolved into 3X mL ethanol (abs.), added to the flask containing BP-1 and then degassed (Figure 94; top, left). The flask was then fitted with a condenser, heated to reflux (70°C) and stirred using a paddle stirrer (Figure 94; bottom, left). After 24 hours the reaction solution was allowed to cool, then removed by vacuum filtration, and washed two times with ethanol and two times with methanol (Figure 94; bottom, right). Tethered BP-1 (BP-1-t) was then air dried to constant mass at 70°C.

Mass gain: 122 – 127%

6.7 Synthesis of Acetate Polyamine Composites (WP-2, BP-2)

A reagent solution was prepared in a three necked round bottom flask (of volume 10 – 15X mL) based upon X grams of dry WP-1 or BP-1. The aqueous reaction solution used to make WP-2 was of volume 4X mL containing 0.83 g sodium chloroacetate per gram of WP-1. BP-2 utilized 1.0 g sodium chloroacetate per gram of BP-1. Once the reaction solution was well mixed, the gel was degassed (Figure 94; top, left). The flask was restored to ambient pressure and fitted with a condenser. The reaction solution was then heated to 65°C using a heating mantle, and stirred with a paddle stirrer (Figure 94; bottom, left). The pH was monitored and kept between 8.5 and 10.0 using 8.0 N NaOH,

added dropwise. After 24 hours the reaction solution was allowed to cool, and then removed by vacuum filtration (Figure 94; bottom, right). WP-2 or BP-2 was then washed three times with water, one time with 1 N HCl, three times with water, and two times with methanol. WP-2 or BP-2 (Figure 4) was then dried to constant mass at 70°C.

Mass gain: 116 – 122%

6.8 Synthesis of Picolylamine Composite (CuWRAM)

Refer to doctoral dissertation of Robert J. Fischer for synthesis of CuWRAM (Figure 5).[18]

6.9 Synthesis of Oxine Polyallylamine Composite (WP-4)

A reagent solution was prepared in a three necked round bottom flask (of volume 15 – 20X mL) based upon X grams of dry BP-1. The aqueous reaction solution used to create the intermediate BP-1-imine composite utilized 5.0X mL 37.7% formaldehyde and 0.10X mL glacial acetic acid. The reaction solution was added to the flask containing BP-1 and the composite was degassed (Figure 94; top, left). The flask was restored to ambient pressure and mixed using a rotary stirrer (Figure 95) for 2 hours at ambient temperature. The intermediate BP-1-imine composite was transferred to a glass-fritted Buchner funnel, washed three times with ethanol and dried by aspiration. A reagent solution was prepared by dissolving 1.0X g 8-hydroxyquinoline (oxine) into 9.0X mL methanol (dried over molecular sieves). The filtered BP-1-imine composite was added to the three necked round bottom flask (of volume 15 – 20X mL), then added the oxine reagent solution, and degassed the composite. The flask was then restored to ambient pressure, fitted with a condenser and heated to 60°C (Figure 94; bottom left). The reaction pH was monitored and adjusted to pH 9 using tetramethylammonium hydroxide (TMAH) (25% in methanol, 5 – 10% H_2O). Seven aliquots of 0.04X mL TMAH were

used over 18 hours at reflux. The solution was then allowed to cool, filtered by vacuum filtration (Figure 94; bottom, right). WP-4 was then washed three times with methanol, two times with 0.025 M NaOH, one time with water, one time with 4.0 N H_2SO_4, two times with water, and two times with methanol. WP-4 (Figure 29) was then dried to constant mass at 70°C.[68,69]

Mass gain: 134 – 142%

Elemental Analysis Table 6 and Appendix A

^{13}C NMR (126 MHz, CP/MAS, 5 mm zirconia rotor spun at 10 kHz, 5004 transients, 1.0 s pulse delay, 3.0 ms contact time) δ 143-115 (9C, aromatic), 46 (broad packet: ~7C polyallyl; 1C, methylene; 1C, C-N), 25 (s, 1C), 9 (s, 1C, C-Si).

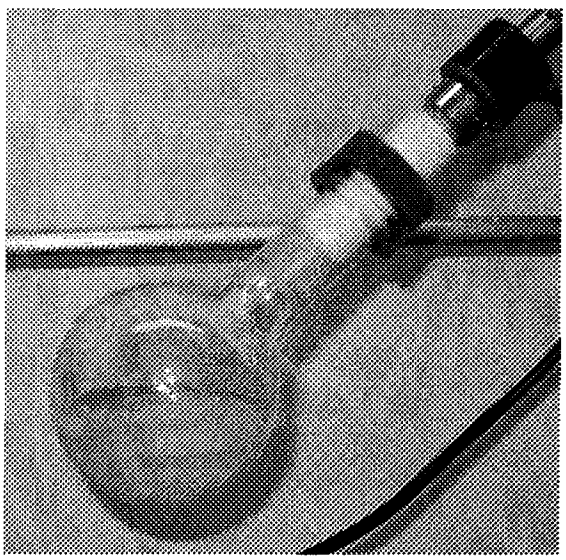

Figure 95. Round bottom flask rotary stirrer.

6.10 Synthesis of Succinamic Acid Polyallylamine Composite (BPSU)

Scheme 5 illustrates the synthesis of BPSU. A reaction solution was prepared based upon X grams of BP-1. The reagent solution was prepared in a three necked round bottom flask (of volume 10 – 15X mL). 1.0X g succinic anhydride was added to 3X mL distilled THF reagent solution. BP-1 was then added, thoroughly mixed (by swirling the

flask), and degassed (Figure 94; top, left). The flask was then restored to ambient pressure, and heated to reflux (~65°C) and stirred using a stir paddle (Figure 94; bottom, left). After 24 hours, the reaction solution was allowed to cool, then removed by vacuum filtration, and washed three times with water, one time with 1.0 N NaOH, three times with water, one time with 1.0 N H_2SO_4, two times with water, and two times with methanol (Figure 94; bottom, right). BPSU was then air dried to constant mass at 70°C.

Mass gain: 119 – 123%

Elemental Analysis Table 7 and Appendix A

^{13}C NMR (126 MHz, CP/MAS, 5 mm zirconia rotor spun at 10 kHz, 2448 transients, 20 s pulse delay, 3.0 ms contact time) δ 148 (s, 1C, C(O)OH), 172 (1C, N-C(O)), 44 (s, 1C, C-N), 32 (broad packet: ~7C, polyallyl; 2C, succinamic methylenes), 24 (s, 1C), 8 (s, 1C, C-Si).

6.11 Synthesis of Tetra-Acetate Polyallyamine Composite (BPDT)

Scheme 6 illustrates the transformation of BP-1 to BPDT. A reaction solution was prepared based upon X grams of BP-1. The reagent solution was prepared in a three necked round bottom flask (of volume 10 – 15X mL). 0.45X mL triethylamine was added to 7X mL DMSO (dried over molecular sieves). 3.5X g diethylenetriamine pentaacetic dianhydride (DTPA) was next added and swirled flask until solution was homogenous. BP-1 was then added, thoroughly mixed (by swirling the flask), and was degassed (Figure 94; top, left). The flask was then restored to ambient pressure, and heated to reflux (~75°C) and stirred using a stir paddle (Figure 94; bottom, left). After 24 hours, the reaction solution was allowed to cool, vacuum filtered, and washed two times with DMSO (heated to 70°C), two times with DI H_2O, one time with 4.0 N H_2SO_4, three times

with water, one time with 4.0 N NH_4OH, four times with water, and two times with methanol (Figure 94; bottom, right). BPDT was then dried to constant mass at 70°C.

Mass gain: 125 – 130%

6.12 Synthesis of Keto Phosphonic Acid Polyamine Composite (BPMA)

Scheme 7 illustrates the synthesis of BPMA utilizing the Michaelis-Arbuzov reaction. A reaction solution was prepared based upon X grams of BP-1. The chlorobutyryl phosphonate reagent was prepared in a three necked round bottom flask (of volume 10 – 15X mL). 0.88X mL tertiary butanol (25% by volume aqueous solution) and 0.68X mL trimethylphosphite were added to the flask, and stirred by rotating the flask in an ice water bath for one hour. 2.0X mL of methanol was added, followed by the addition of BP-1 thoroughly mixed (by swirling the flask), and the silica gel was then degassed (Figure 94; top, left). The solution was adjusted to pH 9.0 using 1.0 N NaOH, heated to 80°C (with condenser), and stirred with a paddle stirrer for 24 hours (Figure 94; bottom, left). The reagent solution was removed by vacuum filtration and washed five times with 4X mL methanol and dried to constant mass at 70°C (Figure 94; bottom, right). The composite was then added to 4X mL dry C_2H_3N containing 0.22X mL bromotrimethylsilane per gram of BP-1, and stirred by rotating flask for 24 hours (Figure 95). The product was washed two times with dry C_2H_3N and two more times with methanol and dried to constant mass at 70°C.

Mass gain: 110 – 114%; Elemental Analysis Table 9 and Appendix A

6.13 Synthesis of Phosphonic Acid Composite via CMPD (BPCD)

Scheme 8 illustrates the synthesis of BPAP utilizing chloromethylphosphonic dichloride reagent. A reaction solution was prepared based upon X grams of BP-1. The chloromethylphosphonate reagent was prepared in a one neck round bottom flask (of

volume 5 – 10X mL). 0.65X mL chloromethylphosphonic dichloride was added to 1.0X mL tertiary butanol (methanol or other alcohol). The solution was stirred using a rotary stirrer (Figure 95) for 4.0 hours. The chloropropyl dialkylphosphonate product was isolated by evaporating the alcohol using a rotovaporator.

^{1}H NMR (400 MHz, $CDCl_3$) δ 6.27 (d, J = 11.0, 6H, $(CH_3O)_2P{=}O$), 5.92 (d, J = 9.3, 2H, $C\underline{H}_2(CH_3O)_2P{=}O$); ^{13}C NMR (100 MHz, $CDCl_3$) δ 54.6 (d, J = 6.4, $(CH_3O)_2P{=}O$), 31.4 (d, J = 159, $(CH_3O)_2P{=}O$); ^{31}P NMR (162 MHz, $CDCl_3$) δ 18.2 (s, $(CH_3O)_2P{=}O$).

The liquid product was then added to 4X mL distilled THF (0.5% DMSO) in a three necked round bottom flask (of volume 10 – 15X mL). BP-1 was then added, thoroughly mixed (by swirling the flask), and degassed (Figure 94; top, right). The flask was then restored to ambient pressure, and heated to reflux (~65°C) and stirred using a stir paddle (Figure 94; bottom, left). After 24 hours, the reaction solution was allowed to cool, removed by vacuum filtration, and washed two times with THF, and two times with methanol (Figure 94; bottom, right). The phosphonate composite was then added to 4X mL 6.0 M HCl in a one neck round bottom flask (of volume 10 – 15X mL), and stirred by rotating for 6.0 hours. The solution was then removed by vacuum filtration and washed two times with water and two times with methanol and dried to constant mass at 70°C.

Mass gain: 108 – 112%

Elemental Analysis Table 10 and Appendix A

6.14 Synthesis of Phosphonic Acid Composite by Mannich Reaction (BPAP)

Scheme 10 illustrates the synthesis of BPAP utilizing BP-1 via the Mannich reaction. X grams of dry BP-1 was massed into a three necked round bottom flask (of volume 10 – 15X mL). 1.0X g phosphorous acid (98% purity) was dissolved in 3X mL 2.0 M HCl, added to the flask containing BP-1, and degassed (Figure 94; top, left). The

flask was then restored to ambient pressure, heated to reflux (~98°C) and mixed using a stir paddle (Figure 94; bottom, left). 0.88X mL CH_2O (37.7%) was added to the flask while heating to reflux. After 4.0 hours at reflux, the reaction solution was allowed to cool and removed by vacuum filtration, and washed three times with water, one time with 1.0 N NaOH, three times with water, one time with 1.0 N H_2SO_4, two times with water, and two times with methanol (Figure 94; bottom, right). BPAP was then dried to constant mass at 70°C.

Mass gain: 116 – 123%

Elemental Analysis Table 11 and Appendix A

^{13}C NMR (126 MHz, CP/MAS, 5 mm zirconia rotor spun at 10 kHz, 4096 transients, 10 s pulse delay, 3.0 ms contact time) δ 70 - 20 (broad packet: ~7C, polyallyl; 1C, CH_2P), 47 (s, 1C, C-N), 28 (s, 1C), 12 (s, 1C, C-Si). ^{31}P NMR (202 MHz, CP/MAS, 5 mm zirconia rotor spun at 10 kHz, 64 transients, 60 s pulse delay) δ 33 (s, 2P, $N(CH_2P(O)(OH)_2)_2$) 23 (s, 1P, $NH(CH_2P(O)(OH))$.

6.15 Synthesis of Methylated BPAP (Phosphonate)

Four reactions were pursued using X g BPAP. Syntheses are summarized below in short due to limited success. BPAP was initially degassed and washed (30 min.) in 3X mL 1 N NaOH, then dried in a Büchner funnel, and then used for the following four reactions. The first methylation utilized 3X mL dimethylsulfate added to BPAP, degassed, and stirred for 12 hours at ambient temperature to produce BPAP-CF 042704-DN. A second attempt used 1X mL ethanol solvent in addition to the 3.0X mL dimethylsulfate, and was refluxed (75°C) for 2 hours (BPAP-CF 042804-DN). In a third study 3.0X mL iodomethane was added to BPAP, degassed, and refluxed at 45°C for 3 hours (BPAP-CF 042904-DN). A fourth attempt utilized 1.0X mL iodomethane and 4X

THF, degassed and refluxed at 50°C for 12 hours (BPAP-CF 043004-DN). Mass gains were negligible as would be expected. BPAP-CF 043004-DN showed a 3.4% mass increase, and the other three showed no mass increase. Elemental analysis (Table 11: Entries 31 – 34) also show limited methylation, although the potential increase in carbon content is small in comparison to the polymer carbon content.

6.16 Synthesis of Phosphinic Acid Polyallylamine Composite (BP-5)

X grams of dry BP-1 was massed into a three necked round bottom flask (of volume 10 – 15X mL). 1.0X g hypophosphorous acid was dissolved in 3X mL 2.0 M HCl, added to the flask containing BP-1, and degassed (Figure 94; top, left). The flask was then restored to ambient pressure, heated to reflux (~98°C) and mixed using a stir paddle (Figure 94; bottom, left). 0.88X mL CH_2O (37.7% solution) was added to the flask while heating to reflux. After 20 hours at reflux, the reaction solution was allowed to cool and removed by vacuum filtration (Figure 94; bottom, right). BP-5 was then washed three times with water, one time with 1.0 N NaOH, three times with water, one time with 1.0 N H_2SO_4, two times with water, and two times with methanol. BP-5 was then dried to constant mass at 70°C.

Mass gain: 123 – 129%

Elemental Analysis Table 12 and Appendix A

6.17 Synthesis of Methyl/Dimethyl Phosphonate Composite (BP-6)

Trimethylphosphite and 1,3-dibromopropane (4 equiv.) were added to a round bottom flask fitted with a reflux condenser and heated to 150°C (external temp.) in an oil bath for 45 minutes (35% yield).[70] Once cooled to ambient temperature the excess dibromopropane was removed by vacuum distillation (65°C, 14 mm Hg). The double displacement product (tetramethyl propane-1,3-diphosphonate) was not removed to give

a clear, colorless liquid (82% pure target phosphonate). Figure 60 shows NMR spectra of the 82% pure product solution.

^{1}H NMR (400 MHz, $CDCl_3$) δ 3.67 (d, J = 10.8, 6H, $(CH_3O)_2P{=}O$), δ 3.40 (t, J = 6.32, 2H, CH_2Br), δ 1.80-1.89, 2.02-2.14 (2m, 4H, $CH_2CH_2P{=}O$); ^{13}C NMR (100 MHz, $CDCl_3$) δ 52.2 (d, J = 6.80, $(CH_3O)_2P{=}O$), 33.3 (d, J = 18.4, $CH_2CH_2P{=}O$), 25.6 (d, J = 4.01, CH_2Br), 23.1 (d, J = 142, $CH_2P{=}O$); ^{31}P NMR (162 MHz, $CDCl_3$) δ 33.8 (s).

X grams of dry BP-1 was massed into a three necked round bottom flask (of volume 10-15X mL). 2.0X mL dimethyl (3-bromopropyl) phosphonate was mixed with 1.5X mL water, added to the flask containing BP-1, and degassed (Figure 94; top, left). The flask was then restored to ambient pressure, fitted with a condenser, heated to 60°C and mixed using a stir paddle (Figure 94; bottom, left). 3.0 M NaOH was added dropwise when the pH dropped to 8.5, adjusting to pH 9.5, adding no more than 1.5X mL (3.0 M NaOH). After 24 hours, the reaction solution was allowed to cool and removed by vacuum filtration (Figure 94; bottom, right). BP-6 was then washed two times with water, one time with 4.0 N NH_4OH, two times with water, one time with 4.0 M HNO_3, two times with water, and two times with methanol. BP-6 was then dried to constant mass at 70°C.

Mass gain: 129 – 135%

Elemental Analysis Table 13 and Appendix A

^{13}C NMR (68.0 MHz, CP/MAS, 5 mm zirconia rotor spun at 10 kHz, 3568 transients, 10 s pulse delay, 3.0 ms contact time) δ 65 - 50 (broad packet: d, 1C, monomethoxy; d, 2C, dimethoxy), 52 (s, 1C, C-N), 45 - 25 (broad packet: ~7C, polyallyl), 25 – 15 (m, 3C, $CH_2CH_2CH_2P$; s, 1C, C-C-Si), 11 (s, 1C, C-Si). ^{31}P NMR (202 MHz, CP/MAS, 4 mm

zirconia rotor spun at 10 kHz, 64 transients, 60 s pulse delay) δ 35 (s, 2P, $P(O)(OMe)_2$) 28 (s, 1P, P(O)(OH)OMe).

6.18 Synthesis of Methyl/Dimethyl Phosphonate Composite (BP-7)

Dimethyl (3-bromopropyl) phosphonate was produced via the Michaelis-Arbuzov rearrangement as reported above in section 6.17. X grams of dry BP-1 was massed into a three necked round bottom flask (of volume 10-15X mL). 2.0X mL dimethyl (3-bromopropyl) phosphonate were mixed with 2.0X mL ethanol (abs.) and 0.63X mL triethylamine. The phosphonate solution was added to the flask containing BP-1 and degassed (Figure 94; top, left). The flask was then restored to ambient pressure, fitted with a condenser, heated to 60°C and mixed using a stir paddle (Figure 94; bottom, left). After 22 hours, the reaction solution was allowed to cool and removed by vacuum filtration (Figure 94; bottom, right). BP-7 was washed three times with water, one time with 4.0 N HNO_3, two times with water, and two times with methanol. BP-7 was then dried to constant mass at 70°C.

Mass gain: 128 – 134%

Elemental Analysis Table 14 and Appendix A

^{13}C NMR (68.0 MHz, CP/MAS, 5 mm zirconia rotor spun at 10 kHz, 3346 transients, 10 s pulse delay, 3.0 ms contact time) δ 65 - 48 (broad packet: d, 1C, monomethoxy; d, 2C, dimethoxy), 52 (s, 1C, C-N), 45 - 25 (broad packet: ~7C, polyallyl), 25 – 15 (m, 3C, $CH_2CH_2CH_2P$; s, 1C, C-C-Si), 10 (s, 1C, C-Si). ^{31}P NMR (202 MHz, CP/MAS, 4 mm zirconia rotor spun at 10 kHz, 64 transients, 60 s pulse delay) δ 35 (s, 2P, $P(O)(OMe)_2$) 28 (s, 1P, P(O)(OH)OMe).

Appendix A – Elemental Analysis Results

Elemental analysis of selected gels and composites found within this thesis are given in Table 17. The absolute error of elemental analyses is reported to be 0.3 (Schwartzkopf Microanalytical Laboratory).

Table 17. Elemental Analysis of various gels and composites.

Entry	Sample Name	Comp. Ref. #	C	H	N	Cl	P	C	H	N	Cl	P	N/P	N*/P
			%	%	%	%	%	mmol/g	mmol/g	mmol/g	mmol/g	mmol/g		
1	CP Gel-QH	091703-DN	6.71	1.11	-	6.35	-	5.6	11	-	1.8	-	-	-
2	CP Gel-QH (2)	092003-CH	6.07	1.35	-	6.05	-	5.1	13	-	1.7	-	-	-
3	CP Gel-QH (3)	092103-CH	7.17	1.47	-	5.65	-	6.0	15	-	1.6	-	-	-
4	CP Gel-QH (A)	022904-DN	6.54	1.25	-	6.00	-	5.4	12	-	1.7	-	-	-
5	CP/M Gel-QH (B)	030104-DN	5.59	0.93	-	4.19	-	4.7	9.2	-	1.2	-	-	-
6	CP/M Gel-QH (C)	030204-DN	4.49	0.75	-	2.24	-	3.7	7.4	-	0.63	-	-	-
7	M Gel-QH (D)	030304-DN	3.33	0.63	-	0.00	-	2.8	6.3	-	0.00	-	-	-
8	CP Gel-CF	040604-DN	7.02	1.46	-	6.24	-	5.8	14	-	1.8	-	-	-
9	WP-1-NJ	012702-DN	11.22	2.47	4.77	-	-	9.3	25	-	-	-	-	-
10	BP-1-QH	120903-DN	16.18	3.54	3.96	1.61	-	13	35	2.8	0.45	-	-	-
11	BP-1-CF	040804-DN	16.05	3.14	3.97	0.98	-	13	31	2.8	0.28	-	-	-
12	WP-4-CF	101205-DN	22.53	3.49	3.99	-	-	19	35	2.8	-	-	-	-
13	BPSU-CF	080404-DN	21.28	3.15	3.43	-	-	18	31	2.4	-	-	-	-
14	BPMA-CF	111702-DN	16.56	3.02	2.87	-	0.57	14	30	2.0	-	0.18	11	5.9
15	BPCD-CF	101602-DN	12.64	2.65	3.00	-	0.35	11	26	2.1	-	0.11	19	10
16	BPCD-CF	100404-DN	16.99	3.87	3.15	-	0.02	14	38	2.2	-	0.01	387	203
17	BPAP-CF	081902-DN	12.92	3.24	4.45	-	<0.10	11	32	3.2	-	-	-	-
18	WPAP-NJ	072902-DN	12.57	2.69	4.44	-	0.20	10	27	3.2	-	0.06	49	26
19	WPAP-NJ	073002-DN	11.59	2.00	4.08	-	0.11	9.7	20	2.9	-	0.04	82	43
20	WPAP-NJ	082202-DN	11.75	2.84	3.87	-	0.88	9.8	28	2.8	-	0.28	9.7	5.1
21	WPAP-CF	090803-DN	11.49	2.74	3.39	-	1.45	9.6	27	2.4	-	0.47	5	2.7
22	BPAP-CF	111302-DN	16.18	3.10	2.89	-	4.05	13	31	2.1	-	1.3	1.6	0.83
23	BPAP-CF	120902-DN	15.00	2.92	2.65	-	4.26	12	29	1.9	-	1.4	1.4	0.72
24	BPAP-CF	041504-DN	15.87	3.40	2.95	0.68	4.71	13	34	2.1	0.19	1.5	1.4	0.73
25	BPAP-QH	121403-DN	15.35	3.64	2.90	1.42	4.98	13	36	2.1	0.40	1.6	1.3	0.68
26	BPAP-CF	100203-DN	14.45	2.99	2.52	-	3.11	12	30	1.8	-	1.0	1.8	0.94
27	BPAP-CF	082003-DN 3	13.59	3.04	2.39	-	4.01	11	30	1.7	-	1.3	1.3	0.69
28	BPAP-CF	082003-DN 13	14.05	3.20	2.34	-	4.60	12	32	1.7	-	1.5	1.1	0.59
29	BPAP-CF	082003-DN 24	14.12	3.07	2.30	-	4.32	12	30	1.6	-	1.4	1.2	0.62
30	BPAP-t-CF	071504-DN	16.71	3.44	3.39	-	5.37	14	34	2.4	-	1.7	1.4	0.73
31	BPAP-CF	042704-DN	16.93	3.44	2.87	-	5.26	14	34	2.0	-	1.7	1.2	0.63
32	BPAP-CF	042804-DN	15.55	3.29	2.75	-	4.21	13	33	2.0	-	1.4	1.4	0.76
33	BPAP-CF	042904-DN	16.88	3.19	2.89	-	4.71	14	32	2.1	-	1.5	1.4	0.71
34	BPAP-CF	043004-DN	15.79	3.33	2.77	-	4.66	13	33	2.0	-	1.5	1.3	0.69
35	BP-5-CF	120804-DN	16.55	3.30	3.15	-	6.36	14	33	2.2	-	2.1	1.1	0.58
36	BP-6-CF	021505-DN	19.54	3.11	4.39	-	3.33	16	31	3.1	-	1.1	2.9	1.5
37	BP-7-CF	022305-DN	18.49	3.55	4.70	-	3.17	15	35	3.4	-	1.0	3.3	1.7

REFERENCES

[1] Moore, J.N.; Luoma, S.N. *Envir. Sci. Technol.* **1990**, *24(9)*, 1278-1285.
[2] Nadeau, T.; Dejak, M. Copper, Nickel, and Chromium Recovery on a Jobshop. *Plating and Surface Finishing* **1986**, *48*.
[3] Tavlarides, L.L.; Deorkar, N. Chemically Active Ceramic Compositions with a Thiol and/or Amine Moiety. U.S. Patent 5,616,533 **1994**.
[4] Beatty, S.T.; Fischer, R.J.; Rosenberg, E.; Pang, D. *Sep Sci. Technol.* **1999**, *34*, 2723 -2739.
[5] Fischer, R. J.; Pang, D.; Beatty, S. T.; Rosenberg. E. *Sep.Sci. Technol.* **1999**, *34*, 3125 -3137.
[6] Gupta, A.; Johnson, E.F.; Schlossel, R.H. *Ind. Eng. Chem. Res.* **1987**, *26*, 588-594.
[7] Lewis, C.J.; Boynton, R.S. Acid Neutralization with Lime, National Lime Association **1995**, Bulletin No. 216.
[8] Ujang, Z.; Anderson, G.K. *Wat. Sci Tech.* **1996**, *34*, 247-253.
[9] Lee, M.-S.; Lee, J.-Y.; Kim, J.-S.; Lee, G.-S. *Sep. Purif. Technol.* **2005**, *46*, 72-78.
[10] Long, H., Formation of Higher Density Sludge on the Treatment of the Berkeley Pit Water, Thesis-Montana Tech of the University of Montana **1995**.
[11] Weingartner, B., Cost Analysis of Treatment Options for the Berkeley Pit Water, Thesis-Montana College of Mineral Science and Technology **1992**.
[12] Weingartner, B., Cost Analysis of Treatment Options for the Berkeley Pit Water, Thesis-Montana College of Mineral Science and Technology **1992**.
[13] Castro, J.M.; Wielinga, B.W.; Gannon, J.E.; Moore, J.N. *Water Environ. Res.* **1999**, *71*, 218-223.
[14] Alexandratos, S.D.; Quillen, D.R.; Bates, M.E. *Macromolecules* **1987**, *20*, 1191-1196.
[15] Personal communication with doctorate student Travis Denton, **2002**.
[16] Geckeler, K.E.; Zhou, R. *Naturwissenschaften* **1993**, *80*, 270-271.
[17] Rosenberg E. Silica Polyamine Composites, Symposium Proceedings, ICMAT **2001**, 173-186.
[18] Fisher, R.J. Doctoral Dissertation, University of Montana, **2002**.
[19] Irving, H.M.N.H.; Williams; R.J.P. *J. Chem. Soc.* **1953**, 3192-3210.
[20] Huheey, J.E. et al. Inorganic Chemistry, 4th Ed. **1993**, 348.
[21] Greenwood, N.N.; Earnshaw, A. The Chemistry of the Elements, 2nd Ed. **1997**, 1058 -1061.
[22] www.calgoncarbon.com/ion_exchange/ **2006**.
[23] www.septor.nl **2006**.
[24] www.pwbrc.org/bmr/ew.htm **2006**.
[25] www.electrometals.com/applications.html **2006**.
[26] Personal communication with Ian Ewert **2003**, www.electrowinning.com.
[27] www.electrowinning.com/tech-paper-zinc-electrowinning.pdf **2006**.
[28] www.netl.doe.gov/publications/proceedings/96/96em/Em96/Em-p1-1.pdf **2006**.
[29] Beatty, S.T.; Fischer R.J.; Hagers, D.L.; Rosenberg, E. *Ind. Eng. Chem. Res.* **1999**, *38*, 4402-4408.
[30] Zaitsev, V. N.; Vassilik, L. *S. Royal Society of Chemistry* **1999**, *235*, 361-368.
[31] Garcia-Valls, R.; Hrdlicka, A.; Perutka, J.; Havel, J.; Deorkar, N.V.; Tavlarides, L.L.; Munoz, M.; Valiente, M. *Anal. Chim. Acta* **2001**, *439*, 247-253.
[32] (a) Fryxell, G.E.; Lin, Y.; Fiskum, S.; Birnbaum, J.C.; Wu, H. *Environ. Sci. Technol.*

2005, *39*, 1324-1331. (b) Yuehe, L.; Fiskum, S.K.; Wassana, Y.; Wu, H.; Mattigod, S.V.; Vorpagel, E.; Fryxell, G. *Environ. Sci. Technol.* **2005**, *39*, 1332-1337.
[33] Davis, A.; Ashenberg, D. *Applied Geochemistry* **1989**, *4*, 23-36.
[34] www.mbmg.mtech.edu/env-berkeley.htm **2006**.
[35] http://ist-socrates.berkeley.edu/~es196/projects/2000final/frank.pdf **2006**.
[36] Stejskal, E.O.; Memory, J.D. High Resolution NMR in the Solid State **1994**.
[37] Zhuravlev, L.T. *Langmuir* **1987**, *3*, 316-318.
[38] Wirth, M.J.; Fatunmbi, O.H. *Anal. Chem.* **1992**, *64*, 2783-2786.
[39] Rosenberg, E., U.S. Patent Number 5,695,882 **1997**.
[40] (a) Wirth, M.J.; Fatunmbi, H.O. *Anal. Chem.* **1993**, *65*, 822-826. (b) Fyfe, C.A.; Zhang, Y.; Aroca, P. *J. Am. Chem. Soc.* **1992**, *114*, 3252-3255.
[41] Wirth, M.J.; Fatunmbi, H.O. *Royal Society of Chemistry* **1994**, *139*, 203-209.
[42] Fatunmbi, H.O.; Bruch, M.D.; Wirth, M.J. *Anal. Chem.* **1993**, *65*, 2048-2054.
[43] Smith R.M. and Martell A.E., Critical Stability Constants Volume 6: Second Supplement **1989**.
[44] Bhattacharya, A.K.; Thyagarajan, G. *Chemical Reviews*, **1981**, *81*, 415-430.
[45] Karaman, R.; Goldblum, A.; Breuer, E. *J. Chem. Soc. Perkin Trans. I* **1989**, 765-774.
[46] Personal communication with Professor Ed Rosenberg, **2002**.
[47] Boduszek, B. *Phosphorus, Sulfur, and Silicon* **1996**, *113*, 209-218.
[48] Smith, M.B. and March, J., March's Advanced Organic Chemistry, 5th ed. **2001**, 1189 -1190.
[49] Blicke, F.F., The Mannich Reaction, Organic Reactions, Chapter 10, **1942**, 303-341.
[50] Geckeler, K.E.; Zhou, R. *Naturwissenschaften.* **1993**, *80*, 270-271.
[51] Crick, D.W.; Alexandratos, S.D. *Magn. Reson. Chem.* **1994**, *32*, S40-S44.
[52] Berthod, A. *J. Chromatography* **1991**, *549*, 1-28.
[53] Selzer, R.B.; Howery, D.G. *Macromolecules* **1986**, *19*, 2673-2682.
[54] Alexandratos, S.D; Smith, S.D. *J. Appl. Polym. Sci.* **2004**, *91*, 463-468.
[55] Deepatana, A.; Marjorie, V. 2004 Conference on Separations Technology VI. Queensland, Australia **2004**, Paper 4.
[56] Park, J.S.; Han, C.; Lee, J.-Y.; Kim, S.-D.; Kim, J.-S.; Wee, J.-H. *Sep. Pur. Tech.* **2005**, *43*, 111-116.
[57] Varga, T.R. *Synthetic Communications* **1997**, *27*, 2899-2903.
[58] Sievers, G.; Hagele, G.; Failla, S.; Finocchiaro, P. *Phosphorus, Sulfur and Silicon* **1999**, *155*, 113-126.
[59] Rixens, B.; Boutevin, G.; Boulahna, A.; Hervaud, Y.; Boutevin, B. *Phosphorus, Sulfur and Silicon and the Related Elements* **2004**, *179*, 2617-2626.
[60] Moore, J.N.; Study conducted Nov. 6th, 2001, HSB analyses courtesy of Montana Bureau of Mines and Geology (sampled May 3rd, 2001).
[61] www.epa.gov **2003**
[62] www.clarkfork.org/milltownfaq.html **2003**
[63] www.milltownfacts.com **2003**
[64] Wiedenheft, B.; Willits, D.; Mosolf, J.; Yeager, M.; Dryden, K.; Young, M.; Douglas, T. Proceedings of the National Academy of Sciences **2005**, 102(30), 10551-10556.
[65] Dellaria, J.F; Jr., Maki, R.G.; Stein, H.H.; Cohen, J.; Whittern, D.; Marsh, K.; Hoffman, D.J.; Plattner, J.J.; and Perun, T.J. *J. Med. Chem.* **1990**, *33*, 534-542.
[66] Fryxell, G.E.; Wu, H.; Lin, Y.; Shaw, W.J.; Birnbaum, J.C., Linehan, J.C.; Nie, Z.; Kemer, K.; Kelly, S. *J. Mater. Chem.* **2004**, *14*, 3356-3363.

[67] Hughes, M.A.; Rosenberg, E. *Ind. Eng. Chem. Res.* **2006**, manuscript under review.
[68] Miranda, P. Doctoral Dissertation, University of Montana, **2005**.
[69] Pyell, U. and Stork, G. *Fresenius J. Anal. Chem.* **1992**, *342*, 281-286.
[70] Maguire, A.R. et al. *Bioorg. Med. Chem.* **2001**, *9*, 745-762.